IMPROVED CONVERGENCE FOR GNSS PRECISE POINT POSITIONING

SIMON BANVILLE

July 2014

IMPROVED CONVERGENCE FOR GNSS PRECISE POINT POSITIONING

Simon Banville

Department of Geodesy and Geomatics Engineering
University of New Brunswick
P.O. Box 4400
Fredericton, N.B.
Canada
E3B 5A3

July 2014

PREFACE

This technical report is a reproduction of a dissertation submitted in partial fulfillment of the requirements for the degree of Doctor of Philosophy in the Department of Geodesy and Geomatics Engineering, July 2014. The research was supervised by Dr. Richard B. Langley, and funding was provided by the Natural Sciences and Engineering Research Council of Canada (NSERC), the Fonds québécois de la recherche sur la nature et les technologies (FQRNT), the School of Graduate Studies (SGS) at the University of New Brunswick (UNB), the Japan Society for the Promotion of Science (JSPS), the Government of Canada, and The Institute of Navigation (ION).

As with any copyrighted material, permission to reprint or quote extensively from this report must be received from the author. The citation to this work should appear as follows:

ABSTRACT

The precise point positioning (PPP) methodology allows for cm-level positioning accuracies using a single GNSS receiver, through careful modelling of all error sources affecting the signals. Adoption of PPP in several applications is however muted due to the time required for solutions to converge or re-converge to their expected accuracy, which regularly exceeds 30 minutes for a moving receiver. In an attempt at solving the convergence issues associated with PPP, three aspects were investigated.

First, signal tracking interruptions are typically associated with integer discontinuities in carrier-phase measurements, often referred to as a cycle slips. A refined method for detecting and correcting cycle slips was thus developed, in which all error sources affecting the observations are either modelled or estimated. Application of this technique allows for instantaneous cycle-slip correction, meaning that continuous PPP solutions can be obtained even in the presence of short losses of lock on satellites.

Second, external information on the ionosphere allows for reduced convergence times, but consistency must be observed in the functional model. A new technique, termed integer levelling, was thus developed to generate ionospheric delay corrections compatible with PPP based on the decoupled-clock model. Depending on the inter-station distances in the network providing ionospheric corrections, instantaneous cm-level accuracies can be obtained in PPP.

Third, processing of GLONASS signals is more problematic than GPS due to frequency division multiple access, leading to inter-frequency carrier-phase and code biases. A novel approach for the estimation of such biases was then proposed and facilitates processing of mixed receiver types. It also allows for undifferenced GLONASS ambiguity resolution based on a heterogeneous network of stations, the first demonstration of such an approach, and therefore has the potential to further reduce PPP convergence times.

This research also emphasized potential benefits of integer-levelled observations for improved ionosphere monitoring. The main justifications for adopting this approach are: a reduction in the determination of slant total electron content errors, a simplification in the GLONASS processing strategy, its applicability in real time, and the generation of satellite biases required for the use of ionospheric constraints in PPP with ambiguity resolution.

ACKNOWLEDGEMENTS

A six-year long project requires help, support and inspiration from several people. First, I would like to acknowledge the role of my supervisor, Dr. Richard B. Langley, for whom I have great respect. His extensive knowledge and rigorous analytical reasoning were an inspiration in improving the quality of my work. He also provided me with countless networking opportunities by encouraging participation in conferences, and by providing points of contact for a 10-week internship position in Japan. I personally believe that inspiration and motivation come from a sense of freedom that Richard created by never objecting to any of my extravagancies from both personal and academic perspectives. It is no coincidence that many students of Richard are now well-respected scientists in the field of GNSS.

Put simply, the influence of Paul Collins shaped the content of this dissertation. First, his innovative "decoupled-clock" model is the foundation of most of the work presented herein. Second, working alongside Paul at NRCan for the past three years helped me understand the intricacies of this model, which led me to cover additional topics in this dissertation. Even though this extra work certainly extended the duration of my degree work by a couple of years, I am certainly grateful for the end result.

I would also like to highlight the contributions of several people who were co-authors of the papers included in this paper-based dissertation, especially Wei Zhang. Wei believed in my idea of "integer levelling" since the beginning and his expertise in

ionosphere modelling was key in concretizing this idea. Reza Ghoddousi-Fard provided extensive advice and came to my rescue in my last-minute work for our ION GNSS 2012 paper. François Lahaye also gave valuable inputs on the GLONASS-related papers. Finally, although it did not make it into this dissertation, Hui Tang built and operated the motion table used in our ION GNSS 2010 student paper.

During my stay at the Electronic Navigation Research Institute (ENRI) in Japan, I had my first real exposure to the effects of disturbed ionospheric conditions on GPS signals. The challenges encountered when processing data provided by ENRI had a significant impact on my research on cycle-slip detection/correction, and I must evidently thank people at ENRI for a warm welcome and constant support: Susumu Saito, Takeyasu Sakai, Takayuki Yoshihara, Keisuke Matsunaga, Kazuaki Hoshinoo, and Seigo Fujita. I truly had a great experience in Japan.

Even though I only spent two years in residency at UNB, I had the chance to participate in Friday meetings at which I got valuable inputs from Yong Won Ahn, Godze Akay, Wei Cao, Peter Dare, Don Kim, Sajan Mushini, Hyunho Rho, Samaneh Sadighi, Marcelo Santos, Hui Tang, and Wei Zhang. I also want to thank Andy Kubiak for taking over some of my duties related to data management of UNB continuously operating receivers.

While it is a complex endeavour to work full time while finishing a Ph.D. degree, I was fortunate enough that my team leader at NRCan, Mark Caissy, was supportive of my

research initiatives. I greatly appreciated the opportunity of working on some dissertation-related matters during work hours.

Last, but not least, I need to mention the constant support of my friends and family, my wife Romy whom I met on my first day in Fredericton, and our beautiful daughter Elizabeth who was born during this long adventure.

Table of Contents

Curriculum Vitae

List of Tables

List of Figures

List of Symbols

GNSS Functional Model

i	identifies frequency-dependant terms
j	identifies a given satellite
Φ	is the carrier-phase measurement (m)
P	is the code measurement (m)
ρ	is the instantaneous range between the phase centres of the satellite and receiver antennas, including displacements due to earth tides and ocean loading and relativistic effects (m)
$\bar{\rho}$	includes all non-dispersive terms such as geometric range, satellite and receiver clock offsets, relativistic effects, tropospheric delay, displacements due to earth tides and ocean loading, etc. (m)
x_r, y_r, z_r	are the Cartesian coordinates of the receiver position (m)
x^j, y^j, z^j	are the Cartesian coordinates of a satellite position (m)
c	is the vacuum speed of light (m/s)
dT	is the receiver clock offset from GPS time for a given observable (m)
dt	is the satellite clock offset from GPS time for a given observable (m)
T	is the tropospheric delay (m)
μ_i	is a constant = f_i^2 / f_1^2, where f_i is the frequency of the L_i carrier
I	is the ionospheric delay on L_1 (m)

M	is a mapping function
λ	is the wavelength of the carrier (m)
N	is the integer carrier-phase ambiguity (cycles)
w	is the receiver wind-up effect (cycles)
b	are instrumental delays (m)
DCB	is the differential code bias, i.e. the difference between instrumental code biases on two frequencies (m)
ε	contains unmodelled quantities such as noise and multipath (m)
δ	is the variation of a quantity over a time interval
$\tilde{\blacksquare}$	is the misclosure (observation minus computed value)
$\blacksquare$	denotes biased quantities
$\bar{\blacksquare}$	denotes integer-levelled observations
$\blacksquare_0$	denotes *a priori* values.

Vectors and Matrices

$\boldsymbol{y}$	is the vector of observations
$\boldsymbol{x}_1$	is the vector of unknown geometric parameters, such as receiver position and receiver clock offset variations. Can also be simply designated as $\boldsymbol{x}$.
$\boldsymbol{x}_2$	is the vector of slant ionospheric parameters
$\boldsymbol{n}$	is the vector of ambiguity parameters

$\delta \boldsymbol{n}$	is the vector of cycle-slip parameters
$\boldsymbol{e}$	is the vector of unmodelled errors associated with each observation
$\boldsymbol{A}_1$	(or $\boldsymbol{A}$) is the design matrix associated with parameters $\boldsymbol{x}_1$
$\boldsymbol{A}_2$	is the design matrix associated with parameters $\boldsymbol{x}_2$
$\boldsymbol{B}$	is the design matrix associated with parameters $\boldsymbol{n}$ and $\delta \boldsymbol{n}$
$\boldsymbol{Q}$	is a covariance matrix
$\boldsymbol{Z}$	is an integer-preserving transformation matrix
$\hat{\blacksquare}$	is a vector of estimated values
$\breve{\blacksquare}$	is a vector of integer values
$\bar{\blacksquare}$	is a vector of biased values
$\blacksquare_0$	is a vector of *a priori* values.

CHAPTER 1

INTRODUCTION

This chapter provides necessary background information on the status of the precise point positioning (PPP) methodology at the time when this research project was initiated. From those explanations emerge the motivations supporting the work conducted for this dissertation. The objectives of the research, the methodology utilized and the main contributions are also presented.

1.1 Background

The Global Positioning System (GPS), initiated by the U.S. Department of Defense, first became operational (initial operational capability) in 1993 [Parkinson, 1994]. By precisely measuring the propagation time of electromagnetic waves from at least four satellites, a GPS receiver can effectively determine its location anywhere on (or in the vicinity of) Earth. The initial purpose of GPS was to serve military operations, allowing positioning of personnel and equipment with metre-level accuracies. However, soon after the first satellites were launched, it became apparent that exploiting the carriers of the GPS signals, as opposed to the pseudorandom noise codes on these carriers, could offer a dramatic increase in the performance of the system. Even though carrier-phase

observations are a relative timing measure, they are approximately one hundred times more precise than code observations.

In satellite navigation, accuracy depends on several error sources affecting the satellites, the signal propagation and the receiver. Errors in satellite positions or in the synchronization of the clocks on board satellites and at the user end all contribute to position uncertainties. Similarly, signal delays caused by the atmosphere contaminate the measurements made by the receiver and translate into positioning inaccuracies. It was however realized that most error sources have a strong spatial correlation, meaning that a pair of closely-spaced receivers could help to mitigate the errors contaminating the observations. Based on this concept and the use of the precise carrier-phase observations, GPS quickly became a high-accuracy system capable of achieving even millimetre-level accuracies [Remondi, 1984].

Over the past decade or so, a technique referred to as precise point positioning (PPP) gained significant ground [Zumberge et al., 1997; Kouba and Héroux, 2001]. It is capable of providing centimetre-level positioning with a single GPS receiver, through careful modelling of all error sources. Precise satellite positions and satellite clock offsets with respect to the GPS time scale are computed based on a permanent network of ground stations. The propagation delays caused by the ionosphere are practically eliminated by using measurements on two frequencies. The hydrostatic part of the tropospheric delay is, for the most part, removed using global pressure and temperature models [Boehm et al. 2009], while the wet delay is estimated in the PPP filter. Another effect to be considered

is the non-spherical phase response of tracking antennas, which causes their actual electrical phase centre to vary as a function of the elevation angle and azimuth of the received signal. For this purpose, calibration procedures for antenna phase-centre variations were defined [Mader, 1999; Schmitz et al., 2002]. Since GPS signals have a right-hand circular polarization, a rotation of the transmitting or receiving antenna leads to a change in the measured phase that must be accounted for [Wu et al., 1993]. Deformation of the solid earth caused by tidal forces and ocean loading must also be considered [Petit and Luzum, 2010]. Relativistic effects, caused by changes in both the gravitational potential and the satellite velocity, are yet another error source requiring proper modelling [Kouba, 2002; Kouba, 2004].

Even though PPP can satisfy high-accuracy requirements, the application of this technique is still limited due to the rather long convergence periods required to obtain its expected accuracy. Several efforts were mounted to overcome this constraint, which led to the recent possibility of fixing carrier-phase ambiguities to integers in PPP [Laurichesse and Mercier, 2007; Collins, 2008; Ge et al., 2008; Mervart et al., 2008], which is an important aspect to reducing the convergence period. Still, ambiguity resolution in PPP is not a trivial task, and on-the-fly algorithms are not yet applicable to this technique. Convergence of conventional kinematic PPP solutions to centimetre-level accuracies can often require an hour of continuous signal tracking [Gao and Shen, 2001]. In the event of complete signal tracking interruptions, such as when a vehicle travels underneath an overpass, users must again wait for several minutes before re-convergence is attained.

3

Several studies have aimed at identifying factors that could reduce initialization times. It was noted that satellite geometry, user environment and dynamics, observation quality and sampling rate could all affect convergence times to a certain level [Héroux et al., 2004]. Other means of improving convergence of PPP solutions include combining GPS and GLONASS constellations [Rocken et al., 2011], and incorporating external information on the ionosphere [Teunissen et al., 2010] or the troposphere [Jokinen et al., 2013]. This dissertation focuses on three main aspects related to this problem: 1) the correction of cycle slips for reducing re-convergence times; 2) the use of global ionospheric delay corrections in PPP with ambiguity resolution; and 3) undifferenced ambiguity resolution for GPS and GLONASS processing.

1.1.1 Cycle-Slip Correction

In the early stages of operation, while the full constellation of satellites was yet to be in orbit, GPS satellite coverage was a significant aspect for obtaining a geometrically strong solution. This problem was amplified when the receiver lost lock on the carrier, a phenomenon commonly referred to as "cycle slip." GPS receivers can measure very precisely the fractional part of the phase of the carrier received from a satellite and also accumulate the total number of carrier cycles over time. However, for a number of reasons such as obstructions or noise, a receiver can miss counting a certain number of

cycles, leading to discontinuities in the integrated phase (i.e., the carrier-phase measurement). When this situation occurs, a new parameter must be introduced in the navigation filter, directly influencing the precision and accuracy of the estimated position parameters.

To minimize the impacts of signal discontinuities on positioning solutions, cycle-slip correction methods were introduced. Since the receiver can measure the fractional part of the sinusoidal phase signal, the magnitude of the discontinuity will be, by definition, an integer. The methods developed then consisted of fitting low-order polynomials to the arcs preceding and following the discontinuity, estimating the offset between polynomials, and rounding it to the nearest integer value [Beutler et al., 1984]. This approach was well suited for static receivers, since the phase signal typically does not undergo irregular variations.

For kinematic applications, receiver dynamics can introduce unpredictable fluctuations in the carrier-phase observations time series. Low-order polynomials are thus not suitable for such situations. Since geometric effects (satellite and receiver displacements, clock variations, etc.) affect similarly all signal types for a given satellite, it is possible to form linear combinations of measurements that eliminate such effects. Hence, by appropriately combining carrier-phase and code observations on both frequencies transmitted by GPS satellites, the magnitude of cycle slips can be recovered even in kinematic application [Mader, 1986; Blewitt, 1990; Bisnath, 2000]. The use of code measurements to eliminate geometric effects implies that polynomials still be fitted

5

to arcs, as to reduce the noise level of this type of observable. Several alternatives, such as the use of filters or wavelets, were also developed for this purpose [Bastos and Landau, 1988; Collin and Warnant, 1995].

Quality control techniques were also used in real-time applications to detect blunders in the observations, such as phase discontinuities, and adapt the positioning filter accordingly [Teunissen and Salzmann, 1989; Teunissen, 1990]. Powerful algorithms for ambiguity resolution (i.e., the process of estimating the initial integer number of cycles between pairs of satellites and receivers) were then developed, allowing centimetre-level positioning within seconds [Hatch, 1990; Euler and Landau, 1992; Abidin, 1993]. This practice somehow alleviated the need for cycle-slip correction, since new ambiguity parameters could simply be estimated and fixed almost instantaneously. Still, for some applications, cycle-slip correction has proven to be a useful component of quality control. Since polynomial fitting is not suitable for real-time applications, a new approach had to be developed, consisting of explicitly estimating the variation of geometric effects between epochs [Kim and Langley, 2002].

PPP, because of the long convergence times required to reach its expected accuracy, has brought back the topics of ambiguity resolution and cycle-slip correction to the front line. Real-time PPP monitoring of stations located in seismically active regions is now an integral part of tsunami-warning systems [Blewitt et al., 2009; Song et al., 2012; Melgar and Bock, 2013], which reinforces the need for a solution immune to discontinuities. Cycle slips are likely to occur during such events due to rapid accelerations of the

antennas caused by the earthquake. A system capable of bridging such signal discontinuities is a safety measure for preserving the valuable information provided by GNSS seismology and is highly desirable. Similar challenges are associated with navigation in urban canyons since obstructions leading to signal tracking interruptions can significantly degrade positioning accuracies [Takasu and Yasuda, 2008].

An initial investigation on instantaneous cycle-slip correction applied to PPP, presented by Banville and Langley [2009] (and detailed in Chapter 2), spurred follow-up work by several researchers. Geng et al. [2010] improved their re-convergence technique based on the prediction of undifferenced slant ionospheric delays, reducing the convergence time from several seconds to a single epoch in most cases. Collins et al. [2012] later generalized this approach to include the algorithm directly into the PPP navigation filter. Li [2012] further expanded it by modelling the ionosphere as a mathematical function rather than using one ionospheric parameter per satellite. Those methods, based on the processing of undifferenced observations, gained remarkable acceptance in the last years. Still, predicting phase variations due to the ionosphere can be challenging in the presence of ionospheric disturbances and remains an important issue for the reliability of PPP.

1.1.2 Ionospheric Corrections for PPP

Electromagnetic waves transmitted by GNSS satellites must go through the ionized part of the atmosphere, the ionosphere, before reaching ground-based receivers. Free electrons present in this region perturb the propagation of GNSS signals causing a group delay and a phase advance inversely proportional to the square of the frequency of the signal. This characteristic is also used to measure the total electron content (TEC), which is the number of free electrons in a column of one square-meter cross section extending from the receiver to the satellite.

Since dual-frequency receivers are typically used in PPP, dispersive effects such as the first-order ionospheric effects can be eliminated by forming linear combinations of observations on two frequencies. While this approach effectively mitigates the impact of the ionosphere on the position solutions, it also prevents the input of additional information on the state of the ionosphere in the navigation filter. Therefore, the use of uncombined signals can be greatly beneficial to PPP since constraining of slant ionospheric delays using external sources is the key to fast convergence times [Odijk, 2002].

Local or regional augmentation capabilities are the foundation of network RTK, which benefits from the spatial correlation of error sources to accurately model such errors for users located within the network [Wübbena et al., 2001; Fotopoulos and Cannon, 2001;

Landau et al., 2002; Rizos, 2002]. While those corrections were originally provided in observation space, it was found that state-space corrections could significantly reduce bandwidth requirements while providing a more accurate modelling of error sources [Wübbena and Willgalis, 2001]. This new formulation was later termed PPP-RTK since it combined the state-space representation of corrections used in PPP with the local augmentation provided by network RTK [Wübbena et al., 2005]. This scalable approach can then allow PPP to be performed on a global scale, while providing rapid convergence for users located within a local or regional network of stations.

Even though the PPP-RTK concept contained all necessary elements for eliminating the convergence time of PPP, it took several years for the GNSS community to fully embrace it. The lack of a detailed description of the underlying technical algorithms most likely contributed to this delayed acceptance. Ambiguity resolution on undifferenced signals (i.e., for PPP) only gained momentum a few years after the introduction of the PPP-RTK concept. The idea of providing state-space ionospheric corrections for instantaneous PPP ambiguity resolution was then explored further by Teunissen et al. [2010].

To assure the consistency of PPP solutions, ionospheric corrections must be provided with a set of compatible satellite equipment delays. For example, slant ionospheric delay corrections computed by Teunissen et al. [2010] contain differential code biases (DCBs) matching their definition of satellite clock corrections, thereby preserving the integer nature of carrier-phase ambiguities. In Collins et al. [2010], satellite phase clock

9

corrections are biased by integer ambiguities, which involves that ionospheric corrections should not be contaminated by DCBs but rather by matching integer-biased satellite equipment delays. This notion was applied to a peer-to-peer cooperative positioning concept in which PPP users located nearby each other exchange such ionospheric corrections to achieve instantaneous ambiguity resolution [Collins et al., 2012].

Currently, DCBs are provided along with global ionospheric maps (GIMs) generated by the International GNSS Service (IGS) [Hernández-Pajares et al., 2009], which prevent the use of such corrections in the decoupled-clock model of Collins et al. [2010]. Therefore, a procedure for the extraction of the integer-biased satellite equipment delays must be defined to ensure the application of consistent external ionospheric constraints for improved PPP solution convergence.

1.1.3 GLONASS Ambiguity Resolution

Another factor influencing the convergence period of PPP solutions is the enhanced geometry of satellites arising from the combination of multiple satellite systems. Several studies demonstrated that processing of GPS and GLONASS observations can reduce the time required to reach centimetre-level accuracies [Rocken et al., 2011; Dai et al., 2011; Cai and Gao, 2013]. Using partial constellations from the European Galileo system, the Japanese quasi-zenith satellite system (QZSS) and the Chinese Beidou system further

improved this performance [Landau et al., 2013]. Combining several systems has also been associated with faster and more reliable (partial) ambiguity resolution in differential mode [Wang and Feng, 2013].

While those benefits could be translated to PPP solutions as well, undifferenced ambiguity resolution for GLONASS is challenging due to the frequency division multiple access (FDMA) technology currently used by this system. Carrier-phase and code inter-frequency biases propagate into the estimated ambiguity parameters, and are a nuisance to ambiguity validation procedures. As a consequence, only ambiguity resolution for satellites using the code division multiple access (CDMA) technology is possible at this stage in PPP. However, with a constellation of 24 GLONASS satellites, one can easily foresee that ambiguity resolution capabilities for this system could be greatly beneficial in reducing the convergence period of PPP solutions.

1.2 Objectives, Methodology, and Contributions

Based on the information provided in the previous section, it becomes clear that several aspects can be investigated with the aim of mitigating the impact of signal discontinuities on PPP solutions and reducing the time required for the initial convergence of the position solutions. Popular cycle-slip correction methods lack some essential characteristics regarding real-time requirements and rigorous handling of ionospheric effects. For PPP based on the decoupled-clock model, external ionospheric

corrections cannot be directly applied without a proper means of estimating consistent satellite equipment delays. Furthermore, undifferenced ambiguity resolution for GLONASS is still affected by improper modelling of inter-frequency biases.

With the goal of reducing the (re-)convergence period of PPP solutions, the objectives of this research are:

- develop a methodology for instantaneous cycle-slip correction based on a single GNSS receiver, with special considerations for ionospheric disturbances;
- develop a methodology for the application of external ionospheric constraints for PPP solutions based on the decoupled-clock model;
- investigate the feasibility of undifferenced ambiguity resolution for GLONASS.

The following subsections describe the methodology used to realize those objectives and summarize the contributions of this dissertation to those topics.

1.2.1 Cycle-Slip Correction

The methodology presented in this dissertation for the correction of cycle slips is based on the initial work of Kim and Langley [2001]. As opposed to popular cycle-slip correction methods processing data on a satellite-by-satellite basis, their approach incorporated all available (triple-differenced) observations (carrier-phase, code and Doppler measurements) into a least-squares adjustment to estimate the unknown receiver displacement as well as cycle-slip parameters. The integration of all measurements into a

single adjustment process with an appropriate weighting scheme is the optimal way of estimating cycle-slip parameters, and allows for single-epoch (i.e., instantaneous) cycle-slip correction. The work presented herein extends this approach for processing of data from a single GNSS receiver, by estimating a receiver clock offset parameter and ionospheric delay parameters.

This novel cycle-slip detection/correction approach has the following characteristics:

- it processes data from a single GNSS receiver;

- it uses both carrier-phase and code measurements based on a rigorous weighting scheme;

- it explicitly estimates all unknown states (receiver displacement, receiver clock variation, slant ionospheric delay variation and cycle slips) in a least-squares adjustment;

- it benefits from carrier-phase observations not affected by cycle slips to accurately model the geometric states of the filter, which constitutes an improvement over noisy "geometry-free" combinations;

- it exploits the correlation between parameters to rigorously define the integer search space of cycle-slip parameters;

- it is capable of handling ionospheric delay variations of up to several decimetres between epochs;

- it offers a means of validating the selected integer candidates based on the strength of the solution and the distance between the float and integer cycle-slip parameters;

13

- it is applicable in real time, and typically solves for cycle slips within a single epoch;

- it is applicable to any GNSS and has a general form allowing processing of multi-frequency signals.

Incorporating cycle-slip correction into a PPP engine therefore allows precise continuous positioning solutions to be obtained even after complete signal tracking interruptions.

1.2.2 Ionospheric Corrections for PPP

A popular approach for removing the arc-dependency of the geometry-free carrier-phase observations used in ionospheric monitoring consists of fitting precise but ambiguous phase observations to noisy code (pseudorange) observations. This process, often referred to as levelling, can however introduce significant errors due to code multipath and intra-day variations of DCBs. In this dissertation, the arc dependency is removed using integer carrier-phase ambiguities obtained from PPP solutions. This novel approach was termed integer levelling. The main benefits of using integer-levelled observations for ionosphere monitoring are:

- a levelling process relying solely on carrier-phase observations, alleviating any dependency on the datum provided by code observations, which was shown to be impacted by intra-day variations of the DCBs;

- the elimination of levelling errors when carrier-phase ambiguities are fixed to correct integer values;

- an improvement in the consistency of slant TEC values in a network;

- a reduction in the RMS of fit when estimating model coefficients in the generation of TEC maps;

- the presence of satellite biases in the geometry-free observables compatible with the PPP model based on the decoupled-clock model, thereby allowing ionospheric constraints to be applied in PPP with ambiguity resolution.

A direct consequence of ionospheric monitoring based on integer-levelled observations is the possibility of applying external ionospheric constraints in the PPP solution, leading to a significant reduction in convergence times.

1.2.3 GLONASS Ambiguity Resolution

To achieve undifferenced ambiguity resolution for GLONASS, it is imperative to carefully model inter-frequency biases for both carrier-phase and code observations. To improve receiver compatibility in differential mode, calibration of inter-frequency phase

biases was proposed by Wanninger [2012]. In this approach, a receiver-specific correction term needs to be applied to each carrier-phase observation in order to remove the linear dependency of carrier-phase biases with respect to the frequency channel number. The success of this approach depends largely on the quality of the metadata associated with each station since inter-frequency phase biases can be impacted by a change in receiver firmware version. For operators of a global network based on publicly-available data, obtaining valid metadata can certainly become a tedious process.

With the purpose of alleviating the dependency on metadata, a new approach for the estimation of inter-frequency phase biases was developed. This method:

- does not require any external information on inter-frequency phase biases;
- relies only on carrier-phase observations, reducing the impacts of possible misalignments between phase and code observables;
- removes the singularity of the GLONASS least-squares solution by defining a set of appropriate minimum constraints;
- is independent of receiver firmware;
- allows for instantaneous ambiguity resolution for mixed receiver types and is therefore suited for real-time applications.

To achieve undifferenced GLONASS ambiguity resolution, inter-frequency code biases also need to be accounted for since they serve in estimating (or eliminating) ionospheric effects. Similar to carrier phases, inter-frequency code biases typically have a

receiver-specific linear dependency on the frequency channel number. However, several factors can impact those biases, such as receiver firmware version and antenna type, which complicates modelling of such biases. To overcome this obstacle, this dissertation proposes to:

- define clusters of stations with similar equipment to assure the compatibility of inter-frequency code biases;

- explicitly estimate the linear dependency of inter-frequency code biases in a least-squares adjustment;

- absorb any residual effects in the satellite clock (or bias) corrections, such that carrier-phase ambiguities estimated by the user naturally converge to integer values.

Although not explicitly demonstrated in this dissertation, it is expected that the possibility of performing undifferenced ambiguity fixing on both GPS and GLONASS will positively impact the convergence time of PPP solutions.

1.3 Dissertation Outline

This thesis follows a paper-based approach, meaning that each chapter is a published paper. Chapter 2 defines the basis of the cycle-slip correction method described in this dissertation. It revisits the time-differenced geometric approach introduced by Kim and

Langley [2001], and proposes modifications for single-receiver processing. This chapter was published as:

Banville, S., and R. B. Langley (2010). "Instantaneous cycle-slip correction for real-time PPP applications," *NAVIGATION: Journal of The Institute of Navigation*, Vol. 57, No. 4, Winter 2010-2011, pp. 325-334.

Applications of this method illustrate that single-epoch recovery of complete satellite tracking interruptions can be achieved in different applications, such as geodynamics and car navigation. Still, the paper emphasizes that some factors could degrade the performance of this technique, such as high ionospheric activity, which is dealt with in the following chapter.

Chapter 3 provides a rigorous means of detecting cycle slips even in the presence of an active ionosphere, as well as insights for correcting cycle slips in such circumstances. It was published as:

Banville, S., and R. B. Langley (2013). "Mitigating the impact of ionospheric cycle slips in GNSS observations," *Journal of Geodesy*, Vol. 87, No. 2, pp. 179-193. doi: 10.1007/s00190-012-0604-1.

Chapter 4 describes the fundamental principles underlying the integer levelling procedure for improved ionospheric monitoring. It was originally published as:

18

Banville, S., W. Zhang, and R. B. Langley (2013). "Monitoring the ionosphere with integer-levelled GPS measurements," *GPS World*, Vol. 24, No. 3, March 2013, pp. 43-49.

This paper is based on two conference proceedings:

Banville, S., and R. B. Langley (2011). "Defining the basis of an integer-levelling procedure for estimating slant total electron content," *Proceedings of the 24th International Technical Meeting of the Satellite Division of The Institute of Navigation (ION GNSS 2011)*, Portland, Ore., 19-23 September, pp. 2542-2551

and

Banville, S., W. Zhang, R. Ghoddousi-Fard, and R. B. Langley (2012). "Ionospheric monitoring using 'integer-levelled' observations," *Proceedings of the 25th International Technical Meeting of the Satellite Division of The Institute of Navigation (ION GNSS 2012)*, Nashville, Tenn., 17-21 September, pp. 2692-2701.

Chapter 5 illustrates that the satellite biases contained in integer-levelled observations can be transmitted to PPP users to ensure ionospheric corrections are compatible with the PPP model. The results were first published as:

Banville, S., P. Collins, W. Zhang, and R. B. Langley (2013). "Global and Regional Ionospheric Corrections for Faster PPP Convergence," *NAVIGATION: Journal of The Institute of Navigation*, Vol. 61, No. 2, Summer 2014, pp. 115-124.

Chapter 6 contains the theoretical aspects for the estimation of GLONASS inter-frequency carrier-phase biases. Application of those concepts is also shown to allow instantaneous ambiguity resolution for short baselines. This work was published as:

Banville, S., P. Collins, and F. Lahaye (2013). "GLONASS ambiguity resolution of mixed receiver types without external calibration," *GPS Solutions*, Vol. 17, No. 3, pp. 275-282. doi: 10.1007/s10291-013-0319-7.

Chapter 7 extends the principles of the previous chapter to accommodate code inter-frequency biases. It is demonstrated that undifferenced widelane ambiguities can be fixed to integers by estimating sets of receiver-dependent satellite widelane biases. This work originates from:

Banville, S., P. Collins, and F. Lahaye (2013). "Concepts for undifferenced GLONASS ambiguity resolution," *Proceedings of the 26th International Technical Meeting of the Satellite Division of The Institute of Navigation (ION GNSS+ 2013)*, Nashville, Tenn., 16-20 September, pp. 1186-1197.

Chapter 8 summarizes the findings presented in this dissertation and suggests further paths to explore.

Appendix I contains derivations explaining the propagation of datum parameters in the decoupled-clock model.

Note that changes to the notation of each paper were made to assure uniformity within this dissertation.

CHAPTER 2

IMPROVING REAL-TIME KINEMATIC PPP WITH INSTANTANEOUS CYCLE-SLIP CORRECTION

This chapter introduces the concept of cycle-slip correction based on the time-differenced model. Application of this method to PPP allows for GPS users to maintain a continuous navigation solution after a momentary signal tracking interruption. The method developed assumes that the ionosphere can be accurately predicted over the duration of the interruption, but this issue will be analyzed in detail in the next chapter.

The following was originally published as:

Banville, S. and R. B. Langley (2010). "Instantaneous cycle-slip correction for real-time PPP applications," *NAVIGATION: Journal of The Institute of Navigation*, Vol. 57, No. 4, Winter 2010, pp. 325–334.

Modifications to the original manuscript were made only for proper identification of sections, figures and tables, as well as to assure the uniformity of symbol and equation notation throughout this dissertation.

Abstract

Real-time precise point positioning (PPP) is limited to only a few applications using a moving receiver, because the quality of the solution is vulnerable to interruptions in signal tracking. A loss of lock on all GPS signals simultaneously even implies that users may have to wait for several minutes before again obtaining cm-level precision. To avoid such a scenario, this paper proposes a method to instantaneously mitigate the impacts of signal interruptions and the resulting cycle slips. The approach is based on a time-differenced solution that allows for estimating the size of cycle slips in a least-squares adjustment. Once cycle slips are corrected, the PPP filter can be modified accordingly so as to prevent the occurrence of discontinuities in the positioning time series. The usefulness of the approach is demonstrated in selected applications such as geodynamics and car navigation.

2.1 Introduction

Over the past decade, precise point positioning (PPP) has proved to be a powerful processing strategy. Its use has spread significantly into application areas such as hydrography, precision agriculture, atmospheric science, geodynamics, surveying in remote regions, and in processing of data from large networks. On the other hand, the success of this technique in kinematic mode is still muted due to the rather long

convergence periods required to obtain a centimetre-level of precision. Several efforts were mounted to overcome this limitation, which led to the recent possibility of fixing carrier-phase ambiguities to integers in PPP [Laurichesse and Mercier, 2007; Collins, 2008; Ge et al., 2008; Mervart et al., 2008], which is one key to reducing the convergence period.

Ambiguity resolution in PPP is still not a trivial task. Several error sources need to be carefully modelled in order to maintain their influence below an acceptable threshold. Hence, on-the-fly ambiguity resolution is not currently achievable, at least not with a high level of confidence. Furthermore, a moving receiver increases the risks of experiencing losses of lock on satellites. In such instances, a new ambiguity resolution attempt needs to be performed. Since most ambiguity resolution approaches in PPP require averaging of the widelane ambiguities, this process is not achievable instantaneously and can lead to a temporary decrease in the overall performance of the system. A method for reducing this re-initialization period has been proposed based on the prediction of satellite-dependent ionospheric delays [Geng, 2009]. While this technique allows for a significant reduction in the re-convergence time, a mean latency of approximately 25 seconds is still required for re-fixing ambiguities.

Current PPP software implementations typically reset ambiguity parameters when cycle slips are detected. This approach does not exploit the integer nature of cycle slips and can result in a degraded performance of PPP processing. Even cycle slips on a single satellite can weaken the geometry and may lead to non-negligible impacts on the

computed positions. Although several cycle-slip correction methods have been developed over the years, not all of them can be applied to the problem at hand. Polynomial fitting of carrier-phase observations [Beutler et al., 1984] or of linear combinations of observations [Blewitt, 1990; Bisnath, 2000] is certainly a widespread approach, which has, however, limited applications in real-time processing. Another method usually providing satisfactory cycle-slip correction capabilities is the one introduced by Mader [1986]. In this approach, integer cycle-slip candidates on L_1 and L_2 are chosen as to minimize the temporal variation of the geometry-free linear combination of carrier-phase measurements over two consecutive epochs. Still, certain pairings of ambiguities on L_1 and L_2 provide similar values for the geometry-free combination, and discriminating the correct candidates requires prior knowledge of the size of the cycle slips to $\pm$ 3 cycles [Bastos and Landau, 1988]. This condition is not trivial in real time due to noise and multipath-contaminated code observations.

An applicable approach is the one developed by Kim and Langley [2001], which estimates the size of cycle slips using a time-differenced solution. In this paper, we first review the principles underlying this technique, and then propose some modifications to account for the fact that the original method was designed for relative positioning rather than for a single receiver. The usefulness of this new implementation is then demonstrated through different examples covering selected applications. Finally, potential shortcomings of the approach are briefly exposed and discussed.

25

2.2 Time-Differenced Functional Model

Time-differenced positioning utilizes variations in GPS measurements over a certain time interval to estimate the change in receiver position and receiver clock offset during this period [Ulmer et al., 1995; Michaud and Santerre, 2001]. In order to obtain an accurate estimate for those quantities, the variation of additional error sources must also be accounted for, which leads to the following functional model:

$$\delta\Phi_i^j = \delta\rho^j + \left(\delta dT - \delta dt^j\right) + \delta T^j - \mu_i\delta I^j + \lambda_i\delta N_i^j + \varepsilon_{\delta\Phi_i^j} \tag{2.1}$$

$$\delta P_i^j = \delta\rho^j + \left(\delta dT - \delta dt^j\right) + \delta T^j + \mu_i\delta I^j + \varepsilon_{\delta P_i^j} \tag{2.2}$$

where

i	identifies frequency-dependant terms
j	identifies a given satellite
$\delta\Phi$	is the variation in carrier-phase measurement, obtained by differencing successive measurements (m)
δP	is the variation in pseudorange measurement, obtained by differencing successive measurements (m)
$\delta\rho$	is the variation in instantaneous range between the phase center of the satellite and receiver antennas, including variations in earth tides, ocean loading and relativistic effects (m)
δdT	is the variation in the receiver clock offset (m)
δdt	is the variation in the satellite clock offset (m)

δT is the variation in tropospheric delay (m)

μ is a constant = f_i^2 / f_1^2, where f_i is the frequency of the L_i carrier

δI is the variation in ionospheric delay on L_1 (m)

λ is the wavelength of the carrier (m)

δN is the variation of the carrier-phase ambiguity (i.e., the size of the cycle slip) (cycles)

$\varepsilon_{\delta\Phi}, \varepsilon_{\delta P}$ are the measurement noise variations, including multipath (m).

The range variation ($\delta\rho$) contains the receiver displacement ($\delta x_r, \delta y_r, \delta z_r$), which is either estimated in the adjustment process, or fixed to zero if the receiver is known to be static. The receiver clock offset variation is also unknown and must also be included in the time-differenced filter. (More details on this topic are provided in a subsequent section.) The variation in satellite clocks and satellite positions can be computed with data retrieved from a reference network [Bertiger et al., 1997; Weber et al., 2005].

The atmospheric delay variations can be approximated as:

$$\delta T = \delta M_T T_z \qquad\qquad\qquad \delta I^j = \delta M_I I_z^j \qquad\qquad (2.3)$$

where δM_T is the change in the tropospheric delay mapping function between sequential epochs, and T_Z is the tropospheric zenith delay obtained from a model, or from the PPP adjustment. Similarly, δM_I is the change in ionospheric delay mapping function between epochs, and I_z^j is the vertical ionospheric delay obtained from a model (e.g., the predicted Klobuchar-style coefficients [Hugentobler et al., 2001] or global ionospheric maps

27

provided by the Center for Orbit Determination in Europe (CODE) [Schaer, 1999]). Note that if no cycle slips are detected on a satellite, the ionosphere-free combination can be used to eliminate the ionospheric delay variation instead of using a correction from a model. For both the tropospheric and ionospheric delay corrections, it is assumed that the value of the delay at the zenith does not fluctuate significantly between sequential epochs, which is usually a reasonable assumption for short time intervals.

The variation in the ambiguity parameter (δN) is zero for continuous carrier-phase measurements, while it is an integer number when cycle slips occur. When a cycle slip is detected, its size (δN) is estimated in the adjustment process.

2.3 Time-Differenced Adjustment Process

The functional model described previously can be expressed in a linearized form as:

$$\delta \boldsymbol{y} = \boldsymbol{A}_1 \delta \boldsymbol{x}_1 + \boldsymbol{B} \delta \boldsymbol{n} + \delta \boldsymbol{e}, \quad \delta \boldsymbol{x}_1 \in \mathbb{R}^{\{1|4\}}, \delta \boldsymbol{n} \in \mathbb{Z}^m$$

$$\boldsymbol{Q}_{\delta \boldsymbol{y}} = \mathrm{cov}(\delta \boldsymbol{y})$$

(2.4)

where

    $\delta \boldsymbol{y}$ is the vector of differences between the time-differenced observations and their computed (modelled) values

    $\delta \boldsymbol{x}_1$ is the vector of unknown geometric parameters such as receiver position

28

and receiver clock offset variations

$\delta \boldsymbol{n}$ is the m-dimensioned vector of cycle-slip parameters

$\delta \boldsymbol{e}$ is the vector of unmodelled errors associated with each observation

$\boldsymbol{A}_1, \boldsymbol{B}$ are the design matrices associated with the unknown geometric parameters and cycle-slip parameters, respectively

For example, let us suppose that, at a given epoch, cycle slips were detected on 2 satellites (hereby identified with superscripts 1 and 3) out of the n satellites observed. In this case, the previously defined vectors would be:

$$\delta \boldsymbol{y} = \begin{bmatrix} \delta \widetilde{\Phi}_1^1 & \delta \widetilde{\Phi}_2^1 & \delta \widetilde{P}_1^1 & \delta \widetilde{P}_2^1 & \dots & \delta \widetilde{\Phi}_1^n & \delta \widetilde{\Phi}_2^n & \delta \widetilde{P}_1^n & \delta \widetilde{P}_2^n \end{bmatrix}^T \tag{2.5}$$

$$\delta \boldsymbol{x}_1 = \begin{bmatrix} \delta x_r & \delta y_r & \delta z_r & \delta dT \end{bmatrix}^T \text{ (moving receiver)} \tag{2.6a}$$

$$\delta \boldsymbol{x}_1 = \begin{bmatrix} \delta dT \end{bmatrix} \text{ (static receiver)} \tag{2.6b}$$

$$\delta \boldsymbol{n} = \begin{bmatrix} \delta N_1^1 & \delta N_2^1 & \delta N_1^3 & \delta N_2^3 \end{bmatrix}^T \tag{2.7}$$

with

$$\delta \widetilde{\Phi}_i^j = \delta \Phi_i^j - \left[\delta \rho_0^j - \delta dt^j + \delta T^j - \mu_i \delta I_i^j \right] \tag{2.8}$$

$$\delta \widetilde{P}_i^j = \delta P_i^j - \left[\delta \rho_0^j - \delta dt^j + \delta T^j + \mu_i \delta I_i^j \right]. \tag{2.9}$$

In equations 2.8 and 2.9, the initial values for the receiver clock offset and ambiguity variations were chosen equal to zero since they are linear terms. The quantity $\delta \rho_0^j$ can be first computed using a predicted receiver displacement of zero, but iterations could be required due to the non-linearity of the observables in the receiver coordinate parameters.

As a first step, the system can be solved by disregarding the integer constraint on cycle-slip parameters. The float values for the estimated cycle-slip parameters ($\hat{\boldsymbol{n}}$) and their covariance matrix ($\boldsymbol{Q}_{\delta\hat{n}}$) could be obtained directly as:

$$\boldsymbol{Q}_{\delta\hat{n}} = [\boldsymbol{FB}]^{-1} \tag{2.10}$$

$$\delta\hat{\boldsymbol{n}} = \boldsymbol{Q}_{\delta\hat{n}}\boldsymbol{F}\delta\boldsymbol{y} \tag{2.11}$$

where

$$\boldsymbol{F} = \boldsymbol{B}^T\boldsymbol{Q}_{\delta y}^{-1}\left[\boldsymbol{I} - \boldsymbol{A}_1\left(\boldsymbol{A}_1{}^T\boldsymbol{Q}_{\delta y}^{-1}\boldsymbol{A}_1\right)^{-1}\boldsymbol{A}_1{}^T\boldsymbol{Q}_{\delta y}^{-1}\right]. \tag{2.12}$$

It is recommended that a cycle-slip parameter be added for a given carrier-phase measurement solely when a cycle slip has been detected. This has been illustrated in equation 2.7, where cycle-slip parameters were introduced only for the satellites labeled as 1 and 3. Introducing extra cycle-slip parameters reduces the geometric strength of the solution and increases the computational burden. For this purpose, cycle-slip detection methods such as the one described by Blewitt [1990] or Bisnath [2000] can be used prior to computing a time-differenced solution. In the event that no cycle slips are detected, the time-differenced solution does not need to be computed.

2.4 Cycle-Slip Correction Procedure

After cycle slips are detected and real-value estimates of their magnitude are available from the time-differenced adjustment process, the next step consists of determining the most probable integer values associated with those estimates. In theory, fixing the cycle-slip candidates $\delta\hat{\boldsymbol{n}}$ to integers could be performed using any ambiguity resolution method developed for this purpose [Kim and Langley, 2000]. On the other hand, since instantaneous cycle-slip correction is expected, the method chosen must allow quick determination of the correct set of integers.

When carrier-phase measurements on at least 4 satellites are free of cycle slips, fixing cycle-slip parameters to integers is, most of the time, a trivial task. Indeed, the precision of the estimated parameters is often within a fraction of a cycle due to the inherent precision of carrier-phase observations. In this case, the Least-Squares Ambiguity Decorrelation Adjustment (LAMBDA) method [Teunissen, 1994] is a quick and efficient way of solving the integer least-squares problem. A critical scenario happens when cycle slips have been detected on all carrier-phase measurements at a given epoch. The ambiguity search space is then defined by the noisy pseudorange measurements and directly applying the LAMBDA method was found not to provide a satisfactory cycle-slip correction success rate. This result can be explained by the fact that the hyper-ellipsoid defining the ambiguity search space is often not centered near the expected set of integers [Teunissen, 2001].

To overcome this limitation, we adopted a different approach, inspired by the work of Colombo et al. [1999]. First, the widelane (WL) cycle slips are fixed with the aid of the LAMBDA method. Since the wavelength of this linear combination is much larger ($\approx$86 cm compared to $\approx$19 cm for the L_1 carrier), it is less sensitive to a bias in the initial solution. Referring back to the example introduced in the previous section, the input matrices needed for the LAMBDA method would be:

$$\begin{bmatrix} \delta\widehat{N}_{WL}^1 \\ \delta\widehat{N}_{WL}^3 \end{bmatrix} = \begin{bmatrix} 1 & -1 & 0 & 0 \\ 0 & 0 & 1 & -1 \end{bmatrix} \begin{bmatrix} \delta\widehat{N}_1^1 \\ \delta\widehat{N}_2^1 \\ \delta\widehat{N}_1^3 \\ \delta\widehat{N}_2^3 \end{bmatrix} = \boldsymbol{D}\delta\widehat{\boldsymbol{n}}$$

(2.13)

$$\boldsymbol{Q}_{\delta\widehat{n}_{WL}} = \boldsymbol{D}\boldsymbol{Q}_{\delta\widehat{n}}\boldsymbol{D}^T.$$

(2.14)

When the widelane cycle-slip parameters can be fixed to integers, the next step consists of using the time-differenced, geometry-free (GF) ambiguities with the introduction of the previously fixed widelane cycle slips ($\delta\widetilde{N}_{WL}$) to determine the size of the cycle slips on L_1:

$$\delta\widetilde{N}_1^j = \text{round}\left[\frac{\delta\widehat{N}_{GF}^j - \lambda_2\delta\widetilde{N}_{WL}^j}{\lambda_1 - \lambda_2}\right]$$

(2.15)

with

$$\delta\widehat{N}_{GF}^j = \lambda_1\delta\widehat{N}_1^j - \lambda_2\delta\widehat{N}_2^j.$$

(2.16)

The time-differenced, geometry-free combination is affected mainly by the variation in ionospheric delay between the two epochs, but this variation is often reduced to a

negligible quantity if the data gap is short enough or the *a priori* ionospheric model is accurate enough. By first introducing the fixed widelane cycle slips, the resulting L_1 cycle-slip parameters have a wavelength of 5.4 cm. The contribution of unmodelled errors should not exceed one quarter of a wavelength, or approximately 1.4 cm, in order to reliably fix the L_1 cycle slips to integers. As will be shown in Section 2.6, this condition is satisfied in most cases for a short time interval. However, residual ionospheric errors and multipath, especially in low-elevation-angle satellites, can sometimes exceed this tight threshold.

Since the quality of the solution in kinematic positioning depends largely on the relative geometry of the satellites and the receiver, uncorrected cycle slips will inevitably degrade the precision of the estimated parameters. Thus, to obtain the most precise solution, it is possible to perform an extra step when only a subset of cycle slips ($\delta \boldsymbol{n}_a$) has been corrected using equation 2.15. Since estimated cycle-slip parameters are strongly correlated with each other, one could make use of the "bootstrapping" technique [Blewitt, 1989] to increase the precision of the remaining unfixed cycle slips ($\delta \boldsymbol{n}_b$):

$$\delta \hat{\boldsymbol{n}}_b' = \delta \hat{\boldsymbol{n}}_b - \boldsymbol{Q}_{\delta \hat{n}_b \delta \hat{n}_a} \boldsymbol{Q}_{\delta \hat{n}_a}^{-1} (\delta \hat{\boldsymbol{n}}_a - \delta \check{\boldsymbol{n}}_a) \tag{2.17}$$

$$\boldsymbol{Q}_{\delta \hat{n}_b'} = \boldsymbol{Q}_{\delta \hat{n}_b} - \boldsymbol{Q}_{\delta \hat{n}_b \delta \hat{n}_a} \boldsymbol{Q}_{\delta \hat{n}_a}^{-1} \boldsymbol{Q}_{\delta \hat{n}_a \delta \hat{n}_b} \tag{2.18}$$

where the sub-matrices are derived from:

$$\boldsymbol{Q}_{\delta \hat{n}} = \begin{bmatrix} \boldsymbol{Q}_{\delta \hat{n}_a} & \boldsymbol{Q}_{\delta \hat{n}_a \delta \hat{n}_b} \\ \boldsymbol{Q}_{\delta \hat{n}_b \delta \hat{n}_a} & \boldsymbol{Q}_{\delta \hat{n}_b} \end{bmatrix} \qquad \delta \hat{\boldsymbol{n}} = \begin{bmatrix} \delta \hat{\boldsymbol{n}}_a \\ \delta \hat{\boldsymbol{n}}_b \end{bmatrix}. \tag{2.19}$$

Another attempt at fixing the components of $\delta\widehat{\boldsymbol{n}}_b'$ to integers can then be performed. The whole process is summarized in Figure 2.1 and the corresponding equations are given between brackets.
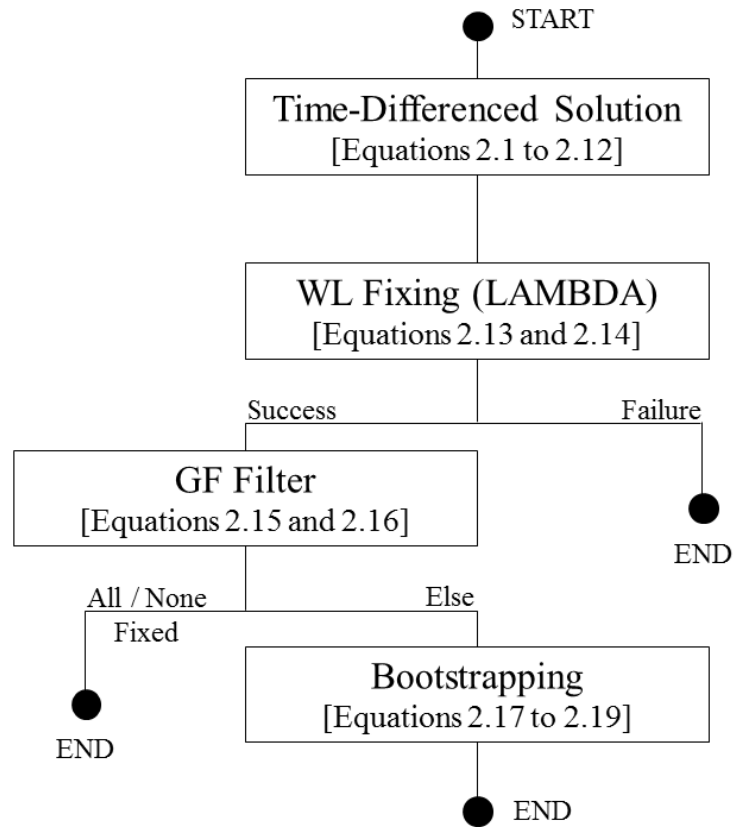
Figure 2.1: Summary of the cycle-slip correction process.

2.5 PPP Solution Update

The size of the cycle slips on both L_1 and L_2 having been determined, the effect of the phase discontinuities in the positioning domain can be eliminated by modifying the predicted values (p) of the ionosphere-free (IF) ambiguity parameters in the PPP filter at the current epoch (t):

$$\lambda_{IF}\left(N_{IF}^j\right)_t^p = \lambda_{IF}\left(\widehat{N}_{IF}^j\right)_{t-1} + \left[(f_1)^2\lambda_1\delta\widetilde{N}_1^j - (f_2)^2\lambda_2\delta\widetilde{N}_2^j\right]/[(f_1)^2 - (f_2)^2] \qquad (2.20)$$

where f_i is the frequency of the carrier. By doing so, the covariance matrix of the predicted ambiguities remains unchanged, which provides continuous coordinate time series. Validation of the chosen integer cycle-slip candidates can be done in the PPP filter by performing a data snooping test [Baarda, 1968]. In the event where the cycle-slip correction procedure is unsuccessful, the ambiguity states are reset in the filter. In this case, cycle-slip correction could be attempted again at subsequent epochs, and the time-differenced observations introduced in equations 2.1 and 2.2 would become:

$$\delta\Phi_i^j = \left(\Phi_i^j\right)_{t_0+k} - \left(\Phi_i^j\right)_{t_0} \qquad (2.21)$$

$$\delta P_i^j = \left(P_i^j\right)_{t_0+k} - \left(P_i^j\right)_{t_0} \qquad (2.22)$$

where t_0 refers to the epoch prior to the cycle slip, and k is the number of epochs since t_0. The update of the PPP filter when cycle-slip correction is delayed becomes more complex and we have not yet implemented this procedure.

2.6 Processing Results

In order to demonstrate the application of our approach, this section presents results obtained in three different contexts: a non-moving receiver, a receiver subject to an earthquake, and a car-mounted receiver. In each example, a kinematic PPP solution was computed in which the coordinates were considered to have a stochastic component that is modelled as white noise. When discontinuities were detected in carrier-phase measurements, the algorithm described in this paper was used to correct cycle slips. In an attempt at simulating real-time performance, the real-time satellite clock corrections estimated by the German Space Operations Center of the German Aerospace Center (DLR), based on the predicted ultra-rapid orbit products provided by the International GNSS Service (IGS), were used in the first and second tests [Hauschild and Montenbruck, 2008]. Since DLR was not yet providing precise real-time clocks at the time of the third test, the final IGS products were used. The tropospheric delay was obtained using pressure values and mapping function coefficients from the forecast Vienna Mapping Function 1 [Boehm et al., 2009], computed following Kouba [2008], and a residual tropospheric zenith delay was estimated. The vertical TEC values for the time-differenced solution were computed using the Klobuchar-style coefficients provided by CODE. All other error sources that must be considered for high-accuracy PPP (earth tides, ocean loading, etc.) were also accounted for. The PPP engine, developed by the first author, uses a conventional Kalman filter estimation procedure. Although the implementation of the software was not designed to be computationally optimal, processing of the PPP solution combined with the whole cycle-slip correction procedure

(i.e., computation of the time-differenced solution and fixing cycle-slip parameters to integers) can usually be achieved in less than 0.2 seconds per epoch on a laptop PC (with a 1.73 GHz processor and 2 GB of RAM) when cycle slips are present on all carrier-phase measurements (worst-case scenario). We then believe that it is a reasonable expectation that the whole process could actually be carried out in real time.

2.6.1 Test #1: Non-moving Receiver

The purpose of the first test is to demonstrate the benefits of using a geometric approach for correcting multiple consecutive cycle slips on a given satellite. Data from 13 March 2010 collected at station UNB3 (located in Fredericton, New Brunswick, Canada) at a 30-second sampling interval was used. The receiver is a Trimble NetR5. This data was selected because cycle slips repeatedly occurred on PRN 21 over a period of approximately 40 minutes, as shown on the top panel of Figure 2.2. This satellite was observed at a low elevation angle (decreasing from 16˚ to 7.5˚) and its signal was affected by noise and multipath. The numerous discontinuities observed in the carrier-phase measurements do not allow this satellite to fully contribute to the positioning solution, unless cycle slips are corrected.
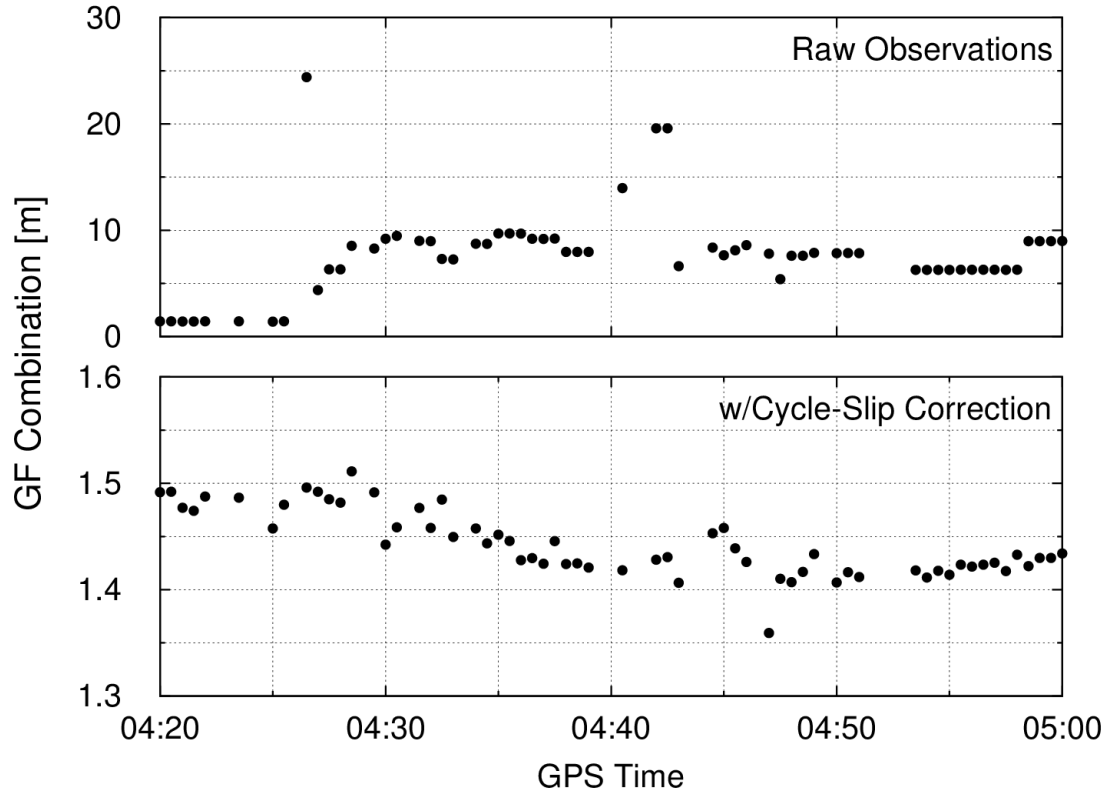
Figure 2.2: Variation of the geometry-free carrier-phase combination of satellite PRN 21, with and without cycle-slip correction, for station UNB3 on 13 March 2010.

The cycle-slip correction procedure introduced in this paper was applied to remove the discontinuities in the measurements, and the reconstructed geometry-free signal has been included in the bottom panel of Figure 2.2. Additionally, Table 2.1 shows the RMS error in the latitude, longitude, and height components with respect to the estimated coordinates obtained from a daily PPP solution in static mode. The RMS errors are based on solely 40 minutes of data, from 04:20 to 05:00 GPST, and exclude the convergence period (from 00:00 to 04:20 GPST). Apparent from the results, the solution is slightly improved when the cycle slips on PRN 21 are fixed to integers as opposed to resetting the

38

ambiguity states in the filter, due to the increased geometric strength of the solution. The benefits of the approach would obviously become more palpable when a larger number of satellites are concurrently affected by cycle slips, as the next examples will demonstrate.

Table 2.1: RMS errors for PPP solutions with and without cycle-slip correction for

PRN 21.

Solution	Latitude (m)	Longitude (m)	Height (m)	3D (m)
No correction	0.053	0.014	0.018	0.057
Cycle slips corrected	0.051	0.011	0.016	0.055

2.6.2 Test #2: Chile Earthquake

On 27 February 2010 at 06:34:29 GPST, a magnitude 8.8 earthquake occurred approximately 100 km northeast of Concepción, Chile. IGS station CONZ, located in the aforementioned city, was able to record GPS observations using a Leica GRX1200 GG Pro receiver throughout the event, providing valuable information on the seismic displacements including the response to surface waves. Even though the real-time Internet data stream was interrupted, the observations were stored in the receiver's internal memory and could be retrieved a few days after the event. Two discontinuities were detected in the GPS data time series: the receiver failed to maintain phase lock on 5

satellites between 06:34:50 and 06:34:54 GPST, dropping the number of continuously tracked GPS satellites in this interval below four, and subsequently it lost lock on all GPS satellites between 06:35:39 and 06:35:42 GPST.

Those GPS signal interruptions would normally lead to a re-initialization period for the PPP solution, which would prevent scientists from exploiting the full potential of GPS observations. While after-the-fact smoothing can help in mitigating this effect, instantaneous cycle-slip correction is an appealing alternative that could potentially be applied in real time. This scenario was simulated here by computing a forward-only solution (no smoothing), using the orbit and clock products available in real time, as mentioned previously. Figure 2.3 shows the estimated displacements, as determined using 1 Hz data, with respect to its IGS reference position. Processing started with data from 05:00 GPST, but the usual PPP convergence is not shown here. Full cycle-slip correction has been achieved for all discontinuities stated previously, which allowed continuous monitoring of the event. The estimated magnitude of the co-seismic displacement, on the order of 3 metres, is in agreement with other preliminary studies [Kouba, 2010; Brooks and Holland, 2010].
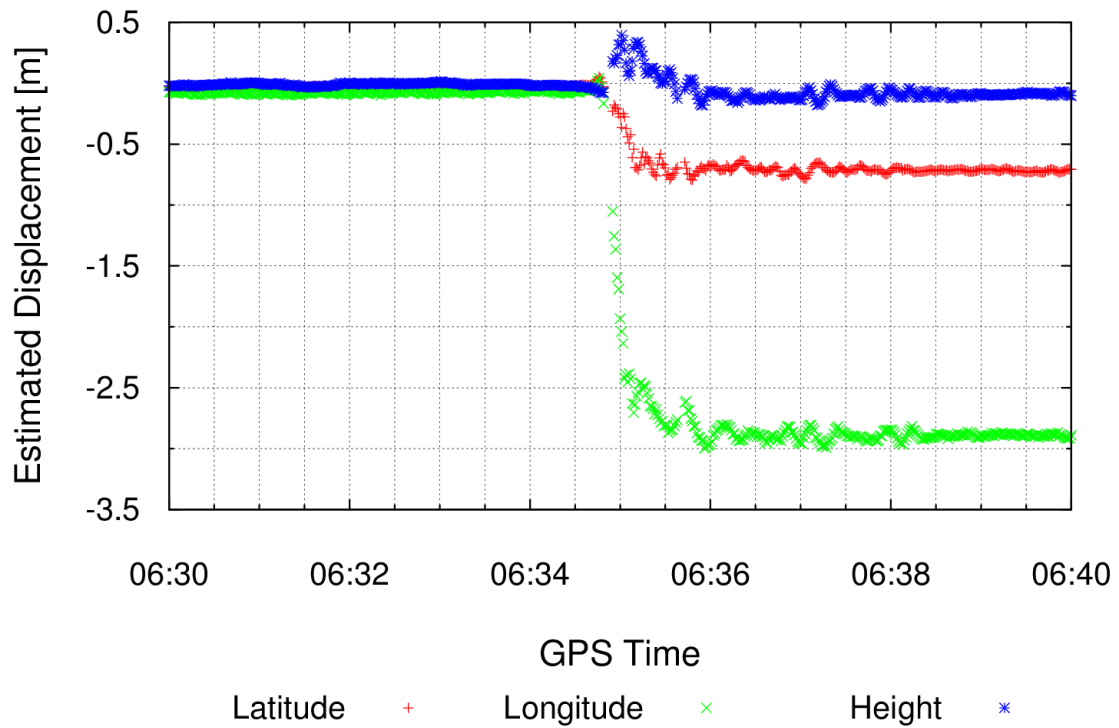
Figure 2.3: Co-seismic displacements at IGS station CONZ on 27 February 2010.

As another means of validation, cycle-slip correction was performed using polynomial fitting with all the data available before the first gap (i.e., prior to 06:34:50 GPST) and after the second gap (i.e., following 06:35:42 GPST). The observations between those two gaps were not used since the time interval is not long enough to reliably fit polynomials. Table 2.2 shows that the sum of the cycle slips corrected after each discontinuity using the method introduced in this paper agrees with the outcome of the polynomial-fitting correction for the total time interval.

Table 2.2: Comparison of the cycle-slip correction outcome (in cycles) for the instantaneous time-differenced approach and polynomial fitting.

| PRN | Instantaneous Time-Differenced Approach | | | | Polynomial Fitting | |
| | 6:34:50 - 6:34:54 GPST | | 6:35:39 - 6:35:42 GPST | | 6:34:50 - 6:35:42 GPST | |
	δN_1	δN_2	δN_1	δN_2	δN_1	δN_2
4	-10	-8	1	-3	-9	-11
11	-	-	-23	-39	-23	-39
13	-	-	-38	-56	-38	-56
17	-	-	-12	1	-12	-1
20	-82	-82	-1	-2	-83	-84
23	-60	-69	-1	-2	-61	-71
31	-22	-30	1	-1	-21	-31
32	-117	-159	-2	-2	-119	-161

2.6.3 Test #3: Car Navigation

The last data set examined in this paper is an excerpt from a car trajectory test that occurred on 10 April 2008. GPS data were collected using a NovAtel OEMV-3 receiver on the streets of Fredericton, New Brunswick, Canada. The section of interest is displayed in Figure 2.4. It was selected since the vehicle traveled beneath two overpasses, which temporarily blocked GPS signals, leading to cycle slips on all carrier-phase

measurements. Some epochs were also discarded after the signal outages because the total number of GPS satellites tracked was below five, while an additional epoch was missing from the RINEX observation file about halfway between the two overpasses. The total duration of the car trajectory is around 30 minutes, which was not sufficient for a complete convergence of the PPP solution. Our focus will then be on the relative displacements between epochs.

Figure 2.4: Car trajectory in Fredericton, New Brunswick, Canada. The receiver lost lock twice on all satellites due to overpasses. (Imagery courtesy of Google.)

In such a scenario, it is quite a complex task to come up with a reference trajectory with at least decimetre-level precision to validate the PPP solution. Processing the data using commercial RTK software with data from a nearby reference station (UNB3) located approximately a kilometre away could not provide reliable ambiguity-fixed solutions for the 17 seconds of data between the two overpasses. For this reason, we only present the estimated height profile obtained from PPP solutions with and without cycle-slip correction (see Figure 2.5). Note that the two time series do not agree perfectly even prior to the gaps since their convergence is still affected by previous cycle slips. Since the road on which the vehicle was travelling is known to be relatively flat, we should not be expecting any sudden jumps in the ellipsoidal height time series. Examining both solutions then lets us suppose that cycle-slip correction indeed improved the estimated trajectory.

2.7 Further Discussions

It should be obvious from the previous examples that instantaneous cycle-slip correction has potential benefits in several applications. Nonetheless, some factors are known to significantly reduce the performance of the proposed approach, namely receiver antenna phase wind-up and strong ionospheric activity.
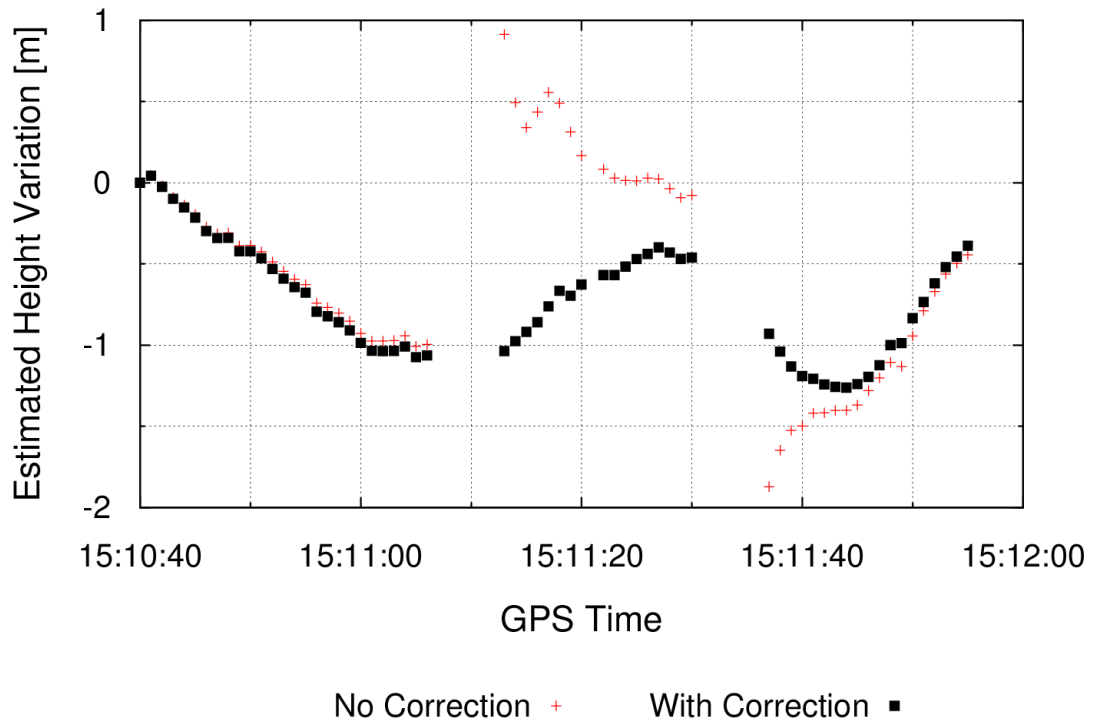
Figure 2.5: Ellipsoidal height variation of the car estimated from PPP solutions with and without cycle-slip correction. The vehicle was known to travel on a relatively flat road.

Since GPS signals have a right-hand circular polarization, a rotation of the transmitting or receiving antenna leads to a change in the measured phase called the wind-up effect [Wu et al., 1993]. Modelling of the satellite component of the wind-up effect is a well-known procedure that should be accounted for in the PPP functional model [Kouba and Héroux, 2001], but the user component of this effect is often ignored due to the absence of information on the orientation of the antenna. Generally, this effect has little impact on the position estimates since it is mainly absorbed by the receiver clock parameter in the PPP filter [Banville and Tang, 2010]. However, when all carrier-

phase measurements are contaminated by cycle slips in the time-differenced solution, the receiver clock variation is solely determined by code measurements (which are not affected by the wind-up effect), and cycle-slip parameters absorb the wind-up effect. Depending on the degree of rotation between epochs, this unmodelled error can compromise considerably the cycle-slip correction success rate [Banville and Langley, 2009]. One means of reducing this effect would be to compute between-satellite cycle-slip differences, which would cancel most of the error. However, we found that using this approach leads to a reduced overall performance of the cycle-slip correction procedure when the antenna is not rotating, due to the increase in noise and the combination of other error sources. Using external information from inertial sensors or a digital magnetic compass would be a viable approach.

The second important limiting factor is ionospheric activity. Using a predictive model to remove the ionospheric delay variation between epochs is certainly a very coarse approximation during ionospheric storms. An in-depth study of this problematic phenomenon, along with an attempt at developing an ionosphere-free cycle-slip correction method, is presented by Banville et al. [2010].

2.8 Summary, Conclusions, and Future Work

Since it is currently a complex task to fix carrier-phase ambiguities on the fly in PPP, a means of effectively accounting for cycle slips is crucial. Failure to do so may seriously degrade the quality of the solution when cycle slips contaminate several carrier-phase measurements simultaneously. In this paper, we presented a method for correcting cycle slips instantaneously: i.e., within a single epoch. It is based on the concept of a time-differenced solution in which the size of cycle slips is estimated as a part of a least-squares adjustment. Cycle slips, being integers by definition, means the next step consists of finding the most-probable set of integers corresponding to the real-valued estimates obtained in the adjustment. This task is achieved by forming linear combinations of the estimated quantities to reduce the impact of geometric errors and improve the performance of the cycle-slip correction process.

The benefits of the method and its potential applicability in real time were demonstrated with three examples. It was shown that instantaneous cycle-slip correction can improve the stability and continuity of the position time series. On the other hand, there are always some risks associated with automated cycle-slip correction in kinematic mode, regardless of the approach used. The main limiting factors are receiver antenna phase wind-up and ionospheric effects. While the wind-up effect could easily be modelled using external information, steep electron density gradients within the ionosphere are currently a serious limitation. Still, the instantaneous cycle-slip correction

47

procedure introduced in this paper could prove useful in several situations and is surely an interesting tool for improving the quality of PPP solutions.

Acknowledgements

References

Baarda, W. (1968). "A testing procedure for use in geodetic networks." Publications on Geodesy, New Series, Vol. 2, No. 5, Netherlands Geodetic Commission, Delft, The Netherlands.

Banville, S., and H. Tang (2010). "Antenna rotation and its effects on kinematic precise point positioning." *Proceedings of the 23rd International Technical Meeting of the Satellite Division of The Institute of Navigation (ION GNSS 2010)*, Portland, Ore., 21-24 September, pp. pp. 2545-2552.

Banville, S., and R. B. Langley (2009). "Improving real-time kinematic PPP with instantaneous cycle-slip correction." *Proceedings of the 22nd International Technical Meeting of the Satellite Division of The Institute of Navigation (ION GNSS 2009)*, Savannah, Ga., 22-25 September, pp. 2470-2478.

Banville, S., R. B. Langley, S. Saito, and T. Yoshihara (2010). "Handling cycle slips in GPS data during ionospheric plasma bubble events." *Radio Science*, Vol. 45, RS6007. doi: doi:10.1029/2010RS004415.

Bastos, L., and H. Landau (1988). "Fixing cycle slips in dual-frequency kinematic GPS-applications using Kalman filtering." *Manuscripta Geodaetica*, Vol. 13, No. 4, pp. 249-256.

Bertiger, W. I., Y. E. Bar-Sever, B. J. Haines, B. A. Iijima, S. M. Lichten, U. J. Lindqwister, A. J. Mannucci, R. J. Muellerschoen, T. N. Munson, A. W. Moore, L. J. Romans, B. D. Wilson, S. C. Wu, T. P. Yunck, G. Piesinger, and M. L. Whitehead (1997). "A real-time wide area differential GPS system." *NAVIGATION: Journal of The Institute of Navigation*, Vol. 44, No. 4, Winter, pp. 433-447.

Beutler, G., D. A. Davidson, R. B. Langley, R. Santerre, P. Vanicek, and D. E. Wells (1984). "Some theoretical and practical aspects of geodetic positioning using carrier phase difference observations of GPS satellites." Department of Geodesy and Geomatics Engineering Technical Report No. 109, University of New Brunswick, Fredericton, N.B., Canada.

Bisnath, S. B. (2000). "Efficient automated cycle-slip correction of dual-frequency kinematic GPS data." *Proceedings of the 13th International Technical Meeting of the Satellite Division of The Institute of Navigation (ION GPS 2000)*, Salt Lake City, Utah, 19-22 September, pp. 145-154.

Blewitt, G. (1989). "Carrier-phase ambiguity resolution for the global positioning system applied to geodetic baselines up to 2000 km." *Journal of Geophysical Research*, Vol. 94, No. B8, pp. 10187-10203. doi:10.1029/JB094iB08p10187.

Blewitt, G. (1990). "An automatic editing algorithm for GPS data." *Geophysical Research Letters,* Vol. 17, No. 3, pp. 199-202. doi:10.1029/GL017i003p00199.

Boehm, J., J. Kouba, and H. Schuh (2009). "Forecast Vienna mapping functions 1 for real-time analysis of space geodetic observations." *Journal of Geodesy*, Vol. 83, No. 5, pp. 397-401. doi:10.1007/s00190-008-0216-y.

Brooks, B., and E. Holland (2010). "Researchers show how far South American cities moved in quake." The Ohio State University Research News. [On-line] 8 March, 2010. http://researchnews.osu.edu/archive/chilemoves.htm.

Collins, P. (2008). "Isolating and estimating undifferenced GPS integer ambiguities." *Proceedings of the 2008 National Technical Meeting of The Institute of Navigation*, San Diego, Calif., 28-30 January, pp. 720-732.

Colombo, O. L., M. Hernández-Pajares, J. M. Juan, J. Sanz, and J. Talaya (1999). "Resolving carrier-phase ambiguities on the fly, at more than 100 km from nearest reference site, with the help of ionospheric tomography," *Proceedings of the 12th International Technical Meeting of the Satellite Division of The Institute of Navigation (ION GPS 1999)*, 14-17 September, Nashville, Tenn., pp. 1635-1642.

Ge, M., G. Gendt, M. Rothacher, M. C. Shi, and J. Liu (2008) "Resolution of GPS carrier-phase ambiguities in precise point positioning (PPP) with daily observations." *Journal of Geodesy*, Vol. 82, No. 7, pp. 389-399. doi:10.1007/s00190-007-0187-4.

Geng, J. (2009). "Rapid re-convergence in real-time precise point positioning with ambiguity resolution." *Proceedings of the 22nd International Technical Meeting of the Satellite Division of The Institute of Navigation (ION GNSS 2009)*, Savannah, Ga., 22-25 September, pp. 2437-2448.

Hauschild, A., and O. Montenbruck (2008). "Real-time clock estimation for precise orbit determination of LEO-satellites." *Proceedings of the 21st International Technical Meeting of the Satellite Division of The Institute of Navigation (ION GNSS 2008)*, Savannah, Ga., 16-19 September, pp. 581-589.

Hugentobler, U., S. Schaer, T. Springer, G. Beutler, H. Bock, R. Dach, D. Ineichen, L. Mervart, M. Rothacher, U. Wild, A. Wiget, E. Brockmann, G. Weber, H. Habrich, and C. Boucher (2001). "CODE IGS analysis center technical report 2000." IGS Central Bureau (Eds.), IGS - 2000 Technical Reports, Jet Propulsion Laboratory Publications 02-012, California Institute of Technology, Pasadena, Calif., November.

Kim, D., and R. B. Langley (2000). "GPS ambiguity resolution and validation: methodologies, trends and issues." *Proceedings of the 7th GNSS Workshop – International Symposium on GPS/GNSS*, Seoul, Korea, 30 November – 2 December, pp. 213–221.

Kim, D., and R. B. Langley (2001). "Instantaneous real-time cycle-slip correction of dual-frequency GPS data." *Proceedings of the International Symposium on Kinematic Systems in Geodesy, Geomatics and Navigation*, Banff, Alta., Canada, 5-8 June, pp. 255-264.

Kouba, J. (2008). "Implementation and testing of the gridded Vienna mapping function 1 (VMF1)." *Journal of Geodesy*, Vol. 82, No. 4-5, pp. 193-205. doi:10.1007/s00190-007-0170-0.

Kouba, J. (2010). "IGS observations during the February 27, 2010 M 8.8 Chilean earthquake." [On-line] 8 March 2010. http://www.igs.org/overview/pubs/2010-8.8-Chilean-Earthquake/.

Kouba, J., and P. Héroux (2001). "Precise point positioning using IGS orbit and clock products." *GPS Solutions*, Vol. 5, No. 2, pp. 12-28. doi:10.1007/PL00012883.

Laurichesse, D., and F. Mercier (2007). "Integer ambiguity resolution on undifferenced GPS phase measurements and its application to PPP." *Proceedings of the 20th International Technical Meeting of the Satellite Division of The Institute of Navigation (ION GNSS 2007)*, Fort Worth, Texas, 25-28 September, pp. 839-848.

Mader, G. (1986). "Dynamic positioning using GPS carrier phase measurements." *Manuscripta Geodaetica*, Vol. 11, No. 4, pp. 272-277.

Mervart, L., Z. Lukes, C. Rocken, and T. Iwabuchi (2008). "Precise point positioning with ambiguity resolution in real-time." *Proceedings of the 21st International Technical Meeting of the Satellite Division of The Institute of Navigation (ION GNSS 2008)*, Savannah, Ga., 16-19 September, pp. 397-405.

Michaud, S., and R. Santerre (2001). "Time-relative positioning with a single civil GPS receiver." *GPS Solutions*, Vol. 5, No. 2, pp. 71-77. doi:10.1007/PL00012888.

Schaer, S. (1999). *Mapping and predicting the Earth's ionosphere using the global positioning system.* Ph.D. dissertation, Astronomical Institute, University of Berne, Switzerland, 205 pp.

Teunissen, P. J. G. (1994). "A new method for fast carrier phase ambiguity estimation." *Proceedings of the IEEE Position, Location and Navigation Symposium (PLANS '94)*, Las Vegas, Nev., 11-15 April, pp. 562-573.

Teunissen, P. J. G. (2001). "Integer estimation in the presence of biases." *Journal of Geodesy*, Vol. 75, No. 7-8, pp. 399-407. doi:10.1007/s001900100191.

Ulmer, K., P. Hwang, B. Disselkoen, and M. Wagner (1995). "Accurate azimuth from a single PLGR+GLS DoD GPS receiver using time relative positioning." *Proceedings of the 8th International Technical Meeting of the Satellite Division of The Institute of Navigation (ION GPS 1995)*, Palm Springs, Calif., 12-15 September, pp. 1733-1741.

Weber, G., D. Dettmering, and H. Gebhard (2005). "Networked transport of RTCM via Internet protocol (NTRIP)." In: *Sanso F. (Ed.): A Window on the Future, Proceedings of the IAG General Assembly*, Sapporo, Japan, 2003, Springer Verlag, Symposia Series, Vol. 128, 2005, pp. 60-64, doi:10.1007/3-540-27432-4_11.

Wu, J., S. Wu, G. Hajj, W. Bertiger, and S. Lichten (1993). "Effects of antenna orientation on GPS carrier phase." *Manuscripta Geodaetica*, Vol. 18, No. 2, pp. 91–98.

CHAPTER 3

MITIGATING THE IMPACTS OF IONOSPHERIC CYCLE SLIPS ON GNSS OBSERVATIONS

Chapter 2 demonstrated the benefits of using a geometric approach to cycle-slip correction and identified the ionosphere as an error source requiring further investigation for improving the reliability of the approach. The purpose of this chapter is thus to provide a rigorous methodology for detecting and correcting cycle slips in the presence of strong ionospheric delay fluctuations.

The following was originally published as:

Modifications to the original manuscript were made only for proper identification of sections, figures and tables, as well as to assure the uniformity of symbol and equation notation throughout this dissertation.

Abstract

Processing of data from global navigation satellite systems (GNSS), such as GPS, GLONASS and Galileo, can be considerably impeded by disturbances in the ionosphere. Cycle-slip detection and correction thus becomes a crucial component of robust software. Still, dealing with ionospheric cycle slips is not trivial due to scintillation effects in both the phase and amplitude of the signals. In this contribution, a geometry-based approach with rigorous handling of the ionosphere is presented. A detailed analysis of the cycle-slip correction process is also tackled by examining its dependence on phase and code noise, non-dispersive effects and, of course, the ionosphere. The importance of stochastic modelling in validating the integer cycle-slip candidates is emphasized and illustrated through simulations. By examining the relationship between ionospheric bias and ionospheric constraint, it is shown that there is a limit in the magnitude of ionospheric delay variation that can be handled by the cycle-slip correction process. Those concepts are applied to GNSS data collected by stations in northern Canada, and show that enhanced cycle-slip detection can lead to decimetre-level improvements in the accuracy of kinematic PPP solutions with a 30-second sampling interval. Cycle-slip correction associated with ionospheric delay variations exceeding 50 cm is also demonstrated, although there are risks with such a procedure and these are pointed out.

54

3.1 Introduction

Global navigation satellite systems (GNSS) signal tracking can be substantially affected by irregularities in the ionosphere. Varying electron densities along the path from a satellite to a receiver can cause GNSS signals to undergo rapid phase and amplitude fluctuations, possibly leading to a loss of lock on those signals and a delay before the signals are reacquired. This event causes the receiver to lose count of the carrier-phase measurement, a condition known as cycle slipping. This situation can significantly affect the performance of GNSS-based applications such as navigation and ionosphere monitoring. For instance, strong ionospheric activity could considerably reduce the availability of ionospheric corrections for satellite-based augmentation systems (SBAS) [Skone and Knudsen, 2000; Komjathy et al., 2003], a crucial component for secure air navigation. With the upcoming next solar cycle maximum expected for 2013 [Jensen and Mitchell, 2011], the time has come to take a critical look at cycle-slip detection/correction methods and to determine how they cope with high ionospheric activity.

A common characteristic of existing cycle-slip detection/correction methods is the assumption that the ionospheric delay varies smoothly over time. When the ionosphere is quiet, the change in ionospheric delay between a satellite and a receiver is mainly a function of the varying elevation angle of that satellite and thus fluctuates slowly indeed. Based on this knowledge, several techniques were developed to detect (and/or repair) carrier-phase discontinuities such as polynomial fitting [Beutler et al., 1984], high-order

differences of phase observations [Hofmann-Wellenhof et al., 1997], or linear combinations of observations [Mader, 1986; Blewitt, 1990; Gao and Li, 1999; Bisnath, 2000; Dai et al., 2009; de Lacy et al., 2012]. When the ionosphere is moderately active, a popular practice consists of tracking the rate of change of the geometry-free linear combination of carrier-phase observations. Several variations of this process were proposed using Kalman filtering [Bastos and Landau, 1988; Kee et al., 1997], wavelets [Collin and Warnant, 1995], polynomial regression [de Lacy et al., 2008], linear functions [Geng et al., 2010; Liu, 2011; Zhang and Li, 2012] or quadratic functions [Cai et al., 2013]. Still, rapid ionospheric fluctuations could impinge on the reliability of those techniques since none of them were conceived with the idea of coping with ionosphere scintillations. For example, Figure 3.1 shows the ionospheric delay variation for each satellite tracked by Natural Resources Canada (NRCan) station IQAL at Iqaluit in northern Canada, on 4 April 2011. Such irregular variations are not uncommon at low and high latitudes, and predicting the ionospheric delay variation will without a doubt impact the performance of cycle-slip detection/correction methods that do not rigorously model this error source.

It is well known that first-order ionospheric effects can be eliminated by forming ionosphere-free combinations of observations. On the other hand, those combinations usually involve noisy code (pseudorange) observations. While it is possible to fit polynomials to long time series of ionosphere-free code-based combinations to estimate the size of carrier-phase discontinuities, this approach suffers from two main drawbacks. First, the occurrence of cycle slips is usually more frequent during ionospheric storms

[Skone et al., 2001], which can significantly reduce the lengths of the arcs used to average code noise. Second, the signal-to-noise ratio often decreases substantially due to amplitude scintillation, leading to noisier code measurements.
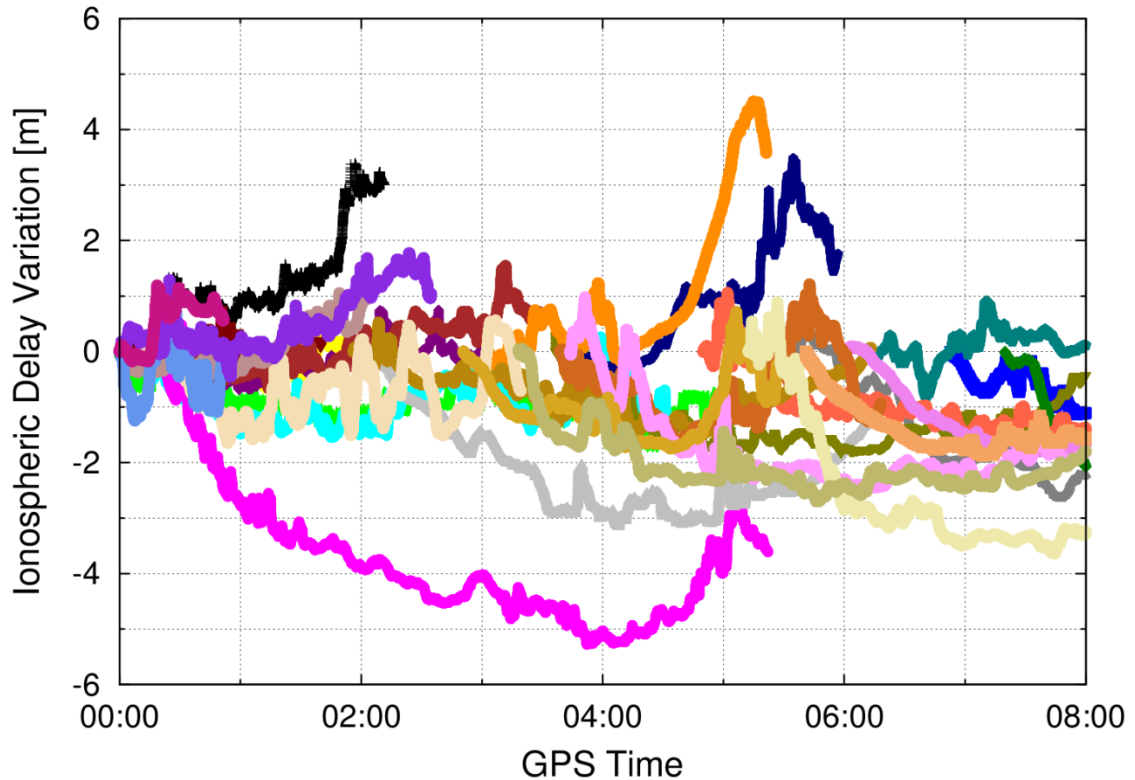
Figure 3.1: Ionospheric delay variation computed using the geometry-free combination of carrier-phase observations on 4 April 2011 at station IQAL. Each color represents a different satellite.

Cycle-slip detection could also be performed using quality control theory, in which residuals from a least-squares (or Kalman filter) adjustment are tested for outliers [Teunissen, 1990]. Since processing all observations in an integrated adjustment offers a

57

mathematically stronger solution than satellite-by-satellite testing [Teunissen, 1999a] improved detection capabilities are expected using this approach [Teunissen, 1991]. Accounting for the ionosphere in the underlying functional model also allows rigorous handling of this quantity in the detection process [de Jong and Teunissen, 2000]. On the other hand, it was shown that the data snooping test [Baarda, 1968] used to detect outliers in the residuals is only rigourous for a single outlier [Baselga, 2011]. A common practice is thus to detect outliers iteratively, removing one measurement at a time from the adjustment [Odijk and Verhagen, 2007]. This process could however be quite tedious if cycle slips contaminate several carrier-phase observations simultaneously. Some studies attempted detecting several simultaneous outliers, but it was found that the measures of internal and external reliability performed worse than when a single outlier was present [Knight et al., 2010].

A review of existing cycle-slip detection/correction methods thus reveals that most approaches lack proper handling of ionospheric delay variations. For this reason, this paper proposes a geometry-based approach to this problem, with an emphasis on proper stochastic modelling and integer validation. First, the cycle-slip detection and estimation process is described, followed by a review of integer least-squares theory and validation. Results of the proposed approaches are then presented from real GPS data collected during high ionospheric activity in northern Canada. Lastly, the methodology described in this paper is summarized and recommendations regarding cycle-slip handling in the presence of high ionospheric activity are presented.

3.2 Cycle-Slip Detection and Estimation

As pointed out in the introduction, most existing cycle-slip detection approaches assume a smooth variation of the ionospheric delay over time. When the ionosphere is disturbed, such approaches could then lead to numerous false detections (see Section 3.5.1). Opting for quality control theory offers an interesting alternative, but might suffer from the presence of multiple outliers. As a solution, we propose a two-step process in which a pre-screening of carrier-phase observations is performed on a satellite-by-satellite basis before including them into an integrated adjustment.

3.2.1 GNSS Functional Model

In order to achieve this objective, one must understand the functional model describing carrier-phase and code observables:

$$\Phi_i^j = \rho^j + \left(dT - dt^j\right) + T^j - \mu_i I^j + \lambda_i N_i^j + \varepsilon_{\Phi_i^j} \tag{3.1}$$

$$P_i^j = \rho^j + \left(dT - dt^j\right) + T^j + \mu_i I^j + b_{P_i}^j + \varepsilon_{P_i^j} \tag{3.2}$$

where

i identifies frequency-dependant terms

j identifies satellite-dependent terms

Φ is the carrier-phase measurement (m)

P	is the code measurement (m)
ρ	is the instantaneous range between the phase centers of the satellite and receiver antennas, including displacements due to earth tides and ocean loading and relativistic effects (m)
dT	is the receiver clock offset from GPS time (m)
dt	is the satellite clock offset from GPS time (m)
T	is the tropospheric delay (m)
μ_i	is a constant $= f_i^2/f_1^2$, where f_i is the frequency of the L_i carrier.
I	is the ionospheric delay on L_1 (m)
λ	is the wavelength of the signal (m)
N	is the (non-integer) carrier-phase ambiguity (cycles)
b	groups instrumental code delays (m)
ε	contains unmodelled quantities such as noise and multipath (m).

For the detection and correction of cycle slips, it is often more appropriate to compute between-epoch differences (δ) of equations 3.1 and 3.2, which eliminates the effects of constant (or slowly-varying) parameters:

$$\delta\Phi_i^j = \Phi_i^j(t + \Delta t) - \Phi_i^j(t)$$
$$= \delta\rho^j + \left(\delta dT - \delta dt^j\right) + \delta T^j - \mu_i\delta I^j + \lambda_i\delta N_i^j + \varepsilon_{\Phi_i^j}$$

(3.3)

$$\delta P_i^j = P_i^j(t + \Delta t) - P_i^j(t)$$
$$= \delta\rho^j + \left(\delta dT - \delta dt^j\right) + \delta T^j + \mu_i\delta I^j + \varepsilon_{P_i^j}$$

(3.4)

where t refers to an epoch and Δt to a time interval. In equation 3.3, the variation of the ambiguity parameter (δN_i^j) is zero for continuous observations, while it is an integer number when a cycle slip occurs. Code instrumental biases have been omitted from equation 3.4 since they are considered constant over a short time interval (typically less than a minute in our application). Several non-dispersive components can easily be modelled using external information such as precise satellite orbit and clock corrections, as well as a tropospheric model. Misclosures can then be computed as:

$$\delta \tilde{\Phi}_i^j = \delta \Phi_i^j - \left(\delta \rho_0^j - \delta dt^j + \delta T_0^j \right) \tag{3.5}$$

$$\delta \tilde{P}_i^j = \delta P_i^j - \left(\delta \rho_0^j - \delta dt^j + \delta T_0^j \right) \tag{3.6}$$

where subscript 0 denotes computed quantities. $\delta \rho_0^j$ can initially be obtained assuming no receiver displacement in the following equation:

$$\delta \rho^j = \sqrt{(\delta x^j - \delta x_r)^2 + (\delta y^j - \delta y_r)^2 + (\delta z^j - \delta z_r)^2} \tag{3.7}$$

where $\left(\delta x^j, \delta y^j, \delta z^j \right)$ is the satellite displacement between epochs and $(\delta x_r, \delta y_r, \delta z_r)$ is the receiver displacement. The remaining unknown quantities in equations 3.3 and 3.4, apart from cycle-slip parameters, are the displacement of the receiver (if it is moving), the receiver clock offset variation and the ionospheric delay variation. A least-squares adjustment using observations from multiple satellites will allow estimation of those parameters, as described next.

3.2.2 Defining Initial Constraints

Estimating the receiver displacement (in the case of a moving antenna), the receiver clock variation and slant ionospheric delay variations can first be achieved by computing a least-squares solution based on code observations only. This process allows verification of the integrity of code observations while providing initial constraints on the unknown parameters. The system of equations involved can be defined as:

$$E\{\delta \boldsymbol{y}_P\} = \boldsymbol{A}_1 \delta \boldsymbol{x}_1 + \boldsymbol{A}_2 \delta \boldsymbol{x}_2 \qquad D\{\delta \boldsymbol{y}_P\} = \boldsymbol{Q}_{\delta \boldsymbol{y}_P}$$

$$E\{\delta \boldsymbol{y}_I\} = \delta \boldsymbol{x}_2 \qquad D\{\delta \boldsymbol{y}_I\} = \boldsymbol{Q}_{\delta \boldsymbol{y}_I} \tag{3.8}$$

where $E\{\cdot\}$ and $D\{\cdot\}$ are the expectation and dispersion operators, respectively. In the case of dual-frequency receivers, the vector of code observations can be expressed as:

$$\delta \boldsymbol{y}_P = [\delta \tilde{P}_1^1 \quad \delta \tilde{P}_2^1 \quad \dots \quad \delta \tilde{P}_1^n \quad \delta \tilde{P}_2^n]^T \tag{3.9}$$

where n is the number of satellites observed. If external information regarding the ionosphere is available, for example by monitoring the rate of change of the geometry-free combination of carrier-phase observations, a vector of pseudo-observations can be added to the system:

$$\delta \boldsymbol{y}_I = [\delta I_0^1 \quad \dots \quad \delta I_0^n]^T. \tag{3.10}$$

More details regarding the selection of those constraints will be provided in Sections 3.3 and 3.4. Parameters have been divided in two groups representing non-dispersive ($\delta \boldsymbol{x}_1$) and dispersive ($\delta \boldsymbol{x}_2$) effects:

$$\delta \boldsymbol{x_1} = [\delta x_r \quad \delta y_r \quad \delta z_r \quad \delta dT]^T \quad \text{(moving receiver)}$$

$$\delta \boldsymbol{x_1} = [\delta dT]^T \quad \text{(static receiver)}$$

(3.11)

$$\delta \boldsymbol{x_2} = [\delta I^1 \quad ... \quad \delta I^n]^T.$$

(3.12)

The design matrices $\boldsymbol{A_1}$ and $\boldsymbol{A_2}$ can easily be obtained by computing the partial derivatives of the code observation equations (equation 3.4) with respect to the estimated parameters. The solution to the system of equation 3.8 will be denoted as $\delta \hat{\boldsymbol{x}}(P)$ with covariance $\boldsymbol{Q}_{\delta \hat{\boldsymbol{x}}(P)}$.

The consistency of this code solution can be assessed by examining the residuals of the adjustment, which constitutes a clear advantage over single-channel processing. Testing of the residuals can be accomplished by computing the normalized residuals and verifying if they exceed a predefined threshold [Baarda, 1968]:

$$\frac{\hat{v}_k}{\sigma_{\hat{v}_k}} > \eta$$

(3.13)

where $\hat{v}_k$ is the estimated residual of the kth measurement, $\sigma_{\hat{v}_k}$ its precision and η is the threshold value from the standard normal distribution. The observation with the largest normalized residual exceeding the threshold, if any, is then discarded from the adjustment and iterations are performed until the test of equation 3.13 is passed for all observations (or until there is no redundancy). Since blunders in code observations typically occur rarely, few iterations should be required at this stage.

3.2.3 Satellite-by-Satellite Detection

The first step of the detection process consists of examining carrier-phase observations for large cycle slips (i.e., above code-noise levels). The purpose of this procedure is to reduce the possible computational load and improve the robustness of data snooping in the case of multiple phase discontinuities. In a similar fashion to that of code observations, the following system can be defined for carrier phases:

$$E\{\delta\boldsymbol{y}_\Phi\} = \boldsymbol{A}_1\delta\boldsymbol{x}_1 - \boldsymbol{A}_2\delta\boldsymbol{x}_2 + \boldsymbol{B}\delta\boldsymbol{n}$$

$$D\{\delta\boldsymbol{y}_\Phi\} = \boldsymbol{Q}_{\delta\boldsymbol{y}_\Phi}.$$

(3.14)

The extra vector of parameters, $\delta\boldsymbol{n}$, contains the cycle-slip parameters and $\boldsymbol{B}$ is the corresponding design matrix. Pre-screening of carrier-phase observations can now be achieved on a satellite-by-satellite basis. Using only data from satellite j and removing the estimated quantities obtained from the code solution leads to:

$$E\{\delta\overline{\boldsymbol{y}}_\Phi^j\} = E\{\delta\boldsymbol{y}_\Phi^j - \boldsymbol{A}_1^j\delta\boldsymbol{x}_1 + \boldsymbol{A}_2^j\delta\boldsymbol{x}_2\} = \boldsymbol{B}^j\delta\boldsymbol{n}^j$$

$$D\{\overline{\delta\boldsymbol{y}}_\Phi^j\} = \boldsymbol{Q}_{\delta\boldsymbol{y}_\Phi^j} + \begin{bmatrix} -\boldsymbol{A}_1^j & \boldsymbol{A}_2^j \end{bmatrix} \boldsymbol{Q}_{\delta\hat{\boldsymbol{x}}(P)} \begin{bmatrix} -\left(\boldsymbol{A}_1^j\right)^T \\ \left(\boldsymbol{A}_2^j\right)^T \end{bmatrix}.$$

(3.15)

The estimated cycle-slip parameters and their covariance matrix can finally be computed as:

$$\boldsymbol{Q}_{\delta\hat{\boldsymbol{n}}^j} = \left[\left(\boldsymbol{B}^j\right)^T \boldsymbol{Q}_{\delta\overline{\boldsymbol{y}}_\Phi^j}^{-1} \boldsymbol{B}^j\right]^{-1}$$

(3.16)

$$\delta \widehat{\boldsymbol{n}}^j = \boldsymbol{Q}_{\delta \widehat{\boldsymbol{n}}^j}^{-1} (\boldsymbol{B}^j)^T \boldsymbol{Q}_{\delta \overline{\boldsymbol{y}}_\Phi^j}^{-1} \delta \overline{\boldsymbol{y}}_\Phi^j.$$

Cycle slips are detected by verifying if the estimated quantities ($\delta \widehat{\boldsymbol{n}}$) are significantly different from zero:

$$(\delta \widehat{\boldsymbol{n}}^j)^T \boldsymbol{Q}_{\delta \widehat{\boldsymbol{n}}^j}^{-1} \delta \widehat{\boldsymbol{n}}^j > \chi^2 \qquad (3.17)$$

where χ^2 is the threshold value from the central chi-square distribution and the variance factor is assumed known [Wells and Krakiwsky, 1971]. This satellite-by-satellite testing will only allow detecting cycle slips that exceed code-noise levels, meaning that discontinuities on the order of 1-2 cycles will most likely remain undetected. Integrating carrier phases in the adjustment will be required for this purpose, which is described next.

3.2.4 Integrated Detection

In order to benefit fully from the precision of carrier-phase observations, measurements from all satellites should be processed simultaneously. Discarding carrier phases flagged as containing cycle slips in the satellite-by-satellite detection step, the least-squares solution obtained from code observations can be updated as:

$$\Delta \delta \boldsymbol{x}(\Phi) = \left(\boldsymbol{D}^T \boldsymbol{Q}_{\delta \boldsymbol{y}_\Phi}^{-1} \boldsymbol{D} + \boldsymbol{Q}_{\delta \widehat{\boldsymbol{x}}(P)}^{-1}\right)^{-1} \boldsymbol{D}^T \boldsymbol{Q}_{\delta \boldsymbol{y}_\Phi}^{-1} \left(\delta \boldsymbol{y}_\Phi - \boldsymbol{D} \delta \widehat{\boldsymbol{x}}(P)\right) \qquad (3.18)$$

$$\delta \widehat{\widehat{\boldsymbol{x}}}(\Phi) = \delta \widehat{\boldsymbol{x}}(P) + \delta \Delta \boldsymbol{x}(\Phi) \qquad (3.19)$$

where $\boldsymbol{D} = \begin{bmatrix} \boldsymbol{A}_1^j & -\boldsymbol{A}_2^j \end{bmatrix}$ and $\delta\Delta\boldsymbol{x}(\varPhi)$ is the parameter update to the *a priori* values provided by the code solution. After computing the residuals, data snooping is performed again as per equation 3.13 and the process is repeated until all remaining cycle slips have been detected. As demonstrated by de Jong and Teunissen [2000], cycle slips with a magnitude of one cycle can be detected using this approach, as long as phase redundancy is available. In the event that this condition is not satisfied, one has to rely on the satellite-by-satellite detection results. Note that when a discontinuity is detected for a satellite, both frequencies are usually flagged as containing cycle slips unless the slant ionospheric delay was tightly constrained.

3.2.5 Estimating Cycle-Slip Parameters

Once cycle slips are detected, the next step consists of estimating the size of the discontinuities. Obtaining unbiased float estimates can only be achieved through careful modelling and estimation of all quantities on the right-hand side of equation 3.3. The estimated parameters $\delta\widehat{\overline{\boldsymbol{x}}}(\varPhi)$, obtained from the integrated detection process, offer the best solution at hand for this purpose. When a receiver maintains lock on most satellites between epochs, non-dispersive effects typically can be modelled with a precision of a few millimetres (static receiver) or centimetres (moving receiver). Ionospheric effects were determined using a combination of code observations and external constraints. Depending on code-noise levels and the predictability of the ionosphere, it is possible that

cycle-slip parameters are still contaminated by this error source. The next sections will explain the role played by the *a priori* constraints set in equation 3.8 in the identification of the proper integer candidates.

If we suppose that non-dispersive effects were indeed precisely modelled, there will be very little correlation between cycle-slip parameters of different satellites. A satellite-by-satellite approach could then still be used for the purpose of cycle-slip correction:

$$E\left\{\delta\overline{\overline{\boldsymbol{y}}}_\Phi^j\right\} = E\left\{\delta\boldsymbol{y}_\Phi^j - \boldsymbol{A}_1^j\delta\widehat{\widehat{\boldsymbol{x}}}_1(\Phi) + \boldsymbol{A}_2^j\delta\widehat{\widehat{\boldsymbol{x}}}_2(\Phi)\right\} = \boldsymbol{B}^j\delta\boldsymbol{n}^j$$

$$D\left\{\delta\overline{\overline{\boldsymbol{y}}}_\Phi^j\right\} = \boldsymbol{Q}_{\delta\boldsymbol{y}_\Phi^j} + \begin{bmatrix} -\boldsymbol{A}_1^j & \boldsymbol{A}_2^j \end{bmatrix}\boldsymbol{Q}_{\delta\widehat{\boldsymbol{x}}(\Phi)}\begin{bmatrix} -\left(\boldsymbol{A}_1^j\right)^T \\ \left(\boldsymbol{A}_2^j\right)^T \end{bmatrix}.$$

(3.20)

An analysis of the estimated cycle-slip parameters and their covariance matrix, again obtained using equation 3.16, can now be performed to identify the most-likely integer candidates.

3.3 Integer Least-Squares Theory

Once the float estimates for the cycle-slip parameters ($\widehat{\boldsymbol{n}}$) are obtained, the next step is to identify the closest integer vector. This section will focus on how this vector should be defined and validated.

67

3.3.1 Integer Pull-In Regions

In order to use the full information from the cycle-slip covariance matrix, $\boldsymbol{Q}_{\delta\widehat{\boldsymbol{n}}}$, the distance between the float estimates and an integer vector ($\delta\widecheck{\boldsymbol{n}}$) should be measured using a special metric sometimes referred to as the Mahalanobis distance [Mahalanobis, 1936], defined as:

$$d_M(\delta\widehat{\boldsymbol{n}}, \delta\widecheck{\boldsymbol{n}}) = (\delta\widehat{\boldsymbol{n}} - \delta\widecheck{\boldsymbol{n}})\boldsymbol{Q}_{\delta\widehat{\boldsymbol{n}}}^{-1}(\delta\widehat{\boldsymbol{n}} - \delta\widecheck{\boldsymbol{n}}). \tag{3.21}$$

This metric takes into account the correlation between the estimated parameters, potentially leading to a completely different distance than the Euclidean norm would provide. When considering the Euclidean norm in two dimensions, all grid points located in a unit square centered on an integer pair are closer to that integer pair than any other one (see Figure 3.2(a)). This unit square defines a Voronoi cell [Xu, 2006], often referred to as a pull-in region in integer least-squares analysis [Teunissen, 1998] since all values located in this cell would be mapped to the closest integer vector.

When the Mahalanobis distance is involved, the shape of those pull-in regions can differ significantly, and depends on the correlation between parameters. The correlation, in turn, is a function of geometry and the stochastic model defined by the observation noise ($\boldsymbol{Q}_{\delta\boldsymbol{y}_\Phi}$, $\boldsymbol{Q}_{\delta\boldsymbol{y}_P}$) and the *a priori* ionospheric constraints ($\boldsymbol{Q}_{\delta\boldsymbol{y}_I}$). It is thus the covariance matrix, $\boldsymbol{Q}_{\delta\widehat{\boldsymbol{n}}}$, in equation 3.21 that allows the stochastic model to contribute in

defining the Voronoi cells. Figure 3.2(b)-(d) demonstrate two-dimensional pull-in regions associated with different stochastic models (actually, only $\sigma_{\delta I_0}$ differs). It can be noticed that, in subplot (d), the grid points (0,0) and (1,0) have no common cell boundary, meaning that the integer pair (1,1) is actually closer to the origin than (1,0) in terms of the Mahalanobis distance.
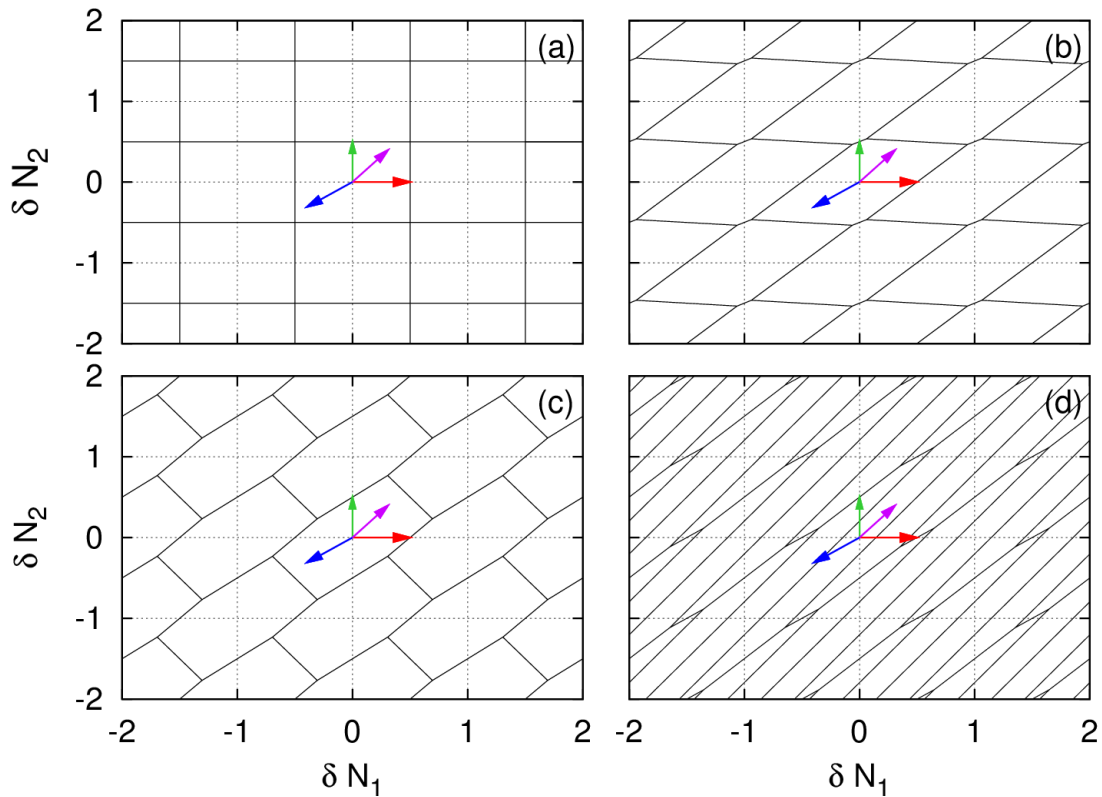
Figure 3.2 : Integer pull-in regions for different ionospheric constraints: (a) uncorrelated cycle-slip parameters (b) $\sigma_{\delta I_0} = 0.001$ m (c) $\sigma_{\delta I_0} = 0.010$ m (d) $\sigma_{\delta I_0} = 0.050$ m. Vectors indicating the direction in which ionospheric (purple), geometric (blue), and parameter-specific (red for N_1 and green for N_2) errors propagate are shown.

The shape of the cells in subplot (d) are much more elongated in the direction of the purple vector, having a slope of λ_2/λ_1, and representing the direction in which the ionospheric delay variation would propagate into the estimates $\delta\widehat{N}_1^j$ and $\delta\widehat{N}_2^j$. In other words, with a looser ionospheric constraint (and a well-defined range), the Mahalanobis distance will to some extent "forgive" any float vector being affected by the ionosphere and still assign it a short distance. This means that our system can accommodate a much larger ionospheric bias as opposed to processing each frequency independently, as represented by subplot (a), or by tightly constraining the ionospheric delay (subplots (b)-(d)).

Figure 3.2 also includes other vectors representing the propagation direction of a geometric error (in blue), having a slope of $-\lambda_1/\lambda_2$, as well as parameter-specific errors such as carrier-phase noise and multipath (in red for δN_1 and in green for δN_2). Since observations are not error free, the vector of estimated cycle-slip parameters might then be contaminated by all those error sources. Hence, Figure 3.2 illustrates that the sensitivity of the cycle-slip correction process to the various error sources depends largely on the ionospheric constraint that was selected. With a looser ionospheric variance, a larger ionospheric error can be accommodated, but the more sensitive the cycle-slip correction process will become towards geometric and parameter-specific errors. It is therefore important to appropriately select the ionospheric variance when using the ionosphere-weighted model, and additional details regarding this topic will be provided in Section 3.4.

3.3.2 Integer Validation

Once the most-likely integer vector has been identified (i.e., the float estimates belong to its pull-in region), the next step is to validate this selection. While this process is fundamental, a rigorous approach is often omitted in the context of cycle-slip correction using geometry-free combinations of observations. Integer cycle-slip validation was suggested by Kim and Langley [2001], and Banville et al. [2010] emphasized the deficits of popular validation methods when dealing with an active ionosphere.

In the literature, several approaches have been proposed to ensure that the proper integer vector is selected, but which approach to choose is still an open issue [Verhagen, 2004]. A very popular method of discriminating between the two closest integer vectors (say $\delta\breve{\boldsymbol{n}}_1$ and $\delta\breve{\boldsymbol{n}}_2$) is the ratio test [Euler and Schaffrin, 1991]. The integer vector $\delta\breve{\boldsymbol{n}}_1$ is accepted if the following condition is met:

$$\frac{d_M(\delta\hat{\boldsymbol{n}}, \delta\breve{\boldsymbol{n}}_1)}{d_M(\delta\hat{\boldsymbol{n}}, \delta\breve{\boldsymbol{n}}_2)} < c_1 \tag{3.22}$$

where c_1 is a constant, usually selected as a fixed value of 1/2 or 1/3. A potential problem with the ratio test is that it does not consider the scale of the covariance matrix. A modified ratio test using a variable threshold value has been proposed by Teunissen and Verhagen [2009]. When the standard deviation of the parameters is large, the threshold value is decreased to reflect this reality. Even though such an approach will perform

better than the fixed-threshold ratio test, computing the threshold value is not trivial and requires look-up tables based on simulations. Another approach would be to define a success probability based on the integral of the probability density function (PDF), centered on the estimates, over the pull-in region of an integer vector. Unfortunately, the integral is quite complex in a multi-dimensional context due to the shape of the pull-in regions (refer back to Figure 3.2) [Xu, 2006; Feng and Wang, 2011]. A multitude of approximations to the success probability have been proposed, such as lower bounds and upper bounds based on the ambiguity dilution of precision (ADOP) [Teunissen, 1997], ellipses [Teunissen, 1998], bootstrapping [Teunissen, 1999b], eigenvalues [Teunissen, 2000], etc. Nevertheless, those approximations ignore the estimated values and only focus on the precision of the estimates, neglecting the potential presence of biases in the observations. The success rate in the presence of biases was also analyzed by Teunissen [2001], where lower and upper bounds were provided for integer least-squares. Still, instantaneous ambiguity resolution could be compromised depending on the sharpness of those bounds.

There are thus two important factors to consider when performing integer validation: 1) the mathematical model must be strong enough for us to have confidence in the selected integer candidates, and 2) only one integer vector must have a significant probability of being the "true" solution. One possible means of considering both the PDF and the estimated values is to use Bayes' marginal *a posteriori* probability of $\delta \boldsymbol{n}_1$ being the "true" integer vector, defined as:

$$\Omega = \frac{f_{\delta\hat{n}}(\delta\breve{\boldsymbol{n}}_1)}{\sum f_{\delta\hat{n}}(\delta\breve{\boldsymbol{n}}_i)} > c_2 \tag{3.23}$$

where the summation is made over all integer vectors, and c_2 is the threshold value, selected as 0.99 in this research. The PDF of the estimated cycle-slip parameters is:

$$f_{\delta\hat{n}}(\delta\breve{\boldsymbol{n}}_i) = \frac{1}{(2\pi)^{k/2}\|\boldsymbol{Q}_{\delta\hat{n}}\|^{1/2}} \exp\left\{-\frac{1}{2}d_M(\delta\hat{\boldsymbol{n}}, \delta\breve{\boldsymbol{n}}_i)\right\} \tag{3.24}$$

where k is the dimension of $\delta\hat{\boldsymbol{n}}$. It was shown that such a formulation also maximizes the probability of successful fixing [Teunissen, 2005]. Simulations have further demonstrated that $1 - \Omega$ represents an unbiased estimate of the failure rate [Van Meerbergen et al., 2010].

Even though the summation in equation 3.23 is made over all integer vectors in $\mathbb{Z}^k$, which is practically impossible to realize, the contribution of some integer vectors obviously becomes negligible. Verhagen and Teunissen [2006] determined that all vectors for which

$$d_M(\delta\hat{\boldsymbol{n}}, \delta\breve{\boldsymbol{n}}_i) > \chi^2 \tag{3.25}$$

where χ^2 is the central chi-square distribution (with two degrees of freedom when dealing with dual-frequency receivers), can be omitted from the summation. An efficient algorithm, such as the one described by de Jonge and Tiberius [1996], allows rapid computation of equation 3.23 constrained by equation 3.25.

3.3.3 On Linear Combinations

A very popular approach to ambiguity resolution and cycle-slip correction is to form linear combinations of observations or parameters to mitigate the presence of some error sources, such as geometric or ionospheric errors. This is typically done using a transformation matrix ($\boldsymbol{Z}$), such that:

$$\delta\hat{\boldsymbol{z}} = \boldsymbol{Z}\delta\hat{\boldsymbol{n}} \tag{3.26}$$

$$\boldsymbol{Q}_{\delta\hat{\boldsymbol{z}}} = \boldsymbol{Z}\boldsymbol{Q}_{\delta\hat{\boldsymbol{n}}}\boldsymbol{Z}^T. \tag{3.27}$$

It can be shown, however, that those transformations will not improve the outcome of the cycle-slip correction, since:

$$
\begin{aligned}
d_M(\delta\hat{\boldsymbol{z}}, \delta\check{\boldsymbol{z}}) &= (\delta\hat{\boldsymbol{z}} - \delta\check{\boldsymbol{z}})^T \boldsymbol{Q}_{\delta\hat{\boldsymbol{z}}}^{-1} (\delta\hat{\boldsymbol{z}} - \delta\check{\boldsymbol{z}}) \\
&= (\boldsymbol{Z}\delta\hat{\boldsymbol{n}} - \boldsymbol{Z}\delta\check{\boldsymbol{n}})^T (\boldsymbol{Z}\boldsymbol{Q}_{\delta\hat{\boldsymbol{n}}}\boldsymbol{Z}^T)^{-1} (\boldsymbol{Z}\delta\hat{\boldsymbol{n}} - \boldsymbol{Z}\delta\check{\boldsymbol{n}}) \\
&= (\delta\hat{\boldsymbol{n}} - \delta\check{\boldsymbol{n}})^T \boldsymbol{Z}^T (\boldsymbol{Z}^T)^{-1} \boldsymbol{Q}_{\delta\hat{\boldsymbol{n}}}^{-1} \boldsymbol{Z}^{-1} \boldsymbol{Z}(\delta\hat{\boldsymbol{n}} - \delta\check{\boldsymbol{n}}) \qquad (3.28) \\
&= (\delta\hat{\boldsymbol{n}} - \delta\check{\boldsymbol{n}})^T \boldsymbol{Q}_{\delta\hat{\boldsymbol{n}}}^{-1} (\delta\hat{\boldsymbol{n}} - \delta\check{\boldsymbol{n}}) \\
&= d_M(\delta\hat{\boldsymbol{n}}, \delta\check{\boldsymbol{n}})
\end{aligned}
$$

where $\boldsymbol{Z}$ is assumed invertible, which is the case by definition for valid integer-preserving transformations [Teunissen and Kleusberg, 1998]. Since the Mahalanobis distance is not affected by the reparameterization, the success rate and Ω (see equation 3.23) will also remain identical. So, using linear combinations (such as the popular widelane) will have no impact on the cycle-slip correction process, provided that the stochastic model was defined properly. Similarly, the Least-squares AMBiguity Decorrelation Adjustment

(LAMBDA) [Teunissen, 1993] is only useful in speeding up the search process, but does not improve ambiguity resolution. An exception to this rule applies when partial fixing is performed, meaning that only a subset of (reparameterized) parameters are fixed [Teunissen et al., 1999].

3.4 Stochastic Analysis

The previous section, in particular Figure 3.2, explained that the outcome of the cycle-slip correction process will greatly depend on the stochastic model. For example, it was shown that a large uncertainty in the ionospheric delay variation makes the process more sensitive to geometric errors and noise or multipath. As mentioned in Section 3.2, several approaches were developed to approximate the success rate as a function of stochastic modelling. Studies have also demonstrated the impact of various types of biases on the success rate [Teunissen et al., 2000; Teunissen, 2001]. In this contribution, we adopt a slightly different approach measuring the impact of both the stochastic model and the presence of biases on Ω (see equation 3.23). Since this quantity is used in practice for integer validation purposes, it is imperative to determine when this value will fall below a certain threshold.

3.4.1 Methodology

For the purpose of simulations, the following system of equations is defined:

$$E\{\delta\boldsymbol{y}_s\} = E\left\{\begin{bmatrix}\delta\widetilde{\Phi}_1^j\\\delta\widetilde{\Phi}_2^j\\\delta\widetilde{P}_1^j\\\delta\widetilde{P}_2^j\\\delta\bar{\rho}_0^j\\\delta I_0^j\end{bmatrix}\right\} = \underbrace{\begin{bmatrix}1 & -\mu_1 & \lambda_1 & 0\\1 & -\mu_2 & 0 & \lambda_2\\1 & \mu_1 & 0 & 0\\1 & \mu_2 & 0 & 0\\1 & 0 & 0 & 0\\0 & 1 & 0 & 0\end{bmatrix}}_{A_s}\begin{bmatrix}\delta\rho^j\\\delta I^j\\\delta N_1^j\\\delta N_2^j\end{bmatrix}$$

(3.29)

$$D\{\delta\boldsymbol{y}_s\} = \boldsymbol{Q}_{\delta y_s}$$

where $\boldsymbol{Q}_{\delta y_s}$ is a diagonal matrix reflecting the precision of phase noise ($\sigma_{\delta\Phi}$), code noise ($\sigma_{\delta P}$), range constraint ($\sigma_{\delta\bar{\rho}_0}$) and *a priori* ionospheric constraint ($\sigma_{\delta I_0}$). The cycle-slip covariance matrix used in the computations of Ω for the simulations will then be:

$$Q_{\delta\hat{n}} = \left[A_s^T Q_{\delta y_s}^{-1} A_s\right]^{-1}.$$

(3.30)

Hence, an analysis of the impacts of the components of $\boldsymbol{Q}_{\delta y_s}$ on Ω can easily be performed. By assuming that $\delta\hat{\boldsymbol{n}} = (0,0)$, a maximal value for Ω will be obtained. The subsequent plots then indicate in which conditions reliable cycle-slip correction (defined here as $\Omega \geq 0.99$) will be possible.

Note that the system of equation 3.29 is equivalent to the cycle-slip estimation process presented in Section 3.2, provided that satellite j was excluded from both the code-based (equation 3.8) and integrated (equation 3.20) solutions. In this case, a range constraint

76

can be defined as $\delta\bar{\rho}_0^j = A^j \delta x_1$ and its precision should reflect the geometric strength of the integrated solution.

3.4.2 Results

Figure 3.3 provides an analysis of the Ω value under different scenarios. In subplot (a), no *a priori* constraints were applied on the range and the ionospheric delay variation. This approach is equivalent to the geometry-free model. It is interesting to note that if both the range and the ionosphere are poorly defined, it is practically impossible to reliably fix cycle slips to integers. In subplot (b), a constraint of 1 cm was applied on the range, which is a reasonable expectation when the receiver displacement and clock offset variation are estimated using the time-differenced approach discussed in Section 3.2. This model thus represents the ionosphere-float model since code measurements offer the only constraint on the ionospheric delay variation. It is no surprise that Ω decreases quickly as code noise increases. Still, it should be emphasized that phase noise also plays a crucial role in the cycle-slip correction process. As pointed out in Figure 3.2(d), the pull-in regions become rather narrow in the propagation direction of parameter-specific errors such as noise. Subplot (c) shows the benefits of adding an ionospheric constraint, and demonstrates that once the range is well defined, it is possible to tolerate a larger uncertainty in the ionospheric delay variation. Finally, subplot (d) again stresses the importance of the range constraint in cycle-slip correction.
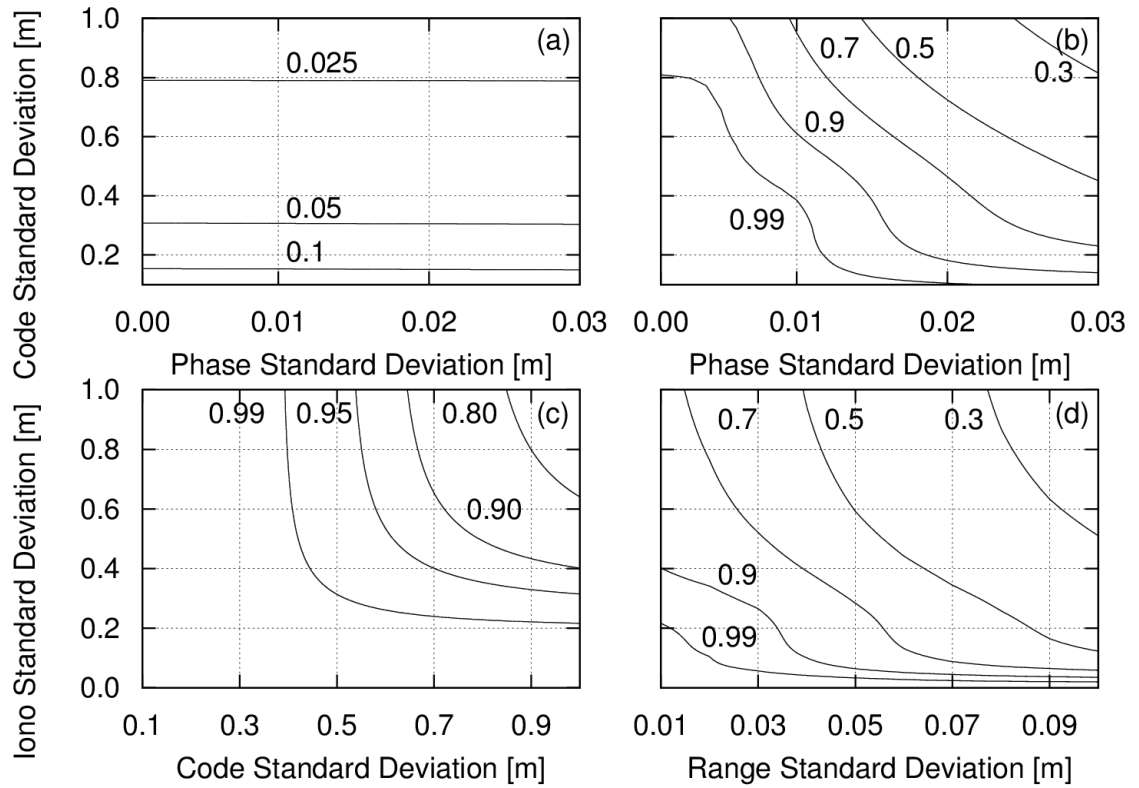
Figure 3.3 : Analysis of Ω under different scenarios: (a) $\sigma_{\delta\bar{p}_0} = \infty$ and $\sigma_{\delta I_0} = \infty$, (b) $\sigma_{\delta\bar{p}_0} = 0.01$ m and $\sigma_{\delta I_0} = \infty$, (c) $\sigma_{\delta\bar{p}_0} = 0.01$ m and $\sigma_{\delta\Phi} = 0.01$ m, (d) $\sigma_{\delta P} = 1.0$ m and $\sigma_{\delta\Phi} = 0.01$ m.

A topic that must now be addressed is how to select the ionospheric constraint. When the ionospheric delay variation between epochs is unknown, is it preferable to opt for the float model or still attempt to constrain this quantity? In order to answer this question, the relationship between ionospheric bias and ionospheric constraint is analyzed for two stochastic models, as illustrated in the plots of Figure 3.4. Some key conclusions can be made from these plots: first, once δI reaches the value of about 67 cm, the estimated

parameters will inevitably lie in the wrong pull-in region, regardless of the constraint selected. This critical value thus constitutes the maximal ionospheric delay variation that can be handled using the ionosphere-weighted model of dual-frequency carrier-phase observations, although a larger delay could be tolerated due to code measurements (see next paragraph). When processing GNSS data at a 30-second sampling interval during high ionospheric activity, ionospheric delay variations exceeding this critical value are indeed possible, implying that it might be safer to disable cycle-slip correction under such circumstances. Furthermore, reliable cycle-slip correction, defined as $\Omega \geq 0.99$, can only be obtained when $\delta I < 0.3$ m with $\sigma_{\delta\Phi} = 5$ mm, and when $\delta I < 0.17$ m when $\sigma_{\delta\Phi} = 1$ cm. Only if one is willing to accept a higher failure rate can an increased ionospheric delay variation be accommodated. One should also keep in mind that the values suggested are maximal values and these could differ in practice due to noise and unmodelled errors.

Note that when code observations are used, code noise will propagate into the estimated cycle-slip parameters and create an apparent ionospheric delay variation. This "interference" could either be constructive or destructive, meaning that it could reduce or amplify the real ionospheric effects. For this reason, cycle-slip correction associated with a value of δI greater than 67 cm can be successful, provided that code measurements help mitigate the ionospheric bias. Similarly, in the ionosphere-float model with noisy code measurements, code noise could push the estimated cycle-slip parameters out of the correct pull-in region and lead to wrong integer candidate identification as will be demonstrated later.
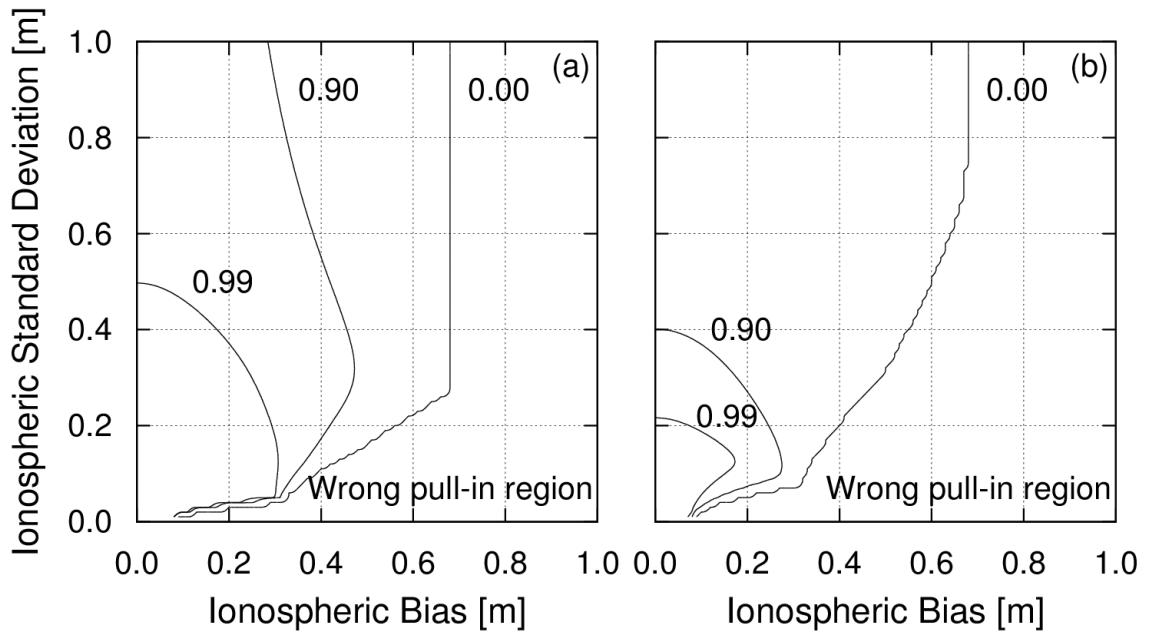
Figure 3.4 : Relationship between ionospheric bias and ionospheric constraint for two stochastic models: (a) $\sigma_{\delta\Phi} = 0.005$ m, $\sigma_{\delta P} = 1.0$ m and $\sigma_{\delta\bar{\rho}_0} = 0.01$ m; (b) $\sigma_{\delta\Phi} = 0.01$ m, $\sigma_{\delta P} = 1.0$ m and $\sigma_{\delta\bar{\rho}_0} = 0.01$ m. The contours indicate levels of Ω.

From Figure 3.4, it seems like selecting $\sigma_{\delta I_0}$ in the vicinity of 10-15 cm is a good compromise in maximizing the sensitivity to an ionospheric bias. Based on the stochastic model of Figure 3.4(a), using such an *a priori* constraint could allow correcting cycle slips even in the presence of an ionospheric bias of nearly 30 cm. This can be explained by the relation between the PDF and the pull-in regions. The tighter the constraint on the ionospheric delay, the more peaked the PDF. Since the success rate is defined as the integral of the PDF over the pull-in region, if a peaked PDF is located close to the border of a cell, the success probability will still be high enough to reliably map the float

estimates to an integer vector. As the PDF gets wider due to a loose ionospheric constraint, it spreads over the boundaries of the pull-in region as it gets closer to the border of a cell, leading to a reduced success rate. It could thus be concluded that it is preferable to slightly over-constrain the ionospheric delay variation, as long as the true delay allows the float estimates to remain within the proper pull-in region.

3.5 Experimental Results

The concepts presented in this paper have been applied to GPS data collected during high ionospheric activity. Ten stations in northern Canada were used (see Table 3.1), all of them located above the 56th parallel, except for station ALGO in Algonquin Park, Ontario, which was used as a benchmark since it was not as affected by ionospheric irregularities. All stations have accurate weekly coordinates estimated by the International GNSS Service (IGS) [Dow et al., 2009] which served as reference positions in subsequent analyses. Satellite orbits and clock corrections were also obtained from the IGS for the computation of PPP solutions [Griffiths and Ray, 2009]. Data from 4 to 7 April 2011 were selected due to the presence of nighttime ionospheric scintillation. An example of the type of ionospheric delay variations observed was already presented in Figure 3.1. The performance of the proposed cycle-slip detection approach is first assessed, followed by an analysis of cycle-slip correction.

Table 3.1: Canadian stations used to assess the performance of the cycle-slip

detection/correction approaches.

Station	Location	Latitude	Longitude	Receiver Type
ALGO	Algonquin Park, Ontario	45º57'21"	-78º04'17"	AOA Benchmark ACT
BAKE	Baker Lake, Nunavut	64º19'04"	-96º00'08"	TPS NetG3
INVK	Inuvik, Northwest Territories	68º18'22"	-133º31'37"	Ashtech UZ-12
IQAL	Iqaluit, Nunavut	63º45'21"	-68º30'38"	TPS NetG3
NAIN	Nain, Newfoundland and Labrador	56º32'13"	-61º41'19"	Ashtech UZ-12
QIKI	Qikiqtarjuaq, Nunavut	67º33'34"	-64º02'01"	Ashtech UZ-12
RESO	Resolute Bay, Nunavut	74º41'27"	-94º53'37"	Ashtech UZ-12
TUKT	Tuktoyaktuk, Northwest Territories	69º26'18"	-132º59'40"	Ashtech UZ-12
WHIT	Whitehorse, Yukon Territory	60º45'01"	-135º13'20"	TPS NetG3
YELL	Yellowknife, Northwest Territories	62º28'51"	-114º28'51"	AOA SNR-12 ACT

3.5.1 Cycle-Slip Detection

When using data at a 30-second sampling interval, ionospheric delay variations of nearly 1 metre can be observed. Therefore, using the geometry-free combination as a means of detecting cycle slips could result in an unnecessarily large number of false detections. This phenomenon can be clearly visualized by examining the performance of kinematic PPP solutions. The datasets selected for this study were processed by three automated online PPP services [Banville et al., 2009]. All PPP engines were using geometry-free linear combinations of observations for the purpose of cycle-slip detection. The RMS errors of the estimated heights, presented in Figure 3.5, offer a clear picture of the problem at hand. When the ionosphere is quiet, typical kinematic PPP height RMS should be around 3 cm for IGS quality data [Kouba, 2009], which could be confirmed for station ALGO (except for one PPP engine). On the other hand, significantly larger RMS errors were obtained for other datasets. Note that the services are labeled as 1, 2 and 3 to maintain anonymity.

The same datasets were also processed by PPP software developed by the first author, which includes the methods described in this paper, such as the improved cycle-slip detection and correction algorithms. For this test, no cycle-slip correction was attempted to emphasize the benefits of the proposed detection procedure. In the cycle-slip detection process, no assumptions were made regarding the dynamics of the receiver, i.e. the receiver displacement was explicitly estimated in the time-differenced solution. When using this approach, the RMS error of the estimated height (labeled as "New Approach"

in Figure 3.5 is clearly smaller than that of the PPP services and is similar to kinematic PPP results with a quiet ionosphere. It is interesting to note that very few cycle slips were present in the carrier-phase observations, but several ambiguity parameters in PPP solutions 1, 2 and 3 were needlessly reset due to the ionospheric effects.
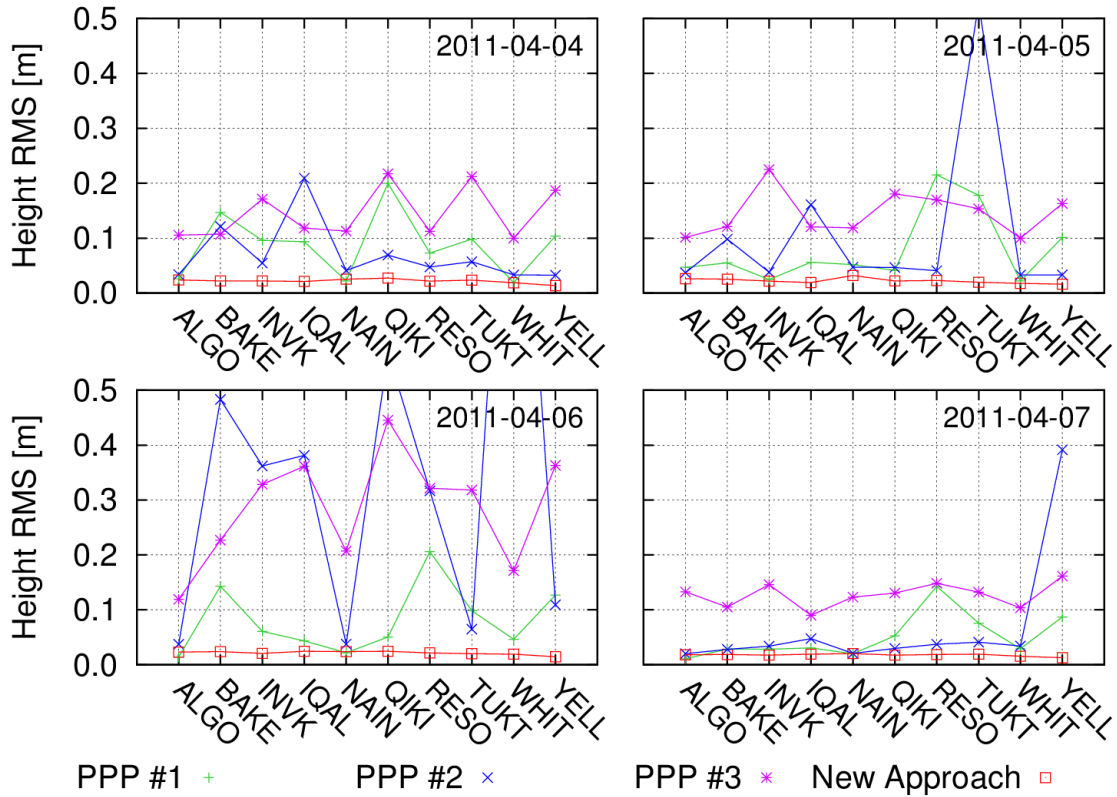
Figure 3.5 : RMS of the estimated station height using the kinematic PPP methodology.

To further illustrate the consequences of this problem, Figure 3.6 presents a 24-hour time series of the estimated ellipsoidal height for station RESO at Resolute Bay, Nunavut, on 6 April 2011. The stability of the solutions suffers greatly from the falsely detected cycle slips, while the new algorithm presented offers more stable height

84

estimates. While kinematic PPP solutions using a 30-second sampling interval have limited applications in practice, this test still illustrates clearly the deficiencies in the cycle-slip detection processes commonly implemented. Having access to a reliable cycle-slip detection method would greatly reduce the number of ambiguity parameters to be estimated for processing IGS station data, in the context of satellite clock estimation or total electron content (TEC) map generation, for instance.
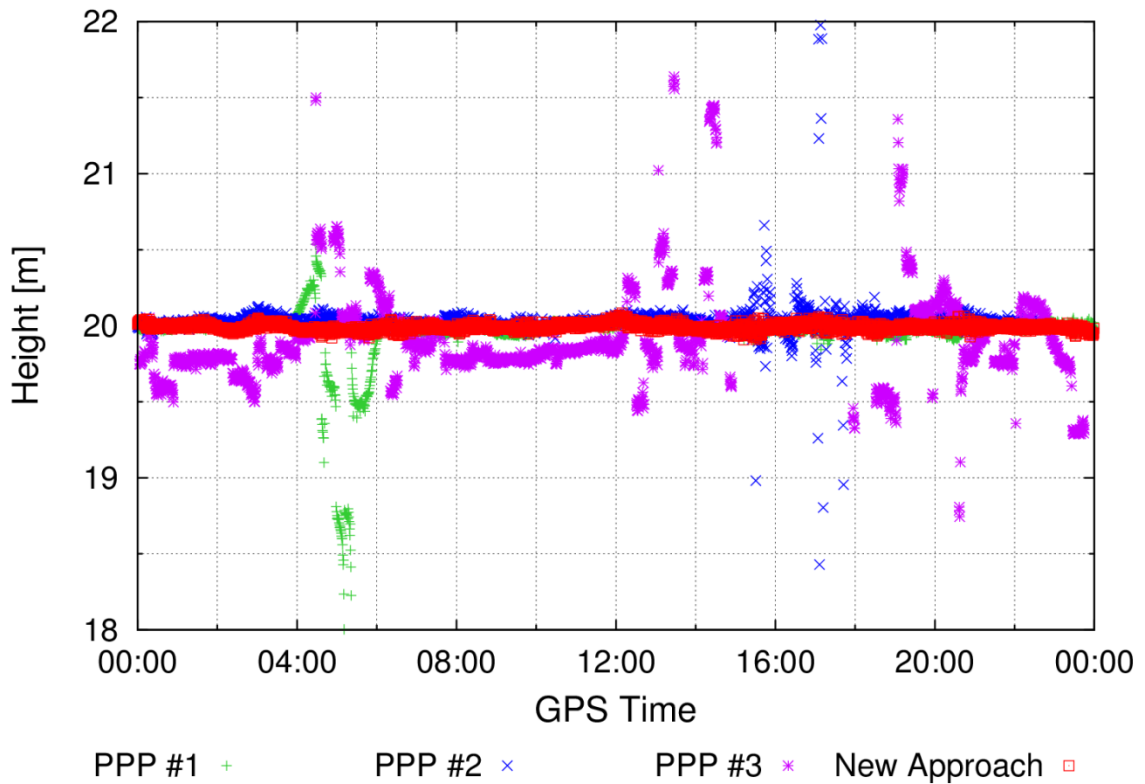
Figure 3.6: Estimated station height for station RESO on 6 April 2011.

3.5.2 Cycle-Slip Correction

With an unstable ionosphere, cycle-slip correction with 30-second epochs should probably be deactivated due to the inherent risk of fixing the estimated parameters to wrong integers. Still, to demonstrate that our method is indeed capable of handling ionospheric delay variations of several decimetres, three examples are provided hereafter.

For every scenario, the receiver was known to be static; i.e., no receiver displacement was estimated in the time-differenced solution. The precision of the estimated receiver clock variation was always in the vicinity of 6 mm. Code and phase noise were monitored using a PPP solution running in parallel, and an appropriate scaling was used to transform the standard deviations from undifferenced ionosphere-free observations to time-differenced uncombined observations. An *a priori* constraint on the ionospheric delay was obtained by computing an RMS value from the between-epoch variation of the geometry-free combination of carrier-phase measurements for the last 5 epochs. All of this information defined the stochastic component required in the correction process.

First, data from satellite PRN 3 on 4 April 2011 at station IQAL was used, and cycle-slip correction was attempted at every epoch. It was verified using 1 Hz data that no cycle slips were present during a 4-hour period, from 00:30 to 04:30 GPST. Figure 3.7 illustrates the ionospheric delay variation during each 30-second interval, as well as the Ω value computed using equation 3.23. It is interesting to note that the proper integer values

(0,0) could be recovered at every epoch, even though the ionospheric delay variation exceeded 50 cm at one epoch. Such results could be achieved thanks to code measurements with relatively low noise, which reduced the ionospheric bias affecting the estimated cycle-slip parameters.
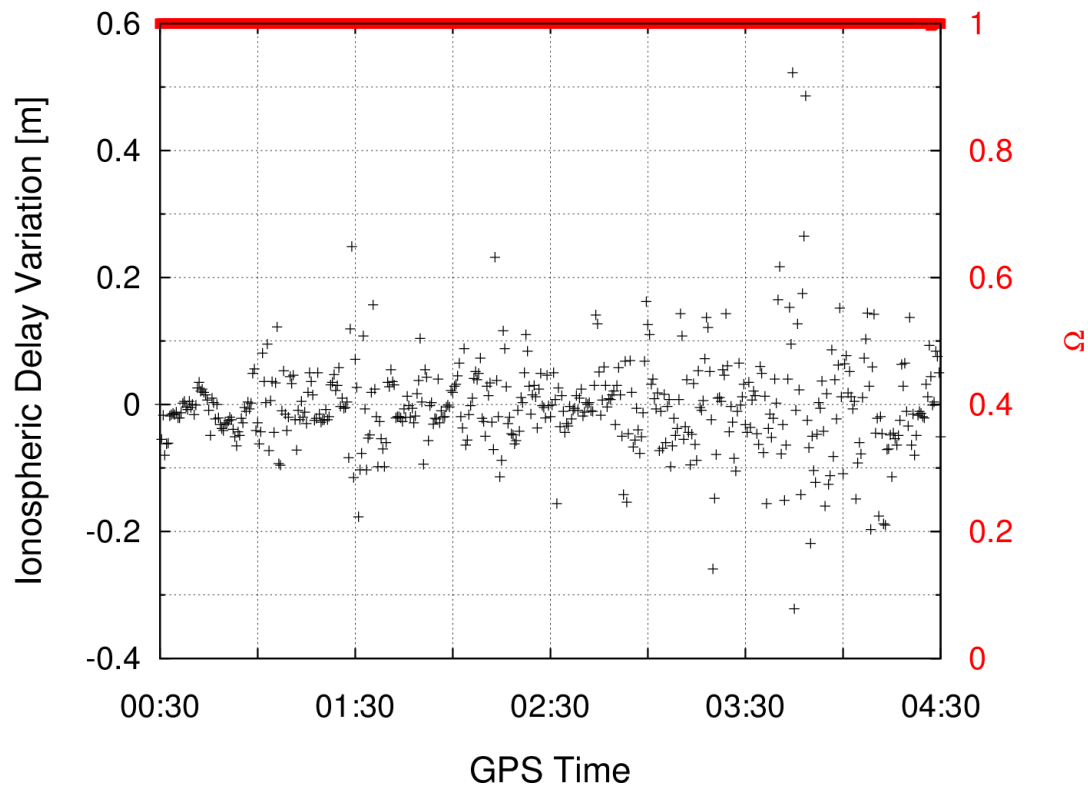
Figure 3.7: Cycle-slip correction results for satellite PRN 3 observed at station IQAL on 4 April 2011.

The same procedure was repeated using data from satellite PRN 4 on 6 April 2011 at station BAKE in Baker Lake, Nunavut. Noisier code measurements were associated with this satellite, affecting the outcome of the cycle-slip correction process, shown in Figure

3.8. In multiple instances, Ω was below the 0.99 threshold value, preventing a reliable identification of integer candidates. In this case, the ambiguity parameters associated with this satellite in the PPP solution would have to be reinitialized. Unfortunately, in six occasions indicated by black squares in Figure 3.8, cycle-slips were fixed to the wrong integer pair (-3, -4). An analysis revealed that misspecifications in the stochastic model as well as code-noise interference (refer to Section 3.4) led to this outcome. Still, for several epochs, the correct integer values were identified even though significant ionospheric fluctuations were present.
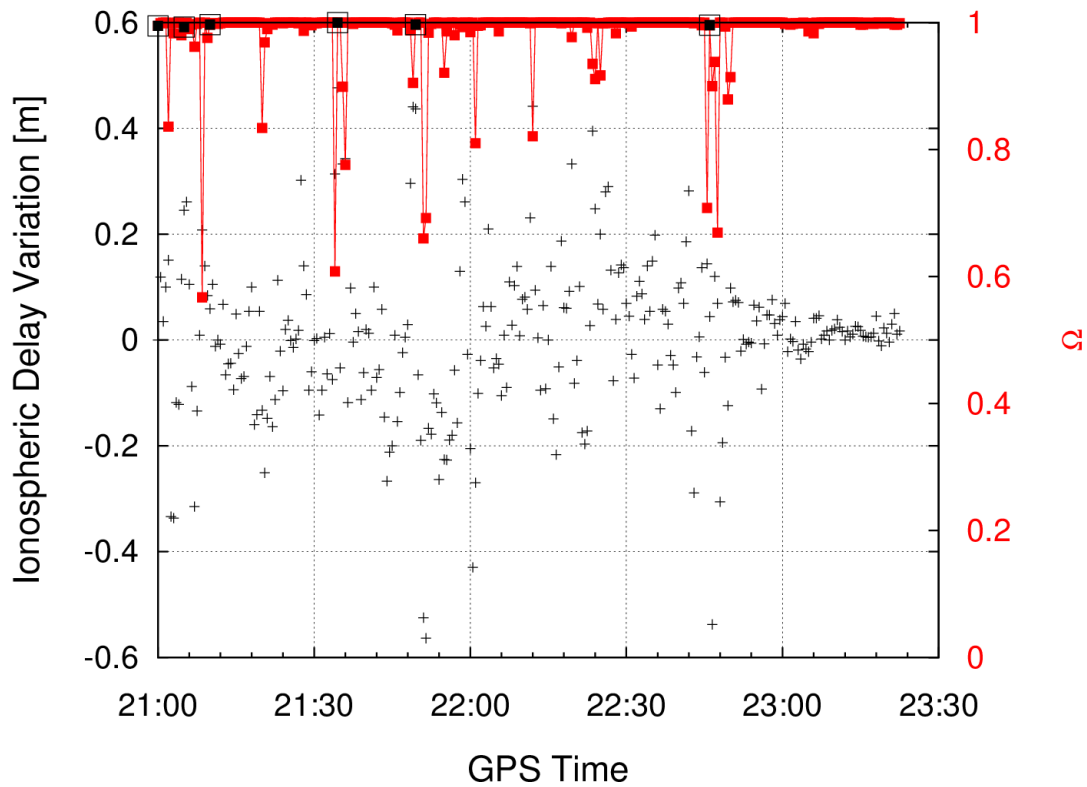
Figure 3.8: Cycle-slip correction results for satellite PRN 4 observed at station BAKE on 6 April 2011. Black squares identify occurrences of wrong cycle-slip fixing.

As mentioned previously, very few cycle slips were observed in the datasets processed in this study. Nonetheless, two occurrences of cycle slips affected satellite PRN 32 at station NAIN in Newfoundland and Labrador on 6 April 2011 over a 10-minute period. The satellite was tracked at a low elevation angle decreasing from approximately 15 to 10 degrees, resulting in noisy code measurements. The rate of change of the ionospheric delay variation increased from 0.02 m to 0.08 m per 30-second epoch over that interval. As discussed throughout this paper, explicitly forming linear combinations of observations and processing the data on a satellite-by-satellite basis is a suboptimal approach for cycle-slip correction. To emphasize this statement, Figure 3.9 presents time series of the Melbourne-Wübbena combination (left panel) and second-order differences of the carrier-phase geometry-free (GF) combination (right panel) over a 90-minute window. An estimate of the widelane cycle slip was obtained by averaging the fractional part of the Melbourne-Wübbena combination over each arc (represented by horizontal blue lines). While the magnitude of the first discontinuity could be computed precisely, the estimate of the second break cannot be reliably rounded to an integer. When the widelane cycle slip can be repaired, the effective wavelength of the geometry-free linear combination becomes 5.4 cm. As apparent from the right panel of Figure 3.9, the estimates at the time of the discontinuities lie very close to the border of the pull-in region (indicated by horizontal blue lines) and prevent proper identification of the cycle-slip candidates. Using the cycle-slip correction approach proposed in this paper then becomes useful in such a context: the range can be accurately defined using the time-differenced solution, and a constraint of $\sigma_{\delta I_0} < 0.1$ m allows one to obtain a

mathematically strong solution, regardless of code noise. In both cases, cycle slips were corrected within a single epoch and fixed as $\boldsymbol{n} = \{-42536340, -33145200\}$ at 22:59:00 and $\boldsymbol{n} = \{-1575420, -1227600\}$ at 23:09:30, with a value of $\Omega > 0.99$.
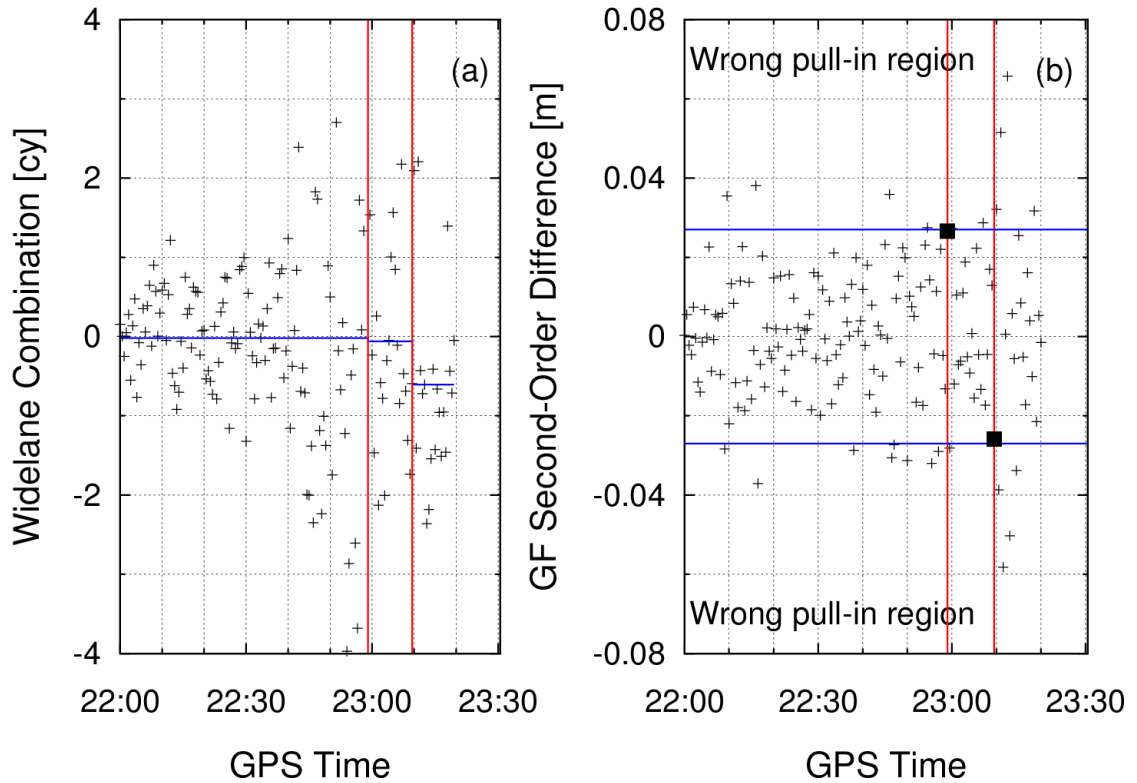
Figure 3.9: Widelane combination and geometry-free combination second-order differences for satellite PRN 32 observed at station NAIN on 6 April 2011.

In summary, cycle-slip correction over a 30-second interval is indeed possible during high ionospheric activity. However, there are risks associated with this procedure and cautious monitoring of the results is recommended. The performance of the proposed approach obviously improves for shorter time intervals, but the stochastic model must

still be carefully selected to avoid an improper selection of integer candidates. Note that this approach could be applied in real time since it allows correcting cycle slips within a single epoch.

3.6 Conclusion

This paper explained how the performance of popular cycle-slip detection and correction approaches could be greatly impacted by disturbances in the ionosphere. To overcome this limitation, alternate detection and correction procedures were proposed. In order to detect discontinuities in carrier-phase measurements, a geometry-based approach using time-differenced observations was suggested. Unknown effects are first estimated using code observations and allow quick satellite-by-satellite screening for cycle slips exceeding code-noise levels. Then, all carrier-phase observations not flagged in the first step are added to the system for a more reliable outlier identification based on quality control theory. Results from northern Canadian stations demonstrated that this technique leads to a significant reduction in the number of false detections.

When cycle slips are detected, their magnitude can also be estimated in a least-squares adjustment. It is, however, crucial that non-dispersive effects be accurately modelled, which can be achieved using observations from satellites not affected by cycle slips. The success rate associated with this approach also depends largely on the stochastic model

used. It is therefore imperative to properly account for observation noise, and to select *a priori* constraints appropriately. A validation procedure based on Bayes' marginal *a posteriori* probability was also adopted which takes into account both the stochastic model and biases in the estimated parameters. Occurrences of wrong cycle-slip fixing seem to mainly occur when the stochastic model is improperly specified.

When it comes to selecting an *a priori* constraint for the ionospheric delay variation, simulations have shown that it is preferable to slightly over-constrain this parameter, as long as the constraint allows the estimated parameters to belong to the proper pull-in region. With a loose constraint, a maximum ionospheric bias of approximately 67 cm can be tolerated until the cycle-slip estimates unavoidably fall within the wrong pull-in region. It is therefore recommended to deactivate the cycle-slip correction procedure in automated processes when an active ionosphere is detected and the time interval between epochs is more than a few seconds. Even if encouraging results are obtained, the increased measurement noise associated with an active ionosphere makes correcting cycle slips an ongoing challenge which requires further investigation.

Acknowledgements

92

editor and reviewers of this paper are also acknowledged for their helpful suggestions in improving this manuscript. This paper is published under the auspices of the NRCan Earth Sciences Sector as contribution number 20120071.

References

Baarda, W. (1968). "A testing procedure for use in geodetic networks." Publications on Geodesy, New Series, Vol. 2, No. 5, Netherlands Geodetic Commission, Delft, The Netherlands.

Banville, S., R. B. Langley, and M. C. Santos (2009). "The Precise Point Positioning Software Centre: an insight into online PPP services." Poster presented at the International Association of Geodesy (IAG) 2009 Meeting, Buenos Aires, Argentina, 31 August - 4 September.

Banville, S., R. B. Langley, S. Saito, and T. Yoshihara (2010). "Handling cycle slips in GPS data during ionospheric plasma bubble events." *Radio Science*, Vol. 45, RS6007. doi: doi:10.1029/2010RS004415.

Baselga, S. (2011). "Nonexistence of rigorous tests for multiple outlier detection in least-squares adjustment." *Journal of Surveying Engineering*, Vol. 137, No. 3, pp. 109-112. doi:10.1061/(ASCE)SU.1943-5428.0000048.

Bastos, L., and H. Landau (1988). "Fixing cycle slips in dual-frequency kinematic GPS-applications using Kalman filtering." *Manuscripta Geodaetica*, Vol. 13, No. 4, pp. 249-256.

Beutler, G., D. A. Davidson, R. B. Langley, R. Santerre, P. Vanicek, and D. E. Wells (1984). "Some theoretical and practical aspects of geodetic positioning using carrier phase difference observations of GPS satellites." Department of Geodesy and Geomatics Engineering Technical Report No. 109, University of New Brunswick, Fredericton, N.B., Canada.

Bisnath, S. B. (2000). "Efficient automated cycle-slip correction of dual-frequency kinematic GPS data." *Proceedings of the 13th International Technical Meeting of the*

Satellite Division of The Institute of Navigation (ION GPS 2000), Salt Lake City, Utah, 19-22 September, pp. 145-154.

Blewitt, G. (1990). "An automatic editing algorithm for GPS data." *Geophysical Research Letters,* Vol. 17, No. 3, pp. 199-202. doi:10.1029/GL017i003p00199.

Cai, C., Z. Liu, P. Xia, and W. Dai (2013). "Cycle slip detection and repair for undifferenced GPS observations under high ionospheric activity." *GPS Solutions*, Vol. 17, No. 2, pp. 247-260. doi:10.1007/s10291-012-0275-7.

Collin, F., and R. Warnant (1995). "Application of the wavelet transform for GPS cycle slip correction and comparison with Kalman filter." *Manuscripta Geodaetica*, Vol. 20, No. 3, pp. 161–172.

Dai, Z., S. Knedlik, and O. Loffeld (2009). "Instantaneous triple-frequency GPS cycle-slip detection and repair." *International Journal of Navigation and Observation*, Vol. 2009. doi:10.1155/2009/407231.

de Jong, K., and P. J. G. Teunissen (2000). "Minimal detectable biases of GPS observations for a weighted ionosphere." *Earth Planets Space* Vol. 52, pp. 857–862.

de Jonge, P. J., and C. C. J. M. Tiberius (1996). "The LAMBDA method for integer ambiguity estimation: implementation aspects." LGR Series 12, Delft Geodetic Computing Center, Delft University of Technology, Delft, The Netherlands.

de Lacy, M.C., M. Reguzzoni, F. Sansò, and G. Venuti (2008). "The Bayesian detection of discontinuities in a polynomial regression and its application to the cycle-slip problem." *Journal of Geodesy*, Vol. 82, No. 9, pp. 527–542. doi:10.1007/s00190-007-0203-8.

de Lacy, M.C., M. Reguzzoni, and F. Sansò (2012). "Real-time cycle slip detection in triple-frequency GNSS." *GPS Solutions*, Vol. 16, No. 3, pp. 353–362. doi:10.1007/s10291-011-0237-5.

Dow, J. M., R. E. Neilan, and C. Rizos (2009). "The International GNSS Service in a changing landscape of global navigation satellite systems." *Journal of Geodesy*, Vol. 83, No. 3-4, pp. 191–198. doi:10.1007/s00190-008-0300-3.

Euler, H.J., and B. Schaffrin (1991). "On a measure for the discernability between different ambiguity solutions in the static-kinematic GPS-mode." *IAG Symposia no. 107, Kinematic Systems in Geodesy, Surveying, and Remote Sensing*, Springer, Berlin Heidelberg, New York, pp. 285–295.

Feng, Y., and J. Wang (2011). "Computed success rates of various carrier phase integer estimation solutions and their comparison with statistical success rates." *Journal of Geodesy*, Vol. 85, No. 2, pp. 93–103. doi:10.1007/s00190-010-0418-y.

Gao, Y., and Z. Li (1999). "Cycle slip detection and ambiguity resolution algorithms for dual-frequency GPS data processing." *Marine Geodesy*, Vol. 22, No. 3, pp. 169–181. doi:10.1080/014904199273443.

Geng, J., X. Meng, A. Dodson, M. Ge, and F. Teferle (2010). "Rapid re-convergences to ambiguity-fixed solutions in precise point positioning." *Journal of Geodesy*, Vol. 84, No. 12, pp. 705–714. doi:10.1007/s00190-010-0404-4.

Griffiths, J., and J. Ray (2009). "On the precision and accuracy of IGS orbits." *Journal of Geodesy*, Vol. 83, No. 3, pp. 277–287. doi:10.1007/s00190-008-0237-6.

Hofmann-Wellenhof, B., H. Lichtenegger, and J. Collins (1997). *Global Positioning System: Theory and Practice*. 4th ed., Springer, Berlin Heidelberg, New York.

Jensen, A. B. O., and C. Mitchell (2011). "GNSS and the ionosphere: What's in store for the next solar maximum?" *GPS World*, Vol. 22, No. 2, pp. 40–48.

Kee, C., T. Walter, P. Enge, and B. Parkinson (1997). "Quality control algorithms on WAAS wide-area reference stations." *NAVIGATION: Journal of The Institute of Navigation*, Vol. 44, No. 1, Spring 1997, pp. 53–62.

Kim, D., and R. B. Langley (2001). "Instantaneous real-time cycle-slip correction of dual-frequency GPS data." *Proceedings of the International Symposium on Kinematic Systems in Geodesy, Geomatics and Navigation*, Banff, Alta., Canada, 5-8 June, pp. 255-264.

Knight, N.L., J. Wang, and C. Rizos (2010). "Generalized measures of reliability for multiple outliers." *Journal of Geodesy*, Vol. 84, No. 10, pp. 625–635. doi:10.1007/s00190-010-0392-4.

Komjathy, A., L. Sparks, A. J. Mannucci, and X. Pi (2003). "On the ionospheric impact of recent storm events on satellite-based augmentation systems in middle and low-latitude sectors." *Proceedings of the 16th International Technical Meeting of the Satellite Division of The Institute of Navigation (ION GPS/GNSS 2003)*, Portland, Ore., 9-12 September, pp. 2769–2776.

Kouba, J. (2009). "Guide to using International GNSS Service (IGS) products." [On-line] 20 May 2012. http://igscb.jpl.nasa.gov/.

Liu, Z. (2011). "A new automated cycle slip detection and repair method for a single dual-frequency GPS receiver." *Journal of Geodesy*, Vol. 85, No. 3, pp. 171–183. doi:10.1007/s00190-010-0426-y.

Mader, G. (1986). "Dynamic positioning using GPS carrier phase measurements." *Manuscripta Geodaetica*, Vol. 11, No. 4, pp. 272-277.

Mahalanobis, P. C. (1936). "On the generalised distance in statistics." *Proceedings of the National Institute of Sciences of India*, Vol. 2, No. 1, pp. 49–55.

Odijk, D., and S. Verhagen (2007). "Recursive detection, identification and adaptation of model errors for reliable high-precision GNSS positioning and attitude determination." *3rd International Conference on Recent Advances in Space Technologies (RAST '07)*, Istanbul, pp. 624–629. doi:10.1109/RAST.2007.4284068.

Skone, S., and K. Knudsen (2000). "Impact of ionospheric scintillations on SBAS performance." *Proceedings of the 13th International Technical Meeting of the Satellite Division of The Institute of Navigation (ION GPS 2000)*, Salt Lake City, Utah, 19-22 September, pp. 284–293.

Skone, S., K. Knudsen, and M. de Jong (2001). "Limitations in GPS receiver tracking performance under ionospheric scintillation conditions." *Physics and Chemistry of the Earth, Part A: Solid Earth and Geodesy*, Vol. 26, No. 6-8, pp. 613-621. doi:10.1016/S1464-1895(01)00110-7.

Teunissen, P. J. G. (1990). "Quality control in integrated navigation systems." *IEEE Aerospace and Electronic Systems Magazine*, Vol. 5, No. 7, pp. 35–41. doi:10.1109/62.134219.

Teunissen, P. J. G. (1991). "On the minimal detectable biases of GPS phase ambiguity slips." *Proceedings of DGPS'91, the First International Symposium on Real Time Differential Applications of the Global Positioning System*, Braunschweig, Germany, Vol. 2, pp. 679–686.

Teunissen, P. J. G. (1993). *Least-squares estimation of the integer GPS ambiguities*. Technical Report, LGR Series 6, Delft Geodetic Computing Centre, Delft University of Technology, Delft, The Netherlands.

Teunissen, P. J. G. (1997). "A canonical theory for short baselines. Part IV: Precision versus reliability." *Journal of Geodesy*, Vol. 71, No. 9, pp. 513–525. doi:10.1007/s001900050119.

Teunissen, P. J. G. (1998). "On the integer normal distribution of the GPS ambiguities." *Artificial Satellites*, Vol. 33, No. 2, pp. 49–64.

Teunissen, P. J. G. (1999a). "Minimal detectable biases of GPS data." *Journal of Geodesy*, Vol. 72, No. 4, pp. 236–244. doi:10.1007/s001900050163.

Teunissen, P. J. G. (1999b). "An optimality property of the integer least-squares estimator." *Journal of Geodesy*, Vol. 73, No. 11, pp. 587-593. doi:10.1007/s001900050269.

Teunissen, P. J. G. (2000). "The success rate and precision of the GPS ambiguities." *Journal of Geodesy*, Vol. 74, No. 3-4, pp. 321–326. doi:10.1007/s001900050289.

Teunissen, P. J. G. (2001). "Integer estimation in the presence of biases." *Journal of Geodesy*, Vol. 75, No. 7-8, pp. 399-407. doi:10.1007/s001900100191.

Teunissen, P. J. G. (2005). "GNSS ambiguity resolution with optimally controlled failure-rate." *Artificial Satellites*, Vol. 40, No. 4, pp. 219–227.

Teunissen, P. J. G., and A. Kleusberg (Eds.) (1998). *GPS for Geodesy*, 2nd ed., Springer, Berlin Heidelberg, New York.

Teunissen, P. J. G., P. Joosten, and C. C. J. M. Tiberius (1999). "Geometry-free ambiguity success rates in case of partial fixing." *Proceedings of the 1999 National Technical Meeting of The Institute of Navigation*, San Diego, Calif., 25-27 January, pp. 201–207.

Teunissen, P. J. G., P. Joosten, and C. C. J. M. Tiberius (2000). "Bias robustness of GPS ambiguity resolution." *Proceedings of the 13th International Technical Meeting of the Satellite Division of The Institute of Navigation (ION GPS-2000)*, Salt Lake City, Utah, 19-22 September, pp. 104–112.

Teunissen, P. J. G., and S. Verhagen (2009). "The GNSS ambiguity ratio-test revisited: a better way of using it." *Survey Review*, Vol. 41, No. 312, pp. 138–151. doi:10.1179/003962609X390058.

Van Meerbergen, G., A. Simsky, and F. Boon (2010). "A novel decision directed Kalman filter to improve RTK performance." *Proceedings of the 23rd International Technical Meeting of the Satellite Division of The Institute of Navigation (ION GNSS 2010)*, Portland, Ore., 21-24 September, pp. 3268–3276.

Verhagen, S. (2004). "Integer ambiguity validation: an open problem?" *GPS Solutions*, Vol. 8, No. 1, pp. 36–43. doi:10.1007/s10291-004-0087-5.

Verhagen, S., and P. J. G. Teunissen (2006). "On the probability density function of the GNSS ambiguity residuals." *GPS Solutions*, Vol. 10, No. 1, pp. 21–28. doi:10.1007/s10291-005-0148-4.

Wells, D. E., and E. J. Krakiwsky (1971). *The Method of Least-squares*. Department of Geodesy and Geomatics Engineering Lecture Notes 18, University of New Brunswick, Fredericton, N.B., Canada.

Xu, P. (2006). "Voronoi cells, probabilistic bounds and hypothesis testing in mixed integer linear models." *IEEE Transactions on Information Theory*, Vol. 52, No. 7, pp. 3122–3138. doi:10.1109/TIT.2006.876356.

Zhang, X., and X. Li (2012). "Instantaneous re-initialization in real-time kinematic PPP with cycle slip fixing." *GPS Solutions*, Vol. 16, No. 3, pp. 315–327. doi:10.1007/s10291-011-0233-9.

CHAPTER 4

MONITORING THE IONOSPHERE USING INTEGER-LEVELLED GPS MEASUREMENTS

This chapter describes a new method for monitoring the ionosphere using GPS measurements. It is shown that, using PPP, a very precise measure of the total electron content between a satellite and a receiver can be obtained. This information can then be used for the computation of ionospheric delay corrections to improve convergence of PPP solutions, as shown in the next chapter. Appendix I provides additional background on the decoupled-clock model.

The following was originally published as:

Banville, S., W. Zhang, and R. B. Langley (2013). "Monitoring the ionosphere with integer-leveled GPS measurements," *GPS World*, Vol. 24, No. 3, March 2013, pp. 43-49, based on the following conference papers:

Banville, S., and R. B. Langley (2011). "Defining the basis of an integer-levelling procedure for estimating slant total electron content," *Proceedings of the 24th International Technical Meeting of the Satellite Division of The Institute of Navigation (ION GNSS 2011)*, Portland, Ore., 19-23 September, pp. 2542-2551,

and

Banville, S., W. Zhang, R. Ghoddousi-Fard, and R. B. Langley (2012). "Ionospheric monitoring using 'integer-levelled' observations," *Proceedings of the 25th International*

Technical Meeting of the Satellite Division of The Institute of Navigation (ION GNSS 2012), Nashville, Tenn., 17-21 September, pp. 2692-2701.

Modifications to the original manuscript were made only for proper identification of sections, figures and tables, as well as to assure the uniformity of symbol and equation notation throughout this dissertation. References were also inserted in this chapter based on the ION GNSS conference papers mentioned above.

4.1 Introduction

Representation and forecast of the electron content within the ionosphere is now routinely accomplished using GPS measurements [Komjathy et al., 2005]. The global distribution of permanent ground-based GPS stations can effectively monitor the evolution of electron structures within the ionosphere, serving a multitude of purposes including satellite-based communication and navigation.

It has been recognized early on that GPS measurements could provide an accurate estimate of the total electron content (TEC) along a satellite-receiver path [Jorgensen, 1978]. However, because of their inherent nature, phase observations are biased by an unknown integer number of cycles and do not provide an absolute value of TEC. Code measurements (pseudoranges), although they are not ambiguous, also contain frequency-

dependent biases, which again prevent a direct determination of TEC. The main advantage of code over phase is that the biases are satellite- and receiver-dependent, rather than arc-dependent. For this reason, the GPS community initially adopted, as a common practice, fitting the accurate TEC variation provided by phase measurements to the noisy code measurements, therefore removing the arc-dependent biases [Lanyi and Roth, 1988]. Several variations of this process were developed over the years, such as phase levelling [Wilson and Mannucci, 1993], code smoothing [Schaer, 1999], and weighted carrier-phase levelling [Stephens et al., 2011].

The main challenge at this point is to separate the code inter-frequency biases (IFBs) from the line-of-sight TEC. Since both terms are linearly dependent, a mathematical representation of the TEC is usually required to obtain an estimate of each quantity [Lanyi and Roth, 1988]. Misspecifications in the model and mapping functions were found to contribute significantly to errors in the IFB estimation, suggesting that this process would be better performed during nighttime when few ionospheric gradients are present [Coco et al., 1991]. IFB estimation has been an ongoing research topic for the past two decades are still remains an issue for accurate TEC determination [Coster and Komjathy, 2008].

A particular concern with IFB is the common assumptions regarding their stability. It is often assumed that receiver IFBs are constant during the course of a day and that satellite IFBs are constant for a monthly period. Studies have clearly demonstrated that intra-day variations of receiver instrumental biases exist, which could possibly be related

to temperature effects [Gao et al., 2001]. This assumption was shown to possibly introduce errors exceeding 5 TEC units (TECU) in the levelling process [Ciraolo et al., 2007], where 1 TECU corresponds to 0.162 metres of code delay or carrier advance at the GPS L_1 frequency (1575.42 MHz).

To overcome this limitation, one could look into using solely phase measurements in the TEC estimation process, and explicitly deal with the arc-dependent ambiguities [Wild et al., 1989; Leandro et al., 2007]. The main advantage of such strategy is to avoid code-induced errors, but a larger number of parameters need to be estimated, thereby weakening the strength of the adjustment. A comparison of the phase-only (arc-dependent) and phase-levelled (satellite-dependent) models showed that no model performs consistently better [Brunini and Azpilicueta, 2009]. It was found that the satellite-dependent model performs better at low-latitudes since the extra ambiguity parameters in the arc-dependent model can absorb some ionospheric features (e.g., gradients). On the other hand, when the mathematical representation of the ionosphere is realistic, the levelling errors are susceptible to impact more significantly the accuracy of the approach.

The advent of precise point positioning (PPP) opened the door to new possibilities for slant TEC (STEC) determination. Indeed, PPP can be used to estimate undifferenced carrier-phase ambiguity parameters on L_1 and L_2, which can then be used to remove the ambiguous characteristics of the carrier-phase observations. In order to obtain undifferenced ambiguities free from ionospheric effects, previous researchers have either

used the widelane/ionosphere-free (IF) combinations [Chen et al., 2004], or the Group and Phase Ionospheric Calibration (GRAPHIC) combinations [Abdel-Salam, 2005]. One critical problem with such approaches is that code biases propagate into the estimated ambiguity parameters [Banville et al., 2008]. Therefore, the resulting TEC estimates are still biased by unknown quantities, and might suffer from the unstable datum provided by the IFBs.

The recent emergence of ambiguity resolution in PPP [Ge et al., 2008; Laurichesse et al., 2009, Collins et al., 2010] presented sophisticated means of handling instrumental biases to estimate integer ambiguity parameters. One such technique is the decoupled-clock method which considers different clock parameters for the carrier-phase and code measurements [Collins et al., 2010]. In the present contribution, we present an "integer-levelling" method, based on the decoupled-clock model, which uses integer carrier-phase ambiguities obtained through PPP to level the carrier-phase observations.

4.2 Standard Levelling Procedure

This section briefly reviews the basic GPS functional model, as well as the observables usually used in ionospheric studies. A common levelling procedure is also presented, since it will serve as a basis for comparing the performance of our new method.

4.2.1 Ionospheric Observables

The standard GPS functional model of dual-frequency carrier-phase and code observations can be expressed as:

$$\Phi_1^j = \bar{\rho}^j - \mu_1 I^j + \lambda_1 \bar{N}_1^j + \varepsilon_{L_1^j} \tag{4.1}$$

$$\Phi_2^j = \bar{\rho}^j - \mu_2 I^j + \lambda_2 \bar{N}_2^j + \varepsilon_{L_2^j} \tag{4.2}$$

$$P_1^j = \bar{\rho}^j + \mu_1 I^j + \left(b_{P_1} - b_{P_1}^j\right) + \varepsilon_{P_1^j} \tag{4.3}$$

$$P_2^j = \bar{\rho}^j + \mu_2 I^j + \left(b_{P_2} - b_{P_2}^j\right) + \varepsilon_{P_2^j} \tag{4.4}$$

where Φ_i^j is the carrier-phase measurement to satellite j on the L_i link and, similarly, P_i^j is the code measurement on L_i. The term $\bar{\rho}^j$ is the biased ionosphere-free range between the satellite and receiver, which can be decomposed as:

$$\bar{\rho}^j = \rho^j + \left(dT - dt^j\right) + T^j. \tag{4.5}$$

The instantaneous geometric range between the satellite and receiver antenna phase centres is ρ^j. The receiver and satellite clock errors, respectively expressed as dT and dt^j, are expressed here in units of metres. The term T^j stands for the tropospheric delay, while the ionospheric delay on L_1 is represented by I^j and is scaled by the frequency-dependent constant μ_i, where $\mu_i = f_1^2/f_i^2$. The biased carrier-phase ambiguities are symbolized by $\bar{N}$ and are scaled by their respective wavelengths (λ_i). The ambiguities can be explicitly written as:

$$\bar{N}_i^j = N_i^j + b_{\Phi_i} + b_{\Phi_i}^j \tag{4.6}$$

where N_i^j is the integer ambiguity, b_{Φ_i} is a receiver-dependent bias, and $b_{\Phi_i}^j$ is a satellite-dependent bias. Similarly, b_{P_i} and $b_{P_i}^j$ are instrumental biases associated with code measurements. Finally, ε contains unmodelled quantities such as noise and multipath, specific to the observable. The overbar symbol indicates biased quantities.

In ionospheric studies, the geometry-free (GF) signal combinations are formed to eliminate non-dispersive terms and thus provide a better handle on the quantity of interest:

$$\Phi_{GF}^j = \Phi_1^j - \Phi_2^j = (\mu_2 - \mu_1)I^j + \lambda_1 \bar{N}_1^j - \lambda_2 \bar{N}_2^j \tag{4.7}$$

$$P_{GF}^j = P_1^j - P_2^j = (\mu_1 - \mu_2)I^j + \underbrace{\left(b_{P_1} - b_{P_2}\right)}_{IFB_r} - \underbrace{\left(b_{P_1}^j - b_{P_2}^j\right)}_{IFB^j} \tag{4.8}$$

where IFB_r and IFB^j represent the code inter-frequency biases for the receiver and satellite, respectively. They are also commonly referred to as differential code biases (DCBs). Note that the noise terms (ε) were neglected in these equations for the sake of simplicity.

4.2.2 Weighted-Levelling Procedure

As pointed out in the introduction, the ionospheric observables of equations 4.7 and 4.8 do not provide an absolute level of ionospheric delay due to instrumental biases

contained in the measurements. Assuming that these biases do not vary significantly in time, the difference between the phase and code observations for a particular satellite pass should be a constant value (provided that no cycle slip occurred in the phase measurements). The levelling process consists of removing this constant from each geometry-free phase observation in a satellite-receiver arc:

$$\bar{\bar{\Phi}}_{GF}^{j} = \Phi_{GF}^{j} - \frac{\sum w\left(\Phi_{GF}^{j} - P_{GF}^{j}\right)}{\sum w} \tag{4.9}$$

where the summation is performed for all observations forming the arc. An elevation-angle-dependent weight (w) can also be applied to minimize the noise and multipath contribution for measurements made at low elevation angles. The double-bar symbol indicates levelled observations.

4.3 Integer-Levelling Procedure

The procedure of fitting a carrier-phase arc to code observations might introduce errors caused by code noise, multipath or intra-day code bias variations. Hence, developing a levelling approach that relies solely on carrier-phase observations is highly desirable. Such an approach is now possible with the recent developments in PPP, allowing for ambiguity resolution on undifferenced observations. This procedure has gained significant momentum in the past few years, with several organizations generating "integer clocks" or fractional offset corrections for recovering the integer nature of the

106

undifferenced ambiguities. Among those organizations are, in alphabetical order, the Centre National d'Études Spatiale (CNES) [Laurichesse et al., 2009], GeoForschungsZentrum (GFZ) [Ge et al., 2008], GPS Solutions Inc. [Mervart et al., 2008], Jet Propulsion Laboratory (JPL) [Bertiger et al., 2010], Natural Resources Canada (NRCan) [Collins et al., 2010], and Trimble Navigation [Leandro et al., 2011]. With ongoing research to improve convergence time, it would be no surprise if PPP with ambiguity resolution would become the *de facto* methodology for processing data on a station-by-station basis. The results presented in this paper are based on the products generated at NRCan, referred to as "decoupled clocks" [Collins et al., 2010].

The idea behind integer levelling is to introduce integer ambiguity parameters on L_1 and L_2, obtained through PPP processing, into the geometry-free linear combination of equation (4.7). The resulting integer-levelled observations, in units of metres, can then be expressed as:

$$\bar{\bar{\Phi}}_{GF}^j = \Phi_{GF}^j - \lambda_1 \widehat{\bar{N}}_1^j + \lambda_2 \widehat{\bar{N}}_2^j = (\mu_2 - \mu_1)I^j + \bar{b}_{\Phi_{GF}} - \bar{b}_{\Phi_{GF}}^j \qquad (4.10)$$

where $\widehat{\bar{N}}_1^j$ and $\widehat{\bar{N}}_2^j$ are the ambiguities obtained from the PPP solution which should be, preferably, integer values. Since those ambiguities were obtained with respect to a somewhat arbitrary ambiguity datum, they do not allow instant recovery of an unbiased slant ionospheric delay [Banville and Langley, 2011]. This fact was highlighted in equation (4.10), which indicates that, even though the arc-dependency was removed from the geometry-free combination, there are still receiver- and satellite-dependent biases ($\bar{b}_{\Phi_{GF}}$ and $\bar{b}_{\Phi_{GF}}^j$, respectively) remaining in the integer-levelled observations. The latter

107

are thus very similar in nature to the standard-levelled observations, in the sense that the biases $\bar{b}_{\Phi_{GF}}$ and $\bar{b}^{j}_{\Phi_{GF}}$ replace the well-known IFBs. As a consequence, integer-levelled observations can be used with any existing software used for the generation of TEC maps. The motivation behind using integer-levelled observations is the mitigation of levelling errors, as explained in the next sections.

4.4 Slant TEC Evaluation

As a first step towards assessing the performance of integer-levelled observations, STEC values are derived on a station-by-station basis. The slant ionospheric delays are then compared for a pair of co-located receivers, as well as with global ionospheric maps (GIMs) produced by the International GNSS Service (IGS).

4.4.1 Levelling Error Analysis

Relative levelling errors between two co-located stations can be obtained by computing between-station differences of levelled observations [Ciraolo et al., 2007]:

$$\bar{\bar{\Phi}}^{j}_{GF(A)} - \bar{\bar{\Phi}}^{j}_{GF(B)} = \bar{b}_{\Phi_{GF}}(A) - \bar{b}_{\Phi_{GF}}(B) + \varepsilon^{j}_{l} \tag{4.11}$$

where subscripts A and B identify the stations involved, and ε_l is the levelling error. Since the distance between stations is short (within 100 metres, say), the ionospheric delays will cancel, and so will the satellite biases ($\bar{b}^j_{\Phi_{GF}}$), which are observed at both stations. The remaining quantities will be the (presumably constant) receiver biases and any levelling errors. Since there are no satellite-dependent quantities in equation (4.11), the differenced observations obtained should be identical for all satellites observed, provided that there are no levelling errors. Hence, equation (4.11) allows comparison of the performance of various levelling approaches.

This methodology has been applied to a baseline of approximately a couple of metres in length between stations WTZJ and WTZZ, in Wettzell, Germany. The observations of both stations from 2 March 2008 were levelled using a standard levelling approach [Wilson and Manucci, 1993], as well as the method described in this paper. Relative levelling errors computed using equation (4.11) are displayed in Figure 4.1, where each color represents a different satellite. It is clear that code noise and multipath does not necessarily average out over the course of an arc, leading to levelling errors sometimes exceeding a couple of TECU for the standard levelling approach (see panel (a)). On the other hand, integer-levelled observations agree fairly well between stations, where levelling errors were mostly eliminated. In one instance, at the beginning of the session, ambiguity resolution failed at both stations for satellite PRN 18, leading to a relative error of more or less 1.5 TECU. Still, the advantages associated with integer levelling should be obvious since the relative error of the standard approach is in the vicinity of -6 TECU for this satellite.
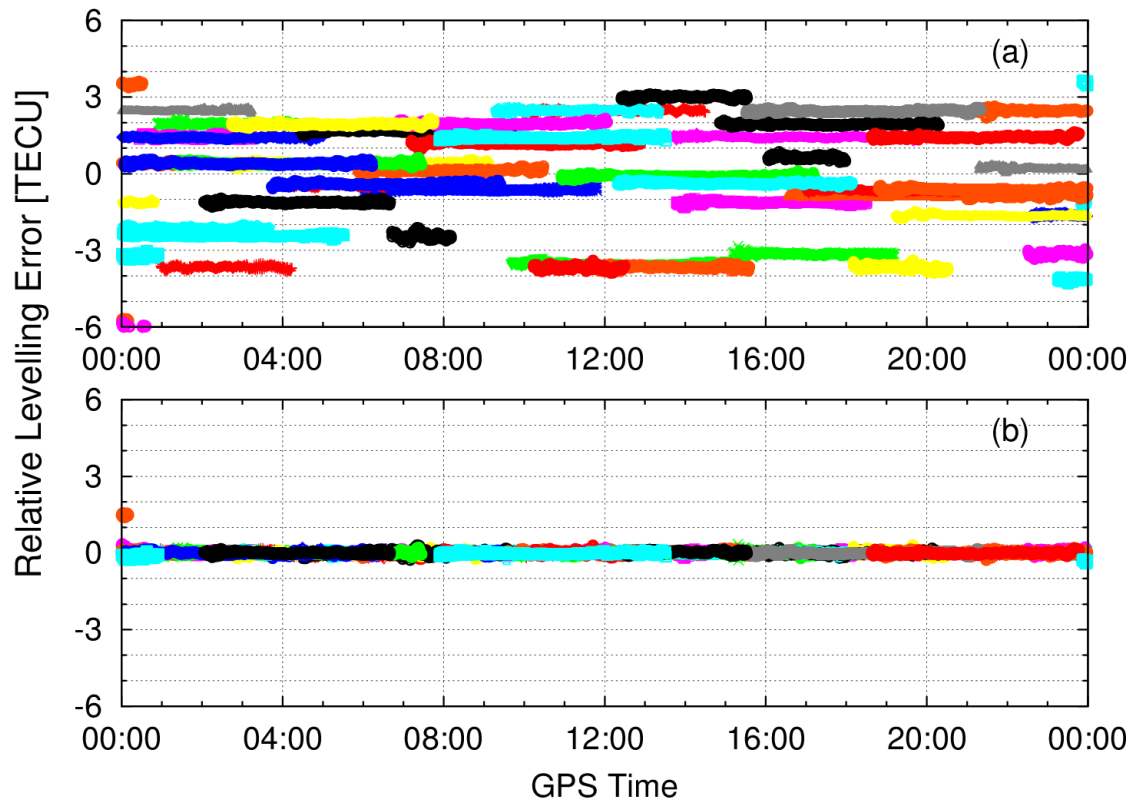
Figure 4.1: Relative levelling errors between stations WTZJ and WTZZ on 2 March 2008. (a) Standard-levelled observations. (b) Integer-levelled observations.

The magnitude of the levelling errors obtained for the standard approach agrees fairly well with previous studies [Ciraolo et al., 2007]. In the event that intra-day variations of the receiver DCBs are observed, even more significant biases were found to contaminate standard-levelled observations [Banville and Langley, 2011]. Since the decoupled-clock model used for ambiguity resolution explicitly accounts for possible variations of any equipment delays, the estimated ambiguities are not affected by such effects, leading to improved levelled observations.

4.4.2 STEC Comparisons

Once levelled observations are available, the next step consists of separating STEC from instrumental delays. As pointed out in the introduction, this task can be accomplished on a station-by-station basis using, for example, the single-layer ionospheric model. Replacing the slant ionospheric delays (I^j) in equation (4.10) by a bilinear polynomial expansion of VTEC leads to:

$$\bar{\bar{\Phi}}_{GF}^j = (\mu_2 - \mu_1)M(e^j)[a_0 + a_1\Delta\lambda + a_2\Delta\phi] + \bar{b}_{\Phi_{GF}} - \bar{b}_{\Phi_{GF}}^j \tag{4.12}$$

where M is the so-called single-layer or thin-shell mapping function (or obliquity factor) depending on the elevation angle (e) of the satellite. The time-dependent coefficients a_0, a_1, and a_2 determine the mathematical representation of the VTEC above the station. Gradients are modelled using $\Delta\lambda$, the difference between the longitude of the ionospheric pierce point and the longitude of the mean sun, and $\Delta\phi$, the difference between the geomagnetic latitude of the ionospheric pierce point and the geomagnetic latitude of the station. The estimation procedure described by Komjathy [1997] is followed in all subsequent tests. An elevation angle cutoff of 10 degrees was applied and the shell height used was 450 km. Since it is not possible to obtain absolute values for the satellite and receiver biases, the sum of all satellite biases was constrained to a value of zero. As a consequence, all estimated biases will contain a common (unknown) offset. STEC values, in TECU, can then be computed as:

$$STEC = \frac{\left(\overline{\overline{\Phi}}_{GF}^j - \hat{\overline{b}}_{\Phi_{GF}} + \hat{\overline{b}}_{\Phi_{GF}}^j\right)}{\mu_2 - \mu_1} \cdot \frac{(f_1)^2}{40.3 \cdot 10^{16}} \tag{4.13}$$

where the hat symbol denotes estimated quantities, and $\hat{\overline{b}}_{\Phi_{GF}}$ is equal to zero (i.e., it is not estimated) when biases are obtained on a station-by-station basis. The frequency, f_1, is expressed in Hz. The numerical constant 40.3, determined from values of fundamental physical constants, is sufficiently precise for our purposes, but is a rounding of the more precise value of 40.308.

While integer-levelled observations from co-located stations show good agreement, an external TEC source is required to make sure that both stations are not affected by common errors. For this purpose, Figure 4.2 compares STEC values computed from global ionosphere maps (GIM) produced by the IGS and STEC values derived from station WTZJ using both standard- and integer-levelled observations. The IGS claims root-mean-square errors on the order of 2-8 TECU for vertical TEC [IGS, 2012], although the ionosphere was quiet on the day selected meaning that errors on the low-end of that range are expected. Errors associated with the mapping function will further contribute to differences in STEC values. As apparent from Figure 4.2, no significant bias can be identified in integer-levelled observations. On the other hand, negative STEC values (not displayed in Figure 4.2) were obtained during nighttimes when using standard-levelled observations, a clear indication that levelling errors contaminated the observations.
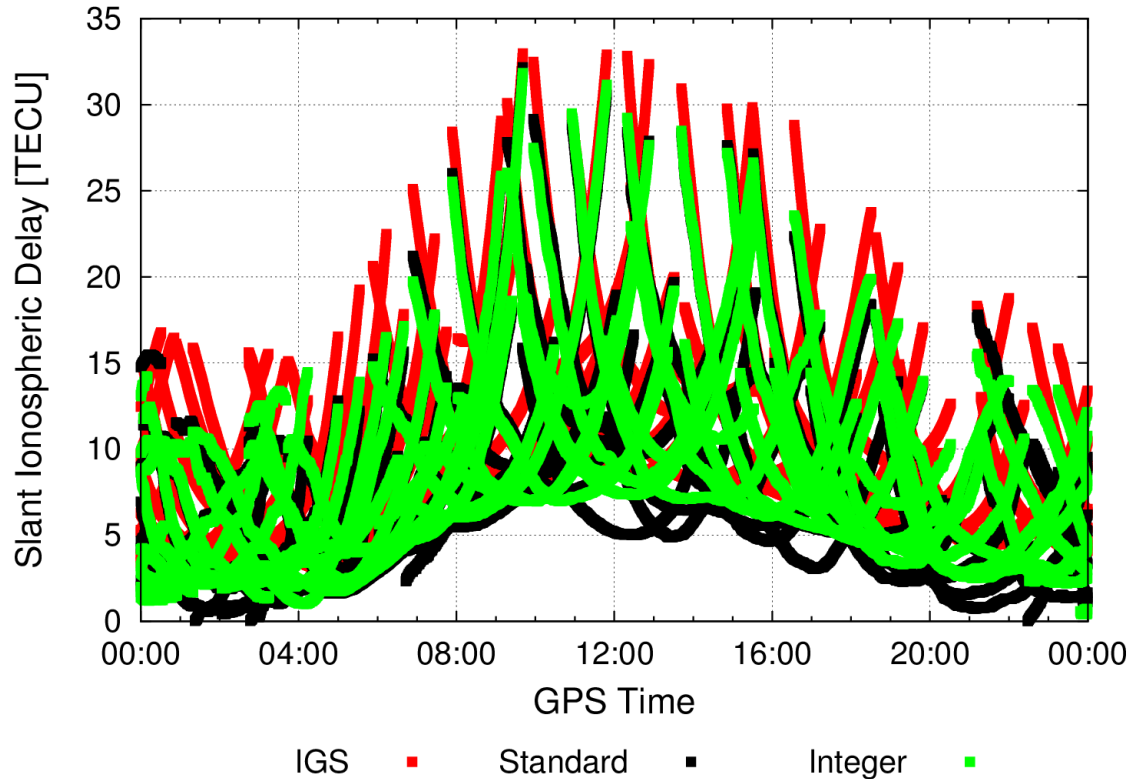
Figure 4.2: Comparison between STEC values obtained from a global ionospheric map, and from station WTZJ using standard- and integer-levelled observations.

4.4.3 STEC Evaluation in the Positioning Domain

Validation of slant ionospheric delays can also be performed in the positioning domain. For this purpose, a station's coordinates in static mode (that is, one set of coordinates estimated per session) are estimated using (unsmoothed) single-frequency code observations with precise orbit and clock corrections from the IGS [Griffiths and

113

Ray, 2009] and various ionosphere correction sources. Figure 4.3 illustrates the convergence of the 3D position error for station WTZZ, using STEC corrections from the three sources introduced previously, namely: 1) global ionospheric maps from the IGS, 2) STEC values from station WTZJ derived from standard levelling, and 3) STEC values from station WTZJ derived from integer levelling. The reference coordinates were obtained from static processing based on dual-frequency carrier-phase and code observations. The benefits of the integer-levelled corrections are obvious, with the solution converging to better than 10 cm. Even though the distance between stations is short, using standard-levelled observations from WTZJ leads to a biased solution as a result of arc-dependent levelling errors. Using a TEC map from the IGS provides a decent solution considering that it is a global model, although the solution is again biased.

This station-level analysis allowed us to confirm that integer-levelled observations can seemingly eliminate levelling errors, provided that carrier-phase ambiguities are fixed to proper integer values. Furthermore, it is possible to retrieve unbiased STEC values from those observations by using common techniques for isolating instrumental delays. The next step will consist of examining the impacts of reducing levelling errors on VTEC.
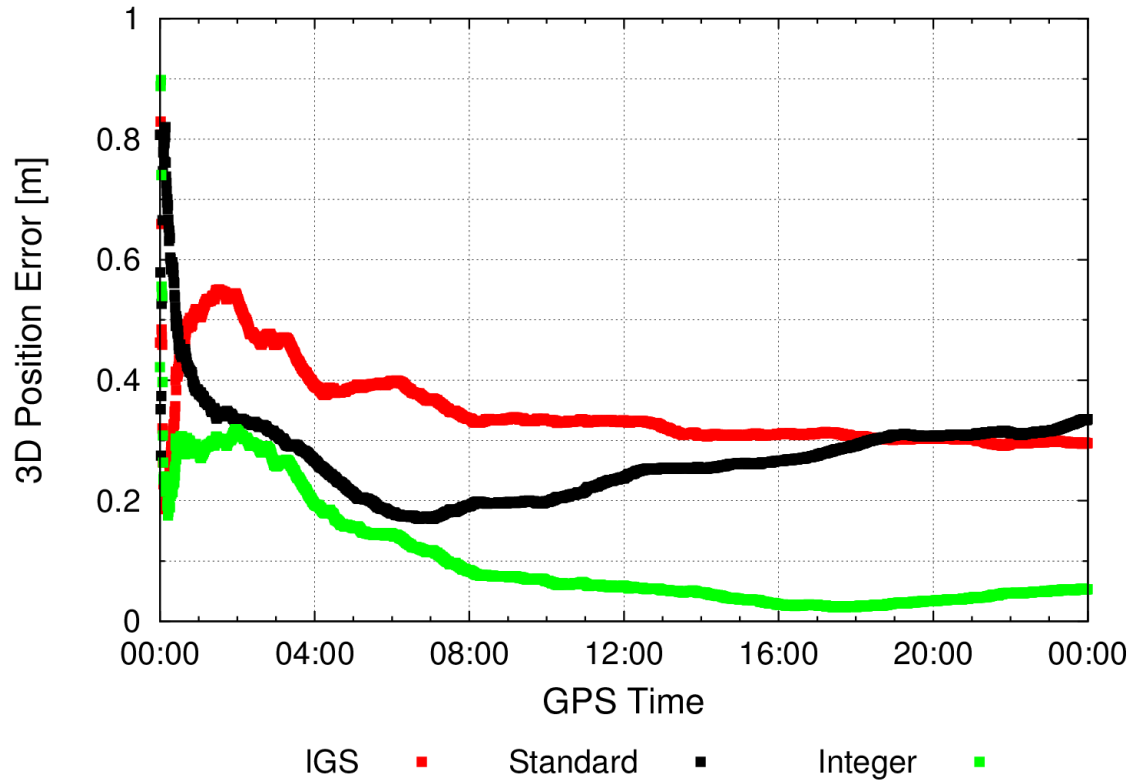
Figure 4.3: Single-frequency code-based positioning results for station WTZZ (in static mode) using different ionosphere correction sources: GIM, and STEC values from station WTZJ using standard- and integer-levelled observations.

4.5 VTEC Evaluation

When using the single-layer model, vertical TEC values can be derived from the STEC values of equation (4.13) using:

115

$$VTEC = \frac{STEC}{M(e^j)}.$$ (4.14)

Dividing *STEC* by the mapping function will also reduce any bias caused by the levelling procedure. Hence, measures of VTEC made from a satellite at a low elevation angle will be less impacted by levelling errors. When the satellite reaches the zenith, then any bias in the observation will fully propagate into the computed VTEC values. On the other hand, the uncertainty of the mapping function is larger at low-elevation angles, which should be kept in mind when analyzing the results.

Using data from a small regional network allows us to assess the compatibility of the VTEC quantities between stations. For this purpose, GPS data collected as a part of the Western Canada Deformation Array (WCDA) network [Dragert et al., 1995], still from 2 March 2008, was used. The stations of this network, located on and near Vancouver Island in Canada, are indicated in Figure 4.4. Following the model of equation (4.12), all stations were integrated into a single adjustment to estimate receiver and satellite biases as well as a triplet of time-varying coefficients for each station. STEC values were then computed as per equation (4.13), and VTEC values were finally derived from equation (4.14). This procedure was again performed for both standard- and integer-levelled observations.

Figure 4.4: Network of stations used in the VTEC evaluation procedures.

To facilitate the comparison of VTEC values spanning a whole day and to account for ionospheric gradients, differences with respect to the IGS GIM were computed. The results, plotted by elevation angle, are displayed in Figure 4.5 for all seven stations processed (all satellite arcs from the same station are plotted using the same color). The overall agreement between the global model and the station-derived VTECs is fairly good, with a bias of about 1 TECU. Still, the top panel demonstrates that, at high elevation angles, discrepancies between VTEC values derived from standard-levelled observations and the ones obtained from the model have a spread of nearly 6 TECU.

117

With integer-levelled observations (see bottom panel), this spread is reduced to approximately 2 TECU. It is important to realize that the dispersion can be explained by several factors, such as remaining levelling errors, the inexact receiver and satellite bias estimates, and inaccuracies of the global model. It is nonetheless expected that levelling errors account for the most significant part of this error for standard-levelled observations.

For satellites observed at a lower elevation angle, the spread between arcs is similar for both methods (except for station UCLU in panel (a) for which the estimated station IFB parameter looks significantly biased). As stated previously, the reason is that levelling errors are reduced when divided by the mapping function. The latter also introduces further errors in the comparisons, which explains why a wider spread should typically be associated with low-elevation-angle satellites. Nevertheless, it should be clear from Figure 4.5 that integer-levelled observations offer a better consistency than standard-levelled observations.
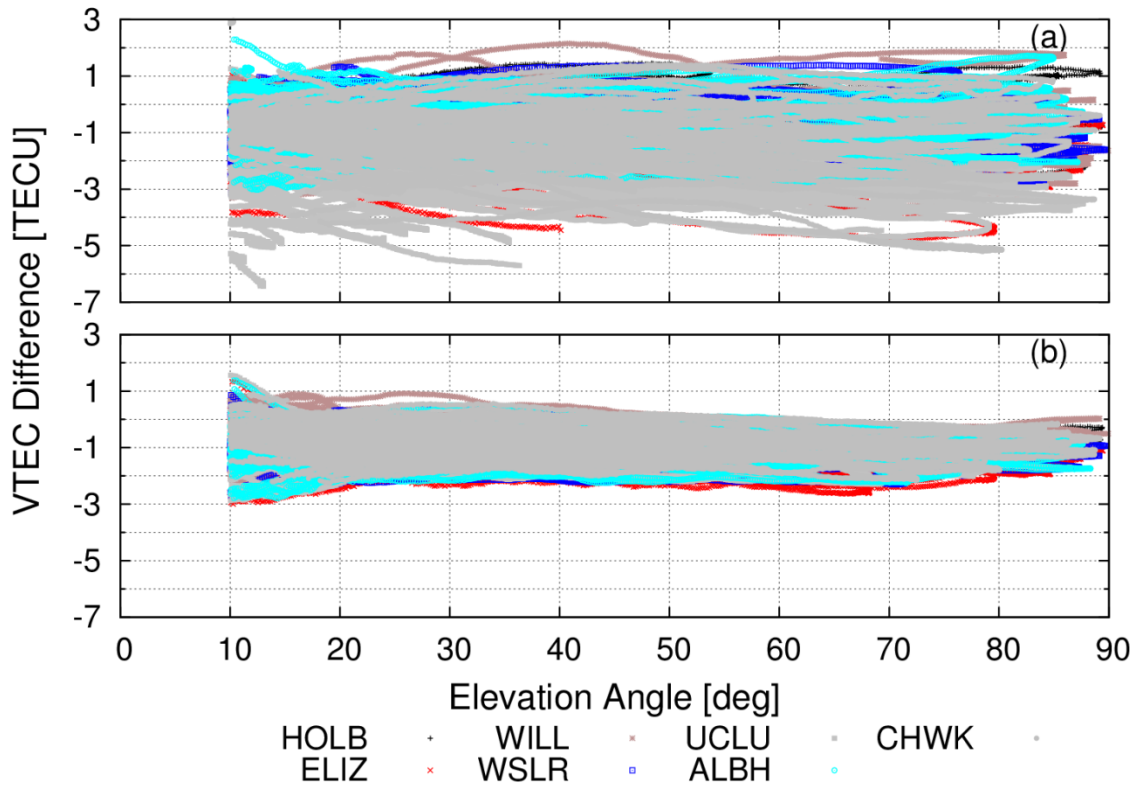
Figure 4.5: VTEC differences with respect to the IGS GIM, for all satellite arcs as a function of the elevation angle of the satellite, using (a) standard-levelled observations and (b) integer-levelled observations.

4.6 Conclusion

The technique of integer levelling consists of introducing (preferably) integer ambiguity parameters obtained from PPP into the geometry-free combination of observations. This process removes the arc dependency of the signals, and allows integer-

levelled observations to be used with any existing TEC estimation software. While levelling errors of a few TECU exist with current procedures, this type of error can be eliminated through use of our procedure, provided that carrier-phase ambiguities are fixed to the proper integer values. As a consequence, STEC values derived from nearby stations are typically more consistent with each other. Unfortunately, subsequent steps involved in generating VTEC maps, such as transforming STEC to VTEC and interpolating VTEC values between stations, attenuate the benefits of using integer-levelled observations.

There are still ongoing challenges associated with the GIM generation process, particularly in terms of latency and three-dimensional modelling [Krankowski, 2011]. Since ambiguity resolution in PPP can be achieved in real time [Laurichesse, 2011], we believe that integer-levelled observations could benefit near-real-time ionosphere monitoring. Since ambiguity parameters are constant for a satellite pass (provided that there are no cycle slips), integer ambiguity values (i.e., the levelling information) can be carried over from one map generation process to the next. Therefore, this methodology could reduce levelling errors associated with short arcs, for instance.

Another prospective benefit of integer-levelled observations is the reduction of levelling errors contaminating data from low-Earth-orbit (LEO) satellites, which are of particular importance for three-dimensional TEC modelling. Due to their low orbits, LEO satellites typically track a GPS satellite for a short period of time. As a consequence, those short arcs do not allow code noise and multipath to average out, potentially leading

to important levelling errors. On the other hand, undifferenced ambiguity fixing for LEO satellites has been demonstrated [Laurichesse et al., 2009], and could be a viable solution to this problem.

Evidently, more research needs to be conducted to fully assess the benefits of integer-levelled observations. Still, we think that the results shown herein are encouraging and offer potential solutions to current challenges associated with ionosphere monitoring.

Acknowledgements

References

Abdel-Salam, M. A. (2005). *Precise Point Positioning Using Un-differenced Code and Carrier Phase Observations*. Ph.D. Dissertation, UCGE Reports No. 20229, University of Calgary, Canada, 206 pp.

Banville, S., and R. B. Langley (2011). "Defining the basis of an integer-levelling procedure for estimating slant total electron content," *Proceedings of the 24th*

International Technical Meeting of the Satellite Division of The Institute of Navigation (ION GNSS 2011), Portland, Ore., 19-23 September 2011, pp. 2542-2551.

Banville, S., R. Santerre, M. Cocard, and R. B. Langley (2008). "Satellite and receiver phase bias calibration for undifferenced ambiguity resolution," *Proceedings of the 2008 National Technical Meeting of The Institute of Navigation*, San Diego, Calif., 28-30 January, pp. 711-719.

Bertiger, W., S. D. Desai, B. Haines, N. Harvey, A. W. Moore, S. Owen, and J. P. Weiss (2010). "Single receiver phase ambiguity resolution with GPS data," *Journal of Geodesy*, Vol. 84, No. 5, pp. 327-337. doi: 10.1007/s00190-010-0371-9.

Brunini, C., and F. J. Azpilicueta (2009). "Accuracy assessment of the GPS-based slant total electron content," *Journal of Geodesy*, Vol. 83, No. 8, pp. 773-785. doi: 10.1007/s00190-008-0296-8.

Chen, W., C. Hu, S. Gao, Y. Chen, X. Ding, and S. C. Kowk (2004). "Precise estimation of absolute ionospheric delay based on GPS active network," *Proceedings of the 17th International Technical Meeting of the Satellite Division of The Institute of Navigation (ION GNSS 2004)*, Long Beach, Calif., 21-24 September, pp. 420-427.

Ciraolo, L., F. Azpilicueta, C. Brunini, A. Meza, and S. M. Radicella (2007). "Calibration errors on experimental slant total electron content (TEC) determined with GPS," *Journal of Geodesy*, Vol. 81, No. 2, pp. 111-120. doi: 10.1007/s00190-006-0093-1.

Coco, D. S., C. E. Coker, S. R. Dahlke, and J. R. Clynch (1991). "Variability of GPS satellite differential group delay biases," *IEEE Transactions on Aerospace and Electronic Systems*, Vol. 27, No. 6, pp. 931-938. doi: 10.1109/7.104264.

Collins, P., S. Bisnath, F. Lahaye, and P. Héroux (2010). "Undifferenced GPS ambiguity resolution using the decoupled clock model and ambiguity datum fixing," *NAVIGATION: Journal of The Institute of Navigation*, Vol. 57, No. 2, Summer 2010, pp. 123-135.

Coster, A., and A. Komjathy (2008). "Space weather and the Global Positioning System," *Space Weather*, Vol. 6, No. 6, S06D04. doi: 10.1029/2008SW000400.

Dragert, H., X. Chen, and J. Kouba (1995). "GPS monitoring of crustal strain in southwest British Columbia with the western Canada deformation array," *Geomatica*, Vol. 49, No. 3, pp. 301-313.

Gao, Y., F. Lahaye, P. Héroux, X. Liao, N. Beck, and M. Olynik (2001). "Modeling and estimation of C1–P1 bias in GPS receivers," *Journal of Geodesy*, Vol. 74, No. 9, pp. 621-626. doi: 10.1007/s001900000117.

Ge, M., G. Gendt, M. Rothacher, C. Shi, and J. Liu (2008). "Resolution of GPS carrier-phase ambiguities in precise point positioning (PPP) with daily observations," *Journal of Geodesy*, Vol. 82, No. 7, pp. 389-399. doi: 10.1007/s00190-007-0187-4.

Griffiths J., and J. Ray (2009). "On the precision and accuracy of IGS orbits," *Journal of Geodesy,* Vol. 83, No. 3, pp. 277–287. doi: 10.1007/s00190-008-0237-6.

IGS (2012). International GNSS Service (IGS) website. [On-line] 18 September 2012. http://igscb.jpl.nasa.gov/components/prods.html.

Jorgensen, P. S. (1978). *Ionospheric Measurements from NAVSTAR Satellites*. Report prepared for Space and Missile Systems Organization, Air Force Systems Command, Los Angeles Air Force Station, Los Angeles, Calif. by Satellite Systems Division of the Aerospace Corporation, El Segundo, Calif., December, SAMSO-TR-79-29, 48 pp.

Komjathy, A. (1997). *Global Ionospheric Total Electron Content Mapping Using the Global Positioning System*. Ph. D. dissertation, Technical Report 188, Department of Geodesy and Geomatics Engineering, University of New Brunswick, Fredericton, New Brunswick, Canada.

Komjathy, A., L. Sparks, B. Wilson, and A. J. Mannucci (2005). "Automated daily processing of more than 1000 ground-based GPS receivers to study intense ionospheric storms," *Radio Science*, Vol. 40, RS6006. doi:10.1029/2005RS003279.

Krankowski, A. (2011). "IGS ionosphere working group technical report 2011," In International GNSS Service Technical Report 2011, Astronomical Institute, University of Bern, [On-line] 18 September 2012. ftp://igs.org/pub/resource/pubs/2011_techreport.pdf

Lanyi, G. E., and T. Roth (1988). "A comparison of mapped and measured total ionospheric electron content using Global Positioning System and beacon satellite observations," *Radio Science*, Vol. 23, No. 4, pp. 483-492. doi:10.1029/RS023i004p00483.

Laurichesse, D. (2011). "The CNES real-time PPP with undifferenced integer ambiguity resolution demonstrator," *Proceedings of the 24th International Technical Meeting of the Satellite Division of The Institute of Navigation (ION GNSS 2011)*, Portland, Ore., 19-23 September 2011, pp. 654-662.

Laurichesse, D., F. Mercier, J.-P. Berthias, P. Broca, and L. Cerri (2009). "Integer ambiguity resolution on undifferenced GPS phase measurements and its application to PPP and satellite precise orbit determination," *NAVIGATION: Journal of The Institute of Navigation*, Vol. 56, No. 2, Summer 2009, pp. 135-149.

Leandro, R., H. Landau, M. Nitschke, M. Glocker, S. Seeger, X. Chen, A. Deking, M. Ben Tahar, F. Zhang, K. Ferguson, R. Stolz, N. Talbot, G. Lu, T. Allison, M. Brandl, V.

Gomez, W. Cao, and A. Kipka (2011). "RTX positioning: the next generation of cm-accurate real-time GNSS positioning," *Proceedings of the 24th International Technical Meeting of the Satellite Division of The Institute of Navigation (ION GNSS 2011)*, Portland, Ore., 19-23 September 2011, pp. 1460-1475.

Leandro, R. F., M. C. Santos, and R. B. Langley (2007). "PPP-based ionosphere activity monitoring," *Proceedings of the 20th International Technical Meeting of the Satellite Division of The Institute of Navigation (ION GNSS 2007)*, Fort Worth, Texas, 25-28 September, pp. 2849-2853.

Mervart, L., Z. Lukes, C. Rocken, and T. Iwabuchi (2008). "Precise point positioning with ambiguity resolution in real-time," *Proceedings of the 21st International Technical Meeting of the Satellite Division of The Institute of Navigation (ION GNSS 2008)*, Savannah, Ga., 16-19 September 2008, pp. 397-405.

Schaer, S. (1999). *Mapping and Predicting the Earth's Ionosphere Using the Global Positioning System.* Ph.D. dissertation, Astronomical Institute, University of Berne, Switzerland, 205 pp.

Stephens, P., A. Komjathy, B. Wilson, and A. Mannucci (2011). "New leveling and bias estimation algorithms for processing COSMIC/FORMOSAT-3 data for slant total electron content measurements," *Radio Science*, Vol. 46, RS0D10. doi:10.1029/2010RS004588.

Wild, U., G. Beutler, W. Gurtner, and M. Rothacher (1989). "Estimating the ionosphere using one or more dual frequency GPS receivers," *Proceedings of the Fifth International Geodetic Symposium on Satellite Positioning*, Vol. 2, Las Cruces, N.M., 13-17 March, pp. 724-736.

Wilson, B. D., and A. J. Mannucci (1993). "Instrumental biases in ionospheric measurements derived from GPS data," *Proceedings of the 6th International Technical Meeting of the Satellite Division of The Institute of Navigation (ION GPS 1993)*, Salt Lake City, Utah, 22-24 September, pp. 1343-1351.

CHAPTER 5

GLOBAL AND REGIONAL IONOSPHERIC CORRECTIONS FOR FASTER PPP CONVERGENCE

The previous chapter described how ionospheric corrections could be generated based on "integer-levelled" observations. In this chapter, it is demonstrated that the differential phase biases obtained from integer levelling are required for including external ionospheric corrections into a PPP solution based on the decoupled-clock model. By using additional constraints on the ionosphere, instantaneous convergence of PPP solutions can be obtained under certain circumstances. Appendix I provides additional details on the propagation of datum parameters in the decoupled-clock model.

The following was originally published as:

Banville, S., P. Collins, W. Zhang, and R. B. Langley (2013). "Global and regional ionospheric corrections for faster PPP convergence," *NAVIGATION: The Journal of The Institute of Navigation*, Vol. 61, No. 2, Summer 2014, pp. 115-124.

Modifications to the original manuscript were made only for proper identification of sections, figures and tables, as well as to assure the uniformity of symbol and equation notation throughout this dissertation.

Abstract

Rapid convergence of precise point positioning (PPP) solutions to cm-level precision is a key factor for many applications. One means of accelerating this convergence is to exploit the benefit of information on the ionosphere. In order to preserve the integer nature of carrier-phase ambiguities in PPP, it is imperative that ionospheric corrections be provided with a set of compatible satellite phase biases. When using the decoupled-clock model, global ionospheric maps (GIMs) currently provided by the International GNSS Service are not directly applicable to PPP with ambiguity resolution. This paper describes a methodology for incorporating external ionospheric corrections into this model. It is shown that the use of both GIMs and ambiguity resolution can potentially reduce the convergence time of PPP to 10-cm horizontal accuracies from 30 to 4.5 minutes (68th percentile), while a regional network with inter-station spacing of 150 km can reach this threshold instantaneously under favourable ionospheric conditions.

5.1 Introduction

One of the main applications of total electron content (TEC) estimation from a ground network of GPS receivers is the mitigation of ionospheric effects for single-frequency code-based users. For instance, satellite-based augmentation systems (SBAS) generate ionospheric corrections allowing improved accuracy and integrity for aviation purposes

[Enge et al., 1996]. Global ionospheric maps (GIMs) are also routinely produced by the International GNSS Service (IGS) [Hernández-Pajares et al., 2009], and were shown to improve post-mission positioning for low-cost receivers [Beran, 2008].

Estimating TEC using dual-frequency GPS receivers typically involves fitting the precise but ambiguous carrier-phase observations to code (pseudorange) observations [Lanyi and Roth 1988]. This process removes the arc dependency of carrier phases, resulting in smooth TEC time series biased only by the so-called receiver and satellite differential code biases (DCBs). Using a mathematical representation of the ionosphere separates TEC from equipment delays, and DCB values are usually obtained as a by-product of TEC estimation [Schaer, 1999]. DCBs are also required to maintain the consistency of single-frequency positioning solutions, as a consequence of satellite clock corrections being computed from ionosphere-free code observations [Collins et al. 2005].

For high-precision applications, the precise point positioning (PPP) methodology typically relies on dual-frequency linear combinations to remove first-order ionospheric effects [Kouba and Héroux, 2001]. With recent advances in PPP, equipment delays can be properly isolated or estimated to recover the integer property of carrier-phase ambiguities [Ge et al., 2008; Laurichesse et al., 2009; Collins et al., 2010]. Even though ambiguity resolution can be achieved in PPP, a convergence time of up to several tens of minutes is still required for reliable fixing of the ambiguities. This is a consequence of using ionosphere-free combinations, which do not allow constraining of slant ionospheric delays using external information. This additional source of information, implicitly

127

present in short-baseline differential positioning, is the key to fast ambiguity resolution [Odijk, 2002]. For this purpose, an extended PPP model allowing explicit estimation of slant ionospheric delay parameters was proposed to allow quick re-convergence to ambiguity-fixed solutions following a discontinuity in measurements [Geng et al., 2010; Collins and Bisnath, 2011].

While this approach permits bridging of discontinuities, it does not directly help in reducing the initial convergence period. A cold start requires ionospheric information external to the PPP solution. In addition, the estimated slant ionospheric delays in PPP contain integer-biased receiver and satellite phase offsets [Collins and Bisnath, 2011] and, as a consequence, are not directly compatible with TEC information. Nevertheless, all PPP users deal with identical satellite offsets, meaning that slant ionospheric delays can be provided from nearby PPP users in a peer-to-peer type of network to potentially allow instantaneous ambiguity resolution [Collins et al., 2012]. Another solution consists of using the single-layer model to benefit from the spatial correlation of the ionosphere over a station [Li, 2012]. The single-layer model allows separation of equipment delays from ionospheric delays and permits constraining of the vertical TEC (VTEC) using external sources.

Ionospheric corrections generated using a regional or even a global network of stations could also be beneficial for reducing the convergence time in PPP [Drescher et al., 2013]. As stated above, those corrections need to be compatible with the PPP functional model. Current GIMs, based on phase-smoothed code observations, can only

provide DCB information beneficial to single-frequency code-based users. To preserve the integer nature of ambiguities in PPP, ionospheric corrections must be combined with satellite phase biases matching the ones contained in the estimated slant ionospheric delays at the user end. Computing of the satellite phase biases required to produce ionospheric corrections compatible with PPP implies that a new set of observables should be used for the generation of TEC maps. Such observables were introduced by Banville and Langley [2011] and termed "integer-levelled observations."

This paper first reviews the underlying concepts of the decoupled-clock model (DCM) for ambiguity resolution in PPP. The extended DCM (EDCM) is then presented to illustrate how external TEC information can be introduced in the PPP solution. The integer-levelling procedure is also described as a means of generating ionospheric corrections with phase biases compatible with the DCM. After assessing the quality of global and regional ionospheric corrections, the benefits of using external ionospheric information for PPP with ambiguity resolution is evaluated using a set of Canadian continuously-operating reference stations.

5.2 The Decoupled-Clock Model (DCM)

The DCM is essentially an extension of the standard PPP model to allow estimation of ambiguity parameters as formal integer values [Collins et al., 2010]. The current

implementation is based on the ionosphere-free (IF) carrier-phase and code measurements, as well as on the Melbourne-Wübbena (MW) combination [Melbourne, 1985; Wübbena, 1985]:

$$\Phi_{IF}^j = \rho^j + T^j + \left(\overline{dT}_{\Phi_{IF}} - \overline{dt}_{\Phi_{IF}}^j\right) + (\alpha_{IF}\lambda_1 + \beta_{IF}\lambda_2)\bar{N}_1^j - \beta_{IF}\lambda_{WL}\bar{N}_{WL}^j + \varepsilon_{\Phi_{IF}}$$

$$P_{IF}^j = \rho^j + T^j + \left(\overline{dT}_{P_{IF}} - \overline{dt}_{P_{IF}}^j\right) + \varepsilon_{P_{IF}} \tag{5.1}$$

$$\Phi_{MW}^j = \left(\bar{b}_{\Phi_{MW}} - \bar{b}_{\Phi_{MW}}^j\right) + \lambda_{WL}\bar{N}_{WL}^j + \varepsilon_{\Phi_{MW}}$$

where the overbar symbol denotes biased quantities, and

j	identifies a given satellite
Φ	is a carrier-phase measurement (m)
P	is a code measurement (m)
ρ	is the instantaneous range between the phase centres of the satellite and receiver antennas, including displacements due to earth tides and ocean loading and relativistic effects (m)
T	is the tropospheric delay (m)
dT	is the receiver clock offset from GPS time and associated receiver equipment delays for a given observable (m)
dt	is the satellite clock offset from GPS time and associated satellite equipment delays for a given observable (m)
α_{IF}	is a constant $= f_1^2/(f_1^2 - f_2^2)$, where f_i is the frequency of the L_i carrier
β_{IF}	is a constant $= 1 - \alpha_{IF}$
λ	is the wavelength of the carrier (m)
N	is the integer carrier-phase ambiguity (cycles)

WL identifies quantities associated with the widelane signal combination

b is a collection of equipment delays (m)

ε contains unmodelled quantities such as noise and multipath (m).

Recovering the integer property of ambiguity parameters with the DCM involves two conditions. First, different clock parameters must be estimated for each signal as a means of isolating equipment delays. The second condition requires the definition of an ambiguity datum to remove the rank deficiency of the system. This means that an ambiguity parameter must be fixed *a priori* to an integer value for each ionosphere-free phase clock and Melbourne-Wübbena bias to be estimated.

As a consequence of imposing those initial constraints on the system, all estimated phase-clock and ambiguity parameters will be biased by the datum ambiguities. With satellite clock corrections being defined in a similar fashion, the estimated ambiguity parameters actually contain datum ambiguities from the reference network stations as well, which are satellite dependent. They can be expressed mathematically as:

$$\bar{N}_1^j = \left[N_1^j - N_1^j(D)\right] - \left[N_1^1 - N_1^1(D)\right]$$

$$\bar{N}_{WL}^j = \left[N_{WL}^j - N_{WL}^j(D)\right] - \left[N_{WL}^1 - N_{WL}^1(D)\right]$$

(5.2)

where the label "D" identifies datum ambiguities originating from the network solution, and the superscript "1" is used to identify the reference satellite. This propagation of datum parameters is fundamental since it also impacts the estimated ionospheric delay parameters in the extended decoupled-clock model, described next.

5.3 The Extended Decoupled-Clock Model (EDCM)

Since the original DCM is based on ionosphere-free linear combinations of observations, it prevents direct access to any ionospheric information. To overcome this limitation, uncombined signals can be used along with an explicit estimation of slant ionospheric delays. However, for compatibility with the satellite clock corrections computed with the DCM, the EDCM presented herein is similar to the one of equation (5.1), except for the Melbourne-Wübbena combination, which is split into the widelane (WL) phase and narrowlane (NL) code observations [Collins and Bisnath, 2011]:

$$\Phi_{WL}^j = \rho^j + T^j + \left(\overline{dT}_{\Phi_{IF}} - \overline{dt}_{\Phi_{IF}}^j\right) + \frac{f_1}{f_2}\bar{I}^j + \lambda_{WL}\bar{N}_{WL}^j + \varepsilon_{\Phi_{WL}}$$
$$P_{NL}^j = \rho^j + T^j + \left(\overline{dT}_{P_{NL}} - \overline{dt}_{\Phi_{IF}}^j\right) + \bar{b}_{\Phi_{MW}}^j + \frac{f_1}{f_2}\bar{I}^j + \varepsilon_{P_{NL}}$$
$$\bar{I}_0^j = \bar{I}^j$$

(5.3)

where $\bar{I}^j$ is the biased slant ionospheric delay between satellite j and the receiver at frequency f_1, and $\bar{I}_0^j$ is an optional constraint on this delay. If mathematical correlations are properly accounted for, the EDCM can be shown to be equivalent to the processing of uncombined signals.

As explained in the previous section, the estimated clock and ambiguity parameters in the DCM are biased by datum ambiguities. Similarly, the estimated ionospheric delays

will be contaminated by receiver- and satellite-dependent geometry-free (GF) biases [Collins et al., 2012]:

$$\bar{I}^j = I^j - \beta_{IF}\big(\bar{b}_{\Phi_{GF}} - \bar{b}^j_{\Phi_{GF}}\big) \tag{5.4}$$

with

$$\bar{b}_{\Phi_{GF}} = DPB_R + (\lambda_1 - \lambda_2) \cdot [N_1^1 - N_1^1(D)] + \lambda_2 \cdot [N_{WL}^1 - N_{WL}^1(D)]$$

$$\bar{b}^j_{\Phi_{GF}} = DPB^j - (\lambda_1 - \lambda_2) \cdot N_1^j(D) - \lambda_2 \cdot N_{WL}^j(D) \tag{5.5}$$

where DPB_R and DPB^j are the receiver and satellite differential phase bias, respectively. The receiver geometry-free bias ($\bar{b}_{\Phi_{GF}}$) contains a contribution from both the datum ambiguities of the station and the network, while satellite geometry-free biases ($\bar{b}^j_{\Phi_{GF}}$) are a function of the network's datum ambiguities. Hence, both quantities are dependent on the satellite clock corrections used. The use of both ionosphere-free satellite clock corrections and Melbourne-Wübbena satellite biases in the functional model of the NL code observations leads to an integer-biased narrowlane code clock ($\overline{dT}_{P_{NL}}$) estimate, but ensures the compatibility of biases within the model.

Since a single receiver-phase-clock parameter is used for both the ionosphere-free and widelane phase observables, it is not possible for this parameter to soak up the receiver bias $\bar{b}_{\Phi_{GF}}$ when external constraints on the ionosphere are used. There are two means of coping with this issue: first, a separate receiver clock parameter could be estimated for the widelane signal; however, this translates into a slightly different functional model and becomes a nuisance to the scalability of the approach. Second, between-satellite ionospheric delays could be estimated. This approach can be used with or without

external information on the ionosphere and is therefore more suitable to seamless transitions from or to a regional network.

From equations (5.4) and (5.5), it should be clear that it is not possible to simply constrain $\bar{I}^j$ using external TEC values due to the presence of the unknown geometry-free biases. Constraining those parameters can only be achieved if compatible satellite geometry-free phase biases ($\bar{b}^j_{\Phi_{GF}}$) are transmitted to the user. Fortunately, those biases can be made available if VTEC maps are computed based on integer-levelled observations, as opposed to phase-smoothed code observations. Details on this approach are provided in the following section.

5.4 Integer Levelling

Ionospheric maps are subject to several error sources originating mainly from the use of a thin-shell model, sparse spatial sampling, and interpolation. The levelling procedure (i.e., the process of fitting carrier-phase to code observations) can also introduce errors of up to 5 TEC units (TECU) on slant ionospheric delay measurements [Ciraolo et al., 2007]. Levelling errors are caused mainly by the fact that code noise and multipath does not necessarily average out over a satellite pass, but there can also be significant errors due to intra-day variations of receiver DCBs.

The concept of integer levelling was developed with the goal of mitigating levelling errors [Banville and Langley, 2011]. As opposed to fitting phase to code, the levelling process is achieved by removing the contribution of carrier-phase ambiguities from the geometry-free carrier-phase observations:

$$\overline{\overline{\Phi}}_{GF}^j = \Phi_{GF}^j - \left[(\lambda_1 - \lambda_2)\widehat{\overline{N}}_1^j + \lambda_2\widehat{\overline{N}}_{WL}^j\right]$$
$$= \left[-\frac{1}{\beta_{IF}}I^j + (\lambda_1 - \lambda_2)N_1^j + \lambda_2 N_{WL}^j + DPB_R - DPB^j\right]$$
$$- \left[(\lambda_1 - \lambda_2)\widehat{\overline{N}}_1^j + \lambda_2\widehat{\overline{N}}_{WL}^j\right]$$

$$(5.6)$$

where the double-bar symbol represents integer-levelled observations, and $\widehat{\overline{N}}_i^j$ are estimated ambiguity values (preferably integers) from a PPP solution. Note that the term Φ_{GF}^j is expanded in the second line of (5.6). Removing the contribution of the carrier-phase ambiguities in (5.6) does not immediately provide unbiased slant ionospheric delays. This is a consequence of the ambiguity datum involved in computing the PPP solution, as explained in the previous sections. Replacing the estimated ambiguities in (5.6) using the definition of equations (5.2) and (5.5) leads to:

$$\overline{\overline{\Phi}}_{GF}^j = -\frac{1}{\beta_{IF}}I^j + \left(\overline{b}_{\Phi_{GF}} - \overline{b}_{\Phi_{GF}}^j\right).$$

$$(5.7)$$

Hence, integer-levelled observations contain receiver and satellite geometry-free biases, functionally similar to DCBs. A benefit of using the observables of (5.7) as opposed to carrier phases fitted to code observations is that integer levelling virtually eliminates levelling errors, provided that ambiguity parameters are fixed to correct

135

integer values. As a result, slant TEC estimates from nearby stations are more consistent, leading to smaller residuals of model fit [Banville et al., 2012].

The receiver ($\bar{b}_{\Phi_{GF}}$) and satellite geometry-free biases ($\bar{b}^j_{\Phi_{GF}}$) are separated from slant ionospheric delays by using a mathematical representation of the ionosphere such as [Komjathy, 1997]:

$$\bar{\bar{\Phi}}^j_{GF} = -\frac{1}{\beta_{IF}} \cdot M(e^j) \cdot (a_0 + a_1\Delta\lambda + a_2\Delta\phi) + \left(\bar{b}_{\Phi_{GF}} - \bar{b}^j_{\Phi_{GF}}\right) \tag{5.8}$$

where M is the so-called single-layer or thin-shell mapping function depending on the elevation angle (e) of the satellite. The time-dependent coefficients a_0, a_1, and a_2 model the VTEC above a station as a bilinear function. Gradients are taken into consideration using $\Delta\lambda$, the difference between the longitude of the ionospheric pierce point and the longitude of the mean sun, and $\Delta\phi$, the difference between the geomagnetic latitude of the ionospheric pierce point and the geomagnetic latitude of the station. When several reference stations are available, one set of coefficients is estimated for each station, and one geometry-free phase bias per station and satellite is set up in the adjustment. To remove the rank deficiency of the system, a zero-mean condition is imposed for the satellite biases. Unbiased slant ionospheric delays are then computed as:

$$I^j = -\beta_{IF}\left(\bar{\bar{\Phi}}^j_{GF} - \hat{\bar{b}}_{\Phi_{GF}} + \hat{\bar{b}}^j_{\Phi_{GF}}\right) \tag{5.9}$$

where the hat symbol again denotes estimated quantities.

Equations (5.7) or (5.9) highlight another important characteristic of integer-levelled observations: they provide ionospheric delays equivalent to the ones derived in equation

(5.4). Both quantities are contaminated by the same station- and receiver-specific geometry-free phase biases. Consequently, if TEC maps are computed based on integer-levelled observations, the estimated geometry-free satellite phase biases should be made available to users in addition to DCBs, which would allow for constraining slant ionospheric delays in PPP with ambiguity resolution.

5.5 Analyzing the Accuracy of Slant Ionospheric Corrections

The concepts presented in this paper were tested using GPS data collected on 2 March 2008, during a quiet phase of the approximately 11-year solar cycle [Jensen and Mitchell, 2011] with a mean Kp index of 2.25. A total of 23 stations located in Canada, shown by triangles in Figure 5.1, were first used to assess the quality of global ionospheric corrections from the IGS GIM. For this purpose, integer-levelled observations were obtained for all stations following equation (5.6). The estimated ambiguity parameters were obtained from PPP solutions using satellite clock corrections provided by Natural Resources Canada (NRCan). The latter are based on the decoupled-clock model and are computed using the IGS Rapid orbits [Griffiths and Ray, 2009]. The integer-levelled observations were then included in a least-squares adjustment to estimate a set of three time-varying coefficients (see equation (5.8)) per station, as well as satellite and receiver geometry-free phase biases. An elevation angle cutoff of 10 degrees was applied and the thin shell height was set to 450 km. Slant ionospheric delays were computed following

equation (5.9). Since levelling errors are reduced to a minimum when using the integer-levelling procedure, ionospheric delays obtained based on this methodology should be accurate enough to provide a good estimate for the quality of the global model, provided that no significant errors were introduced when estimating the satellite and receiver geometry-free biases.
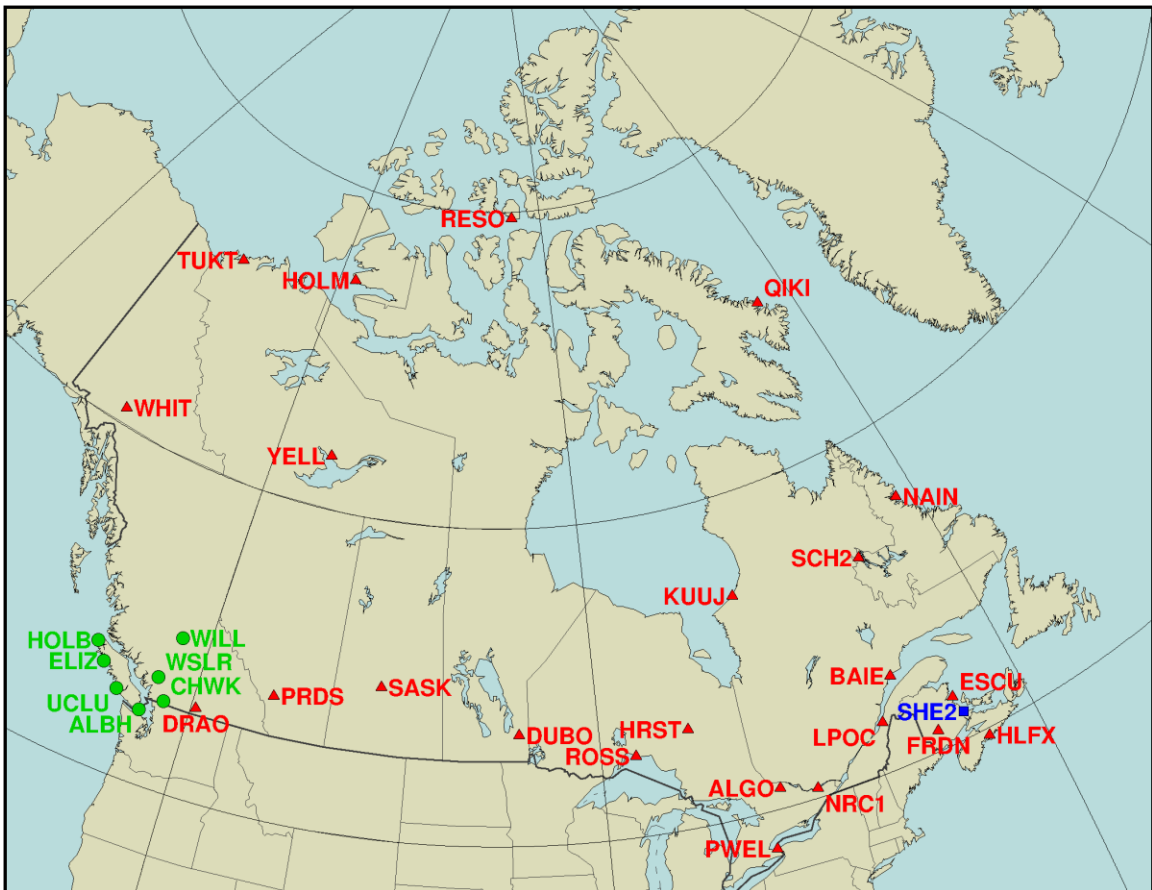
Figure 5.1: Network of stations: green circles are reference stations while blue squares and red triangles are PPP users.

Figure 5.2 shows the RMS differences of slant ionospheric delays between the GIM and the station-derived delays for all stations. The results are divided into two plots showing errors for satellites observed at an elevation angle below and above 20 degrees. Stations are also ordered as a function of latitude, from the most southern (PWEL) to the most northern (RESO) station. The estimated RMS errors are fairly consistent for stations below the 60th parallel (from PWEL to NAIN), and also agree fairly well with the mean RMS errors provided along with the IGS VTEC maps in the IONEX format [Schaer et al., 1998] shown by black squares in Figure 5.2. For stations at latitudes above 60 degrees, the discrepancies between the global corrections and the reference values increase significantly, making the RMS errors reported by the GIM too optimistic. It should however be noted that those discrepancies do not necessarily originate from the GIM itself, but could be attributable to errors in our determination of the receiver geometry-free biases [Themens et al., 2013].

When constraining slant ionospheric delays in the PPP solution, benefits in terms of precisions are expected if the quality of the external corrections is superior to that of code noise. According to Figure 5.2, ionospheric constraints added to the PPP filter would have a mean standard deviation of 15 cm for satellites observed at high elevation angles, and about 25 cm for elevation angles below 20 degrees. Those values are indeed lower than code noise for most receiver types, suggesting that using information from GIMs could be beneficial to PPP users.
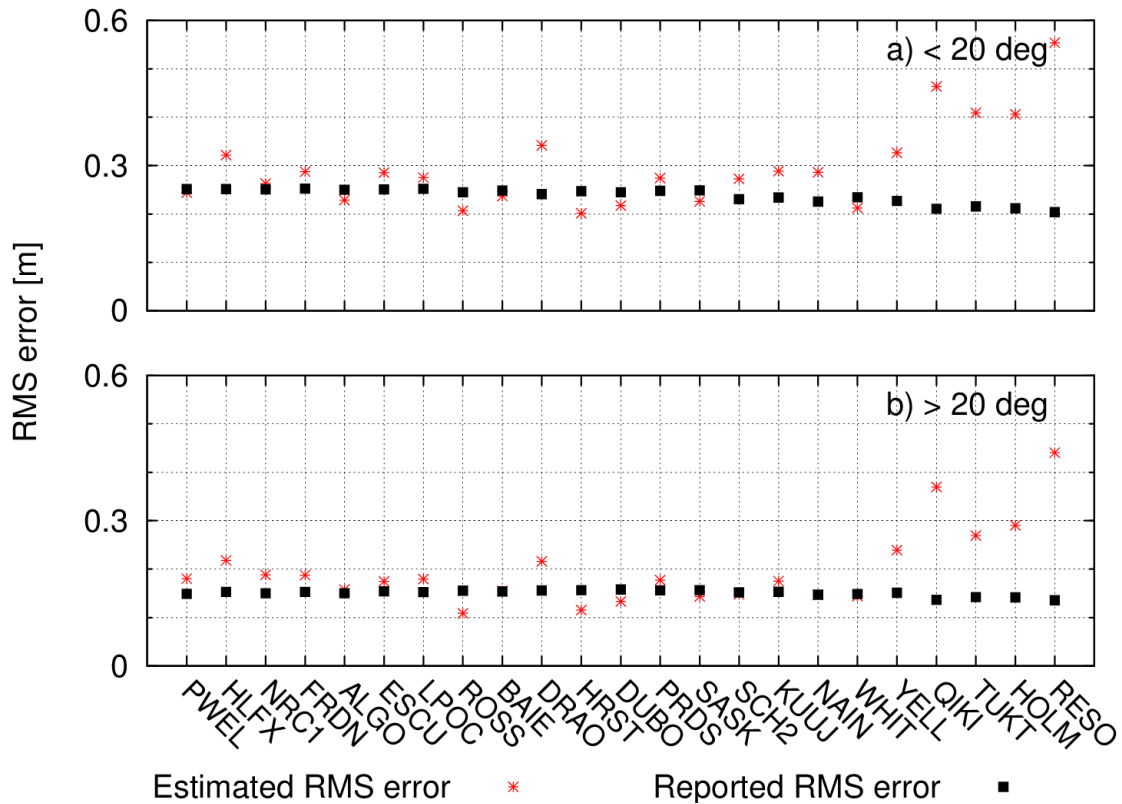
Figure 5.2: Estimated and reported errors in the GIM STEC over Canada on 2 March 2008 for satellites observed at an elevation angle: a) below 20 degrees and b) above 20 degrees.

It is known that estimating station coordinates with a tropospheric zenith delay parameter requires slant ionospheric constraints at the millimetre level to allow for instantaneous ambiguity resolution [Odijk, 2002]. From the results of Figure 5.2, it is unlikely that relying on a thin shell representation of the ionosphere will be accurate enough for this purpose. Ionospheric constraints should therefore be provided as line-of-sight corrections from either a regional network of stations or even a single station. The

quality of ionospheric corrections from a regional network on the east coast of Canada was therefore assessed as well. Station SHE2 was designated as a rover, and the three closest NRCan stations (ESCU, FRDN, and HLFX) were considered as reference stations. The mean distance between the rover and the reference stations is approximately 150 km, while the closest station (ESCU) is located at 97 km. Slant ionospheric delays at the rover and their precisions were computed as:

$$\bar{I}_0^j = \frac{\sum_{k=1}^{3} \frac{1}{d_k^2} \cdot \left[\beta_{IF} \cdot \left(\hat{\bar{b}}_{\Phi_{GF}} - \bar{\bar{\Phi}}_{\Phi_{GF}}^j \right)_k \right]}{\sum_{k=1}^{3} \frac{1}{d_k^2}} \tag{5.10}$$

$$\sigma_{\bar{I}_0^j}^2 = \frac{\sum_{k=1}^{3} \frac{1}{d_k^2} \cdot \left(\beta_{IF} \cdot \left(\hat{\bar{b}}_{\Phi_{GF}} - \bar{\bar{\Phi}}_{\Phi_{GF}}^j \right)_k - \bar{I}_0^j \right)^2}{2 \cdot \sum_{k=1}^{3} \frac{1}{d_k^2}} \tag{5.11}$$

where $\bar{I}_0^j$ is the interpolated slant ionospheric delay at the rover for satellite j, and d_k is the distance between the user and reference station k. Slant ionospheric delays between satellite j and station k are obtained by removing the receiver geometry-free bias from integer-levelled observations. Note that more rigorous interpolation methods such as Kriging could have been used to obtain the slant delays at the rover, but the weighted mean of equation (5.10) was adopted here for simplicity. Integer-levelled observations are also obtained at the rover (R) and the error in the interpolated delay is evaluated as:

$$\varepsilon_{\bar{I}_0^j} = \beta_{IF} \left[\bar{\bar{\Phi}}_{GF}^j \right]_R + \bar{I}_0^j = \beta_{IF} \left[\bar{b}_{\Phi_{GF}} \right]_R. \tag{5.12}$$

This quantity provides an estimate of the receiver geometry-free phase bias. Removing the mean from all values computed allows assessing the quality of the regional

141

corrections, as presented in Figure 5.3. This figure demonstrates the significant gain in accuracy obtained by going from a global to a regional source of ionospheric information. The RMS error for satellites observed at elevation angles below 20 degrees is 3.5 cm while it is 1.8 cm for elevation angles above 20 degrees. Panel 'a' of Figure 5.3 suggests that unmodelled errors, originating from either integer levelling with float ambiguities or instrumental bias estimation, remain for some satellites causing constant biases of a few centimetres over a satellite arc. As a consequence, optimistic precisions computed from (5.11) can be associated with regional ionospheric corrections, as shown in panel 'b'. Figure 5.3 also suggests that shorter inter-station distances would be required to provide slant ionospheric corrections with mm-level precisions to allow for systematic instantaneous ambiguity resolution.

5.6 PPP with Global Ionospheric Corrections

The quality of the global ionospheric product introduced in the previous section was evaluated in the positioning domain for 24 Canadian stations represented by triangles and a square in Figure 5.1. PPP solutions computed following the methodologies described in Table 5.1 were used to study the impact of external ionospheric constraints and ambiguity resolution on the convergence period.
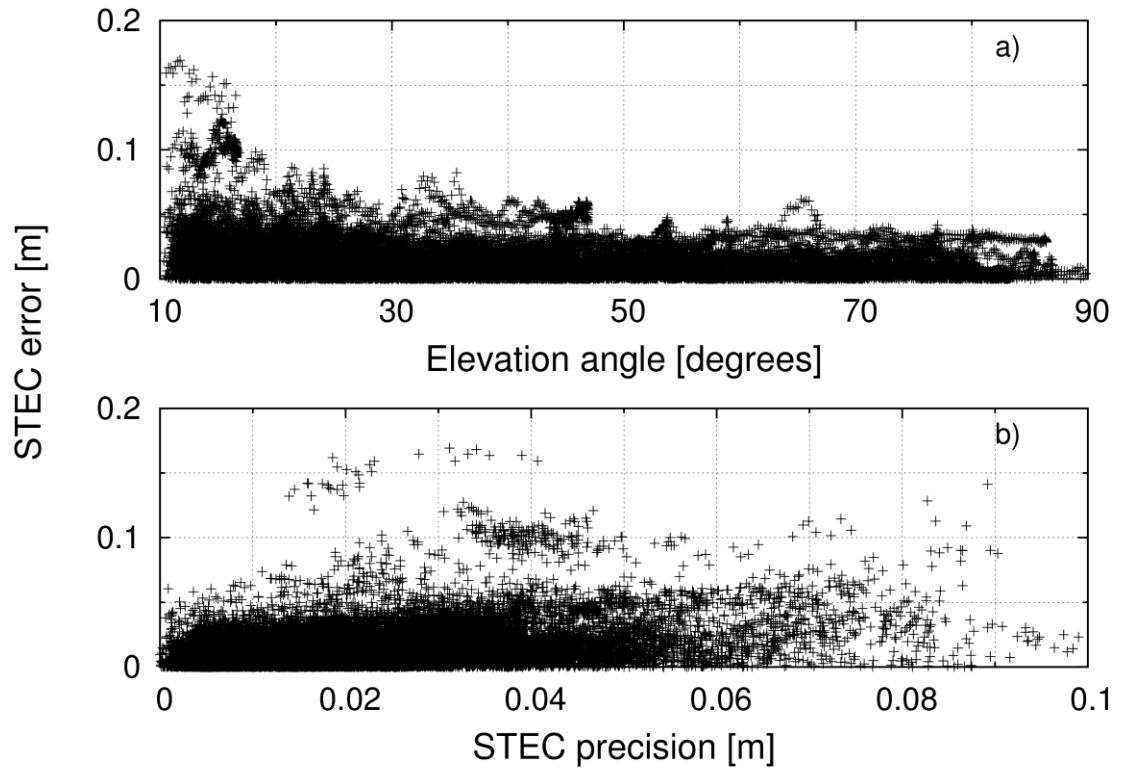
Figure 5.3: Estimated errors in the regional ionospheric corrections in eastern Canada on

2 March 2008 as a function of a) elevation angle, and b) STEC precision.

Table 5.1: Description of the PPP solutions

Solution Type	STEC constraints	Ambiguity Resolution
PPP	No	No
PPP-AR	No	Yes
PPP + GIM	Yes	No
PPP-AR + GIM	Yes	Yes

All solutions in Table 5.1 were computed using the functional model of the EDCM, but solutions with the label 'GIM' used external ionospheric constraints from a GIM. Ambiguity resolution was only attempted for the 'PPP-AR' solutions, while the 'PPP' solutions kept ambiguities as real numbers in the adjustment process. To keep the results independent of any specific ambiguity validation method, ambiguity resolution was based on the integer least-squares solution [Teunissen, 1993] on an epoch-by-epoch basis; i.e., the closest integer vector to the float ambiguities at each epoch, based on the metric of the ambiguity covariance matrix, was selected as being the "true" values while the float solution was maintained in the PPP filter.

The satellite clock corrections used were provided by NRCan based on the decoupled-clock model. The precision of the observations at zenith was set to 3 mm and 30 cm for uncombined phase and code measurements, respectively, and an elevation-angle-dependent weighting was applied. GPS data at a sampling interval of 30 seconds was used to estimate station coordinates independently at each epoch, often referred to as a kinematic solution. The tropospheric zenith delay was estimated as a random walk process with process noise of 3 mm/$\sqrt{\text{hour}}$. Time correlation of all receiver clock parameters was modelled as white noise. Constraining of slant ionospheric delay parameters was done only for one epoch when the satellite is first observed or suffers from a cycle slip; otherwise, ionospheric delay parameters are estimated as a white noise process to account for possible scintillation effects. The ionospheric constraints are introduced in the PPP filter as pseudo-observations:

$$\bar{I}_0^j = M(e^j) \cdot I(v)_{GIM}^j - \beta_{IF} \hat{\bar{b}}_{\Phi_{GF}}^j \qquad (5.13)$$

$$\sigma_{\bar{I}_0^j}^2 = \left[M(e^j)\right]^2 \sigma_{I(v)_{GIM}^j}^2 + \beta_{IF}^2 \sigma_{\hat{\bar{b}}_{\Phi_{GF}}^j}^2 \qquad (5.14)$$

where $I(v)_{GIM}^j$ is the vertical ionospheric delay, in metres, from the IGS GIM at the pierce point on the thin-shell model. The precision of this quantity is derived from the RMS maps also included in the IONEX-format data. Geometry-free satellite phase biases ($\hat{\bar{b}}_{\Phi_{GF}}^j$), required for the consistency of ionospheric corrections, were estimated using a regional network of seven stations represented by circles in Figure 5.1. The procedure described in the previous section was used for this purpose. Applying geometry-free satellite phase biases computed using a regional network to the IGS GIM should be consistent provided that TEC values from the GIM are not corrupted by unmodelled DCB effects.

Data from all 24 stations was processed in independent segments of one hour, leading to a total of $24 \cdot 24 = 576$ solutions. This process was repeated for every solution type in Table 5.1. The reference coordinates for each station were obtained using a static PPP solution based on the full 24-hour data sets. Our metric for evaluating convergence time is based on the horizontal (2D) error reaching an accuracy of better than 10 cm. Comparison between methodologies is achieved using the 68th and 95th percentiles. Results are presented in Figure 5.4.
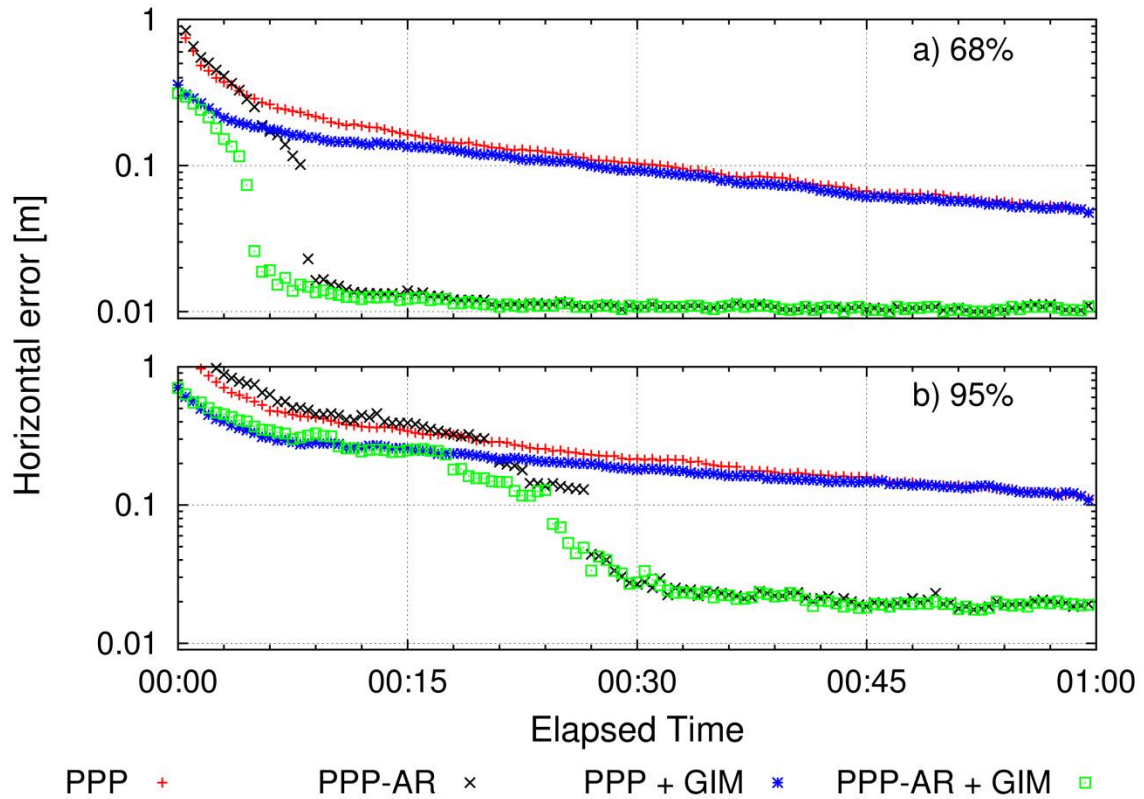
Figure 5.4: Hourly horizontal error percentiles for 24 Canadian stations on 2 March 2008: a) 68th percentile values, and b) 95th percentile values.

Figure 5.4 illustrates the typical PPP convergence period in which more than 30 minutes of data are required for 68% of the solutions to reach an accuracy of 10 cm horizontally. Approximately 5% of the solutions still had not attained this threshold after an hour. Using ambiguity resolution, as shown by the 'PPP-AR' values, reduces convergence time to about 8.5 minutes (68%), and improves the stability of the solutions. The benefits of ambiguity resolution are, however, not as notable when looking at the 95th percentile values where solutions with ambiguity resolution only surpass float solutions after nearly 20 minutes. Applying ionospheric constraints from a GIM clearly

improves positioning accuracies at the beginning of the sessions. At the first epoch, the 68th percentile curve is at the metre mark for the 'PPP' solutions due to noisy code measurements. Introducing external information on the ionosphere decreases this value to 35 cm, an improvement of 65%. Adding ambiguity resolution capabilities can allow reaching the 10-cm threshold in about 4.5 minutes, an improvement of nearly 50% over the 'PPP-AR' solution (68%).

The benefits of applying ionospheric constraints are, however, attenuated after a few minutes of observations. Since TEC errors from GIMs are strongly correlated over short time intervals, there is no gain in incorporating TEC information at every epoch. Hence, slant ionospheric delays explicitly or implicitly estimated in the standard PPP model quickly reach the same level of precision as the external constraints when averaging code noise over a few epochs. As expected, instantaneous ambiguity resolution is not likely to be achieved with a global ionospheric map, but a reduction in convergence time is possible under favourable ionospheric conditions. Also note that no significant accuracy degradation was observed on this day for high-latitude stations.

Since the AR-based solutions are computed using integer least-squares without validating the selected integer ambiguity candidates, they indicate the time required for the closest integer vector from the float solution to be the "true" ambiguity values. In other words, the 'PPP-AR' solutions suggest that attempting to fix ambiguities before a period of half an hour is likely to fail about 5% of the time, which confirms earlier findings [Zhang and Li, 2013]. Adding ionospheric corrections from GIM does not seem

to provide significant benefits in this regard. While geometry plays an important role in the convergence period, the exactness of the stochastic model, that is, how well the covariance matrix of the ambiguities describes their distance to the closest integer vector, seems a crucial component of quick and reliable ambiguity resolution and requires further investigation.

5.7 Regional Ionospheric Corrections for PPP with Ambiguity Resolution

The assessment of regional ionospheric corrections is demonstrated using a network located on the east coast of Canada (see Figure 5.1). Hourly PPP solutions for station SHE2 were computed using the same methodology as described in the previous section. In addition to the four scenarios enumerated in Table 5.1, two solutions using slant ionospheric corrections interpolated from the three nearest reference stations (ESCU, FRDN and HLFX) were computed. They are labeled as 'PPP + REG' and 'PPP-AR + REG' to emphasize the dependency on a regional network for providing ionospheric corrections. As stated previously, the mean distance between the PPP user and the reference stations is approximately 150 km, while the closest station (ESCU) is located at 97 km. The ionospheric pseudo-observations introduced in the PPP filter and their variances were computed as per equations (5.10) and (5.11). Geometry-free satellite

biases were obtained using the network of 23 stations represented by triangles in Figure 5.1.

Figure 5.5 shows, for each scenario, the horizontal errors for the 24 hourly solutions, as well as the 68th percentile values. The plots on the left-hand side demonstrate the influence of various ionospheric models on the float solutions. As pointed out in the previous section, ionospheric constraints mainly reduce the position errors for the first epochs. However, even when precise ionospheric delays are available from external sources, position estimates are still greatly dependent on code measurements. The impact of ambiguity resolution is shown on the right-hand side. The step-like changes in horizontal error originate from the outcome of the integer least-squares solution, where different integer vectors are selected for consecutive epochs. It is apparent that consistent convergence to cm-level accuracies requires ambiguity resolution for short observation sessions. Furthermore, tightly constrained ionospheric delays reduce the size of the ambiguity search space, which allows for quicker ambiguity resolution. This result can be seen from the 'PPP-AR + REG' solutions, where horizontal accuracies below 10 centimetres were achieved instantaneously for 21 hours out of 24. The 68th percentile values suggest that horizontal accuracies around 2.4 cm can be obtained from a single epoch of data.
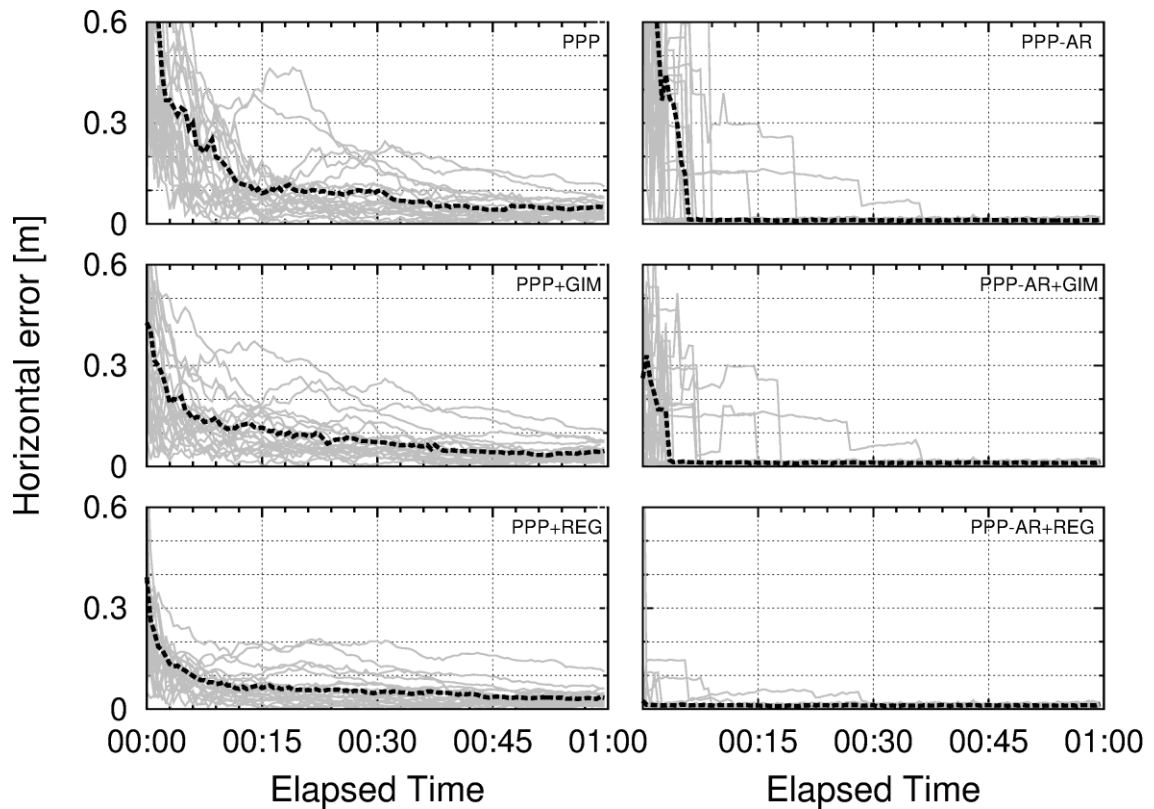
Figure 5.5: Hourly horizontal error based on 24 hourly solutions for station SHE2 on 2 March 2008. The dashed curves show the 68th percentiles.

5.8 Conclusion

This paper described how using phase-based satellite clock corrections in PPP yields integer-biased clock, ambiguity and ionospheric parameters. Due to this characteristic, a set of consistent satellite phase biases must be provided along with external TEC corrections for their inclusion in the PPP model. Such biases can be obtained by replacing phase-smoothed code observations by integer-levelled observations in the generation of

TEC maps. The integer levelling procedure can be achieved explicitly by introducing integer ambiguity parameters obtained from a PPP solution into the geometry-free carrier-phase observables, or implicitly by using the slant ionospheric delay parameters estimated in the PPP filter.

While the benefits of applying external TEC constraints from a global source depends significantly on the ionospheric activity, it was demonstrated that such corrections can improve position accuracies by over 60% at the beginning of a session when the ionosphere is quiet. Due to the time-correlated nature of TEC errors, this benefit is, however, quickly mitigated as the noise in code observations is averaged out and reaches the same level of precision as the external constraints. With ambiguity resolution capabilities, a GIM can speed up convergence time of PPP solutions to the 10-cm level horizontally to 4.5 minutes (68th percentile). This level of accuracy was obtained in 8.5 minutes without using ionospheric corrections from the global map. Those results are a substantial improvement over the standard PPP solution which takes nearly 30 minutes to converge to this level of accuracy. Using ionospheric corrections from a regional network with inter-station distances of approximately 150 km can allow convergence to the 10-cm threshold instantaneously under favourable ionospheric conditions and good satellite geometry. These results were validated by comparing the estimated positions to known coordinates; a rigorous validation procedure is still required to exclude incorrectly-fixed ambiguities. With a disturbed ionosphere, constraining the ionospheric effect using external sources should not negatively impact PPP solutions, provided that the precision of those constraints reflect their deficiencies.

Since the extended decoupled-clock model can be used regardless of the availability of external ionospheric constraints, it allows for a scalable PPP solution to be obtained. Rapid initialization can be achieved when the user is located in the vicinity of a local or regional network, although such a network is not essential for maintaining cm-level accuracies. In the event that users are located in a remote area, solutions can still benefit from global ionospheric corrections to gain a few minutes on their convergence times.

Acknowledgements

References

Banville, S., and R. B. Langley (2011). "Defining the basis of an integer-levelling procedure for estimating slant total electron content," *Proceedings of the 24th International Technical Meeting of the Satellite Division of The Institute of Navigation (ION GNSS 2011)*, Portland, Ore., 19-23 September 2011, pp. 2542-2551.

Banville, S., W. Zhang, R. Ghoddousi-Fard, and R. B. Langley (2012). "Ionospheric monitoring using 'integer-levelled' observations," *Proceedings of the 25th International Technical Meeting of the Satellite Division of The Institute of Navigation (ION GNSS 2012)*, Nashville, Tenn., 17-21 September 2012, pp. 2692-2701.

Beran, T. (2008). *Single-frequency, single-receiver terrestrial and spaceborne point positioning*. Ph.D. dissertation, Technical Report 257, Department of Geodesy and Geomatics Engineering, University of New Brunswick, Fredericton, New Brunswick, Canada.

Ciraolo, L., F. Azpilicueta, C. Brunini, A. Meza, and S. M. Radicella (2007). "Calibration errors on experimental slant total electron content (TEC) determined with GPS," *Journal of Geodesy*, Vol. 81, No. 2, pp. 111-120. doi: 10.1007/s00190-006-0093-1.

Collins, P., F. Lahaye, and S. Bisnath (2012) "External ionospheric constraints for improved PPP-AR initialisation and a generalised local augmentation concept," *Proceedings of the 25th International Technical Meeting of the Satellite Division of The Institute of Navigation (ION GNSS 2012)*, Nashville, Tenn., 17-21 September 2012, pp. 3055-3065.

Collins, P., and S. Bisnath (2011). "Issues in ambiguity resolution for precise point positioning," *Proceedings of the 24th International Technical Meeting of the Satellite Division of The Institute of Navigation (ION GNSS 2011)*, Portland, Ore., 19-23 September 2011, pp. 679-687.

Collins, P., S. Bisnath, F. Lahaye, and P. Héroux (2010). "Undifferenced GPS ambiguity resolution using the decoupled clock model and ambiguity datum fixing," *NAVIGATION: Journal of The Institute of Navigation*, Vol. 57, No. 2, Summer 2010, pp. 123-135.

Collins, P., Y. Gao, F. Lahaye, P. Héroux, K. MacLeod, and K. Chen (2005). "Accessing and processing real-time GPS corrections for precise point positioning: some user considerations," *Proceedings of the 18th International Technical Meeting of the Satellite Division of The Institute of Navigation (ION GNSS 2005)*, Long Beach, Calif., 13-16 September 2005, pp. 1483-1491.

Drescher, R., X. Chen, H. Landau, A. Kipka, M. Glocker, and V. Gomez (2013). "Accelerating the convergence of Trimble CenterPoint RTX Positioning by using a global ionospheric model," *Presented at the GNSS PPP Workshop: Reaching Full Potential*, Ottawa, Ont., Canada, 12-14 June.

Enge, P., T. Walter, S. Pullen, C. Kee, Y. C. Chao, and Y.-J. Tsai (1996). "Wide area augmentation of the Global Positioning System," *Proceedings of the IEEE*, Vol. 84, No. 8, August 1996, pp.1063-1088. doi: 10.1109/5.533954.

Ge, M., G. Gendt, M. Rothacher, C. Shi, and J. Liu (2008). "Resolution of GPS carrier-phase ambiguities in precise point positioning (PPP) with daily observations," *Journal of Geodesy*, Vol. 82, No. 7, pp. 389-399. doi: 10.1007/s00190-007-0187-4.

Geng, J., X. Meng, A. H. Dodson, M. Ge, and F. N. Teferle (2010). "Rapid re-convergences to ambiguity-fixed solutions in precise point positioning," *Journal of Geodesy*, Vol. 84, No. 12, pp. 705-714. doi: 10.1007/s00190-010-0404-4.

Griffiths, J. and J. Ray (2009) "On the precision and accuracy of IGS orbits," *Journal of Geodesy*, Vol. 83, No. 3, pp. 277–287. doi:10.1007/s00190-008-0237-6.

Hernández-Pajares, M., J. M. Juan, J. Sanz, R. Orus, A. Garcia-Rigo, J. Feltens, A. Komjathy, S. C. Schaer and A. Krankowski (2009). "The IGS VTEC maps: a reliable source of ionospheric information since 1998," *Journal of Geodesy*, Vol. 83, No. 3-4, pp. 263-275. doi: 10.1007/s00190-008-0266-1.

Jensen, A. B. O., and C. Mitchell (2011). "GNSS and the ionosphere: What's in store for the next solar maximum?" *GPS World*, Vol. 22, No. 2, pp. 40–48.

Komjathy, A. (1997). *Global Ionospheric Total Electron Content Mapping Using the Global Positioning System*. Ph.D. dissertation, Technical Report 188, Department of Geodesy and Geomatics Engineering, University of New Brunswick, Fredericton, New Brunswick, Canada.

Kouba, J. and P. Héroux (2001). "Precise point positioning using IGS orbit and clock products," *GPS Solutions*, Vol. 5, No. 2, pp. 12-28. doi: 10.1007/PL00012883.

Lanyi, G. E., and T. Roth (1988). "A comparison of mapped and measured total ionospheric electron content using Global Positioning System and beacon satellite observations," *Radio Science*, Vol. 23, No. 4, pp. 483-492. doi: 10.1029/RS023i004p00483.

Laurichesse, D., F. Mercier, J.-P. Berthias, P. Broca, and L. Cerri (2009). "Integer ambiguity resolution on undifferenced GPS phase measurements and its application to PPP and satellite precise orbit determination," *NAVIGATION: Journal of The Institute of Navigation*, Vol. 56, No. 2, Summer 2009, pp. 135-149.

Li, X. (2012) "Improving real-time PPP ambiguity resolution with ionospheric characteristic consideration," *Proceedings of the 25th International Technical Meeting of the Satellite Division of The Institute of Navigation (ION GNSS 2012)*, Nashville, Tenn., 17-21 September 2012, pp. 3027-3037.

Melbourne, W. G. (1985). "The case for ranging in GPS based geodetic systems," *Proceedings of 1st International Symposium on Precise Positioning with the Global Positioning System*, edited by Clyde Goad, U.S. Department of Commerce, Rockville, Md., 15-19 April, pp. 373-386.

Odijk, D. (2002). *Fast precise GPS positioning in the presence of ionospheric delays*. Ph.D. dissertation, Publications on Geodesy 52, Delft University of Technology, Netherlands Geodetic Commission, Delft, The Netherlands.

Schaer, S. (1999). *Mapping and Predicting the Earth's Ionosphere Using the Global Positioning System.* Ph.D. dissertation, Astronomical Institute, University of Berne, Switzerland, 205 pp.

Schaer, S., W. Gurtner, and F. Feltens (1998). "IONEX: the IONosphere map Exchange format version 1, February 25, 1998," *Proceedings of the 1998 IGS Analysis Centers Workshop*, ESOC, Darmstadt, Germany, 9-11 February.

Teunissen, P. J. G. (1993). *Least-squares estimation of the integer GPS ambiguities*. Technical Report, LGR Series 6, Delft Geodetic Computing Centre, Delft University of Technology, Delft, The Netherlands.

Themens, D. R., P. T. Jayachandran, R. B. Langley, J. W. MacDougall, and M. J. Nicolls (2013) "Determining receiver biases in GPS-derived total electron content in the auroral oval and polar cap region using ionosonde measurements," *GPS Solutions*, Vol. 17, No. 3, pp. 357-369. doi: 10.1007/s10291-012-0284-6.

Wübbena, G. (1985). "Software developments for geodetic positioning with GPS using TI 4100 code and carrier measurements," *Proceedings of 1st International Symposium on Precise Positioning with the Global Positioning System*, edited by Clyde Goad, U.S. Department of Commerce, Rockville, Md., 15-19 April, pp. 403-412.

Zhang, X., and P. Li (2013). "Assessment of correct fixing rate for precise point positioning ambiguity resolution on a global scale," *Journal of Geodesy*, Vol. 87, No. 6, pp. 579-589. doi: 10.1007/s00190-013-0632-5.

CHAPTER 6

GLONASS AMBIGUITY RESOLUTION OF MIXED RECEIVER TYPES WITHOUT EXTERNAL CALIBRATION

This chapter describes a methodology for handling inter-frequency carrier-phase biases occurring when mixing receiver types in the processing of GLONASS observations. It constitutes the groundwork for undifferenced ambiguity resolution for GLONASS.

The following was originally published as:

Modifications to the original manuscript were made only for proper identification of sections, figures and tables, as well as to assure the uniformity of symbol and equation notation throughout this dissertation.

Abstract

GLONASS processing from mixed receiver types is typically subject to unmodelled inter-frequency phase biases which prevent carrier-phase ambiguity parameters from converging to integers. Receiver-dependent values have been proposed to mitigate the contribution of these biases, but are still subject to a number of issues, such as firmware updates. Recent studies have demonstrated that the origin of inter-frequency biases is a misalignment between phase and code observations, and could be calibrated to first order by manufacturers. In this contribution, a calibration-free method for GLONASS ambiguity resolution is presented in which ambiguities naturally converge to integers. A mandatory condition is that two GLONASS satellites with adjacent frequency numbers are observed simultaneously, although this condition can be relaxed once a fixed solution has been obtained. This approach then permits the integration of different receiver types and firmware versions into seamless processing.

6.1 Introduction

Reliable ambiguity resolution in any Global Navigation Satellite System (GNSS) requires rigorous modelling of all error sources affecting carrier-phase and code observations. This is especially true for GLONASS due to the frequency division

157

multiple access (FDMA) technique used to define the signals. This approach adds a level of complexity to ambiguity resolution because of resulting inter-frequency biases [Takac, 2009]. To clarify the problems associated with GLONASS ambiguity resolution, a simplified functional model for between-receiver single-differenced GNSS observations can be used, where the baseline and atmospheric effects are assumed known. An explicit estimation of slant ionospheric delays will be the subject of future work. Under these assumptions, the carrier-phase and code observables can be expressed as:

$$\Delta \widetilde{\Phi}_i^j(S,m) = \Delta dT_{\Phi_i}(S,m) + \lambda_i^j(S)\Delta N_i^j(S,m) \qquad (6.1)$$

$$\Delta \widetilde{P}_i^j(S,m) = \Delta dT_{P_i}(S,m) \qquad (6.2)$$

where Δ denotes between-receiver single-differenced quantities, $\widetilde{\Phi}$ is the carrier-phase misclosure (m), $\widetilde{P}$ is the code misclosure, i identifies frequency-dependent quantities, j identifies a satellite, S identifies the system (G = GPS, R = GLONASS), m identifies the signal modulation, dT is the combined clock offset from GPS time and equipment delays (m), λ is the wavelength of the carrier, and N is the integer ambiguity in cycles.

Equations (6.1) and (6.2) emphasize the dependency of clock parameters on: the system, the observable (phase or code), the frequency, and the modulation of the signal (simplifications to this notation are used for clarity only). These distinctions are necessary due to the presence of equipment delays between signals, and decoupling clock parameters is a rigorous means of handling those biases [Collins et al., 2010]. Explicitly estimating between-receiver clock parameters on all signals is equivalent to forming double-differenced observations and taking into account the mathematical correlations.

158

The notation of (6.1) and (6.2) is preferred since it permits the method to be more easily generalized. FDMA implies that each signal on any GLONASS satellite is subject to a unique bias, and properly defined clock parameters are required for rigorous bias handling.

When n satellites are observed on a single frequency, a total of n carrier-phase observations are available, while there are $n+1$ phase parameters to solve for: the difference in receiver phase clock between stations and n ambiguity parameters. To remove the rank deficiency, a biased clock parameter can be defined according to (6.3). Dependency on modulation will be dropped from here on for the sake of simplicity.

$$\Delta \overline{dT}_{\Phi_i}(S) \equiv \Delta dT_{\Phi_i}(S) + \lambda_i^1(S)\Delta N_i^1(S) \tag{6.3}$$

In (6.3), the newly-defined clock parameter ($\Delta \overline{dT}$) now contains the carrier-phase ambiguity of satellite 1, therefore reducing the number of parameters to estimate by one. The overbar symbol will denote biased quantities. When introducing (6.3) into (6.1), a system of equations can be defined for all GPS satellites observed as:

$$\Delta \widetilde{\Phi}_i^1(G) = \Delta \overline{dT}_{\Phi_i}(G) \tag{6.4a}$$

$$\Delta \widetilde{\Phi}_i^n(G) = \Delta \overline{dT}_{\Phi_i}(G) + \lambda_i \Delta N_i^{1n}(G) \tag{6.4b}$$

with $n > 1$ and where dependency of the wavelength on the satellite is omitted, but explicit reference to the GPS (G) system is retained, and

$$\Delta N_i^{1n} = \Delta N_i^n - \Delta N_i^1. \tag{6.5}$$

As a consequence of defining an ambiguity-biased receiver clock parameter, double-differenced ambiguities between stations and with respect to satellite 1 are obtained. Since the frequency number is the same for all GPS satellites, the system of equations now has n unknowns and is solvable using a least-squares adjustment.

Applying the same concept to GLONASS is not as straightforward due to FDMA. Using the same variable change defined by (6.3), the system of GLONASS (R) equations becomes:

$$\Delta\widetilde{\Phi}_i^1(R) = \Delta\overline{dT}_{\Phi_i}(R) \tag{6.6a}$$

$$\Delta\widetilde{\Phi}_i^n(R) = \Delta\overline{dT}_{\Phi_i}(R) + \lambda_i^n \Delta N_i^n(R) - \lambda_i^1 \Delta N_i^1(R) \tag{6.6b}$$

where the wavelength of satellite n is identified using the corresponding superscript. Since inter-frequency analog hardware phase biases are known to be at the sub-millimeter level [Sleewaegen et al., 2012], a common clock parameter can be used for all GLONASS satellites in the same frequency band. As apparent from (6.6), the different wavelengths between satellites prevent obtaining directly double-differenced ambiguities. A common, and equivalent, reformulation of (6.6) consists of the following:

$$\Delta\widetilde{\Phi}_i^1(R) = \Delta\overline{dT}_{\Phi_i}(R) \tag{6.7a}$$

$$\Delta\widetilde{\Phi}_i^n(R) = \Delta\overline{dT}_{\Phi_i}(R) - (\lambda_i^1 - \lambda_i^n)\Delta N_i^1(R) + \lambda_i^n \Delta N_i^{1n}(R) \tag{6.7b}$$

where double-differenced ambiguities are now estimated, and the reference ambiguity is multiplied by the difference in wavelengths between satellites. Because the reference ambiguity remains an explicit parameter, the system defined by (6.7) is still singular.

Using this model, several approaches have been defined to deal with the system's rank deficiency [Wang et al., 2001]. A popular method consists of computing an approximate value for the reference ambiguity using code observations [Mader et al., 1995], such that:

$$\Delta N_i^1 \approx \frac{\Delta \widetilde{\Phi}_i^1(R) - \Delta \widetilde{P}_i^1(R)}{\lambda_i^1}. \tag{6.8}$$

Due to the uncertainty in determining the reference ambiguity using code observations, a pseudo-observation reflecting the precision of the ambiguity computed using (6.8) can be added to the system. The ambiguity covariance matrix will then properly reflect the uncertainty in this quantity: the ambiguities for which the difference in wavelengths $\lambda_i^1 - \lambda_i^n$ is the largest will have a larger variance. Using this information, a sequential rounding of ambiguities, starting with the most precise ones, can be performed [Habrich et al., 1999]. Once an ambiguity parameter can be fixed to an integer, it is then possible to explicitly estimate the error in the reference ambiguity.

Even when the contribution of the reference ambiguity is removed from (6.7) using low-noise code measurements, GLONASS ambiguities do not always converge naturally to integers. This led to the hypothesis that phase biases were also present in carrier-phase observations, and that those biases had a linear response to frequency [Pratt et al., 1997]. Furthermore, the biases seemed to be receiver-dependent and, for the most part, constant in time [Wanninger and Wallstab-Freitag, 2007]. Calibration procedures were then carried out to estimate the magnitude of the biases and the values obtained could be used

to correct carrier-phase observations to recover the integer nature of the ambiguities [Wanninger, 2012; Al-Shaery et al., 2013].

It has recently been discovered that the linear phase biases observed are in fact not true analog hardware biases [Sleewaegen et al., 2012]. Equation (6.8) assumes that phase and code observations are synchronized, which is not always the case. When a significant synchronization offset occurs between the two observables, the reference ambiguity computed using (6.8) could be in error by several cycles, even if low-noise code observations are available. An error in the *a priori* value of the reference ambiguity is then multiplied by the difference in wavelengths (6.7), which creates an apparent linear frequency response and becomes a nuisance to the ambiguity resolution process. As explained in Sleewaegen et al. [2012], the offset between code and phase observations can be accurately calibrated by the receiver manufacturers and is constant in time.

While such a correction goes a long way toward solving the problems associated with ambiguity resolution for GLONASS, it is still subject to compatibility issues. It is relatively simple for the observations of two receivers forming a single baseline to be corrected using the manufacturers' calibration values. On the other hand, when operating from a network of mixed receiver types using publicly available GNSS data, valid metadata regarding receiver types and firmware versions must be available for all stations to ensure that inter-frequency biases are properly accounted for. In the worst case, inaccurate information could compromise the validity of the products generated using this network. Therefore, to minimize the risks of applying improper inter-frequency bias

corrections, we propose an alternative means of dealing with the reference ambiguity parameter which does not require any calibration. The next sections will explain the underlying theoretical concepts, followed by a demonstration that GLONASS ambiguities naturally converge to integers with the new method.

6.2 Defining Minimum Constraints

This section proposes an alternate formulation for dealing with the reference ambiguity in GLONASS ambiguity resolution. As stated previously, the system of (6.7) has a rank deficiency of one, since defining the re-parameterization of (6.3) did not resolve the singularity problem. For the system to be solvable in a least-squares adjustment without introducing any *a priori* information, an additional constraint needs to be defined. The selection of this constraint is critical since it must preserve the integer nature of the GLONASS ambiguities.

Following the same reasoning as in the definition of (6.3), the idea is now to merge the double-differenced ambiguity of satellite 2 with the reference ambiguity parameter to obtain:

$$\Delta \widetilde{\Phi}_i^2(R) = \Delta \overline{dT}_{\Phi_i}(R) - (\lambda_i^1 - \lambda_i^2)\Delta \overline{N}_i^1. \tag{6.9}$$

From (6.7) and (6.9), the value for the estimated reference ambiguity can be determined as being:

$$\Delta \bar{N}_i^1 \equiv \Delta N_i^1(R) - \frac{\lambda_i^2 \Delta N_i^{12}(R)}{\lambda_i^1 - \lambda_i^2}. \tag{6.10}$$

The definition of (6.3) and (6.9) involves the presence of two reference satellites. Since no double-differenced ambiguity parameter is estimated for those two satellites, they allow estimating both the biased receiver clock and the biased reference ambiguity parameters. Estimating a biased receiver clock and reference ambiguity will obviously lead to biased estimates for all ambiguity parameters because of the linear dependencies between those quantities. Obtaining biased ambiguity parameters is not a problem, provided their integer property is maintained. Isolating the term $\Delta N_i^1(R)$ from (6.10) and introducing it in (6.7) for satellite n leads to:

$$\Delta \widetilde{\Phi}_i^n(R) = \Delta \overline{dT}_{\Phi_i}(R) + \lambda_i^n \Delta N_i^{1n}(R) - (\lambda_i^1 - \lambda_i^n)\left[\Delta \bar{N}_i^1 + \frac{\lambda_i^2 \Delta N_i^{12}(R)}{\lambda_i^1 - \lambda_i^2}\right]. \tag{6.11}$$

By using the relation:

$$\frac{\lambda_i^1 - \lambda_i^n}{\lambda_i^1 - \lambda_i^2} = \frac{\lambda_i^n}{\lambda_i^2}\left[\frac{k^1 - k^n}{k^1 - k^2}\right] \tag{6.12}$$

where k is the frequency channel number, equation (6.11) simplifies to:

$$\Delta \widetilde{\Phi}_i^n(R) = \Delta \overline{dT}_{\Phi_i}(R) - (\lambda_i^1 - \lambda_i^n)\Delta \bar{N}_i^1 + \lambda_i^n \Delta \bar{N}_i^{1n} \tag{6.13}$$

where

$$\Delta \bar{N}_i^{1n} = \Delta N_i^{1n}(R) - \left[\frac{k^1 - k^n}{k^1 - k^2}\right]\Delta N_i^{12}(R) \tag{6.14}$$

164

Equation (6.14) is the core of the method presented herein. It indicates that the estimated double-differenced ambiguities will be biased by a multiple of the integer double-differenced ambiguities between satellites 1 and 2. Since the frequency number values (k) are integers, this multiplication factor will only be an integer when the frequency numbers of the two reference satellites differ by one. In other words, selecting two GLONASS reference satellites with adjacent frequency numbers allows for ambiguity parameters to be estimated formally as integer values.

Summarizing, the system of equations for this new approach reads:

$$\Delta \widetilde{\Phi}_i^1(R) = \Delta \overline{dT}_{\Phi_i}(R) \tag{6.15a}$$

$$\Delta \widetilde{\Phi}_i^2(R) = \Delta \overline{dT}_{\Phi_i}(R) - (\lambda_i^1 - \lambda_i^2)\Delta \overline{N}_i^1 \tag{6.15b}$$

$$\Delta \widetilde{\Phi}_i^n(R) = \Delta \overline{dT}_{\Phi_i}(R) - (\lambda_i^1 - \lambda_i^n)\Delta \overline{N}_i^1 + \lambda_i^n \Delta \overline{N}_i^{1n} \tag{6.15c}$$

with $n > 2$. This method is independent of the code observations, and is thus free from potential biases existing between carrier-phase and code observables. As a consequence, no calibration is required for the estimated ambiguities to naturally converge to integer values. Such an approach greatly simplifies the integration of receiver types and firmware versions since it is completely independent from any biases specific to any of those entities.

6.3 Datum Transformation

The specification of decoupled clock parameters implies the need for a time-reference for the carrier-phase clock estimates, one that would otherwise be provided by the code clocks. The most obvious choice for such a reference is one of the arbitrary, but constant-valued ambiguities [Collins et al., 2010]. This concept has been extended in the previous section to two ambiguities to accommodate the apparent frequency response of fixing the first ambiguity when dealing with GLONASS observations. Hence, it is useful to refer to the initially fixed ambiguities as the datum ambiguities. Provided the minimum number of datum ambiguities is fixed, a solution can be computed.

When a change of reference satellites is necessary, and no other ambiguities have been explicitly fixed, a rigorous datum transformation is required to maintain the formal integer nature of the remaining ambiguity parameters. Writing the system of (6.15) in matrix form:

$$\boldsymbol{l} = \boldsymbol{A}\boldsymbol{x} \tag{6.16}$$

where $\boldsymbol{l}$ is the vector of observations, $\boldsymbol{A}$ is the design matrix, and $\boldsymbol{x}$ is the vector of parameters, permits a change in datum using the following transformation [Grafarend and Schaffrin, 1976]:

$$\boldsymbol{A}_{D1}\boldsymbol{x}_{D1} = \boldsymbol{A}_{D2}\boldsymbol{x}_{D2}$$

$$\boldsymbol{x}_{D2} = (\boldsymbol{A}_{D2}^{T}\boldsymbol{A}_{D2})^{-1}\boldsymbol{A}_{D2}^{T}\boldsymbol{A}_{D1}\boldsymbol{x}_{D1} = \boldsymbol{D}_{D21}\boldsymbol{x}_{D1} \tag{6.17}$$

where the subscript denotes datum identification. The datum definitions are fully contained within the design matrices, and the transformation presented in (6.17) constitutes a simple recombination of parameters. Matrix $\boldsymbol{D}_{D21}$ can be shown to be a similarity transformation in the *S-Basis* method [Teunissen, 1985]. The covariance matrix should also be propagated as:

$$\boldsymbol{Q}_{x_{D2}} = \boldsymbol{D}_{D21}\boldsymbol{Q}_{x_{D1}}\boldsymbol{D}_{D21}^{T}. \tag{6.18}$$

Since the estimated parameters are biased by ambiguity values, a change in datum could result in discrete jumps in the clock and ambiguity parameters. This, however, is not a concern since it will not affect the position solution, provided that the transformation is handled properly. In fact, if coordinate estimates were included in the vector of parameters, the transformation defined by (6.17) would yield the identity matrix for this group of parameters, meaning that their values would remain unaltered. Once two non-datum GLONASS carrier-phase ambiguities are fixed to integers, regardless of their frequency number, datum continuity is preserved without any explicit datum transformation.

6.4 Estimation of GLONASS Inter-frequency Code Biases

For a reliable estimation of integer carrier-phase ambiguities, it is imperative that the underlying code-based solution be unbiased. For this reason, inter-frequency code biases

(IFCB) of GLONASS satellites need to be properly accounted for [Felhauer, 1997; Yamada et al., 2010]. While de-weighting of GLONASS code observations in a combined GPS+GLONASS solution might be a feasible approach [Cai and Gao, 2013], it will not benefit a GLONASS-only solution. Performing an *a priori* calibration of IFCB using a linear model was proposed by Al-Shaery et al. [2013], although previous studies have demonstrated that IFCB could have a non-linear response to the frequency number and as well as a code-type dependency [Kozlov et al., 2000]. Such characteristics are certainly a nuisance for calibration purposes [Reussner and Wanninger, 2011]. Another approach consists of estimating one bias parameter per frequency number [Defraigne and Baire, 2011]. Even though it is a more rigorous approach, it significantly increases the total number of unknowns.

In our approach, the GLONASS code-clock model is augmented to account for a possible linear response to frequency:

$$\Delta \overline{dT}_{P_i}^j(R) = \Delta dT_{P_i}(R) + k^j \Delta b_{P_i}. \tag{6.19}$$

Equation (6.19) effectively takes into account a time-dependent common offset for all GLONASS satellites on a given signal, in addition to a possible frequency-dependent linear trend, typically modelled as slowly-varying parameters. Such an approach is self-calibrating and could potentially deal with inter-frequency bias fluctuations related to temperature, firmware updates, etc. While the frequency response of some receiver types might not be perfectly modelled using a linear fit, estimating the slope of the IFCB will at least remove first-order effects. If needed, equation (6.19) can easily be expanded to include a quadratic term to handle non-linear frequency responses.

168

6.5 Proof of Concept

As a proof of concept, the method presented was applied to a number of zero and short baselines with mixed receiver types. The use of short baselines was chosen to remove or greatly reduce atmospheric effects from the problem, focusing on showing the recovered integer nature of GLONASS ambiguities with the proposed modelling. Three receivers located on the University of New Brunswick (UNB) campus in Fredericton, Canada, share the same antenna and thus form a zero-baseline. Natural Resources Canada's (NRCan) FRDN station is situated 2.3 km away and allows for short-baseline evaluation. Table 6.1 summarizes the equipment used at each station, as extracted from the RINEX file header. Data from January 1, 2012, was arbitrarily selected and a sampling interval of 30 seconds was used.

As a first test, a GPS+GLONASS single-frequency (SF) solution on L_1 is computed for stations UNB3 and UNBN. The purpose of adding GPS data to the solution is purely geometric. Since L_1 and C_1 observables are used for both systems, a total of 4 clock parameters are estimated to properly isolate equipment delays, as emphasized by (6.1) and (6.2). Following (6.19), GLONASS inter-frequency code biases are modelled as a linear function with respect to the frequency number. Additionally, epoch-independent baseline components and float carrier-phase ambiguities are estimated in a least-squares

169

filter. A summary of the parameters involved, omitting carrier-phase ambiguities, is presented in the column labelled 'GPS+GLO (SF)' in Table 6.2.

Table 6.1: Stations and equipment used following the International GNSS Service (IGS) nomenclature.

Station	Receiver	Antenna
UNBJ	TPS LEGACY	JPSREGANT_DD_E NONE
UNB3	TRIMBLE NETR5	JPSREGANT_DD_E NONE
UNBN	NOV OEMV3	JPSREGANT_DD_E NONE
FRDN	TPS NETG3	TPSCR.G3 NONE

Figure 6.1 illustrates the estimated carrier-phase ambiguities for every GLONASS satellite. The value for each arc is shifted by an integer constant so that the values displayed match the frequency number (k) of the satellite. A different color is used for satellites sharing the same frequency number. It is clear from this plot that all estimated ambiguity parameters naturally converge to integer values. Previous studies indicated that a 3 cm bias per frequency number existed between Trimble and NovAtel receivers [Wanninger, 2012], and it is emphasized that no *a priori* calibration values were applied in this study. Some small discontinuities can at times be observed in the times series of Figure 6.1 and are associated with datum changes. Those jumps would not occur if

ambiguities were explicitly fixed to integers in the filter as opposed to keeping float values.

Table 6.2: Number of parameters involved in short-baseline processing of GPS and GLONASS (GLO) single-frequency (SF) or dual-frequency (DF) observations. Approach #1 is using external calibration values, while approach #2 is the proposed calibration-free method.

Parameters	Solutions					
	GPS + GLO (SF)	GPS only (DF)	GLO only (DF)		GPS + GLO (DF)	
	#2		#1	#2	#1	#2
Baseline components	3	3	3	3	3	3
Receiver phase clocks	2	2	2	2	4	4
Reference ambiguities	1	0	0	2	0	2
Receiver code clocks	2	2	2	2	4	4
IFCB	1	0	2	2	2	2
Total	9	7	9	11	13	15
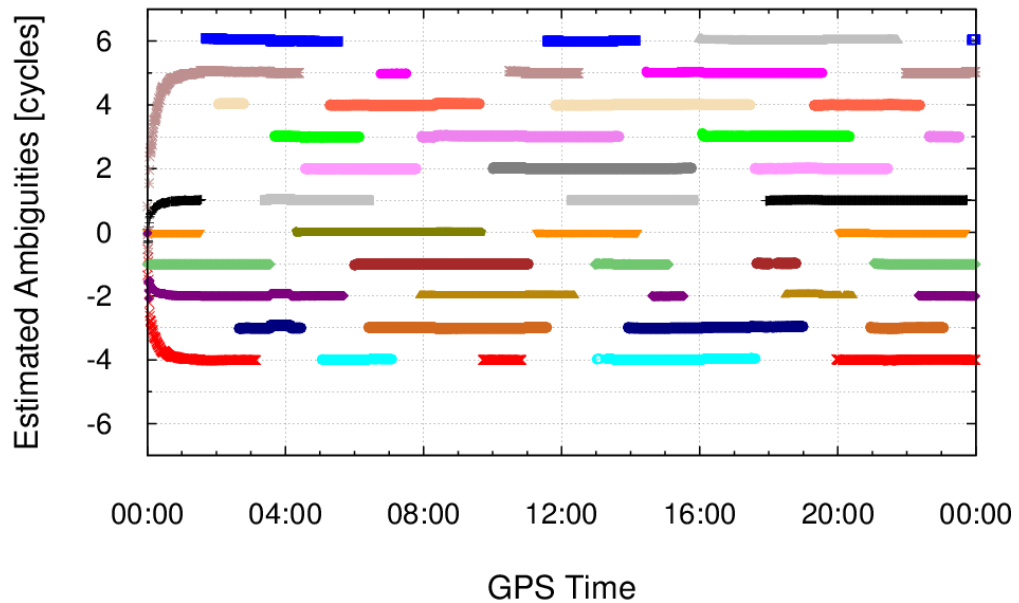
Figure 6.1: Estimated GLONASS carrier-phase ambiguity parameters for the UNBN (NovAtel OEMV3) and UNB3 (Trimble NetR5) baseline. The value for each arc was shifted by an integer constant so that the values displayed match the frequency number (k) of the satellite.

To further confirm the validity of our approach, Figure 6.2 and Figure 6.3 present the estimated baseline components and the carrier-phase residuals of all GLONASS satellites, respectively. Since both receivers share the same antenna, the expected baseline length is zero. This configuration also greatly mitigates multipath errors, resulting in carrier-phase residuals representing phase noise. The zero-mean characteristic of the residuals, along with an accurate determination of the baseline components, emphasizes

172

that no bias or unmodelled quantity contaminates the observations. Inter-frequency code biases appear clearly in code residuals when not properly accounted for in the functional model (see Figure 6.4a). Using the linear representation of (6.19) allows for unbiased code residuals and thus for a more coherent solution to be obtained, as illustrated in Figure 6.4b.
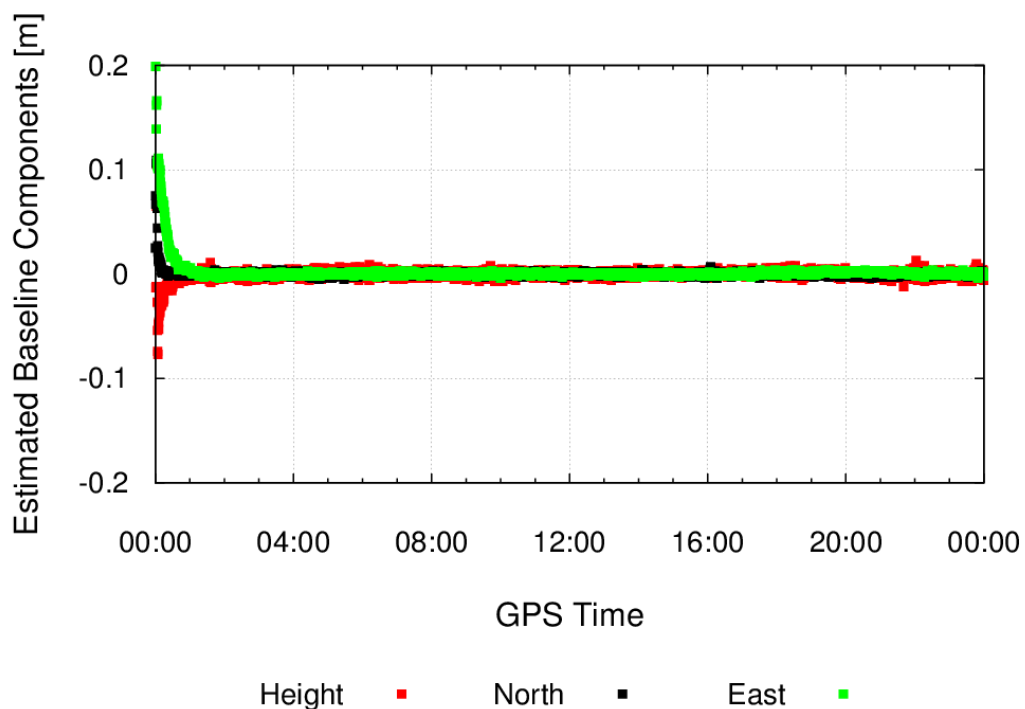
Figure 6.2: Estimated baseline components for GPS+GLO (SF) UNBN-UNB3 solution.

Equation (6.3) indicates that the estimated receiver phase-clock parameter is biased by the choice of a reference ambiguity which is different for each signal type. Hence, the estimated receiver phase clock does not represent the "true" clock offset but rather an integer-biased relative equipment delay. Due to this characteristic, it is subject to

173

discontinuities when a datum change occurs. This fact is highlighted in Figure 6.5 where the offset between the GPS and GLONASS receiver phase clocks is displayed. Every time a datum change occurs, the value for the system offset is affected. A similar phenomenon also affects the GLONASS reference ambiguity. These parameter variations are only artifacts of the datum definition and do not affect the estimated baseline components. Also displayed in Figure 6.5 is the difference between the estimated code clocks (for $k^j = 0$ in (6.19)), which represents the inter-system bias. Even though this quantity is often modelled as a random walk process [Cai and Gao, 2008], code clocks for each system are estimated as a white noise process to model all possible clock effects, including arbitrary clock jumps.
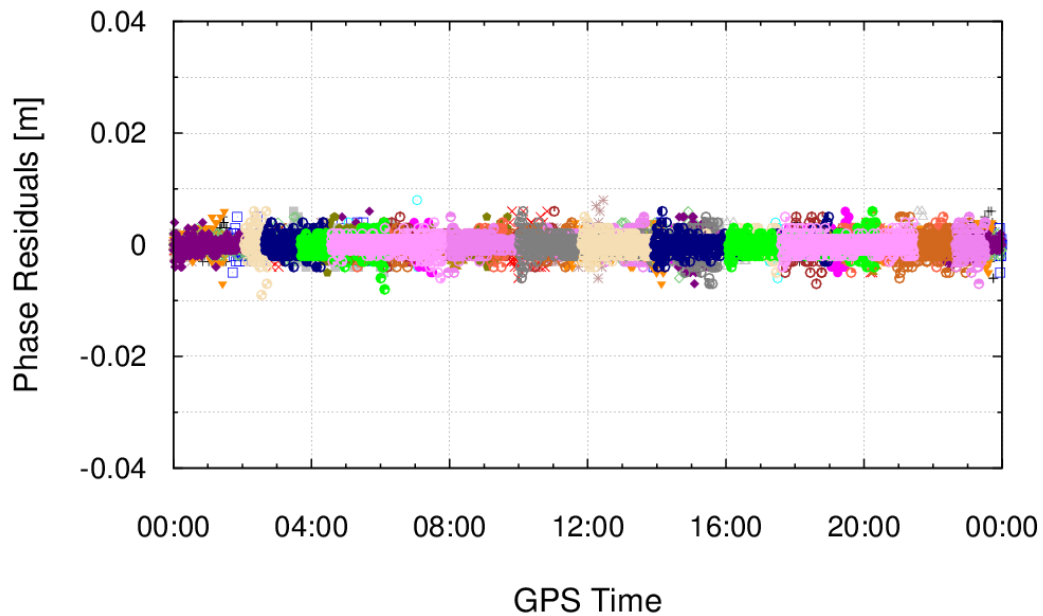
Figure 6.3: GLONASS carrier-phase residuals for baseline UNBN-UNB3 (GPS+GLO (SF) solution).

174
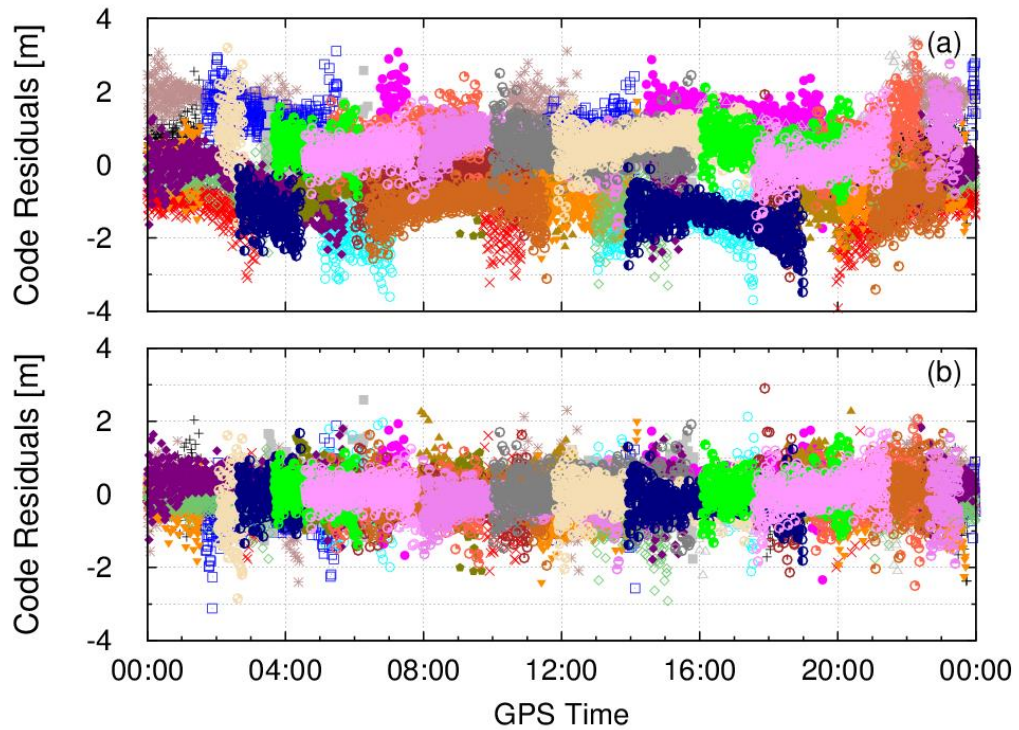
Figure 6.4: GLONASS code residuals for baseline UNBN-UNB3 without inter-frequency code bias (IFCB) estimation (panel *a*), and using the linear representation of (6.19) (panel b) (GPS+GLO (SF) solution).

A Javad Legacy receiver, used for International GNSS Service (IGS) station UNBJ, is also connected to the same antenna. A zero-baseline was again formed with station UNBN and the same methodology was applied for data processing. Regardless of the receiver types involved, selecting two GLONASS satellites with adjacent frequency numbers as reference satellites allows recovering the integer nature of the estimated GLONASS carrier-phase ambiguities. This fact is again confirmed by examining Figure 6.6 which shows the initial convergence of the GLONASS ambiguities to integer values.

175

At the beginning of the session, ambiguities for satellites R11 and R12, with frequency numbers 0 and -1 respectively, were selected as reference satellites. This constraint was sufficient for all other ambiguities to converge to integer values as well. Shortly after 01:30 GPST, satellite R11 was tracked at an elevation angle below 10 degrees, triggering a datum change. At this point, satellites R12 and R13, with frequency numbers -1 and -2, became the reference satellites. As apparent from Figure 6.6, the requirement of simultaneously tracking GLONASS satellites with adjacent frequency numbers does not impose any limitation in this case. Figure 6.1 also demonstrates that this condition is almost always satisfied with good satellite coverage. Still, when satellite tracking is obstructed, it is possible that formal integer-valued ambiguity estimation will be temporarily impractical, but it is emphasized that the requirement to fix the ambiguities of two satellites with adjacent *k*-values is an initial condition only.

To evaluate the performance of instantaneous ambiguity resolution without external calibration, short baselines were defined between stations FRDN and all three UNB receivers. Dual-frequency signals were processed, and three solutions were computed: 1) a GPS-only solution, 2) a GLONASS-only solution, and 3) a GPS+GLONASS solution. The parameters involved for each solution are described in Table 6.2. Two approaches were used to handle the GLONASS reference ambiguities and carrier-phase inter-frequency biases. The first approach computes reference ambiguities using code observations and uses calibration values suggested by Wanninger [2012] to mitigate the impacts of misaligned code and phase observations. The second approach is based on the theoretical developments presented here; i.e. no calibration values are used and the

integer nature of the GLONASS ambiguities is retrieved by selecting two reference satellites with adjacent frequency numbers. At every epoch, ambiguity parameters were reset and full ambiguity resolution was attempted. Ambiguity resolution was considered successful if the selected integer candidates match the final ambiguity estimates of a daily batch solution and the ratio test is above 2 [Landau and Euler, 1992]. The ambiguity resolution success rates are presented in Table 6.3.
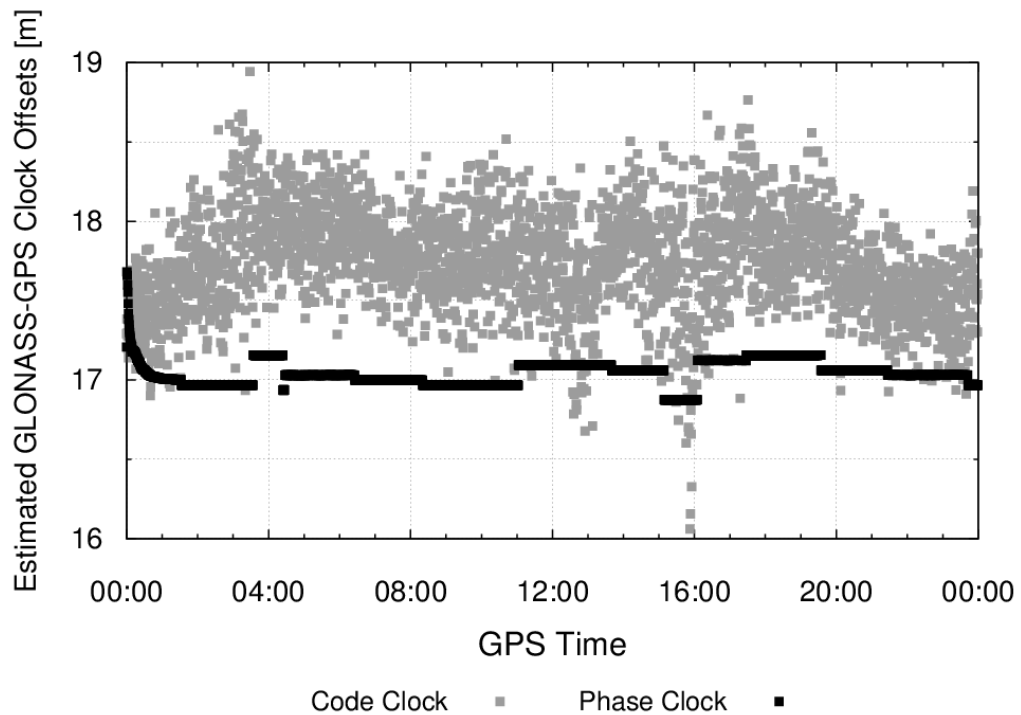
Figure 6.5: Estimated GLONASS-GPS receiver clock offsets for baseline UNBN-UNB3 (GPS+GLO (SF) solution).
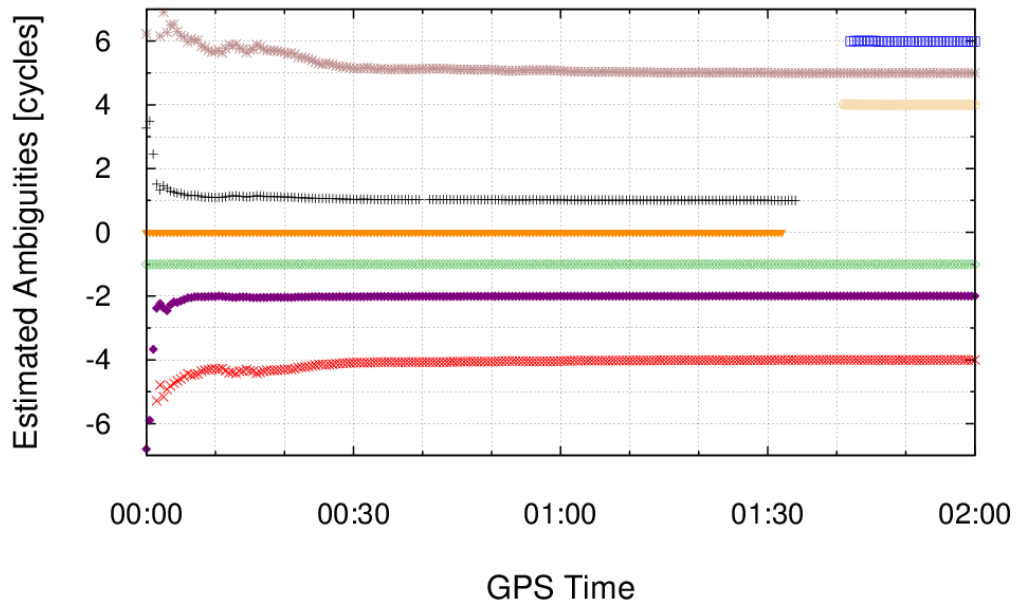
Figure 6.6: GLONASS ambiguity convergence for the UNBN (NovAtel OEMV3) and UNBJ (Javad Legacy) baseline. The value for each arc was shifted by an integer constant so that the values displayed match the frequency number (*k*) of the satellite.

Table 6.3 suggests that the performance of instantaneous ambiguity resolution depends largely on the underlying code solution. The weaker geometry associated with a GLONASS-only solution, combined with the extra parameters required for proper bias handling, translates into a lower probability of single-epoch ambiguity resolution. Those results are confirmed by looking at the average precision of the estimated ambiguities, expressed using the ambiguity dilution of precision (ADOP) factor [Teunissen and Odijk, 1997]. The (mean) value per processing strategy is provided in Table 6.3. Estimating reference ambiguity parameters (case #2) leads to ambiguities that are less precisely

178

defined as opposed to fixing those quantities using *a priori* calibration values. Hence, while opting for a calibration-free approach reduces the dependency on external information, it also leads to a performance loss with regard to instantaneous ambiguity resolution. However, this problem is mitigated to a great extent when integrating GPS and GLONASS since the enhanced geometry of the joint solution allows for a better determination of the ambiguities.

Table 6.3: Instantaneous ambiguity resolution success rate in percent and mean ADOP for three mixed-receiver baselines based on dual-frequency (DF) processing of GPS and/or GLONASS data. Approach #1 is using external calibration values, while approach #2 is the proposed calibration-free method.

Baseline	GPS only (DF)	GLO only (DF)		GPS + GLO (DF)	
		#1	#2	#1	#2
UNBJ-FRDN	99.4	95.6	76.1	99.3	98.6
UNB3-FRDN	99.4	96.0	70.6	99.7	99.0
UNBN-FRDN	99.0	94.8	70.9	99.7	99.0
Mean ADOP [cycles]	0.08	0.12	0.20	0.05	0.07

6.6 Conclusion

GLONASS ambiguity resolution with mixed receiver types is more complicated than its GPS counterpart due to the FDMA signals and the non-alignment of code and phase observables. While calibration can be done to solve this problem, we demonstrated that carrier-phase ambiguities can be modelled as formal integer parameters and therefore naturally converge to integer values. This is achieved by defining a set of minimum constraints to solve for the system's rank deficiency. It was shown that, for frequency-dependent GLONASS carrier phases, selecting two reference satellites with adjacent frequency numbers for datum ambiguity definition is the key to preserving the integer nature of the ambiguities. Using this model permits processing of baselines with mixed receiver types showing unbiased estimates of baseline components and carrier-phase residuals, demonstrating the validity of our approach.

Explicitly estimating GLONASS reference ambiguity parameters does weaken the solution compared to using external calibration values. However, removing the dependency on external information for GLONASS ambiguity resolution is of critical importance when processing a network of publicly available stations, especially in real time. This approach will be further developed and generalized to handle ionospheric effects for longer baselines, and the processing of undifferenced GLONASS observations for precise point positioning.

Acknowledgements

References

Al-Shaery, A., S. Zhang, and C. Rizos (2013). "An enhanced calibration method of GLONASS inter-channel bias for GNSS RTK," *GPS Solutions*, Vol. 17, No. 2, pp. 165-173. doi: 10.1007/s10291-012-0269-5.

Cai, C., and Y. Gao (2008). "Estimation of GPS-GLONASS system time difference with application to PPP," *Proceedings of the 21st International Technical Meeting of the Satellite Division of The Institute of Navigation (ION GNSS 2008)*, Savannah, Ga., 16-19 September 2008, pp. 2880-2887.

Cai, C., and Y. Gao (2013). "Modeling and assessment of combined GPS/GLONASS precise point positioning," *GPS Solutions*, Vol. 17, No. 2, pp. 223-236. doi: 10.1007/s10291-012-0273-9.

Collins, P., S. Bisnath, F. Lahaye, and P. Héroux (2010). "Undifferenced GPS ambiguity resolution using the decoupled clock model and ambiguity datum fixing," *NAVIGATION: Journal of The Institute of Navigation*, Vol. 57, No. 2, Summer 2010, pp. 123-135.

Defraigne, P., and Q. Baire (2011). "Combining GPS and GLONASS for time and frequency transfer," *Advances in Space Research*, Vol. 47, No. 2, pp. 265-275. doi: 10.1016/j.asr.2010.07.003.

Felhauer, T. (1997). "On the impact of RF front-end group delay variations on GLONASS pseudorange accuracy," *Proceedings of the 10th International Technical Meeting of the Satellite Division of The Institute of Navigation (ION GPS 1997)*, Kansas City, Mo., 16-19 September 1997, pp. 1527-1532.

Grafarend, E., and B. Schaffrin (1976). "Equivalence of estimable quantities and invariants in geodetic networks," *Zeitschrift für Vermessungswesen*, Vol. 101, pp. 485-491.

Habrich, H., G. Beutler, W. Gurtner, and M. Rothacher (1999). "Double difference ambiguity resolution for GLONASS/GPS carrier phase," *Proceedings of the 12th International Technical Meeting of the Satellite Division of The Institute of Navigation (ION GPS 1999)*, Nashville, Tenn., 14-17 September 1999, pp. 1609-1618.

Kozlov, D., M. Tkachenko, and A. Tochilin (2000). "Statistical characterization of hardware biases in GPS+GLONASS receivers," *Proceedings of the 13th International Technical Meeting of the Satellite Division of The Institute of Navigation (ION GPS 2000)*, Salt Lake City, Utah, 19-22 September 2000, pp. 817-826.

Landau, H., and H.-J. Euler (1992). "On-the-fly ambiguity resolution for precise differential positioning," *Proceedings of the 5th International Technical Meeting of the Satellite Division of The Institute of Navigation (ION GPS 1992)*, Albuquerque, N.M., 16-18 September 1992, pp. 607-613.

Mader, G., J. Beser, A. Leick, and J. Li (1995). "Processing GLONASS carrier phase observations - theory and first experience," *Proceedings of the 8th International Technical Meeting of the Satellite Division of The Institute of Navigation (ION GPS 1995)*, Palm Springs, Calif., 12-15 September 1995, pp. 1041-1047.

Pratt, M., B. Burke, and P. Misra (1997). "Single-epoch integer ambiguity resolution with GPS L1-L2 carrier phase measurements," *Proceedings of the 10th International Technical Meeting of the Satellite Division of The Institute of Navigation (ION GPS 1997)*, Kansas City, Mo., 16-19 September 1997, pp. 1737-1746.

Reussner, N., and L. Wanninger (2011). "GLONASS inter-frequency biases and their effects on RTK and PPP carrier-phase ambiguity resolution," *Proceedings of the 24th International Technical Meeting of the Satellite Division of The Institute of Navigation (ION GNSS 2011)*, Portland, Ore., 19-23 September 2011, pp. 712-716.

Sleewaegen, J. M., A. Simsky, W. de Wilde, F. Boon, and T. Willems (2012). "Demystifying GLONASS inter-frequency carrier phase biases," *InsideGNSS*, Vol. 7, No. 3, pp. 57-61.

Takac, F. (2009) "GLONASS inter-frequency biases and ambiguity resolution," *InsideGNSS*, Vol. 4, No. 2, pp. 24-28.

Teunissen, P. J. G. (1985). "Zero order design: generalized inverses, adjustment, the datum problem and S-transformations," In: Grafarend E. W., and Sansò F (eds) Optimization and Design of Geodetic Networks, Springer-Verlag, pp 11-55.

Teunissen, P. J. G., and D. Odijk (1997). "Ambiguity dilution of precision: definition, properties and application," *Proceedings of the 10th International Technical Meeting of the Satellite Division of The Institute of Navigation (ION GPS 1997),* Kansas City, Mo., 16-19 September 1997, pp. 891-899.

Wang, J., C. Rizos, M. P. Stewart, and A. Leick (2001). "GPS and GLONASS integration: modeling and ambiguity resolution issues," *GPS Solutions*, Vol. 5, No. 1, pp. 55-64. doi: 10.1007/PL00012877.

Wanninger, L. (2012). "Carrier-phase inter-frequency biases of GLONASS receivers," *Journal of Geodesy*, Vol. 86, No. 2, pp. 139-148. doi: 10.1007/s00190-011-0502-y.

Wanninger, L., and S. Wallstab-Freitag (2007). "Combined processing of GPS, GLONASS, and SBAS code phase and carrier phase measurements," *Proceedings of the 20th International Technical Meeting of the Satellite Division of The Institute of Navigation (ION GNSS 2007)*, Fort Worth, Texas, 25-28 September 2007, pp. 866-875.

Yamada, H., T. Takasu, N. Kubo, and A. Yasuda (2010). "Evaluation and calibration of receiver inter-channel biases for RTK-GPS/GLONASS," *Proceedings of the 23rd International Technical Meeting of the Satellite Division of The Institute of Navigation (ION GNSS 2010)*, Portland, Ore., 21-24 September 2010, pp. 1580-1587
.

CHAPTER 7

CONCEPTS FOR UNDIFFERENCED GLONASS AMBIGUITY RESOLUTION

This chapter applies the concepts developed in the previous chapter to demonstrate the feasibility of undifferenced GLONASS ambiguity resolution. The possibility of fixing ambiguities for both GPS and GLONASS is yet another aspect for faster convergence of PPP solutions.

The following was originally published as:

Banville, S., P. Collins, and F. Lahaye (2013). "Concepts for undifferenced GLONASS ambiguity resolution," *Proceedings of the 26th International Technical Meeting of the Satellite Division of The Institute of Navigation (ION GNSS+ 2013)*, Nashville, Tenn., 16-20 September, pp. 1186-1197.

Modifications to the original manuscript were made only for proper identification of sections, figures and tables, as well as to assure the uniformity of symbol and equation notation throughout this dissertation. An additional reference to Mervart [1995] was also added, and Figures 11 to 16 of the original manuscript were also combined to form Figure 7.11.

Abstract

To achieve undifferenced GLONASS ambiguity resolution, it is imperative to adequately model both inter-frequency carrier-phase and code biases. This paper demonstrates that the apparent linear frequency response associated with carrier phases can be rigorously modelled by selecting two reference satellites with adjacent frequency channels. This condition allows explicit estimation of the frequency response, while preserving the integer properties of all ambiguity parameters. Applying this concept to the Melbourne-Wübbena (MW) combination also removes the linear dependency of the narrowlane inter-frequency code biases (IFCBs) to the frequency channel number. Unfortunately, this method alone is not sufficient for recovering the integer properties of GLONASS widelane ambiguities, and satellite MW biases are estimated based on clusters of stations with similar equipment. To accommodate stations with unique IFCB characteristics, ambiguity resolution in the presence of biases is discussed. Application of these concepts shows that GLONASS ambiguity resolution for mixed receiver types is feasible based on the MW combination.

7.1 Introduction

Precise point positioning (PPP) allows single-receiver accurate positioning through the use of precise satellite orbit and clock products. Recently, fixing of GPS carrier-phase

ambiguities in PPP has become possible through proper handling of satellite and receiver equipment delays, leading to reduced convergence time and improved stability of the position estimates [Ge et al., 2008; Laurichesse et al., 2009; Collins et al., 2010]. Combining GPS and GLONASS has been shown to be beneficial as a result of increased redundancy and enhanced geometry [Cai and Gao, 2013], however GLONASS ambiguity resolution is problematic because of the nature of frequency division multiple access (FDMA).

Even in differential mode, processing of GLONASS data from mixed receiver types is impacted by receiver design. It was demonstrated by Sleewaegen et al. [2012] that a misalignment between code and phase observables results in apparent inter-frequency carrier-phase biases, which need to be properly handled in order to perform ambiguity resolution. For this purpose, receiver-dependent inter-frequency phase corrections were proposed by Wanninger [2012]. Residual effects, caused by antenna type or receiver firmware for instance, can then be estimated as a part of the navigation filter. When no *a priori* values are available, a sequential ambiguity fixing procedure can be used to estimate the inter-frequency phase biases but requires longer observation sessions [Habrich et al., 1999].

GLONASS code measurements are also affected by inter-frequency code biases (IFCBs) which should be taken into consideration even for improved processing of short baselines [Kozlov et al., 2000]. Calibration values of such biases for several receiver types was proposed by Al-Shaery et al. [2013], although variations due to firmware

version and antenna have been observed by Chuang et al. [2013]. When it comes to processing of long baselines, code observations play a crucial role by providing information on the ionosphere. Hence, the presence of umodelled IFCBs typically limits GLONASS ambiguity resolution for baseline lengths over which the ionosphere cancels out or can be predicted using external information.

The ambiguity resolution challenges associated with PPP are fundamentally the same as for long-baseline differential positioning. Undifferenced GLONASS ambiguity resolution could be performed provided that a precise representation of the ionosphere is available [Reussner and Wanninger, 2011]. However, for PPP with ambiguity resolution to be applicable globally, it is necessary to investigate the possibility of mitigating the impacts of IFCBs. For this purpose, this paper first explains how linear inter-frequency biases can be estimated on the fly. To account for residual IFCB effects, ambiguity resolution in the presence of biases is also discussed. An analysis is then conducted to identify how various pieces of equipment affect IFCBs and to determine the consistency of such biases for stations with similar hardware.

7.2 Estimating Inter-Frequency Biases

When dealing with mixed receiver types, it is common practice to apply *a priori* corrections to account for inter-frequency phase biases [Wanninger, 2012]. Since those

biases really originate from timing considerations between carrier-phase and code observables, an approach that relies solely on phase measurements was proposed by Banville et al. [2013]. This section first reviews the theoretical developments underlying this method, and then applies those concepts to the Melbourne-Wübbena combination.

7.2.1 Generic Case

A simplified functional model for carrier-phase and code observables can be defined as:

$$\Phi_i^j + dt_{\Phi_i}^j = dT_{\Phi_i} + \lambda_i^j N_i^j \tag{7.1}$$

$$P_i^j + dt_{P_i}^j = dT_{P_i} + k^j \lambda_i^j B_{P_i} \tag{7.2}$$

where

Φ is the carrier-phase measurement (m)

P is the code measurement (m)

i identifies signal-dependent quantities

j identifies satellite-dependent quantities

dt is the combined satellite clock offset and equipment delays (m)

dT is the combined receiver clock offset and equipment delays (m)

λ is the wavelength of the carrier on the L_i link (m)

N is the integer carrier-phase ambiguity (cycles)

k is the frequency channel number

B contains instrumental biases (cycles).

Equations (7.1) and (7.2) assume, without loss of generality, that the user and satellite positions as well as the atmospheric delays are known. It is important to note that different clock parameters were defined for each observable on each frequency, which is the key to properly isolate equipment delays [Collins et al., 2010]. At this point, satellite clock offsets are included on the left side of the equations since, for PPP users, they are considered as known quantities. Additional considerations for estimating satellite clock offsets will be provided in a subsequent section. Inter-frequency code biases are modelled as a linear function of the frequency channel number to remove first-order effects.

Forming a system of equations using n satellites will lead to a rank-deficient system for carrier phases because each phase measurement is biased by an unknown integer number of cycles. To remove this singularity, it is possible to fix, i.e. not estimate, the ambiguity of one satellite. As a consequence, the estimated receiver clock will be biased by this reference ambiguity, labeled with superscript "1":

$$\overline{dT}_{\Phi_i} = dT_{\Phi_i} + \lambda_i^1 N_i^1 \tag{7.3}$$

where the overbar symbol denotes biased quantities. Isolating dT_{Φ_i} from equation (7.3) and introducing it into equation (7.1) leads to the following system of equations:

$$\Phi_i^1 + dt_{\Phi_i}^1 = \overline{dT}_{\Phi_i} \tag{7.4a}$$

$$\Phi_i^n + dt_{\Phi_i}^n = \overline{dT}_{\Phi_i} - (\lambda_i^1 - \lambda_i^n)N_i^1 + \lambda_i^n N_i^{1n} \tag{7.4b}$$

where $n > 1$ and $N^{1n} = N^n - N^1$. Since every GLONASS satellite in view transmits signals at a slightly different frequency, the reference ambiguity still appears as an

189

unknown quantity in equation (7.4b) and causes another singularity. To overcome this problem, it is possible to fix the ambiguity of another satellite for the purpose of estimating a biased reference ambiguity parameter ($\bar{N}_i^1$), leading to:

$$\Phi_i^1 + dt_{\Phi_i}^1 = \overline{dT}_{\Phi_i} \tag{7.5a}$$

$$\Phi_i^2 + dt_{\Phi_i}^2 = \overline{dT}_{\Phi_i} - (\lambda_i^1 - \lambda_i^2)\bar{N}_i^1 \tag{7.5b}$$

$$\Phi_i^n + dt_{\Phi_i}^n = \overline{dT}_{\Phi_i} - (\lambda_i^1 - \lambda_i^n)\bar{N}_i^1 + \lambda_i^n \bar{N}_i^{1n} \tag{7.5c}$$

where $n > 2$. In equation (7.5), the newly defined terms can be expressed as:

$$\bar{N}_i^1 = N_i^1 + \frac{\lambda_i^2}{\lambda_i^1 - \lambda_i^2} N_i^{12} \tag{7.6}$$

$$\bar{N}_i^{1n} = N_i^{1n} - \left[\frac{k^1 - k^n}{k^1 - k^2}\right] N_i^{12}. \tag{7.7}$$

The system of equations (7.5) now contains n carrier-phase observations and n unknowns (the receiver clock offset, reference ambiguity parameter and (n - 2) ambiguity parameters) and is thus of full rank. Equation (7.7) indicates that selecting two reference satellites with adjacent frequency channel numbers, i.e. $|k^1 - k^2| = 1$, allows estimating GLONASS ambiguities as formal integer values with full wavelength. A practical demonstration of this concept was presented by Banville et al. [2013], where estimated ambiguity parameters between mixed receiver types naturally converge to integers without applying any *a priori* corrections for inter-frequency phase biases.

7.2.2 Melbourne-Wübbena Combination

Ambiguity resolution in PPP often relies on the Melbourne-Wübbena (MW) combination [Melbourne, 1985; Wübbena, 1985]:

$$\Phi_{MW}^j + b_{\Phi_{MW}}^j = b_{\Phi_{MW}} + \lambda_{WL}^j N_{WL}^j + k^j \lambda_{NL}^j B_{NL} \tag{7.8}$$

where clock offsets are replaced by biases (b). While equation (7.8) has a similar structure as equation (7.1), the presence of the narrowlane (NL) IFCBs must be properly accounted for to preserve the integer characteristics of the widelane (WL) ambiguity parameters. The procedure outlined previously can be applied by first defining:

$$\bar{b}_{\Phi_{MW}} = b_{\Phi_{MW}} + \lambda_{WL}^1 N_{WL}^1 + k^1 \lambda_{NL}^1 B_{NL}. \tag{7.9}$$

Isolating $b_{\Phi_{MW}}$ in equation (7.9) and introducing it in equation (7.8) leads to the following system of equations:

$$\Phi_{MW}^1 + b_{\Phi_{MW}}^1 = \bar{b}_{\Phi_{MW}} \tag{7.10a}$$

$$\Phi_{MW}^n + b_{\Phi_{MW}}^n = \bar{b}_{\Phi_{MW}} - (\lambda_{WL}^1 - \lambda_{WL}^n) N_{WL}^1 + \lambda_{WL}^n N_{WL}^{1n}$$
$$-(k^1 \lambda_{NL}^1 - k^n \lambda_{NL}^n) B_{NL} \tag{7.10b}$$

where $n > 1$. In order to obtain a form similar to the one of equation (7.5), we define:

$$\bar{N}_{WL}^1 = N_{WL}^1 - \frac{\lambda_{WL}^2}{\lambda_{WL}^1 - \lambda_{WL}^2} N_{WL}^{12} + \left[\frac{k^1 \lambda_{NL}^1 - k^2 \lambda_{NL}^2}{\lambda_{WL}^1 - \lambda_{WL}^2} \right] B_{NL}. \tag{7.11}$$

By using the relation $f_2^n = \frac{7}{9} f_1^n$, and after some algebraic manipulations, the term in brackets in the previous equation simplifies to:

$$\frac{k^1 \lambda_{NL}^1 - k^2 \lambda_{NL}^2}{\lambda_{WL}^1 - \lambda_{WL}^2} = -\frac{f_1 - f_2}{f_1 + f_2} \cdot \frac{f_1}{\Delta f_1} \equiv r_f \tag{7.12}$$

where $f_1 = 1602$ MHz and $f_2 = 1246$ MHz are the nominal frequencies of the L_1 and L_2 carriers, while $\Delta f_1 = 0.5625$ MHz is the frequency spacing between adjacent frequency channels of the L_1 carrier. Hence, the quantity of equation (7.12) is independent of the satellites involved in its computation. Isolating N_{WL}^1 from equation (7.11) and substituting it back into equation (7.10) gives:

$$\Phi_{MW}^1 + b_{\Phi_{MW}}^1 = \bar{b}_{\Phi_{MW}} \tag{7.13a}$$

$$\Phi_{MW}^2 + b_{\Phi_{MW}}^2 = \bar{b}_{\Phi_{MW}} - (\lambda_{WL}^1 - \lambda_{WL}^2)\bar{N}_{WL}^1 \tag{7.13b}$$

$$\Phi_{MW}^n + b_{\Phi_{MW}}^n = \bar{b}_{\Phi_{MW}} - (\lambda_{WL}^1 - \lambda_{WL}^n)\bar{N}_{WL}^1 + \lambda_{WL}^n \bar{N}_{WL}^{1n} - \omega \cdot B_{NL} \tag{7.13c}$$

where $\bar{N}_{WL}^{1n}$ takes the form of equation (7.7), and:

$$\begin{aligned}
\omega &= (\lambda_{WL}^1 - \lambda_{WL}^n) \cdot r_f - (k^1 \lambda_{NL}^1 - k^n \lambda_{NL}^n) \\
&= (\lambda_{WL}^1 - \lambda_{WL}^n) \cdot \left[r_f - \frac{k^1 \lambda_{NL}^1 - k^n \lambda_{NL}^n}{\lambda_{WL}^1 - \lambda_{WL}^n} \right] \\
&= (\lambda_{WL}^1 - \lambda_{WL}^n) \cdot [r_f - r_f] \\
&= 0.
\end{aligned} \tag{7.14}$$

With ω taking a value of zero, the system of equation (7.13) for the Melbourne-Wübbena combination takes the same form as the generic case of equation (7.5). This implies that explicit estimation of the reference ambiguity parameter absorbs narrowlane IFCBs, provided that they are a linear function of the frequency channel number.

7.3 Ambiguity Resolution in the Presence of Biases

The integer least-squares approach to ambiguity resolution consists of finding the vector of integer values that minimizes the distance to the float ambiguity estimates in the metric of the ambiguity covariance matrix [Teunissen, 1993]. This approach was shown to be optimal [Teunissen, 1999b], but this statement only holds provided that the ambiguity covariance matrix is properly defined. Hence, the performance of ambiguity resolution can be greatly affected by the presence of unmodelled biases [Teunissen, 2001].

If the hypothesis made in equation (7.2) regarding the linear dependency of the IFCBs to the frequency channel number does not hold, second-order IFCB effects will likely propagate into the estimated ambiguity parameters. As a consequence, the ambiguity covariance matrix could become too optimistic which might negatively impact the outcome of ambiguity resolution based on integer least squares.

The quasi-ionosphere-free (QIF) approach to ambiguity resolution offers a practical solution to this issue [Mervart, 1995; Dach et al., 2007, pp. 177-180]. This method fixes ambiguities on a satellite-by-satellite basis, by searching for integer candidates minimizing the following objective function:

$$\Omega^j = \left| a_1^j \left(\widehat{N}_1^j - \breve{N}_1^j \right) - a_2^j \left(\widehat{N}_{WL}^j - \breve{N}_{WL}^j \right) \right| < c_1 \tag{7.15}$$

where $\widehat{N}_i^j$ is the float ambiguity estimate, $\breve{N}_i^j$ is an integer candidate, and

193

$$a_1^j = \alpha_{IF}^j \lambda_1^j + \beta_{IF}^j \lambda_2^j \qquad (7.16a)$$

$$a_2^j = \beta_{IF}^j \lambda_2^j \qquad (7.16b)$$

with the frequency-dependent $(f_i^{\,j})$ scalars:

$$\alpha_{IF}^j = \frac{\left(f_1^{\,j}\right)^2}{\left(f_1^{\,j}\right)^2 - \left(f_2^{\,j}\right)^2} \qquad\qquad \beta_{IF}^j = 1 - \alpha_{IF}^j. \qquad (7.17)$$

Since the coefficients a_1^j and a_2^j originate from the ionosphere-free combination, the objective function cancels ionospheric errors. However, the QIF approach is not entirely independent from this error source because the latter plays a role in the definition of the search space for N_1 and N_{WL}. To take into account a possible ionospheric bias in the estimated ambiguities, a fixed number of candidates are tested, without considering the actual ambiguity covariance matrix:

$$\breve{N}_1^j \in \left[\text{round}\big(\widehat{N}_1^j\big) \pm \Delta N_1^j\right] \qquad (7.18a)$$

$$\breve{N}_{WL}^j \in \left[\text{round}\big(\widehat{N}_{WL}^j\big) \pm \Delta N_{WL}^j\right] \qquad (7.18b)$$

where $\text{round}(\cdot)$ denotes the rounding operator, and ΔN_i^j is the size of the search space for each ambiguity parameter. A pair of candidates is selected if it is the only one for which $\Omega^j < c_1$, with c_1 selected as 1 cm in this study. Due to this tight threshold and the risks of Ω^j to be contaminated by non-dispersive effects, the QIF approach is typically used in static mode with session lengths of a few hours.

Table 7.1 shows the value of the objective function Ω^j as a function of selected ambiguity candidates, assuming that the float ambiguities are errorless. It suggests that

the larger the uncertainty in the widelane ambiguity, the harder it becomes to discriminate certain pairings of ambiguities. Ideally, to retain an effective wavelength of 10 cm, ΔN_{WL}^j in equation (7.18b) would need to be set to zero, meaning that rounding of the widelane float ambiguity should readily provide the correct integer candidate. The last column of Table 7.1 indicates to which accuracy non-dispersive effects must be modelled in order to avoid incorrect fixing of the N_1 ambiguity when the wrong widelane candidate is being tested.

Table 7.1: Variations in the QIF objective function as a function of selected ambiguity candidates, assuming that float ambiguities are errorless.

$\left(\widehat{N}_1^j - \breve{N}_1^j\right)$ [cycles]	$\left(\widehat{N}_{WL}^j - \breve{N}_{WL}^j\right)$ [cycles]	Ω^j (for $k^j = 0$) [m]
0	0	0.000
1	0	0.105
3	-1	0.053
4	-1	0.053
7	-2	0.000
8	-2	0.105

A generalization of the QIF approach was proposed by Kim and Langley [2007] to incorporate ambiguities from all satellites into a single search process and therefore

benefit from the geometric strength of the solution. While instantaneous ambiguity resolution can potentially be achieved, validation of the selected integer vector must be performed and constitutes another challenge by itself. For this reason, we used the original QIF approach in the tests presented hereafter.

7.4 Application of Concepts

The concepts presented in the previous sections were applied to a short baseline of 8.6 km between stations BADH and KLOP, located in Germany. Station BADH is equipped with a Leica GRX1200GGPRO receiver, while station KLOP operates a Trimble NetR5 receiver. Using data from 1 March 2013 and keeping coordinates fixed to their known values, the between-station receiver clock offset was estimated using narrowlane code observations. Since it is a short baseline, most error sources such as atmospheric effects and orbit errors are expected to be eliminated by between-station observation differencing. The IFCBs were then obtained by computing the mean of the estimated residuals for each frequency channel. The results are displayed in Figure 7.1.
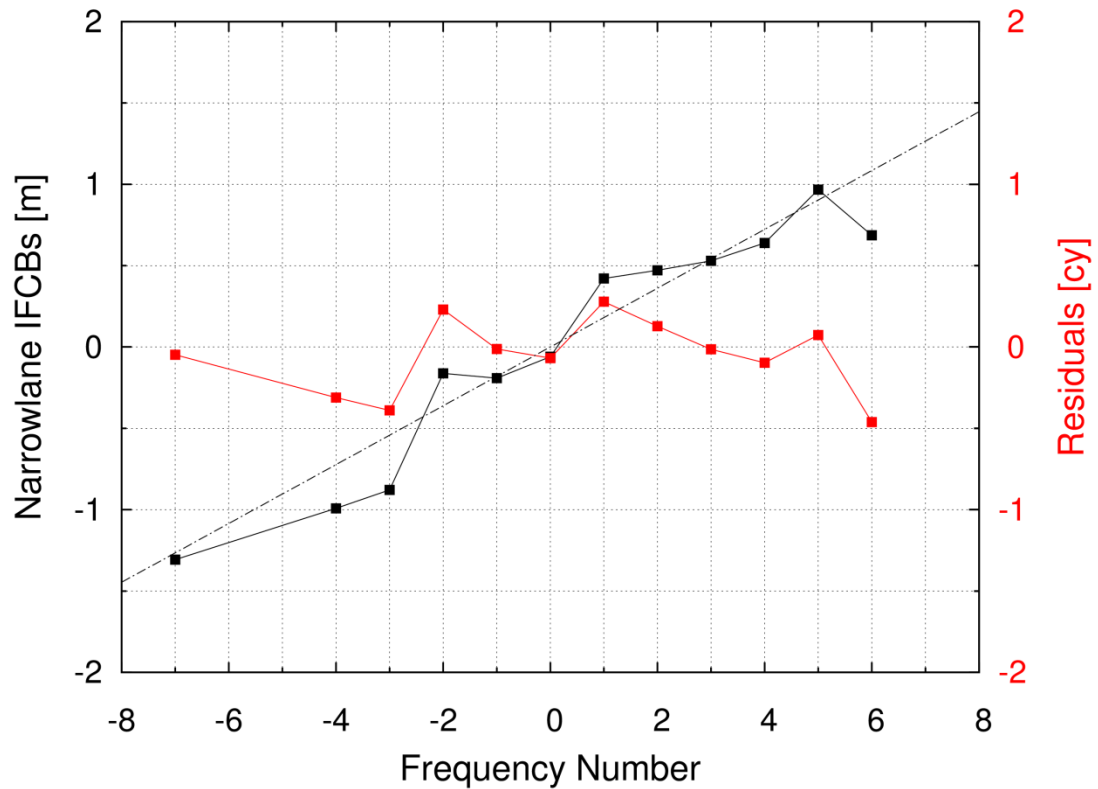
Figure 7.1: Narrowlane IFCBs between stations BADH and KLOP on 1 March 2013, and residuals from a linear fit in units of widelane cycles.

Figure 7.1 shows that the narrowlane IFCBs between stations have a quasi-linear dependency with respect to the frequency channel number. However, removing a linear fit from the IFCBs still leaves significant second-order effects, with a magnitude of up to half a widelane cycle. It is then expected that using the model of equation (7.13) for processing of the MW combination will not allow ambiguities to naturally converge to integer values. An additional mechanism, such as the QIF approach, is then necessary for proper identification of the widelane integers.

GLONASS observations from the BADH-KLOP baseline were then processed following a methodology typically used for long-baseline differential positioning or PPP. Between-station single-differenced ionosphere-free carrier-phase and code observations, as well as the MW combination, are integrated into a least-squares adjustment to estimate:

- a set of daily baseline components;

- a between-station tropospheric zenith delay modelled as a random walk process;

- epoch-independent receiver clock offsets for each signal;

- a reference ambiguity parameter $(\overline{N}_i^1)$ for each of the ionosphere-free and MW signals, constant over the day;

- $\overline{N}_1^{1n}$ and $\overline{N}_{WL}^{1n}$ carrier-phase ambiguities, constant over a satellite pass.

Two satellites with adjacent frequency channel numbers are selected as reference satellites, following the model of equations (7.5) and (7.13). Ambiguity resolution is performed based on the QIF approach, as described in the previous section. Since the BADH-KLOP baseline is short, "true" values for the ambiguities could be easily identified by processing of uncombined signals, and will serve as a benchmark for evaluating the performance of ambiguity resolution based on the concepts proposed in this paper.

Figure 7.2 shows the initial convergence of the estimated widelane ambiguities. The ambiguities for satellites R15 and R16, with frequency channel number 0 and -1

respectively, were initially fixed to define the datum. Since the QIF approach fixes ambiguities on a satellite-by-satellite basis, non-dispersive effects are required to be modelled precisely. For this reason, ambiguity resolution was not attempted for at least 45 minutes to allow the float solution to converge. As expected, the estimated widelane ambiguities do not converge to integers due to second-order narrowlane IFCB effects. Nonetheless, by performing a simultaneous ambiguity search on the N_1 and N_{WL} ambiguities, the correct integer values could be identified for all satellites. This was even the case for satellite R09 for which the widelane estimate was close to the half-cycle mark prior to being fixed. Processing of the full data set led to no wrong fixes, and the ambiguities of only two arcs longer than one hour could not be resolved.

Between-station single differencing eliminated the contribution of MW satellite biases and ionosphere-free satellite clocks. To extend the concepts to a practical PPP implementation, MW satellite biases must be explicitly estimated. As Figure 7.1 illustrates, IFCBs differ among receiver types and do not necessarily have a perfectly linear dependency on the frequency channel number. As a consequence, it is not expected that a set of consistent MW satellite biases can be obtained by mixing receiver types. An analysis of the characteristics of IFCBs is then required to assess the compatibility of receiver types for estimation of these biases.
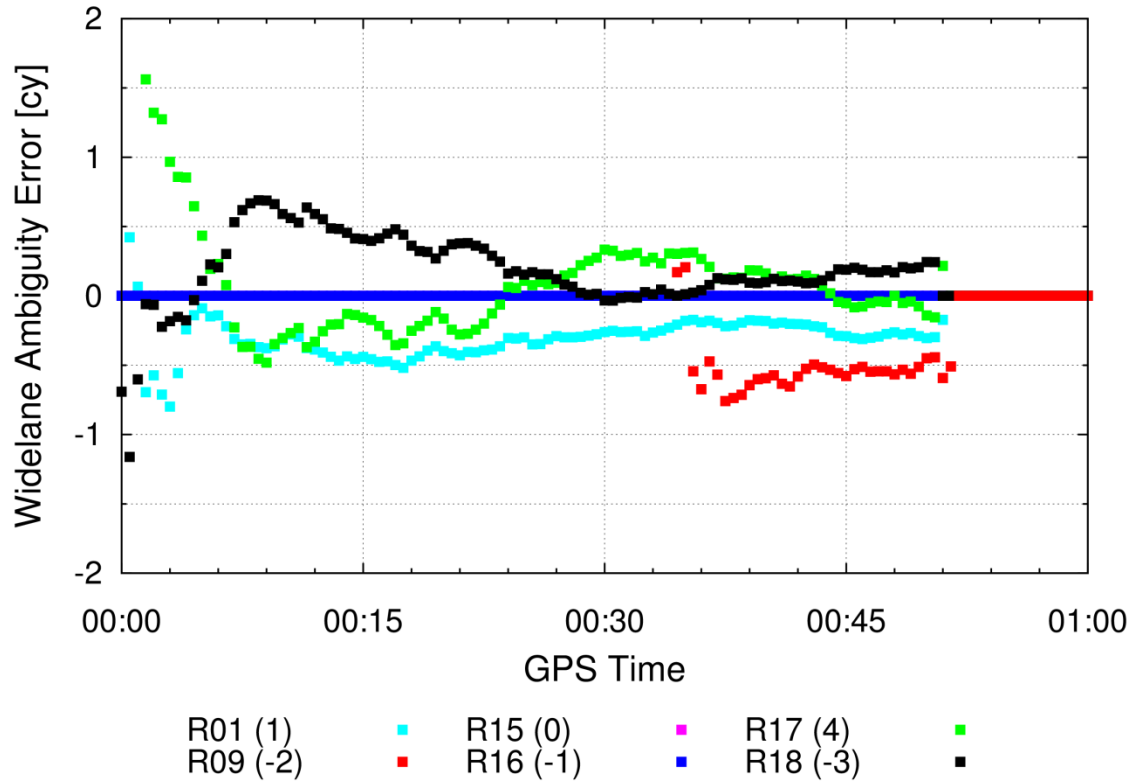
Figure 7.2: Convergence of the widelane ambiguities for baseline BADH-KLOP.

7.5 Characteristics of IFCBs

Accessing undifferenced narrowlane IFCBs is a complex task due to the ionosphere. As a workaround, one can examine the ionosphere-free IFCBs which are simply another linear combination of the IFCBs on P_1 and P_2. Hence, if ionosphere-free IFCBs are consistent for a receiver type, it is expected that the narrowlane IFCBs will also share similar characteristics.

Ionosphere-free IFCBs were obtained from the residuals of GPS+GLONASS PPP solutions, computed using Natural Resources Canada's online PPP service [Mireault et al., 2008]. Since GLONASS code measurements are down-weighted with respect to those of GPS in this software, any bias in the GLONASS ionosphere-free code observables should propagate into the estimated residuals. For all receiver types, the C_1 and P_2 observables were processed to provide a consistent analysis across all receiver makes. While the results obtained with this approach are dependent upon the satellite clock corrections used, all stations located in the same geographical region should be affected similarly. To account for this issue, we use data from a total of 145 stations belonging to the EUREF network [Bruyninx, 2004], collected on 1 March 2013 (see Figure 7.3).

Figure 7.4-Figure 7.9 show the daily average of the ionosphere-free code residuals (assumed to be equal to IFCBs) as a function of the frequency channel number for each of the six receiver types involved in this study. Figure 7.4 demonstrates that the 32 Trimble receivers offer a quasi-linear dependency of the IFCBs on the frequency channel number. However, two receivers have clearly distinct patterns: 1) station GRAS was equipped with an Ashtech antenna (ASH701945E_M) while all other Trimble receivers are connected to Trimble antennas; 2) station OSJE was the only Trimble receiver running firmware version 3.50, as opposed to a release of version 4.
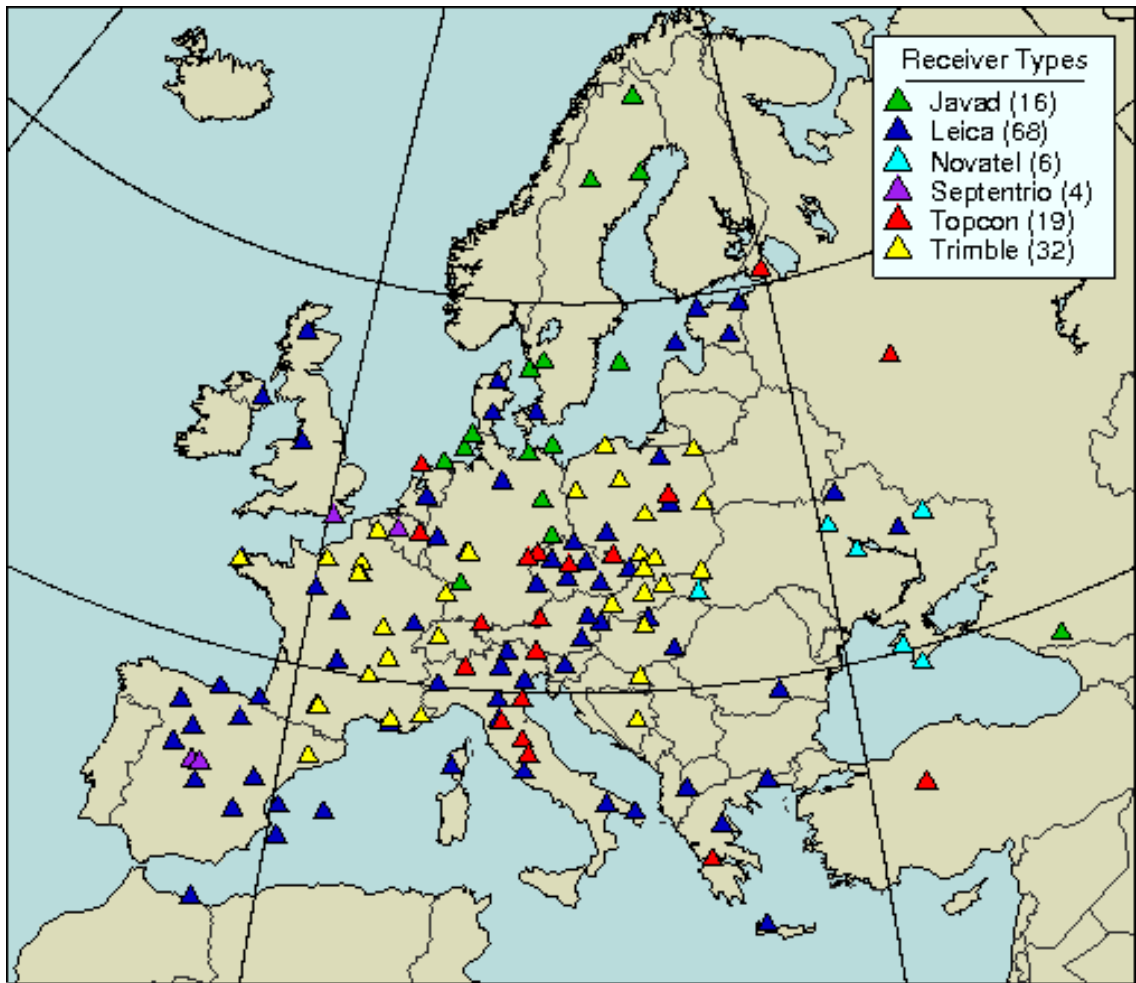
Figure 7.3: Network of stations used for the analysis of IFCBs.

Similar consistency can likewise be observed in Figure 7.5, displaying the IFCBs for a group of 68 Leica receivers. The use of an Ashtech antenna (ASH701945E_M) at station SULD, as opposed to Leica antennas for the majority of stations, is associated with an entirely different slope. Even among stations equipped with Leica antennas of type LEIAR25, the presence or absence of a dome causes significant variations of IFCBs, as shown in green in Figure 7.5.

Figure 7.4: Ionosphere-free IFCBs (C_1/P_2) for 32 Trimble receivers on 1 March 2013. Stations with outstanding characteristics are represented in colors.

Figure 7.6 shows the IFCBs for 6 NovAtel OEMV3 receivers, all connected to identical NovAtel antennas (NOV702GG) without domes. As a consequence, the agreement between stations is fairly good, except for station EVPA which had a data gap of 14 hours on this day, leading to shorter satellite passes for some satellites. Similar conclusions can be drawn from the 4 Septentrio receivers (Figure 7.7), although slightly different characteristics can be observed for the POLARX3 and POLARX4 models.

Figure 7.5: Ionosphere-free IFCBs (C_1/P_2) for 68 Leica receivers on 1 March 2013. Stations with outstanding characteristics are represented in colors. The asterisk in the legend is a wildcard that can be expanded into any set of characters.

Figure 7.8 demonstrates that IFCBs can be significantly different among receivers of a same manufacturer. The set of 16 Javad receivers contains a mix of Javad Legacy and the newer Delta series, which do not seem to have comparable IFCBs. In addition, a total of 11 different antenna types are being used at those 16 stations, which can contribute to the discrepancies. Stations KIR0 and VIS0 were both equipped with the same hardware (Javad EGGDT receivers running firmware 2.6.1 and AOAD/M_T antennas with the OSOD dome), but display clearly different patterns of IFCBs. Other stations operate with

the EGGDT receiver (VIL0) or the same antenna model (SPT0) but do not show such important fluctuations with frequency. Processing only the Legacy model (7 stations) using the less noisy P_1 observable as opposed to C_1 results in a better consistency, similar to the receiver types previously analyzed (results not shown here). The sample of Javad Delta receivers available was not large enough to draw significant conclusions at this point.
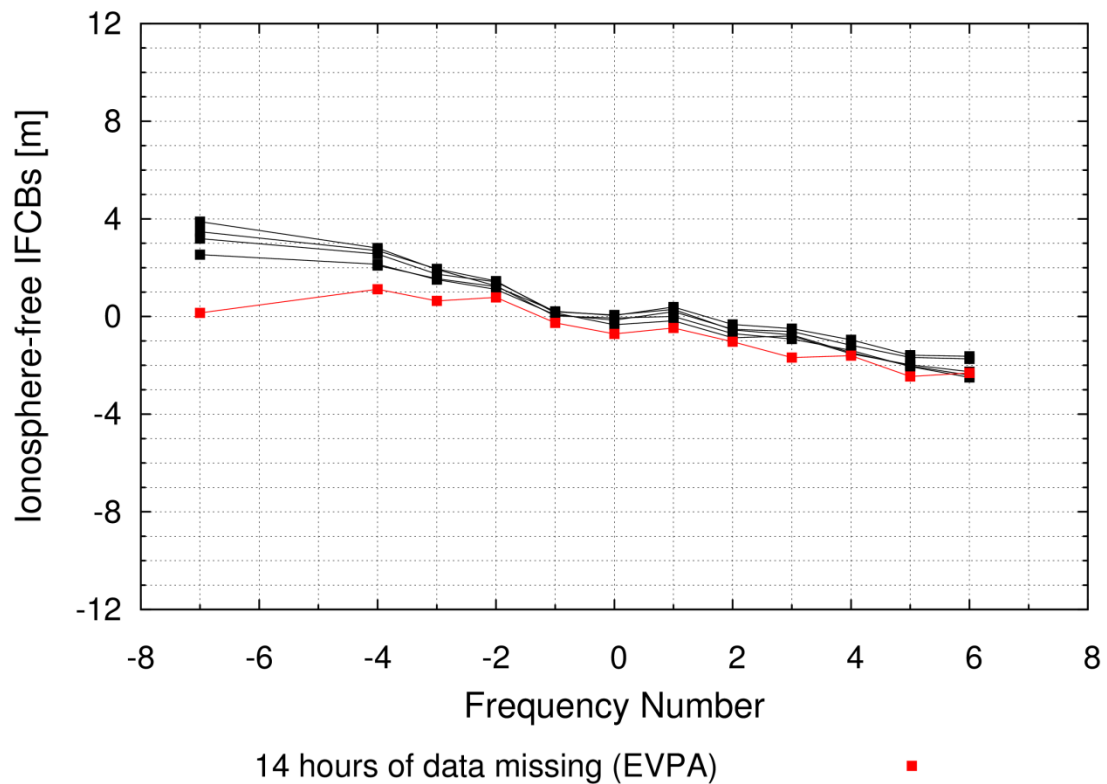
Figure 7.6: Ionosphere-free IFCBs (C_1/P_2) for 6 NovAtel receivers on 1 March 2013. A station with outstanding characteristics is represented in colors.
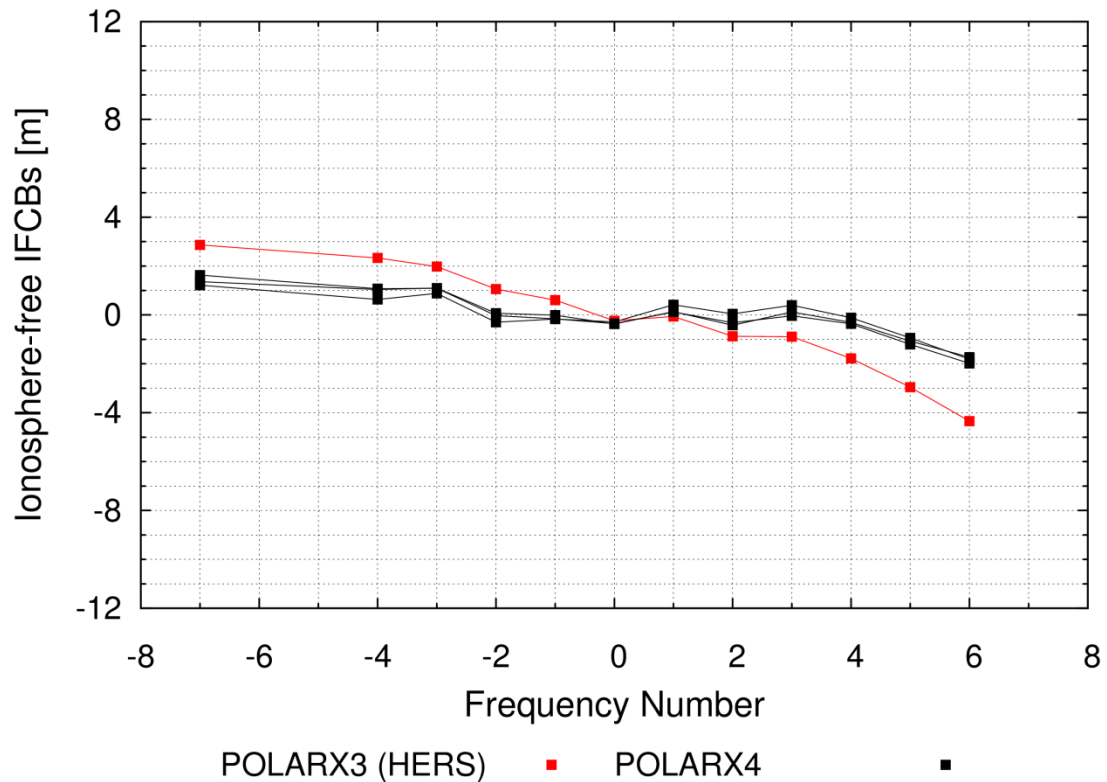
Figure 7.7: Ionosphere-free IFCBs (C_1/P_2) for 4 Septentrio receivers on 1 March 2013. A stations with outstanding characteristics is represented in colors.

Similar results are obtained for the Topcon receivers, as shown in Figure 7.9. While different models seem to exhibit dissimilar IFCB characteristics, Topcon receivers also tend to be connected to a wide variety of antennas. As a result, there is little compatibility between the IFCBs of stations equipped with Topcon receivers, and no apparent linear trend can be observed. Differences exceeding 10 metres even exist between IFCBs at the edge frequencies.
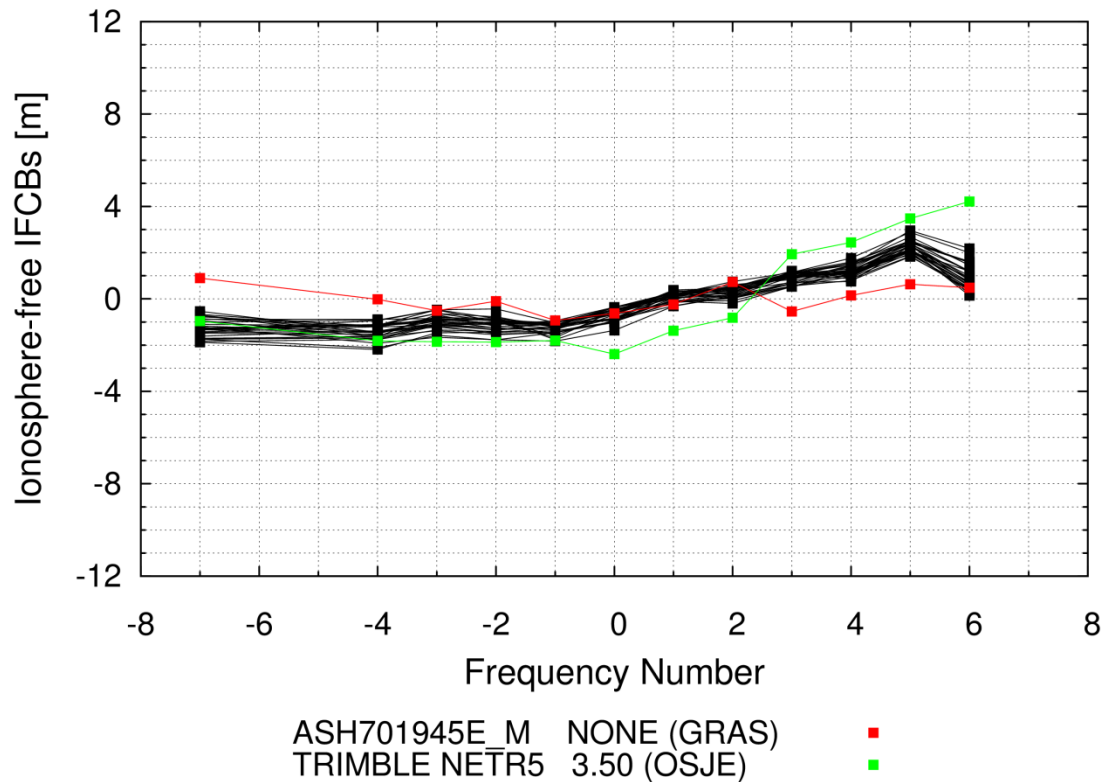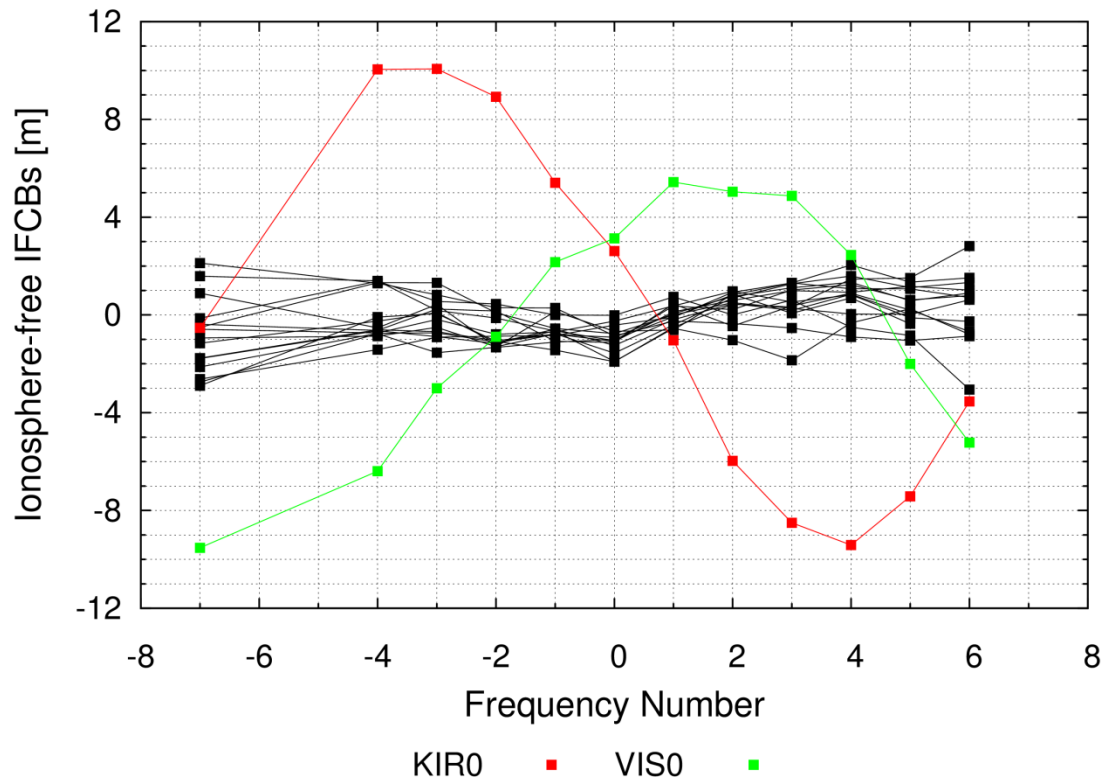
Figure 7.8: Ionosphere-free IFCBs (C_1/P_2) for 16 Javad receivers on 1 March 2013. Stations with outstanding characteristics are represented in colors.

Isolating only the Topcon NetG3 model (5 stations from EUREF plus an additional 8 stations from Canada) reveals an improvement in consistency, especially when processing the P_1 observable (see Figure 7.10). However, it can be seen that the IFCBs of this observable have a clear non-linear response to frequency. Furthermore, individual stations such as BAKE have unique IFCB characteristics that cannot be associated with the receiver and antenna used.
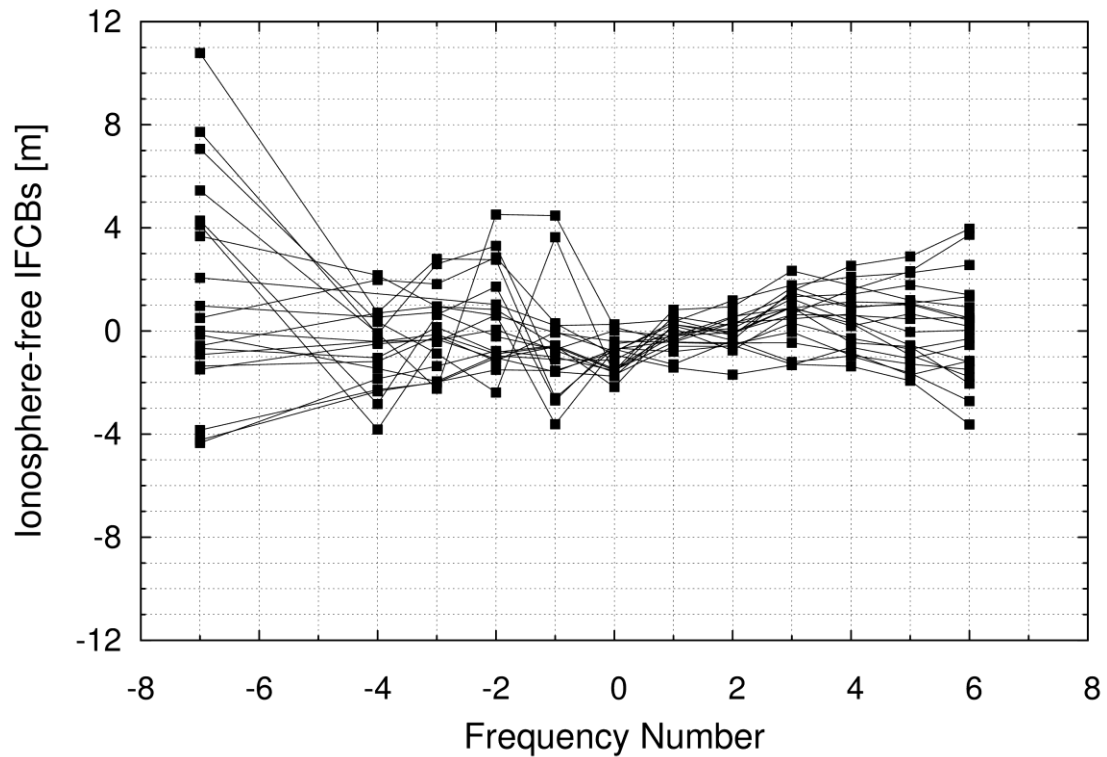
Figure 7.9: Ionosphere-free IFCBs (C_1/P_2) for 19 Topcon receivers on 1 March 2013.

The results presented in this section confirm the findings of Chuang et al. [2013] claiming that IFCBs are affected by receiver type and firmware version, as well as antenna type. Our analysis also allowed gaining some insights on the strategy to be used for the estimation of MW satellite biases. Estimating meaningful satellite biases requires a set of compatible stations, which can only be obtained by isolating subsets of stations with equipment sharing similar characteristics.
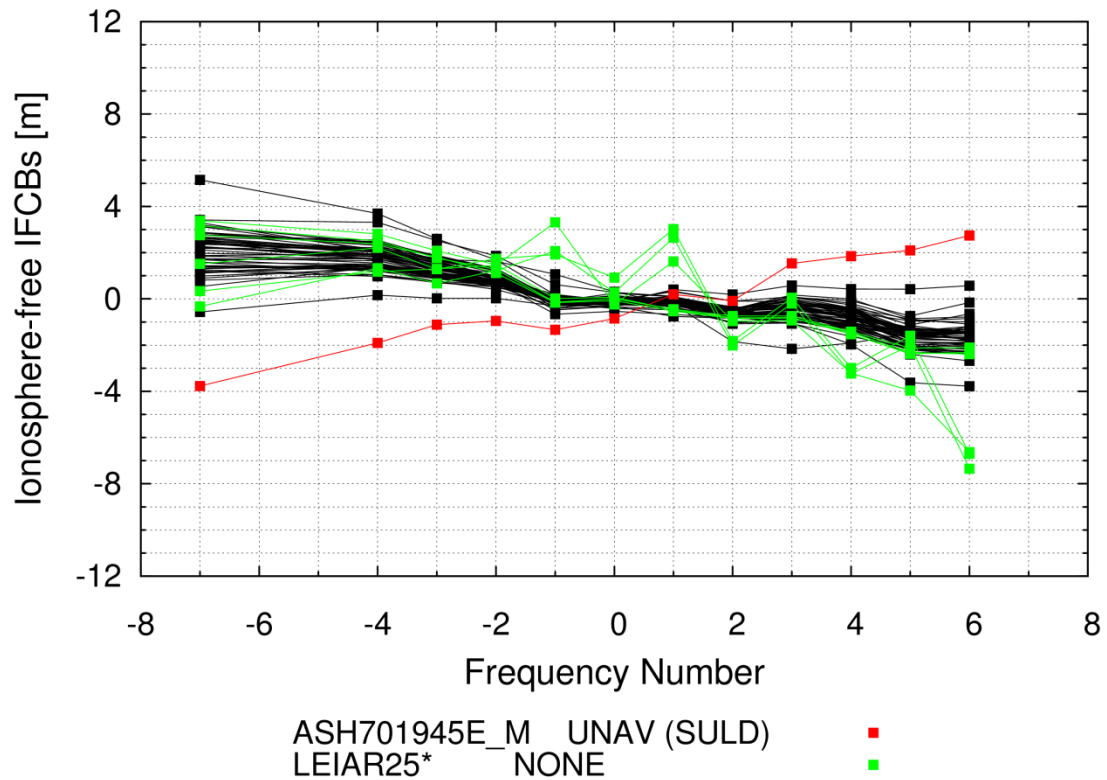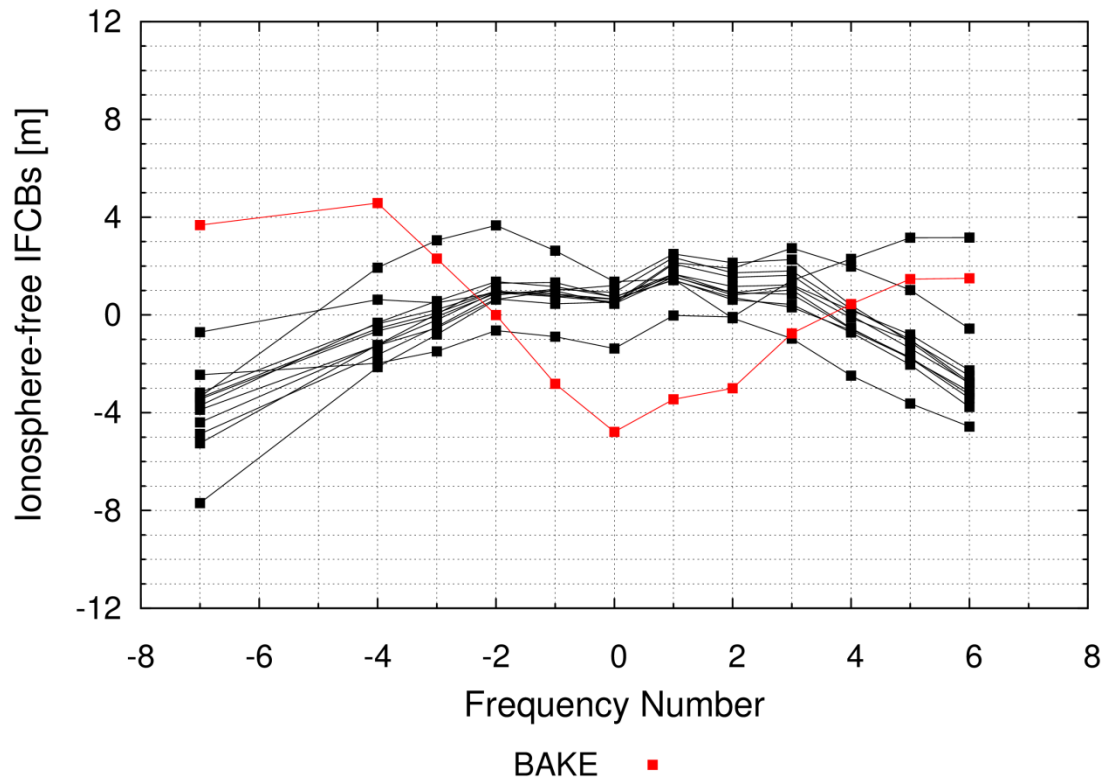
Figure 7.10: Ionosphere-free IFCBs (P_1/P_2) for 13 Topcon NetG3 receivers on 1 March 2013. A station with outstanding characteristics is represented in colors.

7.6 Melbourne-Wübbena Satellite Biases

To verify that stations with similar hardware are indeed compatible for ambiguity resolution using the MW combination, six clusters based on receiver and antenna types were defined, as shown in Table 7.2. The group of Topcon receivers was added only to demonstrate that, at this point, not all receiver types are suitable for satellite bias

estimation based on the MW combination. The last column of Table 7.2 indicates the number of stations from Figure 7.3 included in each cluster.

A prototype network solution for the estimation of the MW satellite biases is performed under the assumption that satellite and receiver biases are constant for a day. This methodology was implemented as a prelude to a full decoupled-clock solution in which no assumption is made regarding the stability of the biases [Collins et al., 2010]. In a first step, the MW combination is processed separately for each receiver-satellite pair (in units of cycles). All arcs longer than one hour during the 24-hour period are aligned by estimating an integer offset between each arc. A combined receiver-satellite bias is then obtained by averaging all aligned MW observations for this receiver-satellite pair. Based on the functional model of equation (7.13), the second step consists of including all averaged receiver-satellite biases into a single least-squares adjustment to estimate, independently for each cluster defined in Table 7.2:

- one MW station bias ($\bar{b}_{\Phi_{MW}}$) and reference ambiguity parameter ($\bar{N}_{WL}^1$) per station;
- one widelane ambiguity ($\bar{N}_{WL}^{1n}$) per satellite for each station, and;
- one MW satellite bias ($b_{\Phi_{MW}}^n$) per satellite (which is now considered unknown).

Table 7.2: Cluster definitions for MW satellite bias estimation.

Cluster	Definition		
	Receiver type	Antenna type	# sta
1	Leica	Leica, except LEIAR25*NONE	50
2	Trimble with firmware v. 4	Trimble	30
3	NovAtel	NovAtel	6
4	Septentrio POLARX4	All	3
5	Javad Legacy	All	7
6	Topcon	All	19

For the system to be solvable, a set of minimum constraints must be defined. For each station, two ambiguity parameters for satellites with adjacent frequency channel numbers are fixed, as suggested by equation (7.13). Additionally, one widelane ambiguity parameter must be fixed for each MW satellite bias to be estimated. Finally, the receiver bias and reference ambiguity parameter of one station is held fixed. The integer nature of the widelane ambiguities is first disregarded and a float solution is obtained. Then, all ambiguities are fixed to their closest integer value on a station-by-station basis and an ambiguity-fixed solution is computed for the remaining parameters. Residuals are also estimated from the ambiguity-fixed solution, and results are displayed for each cluster in Figure 7.11.
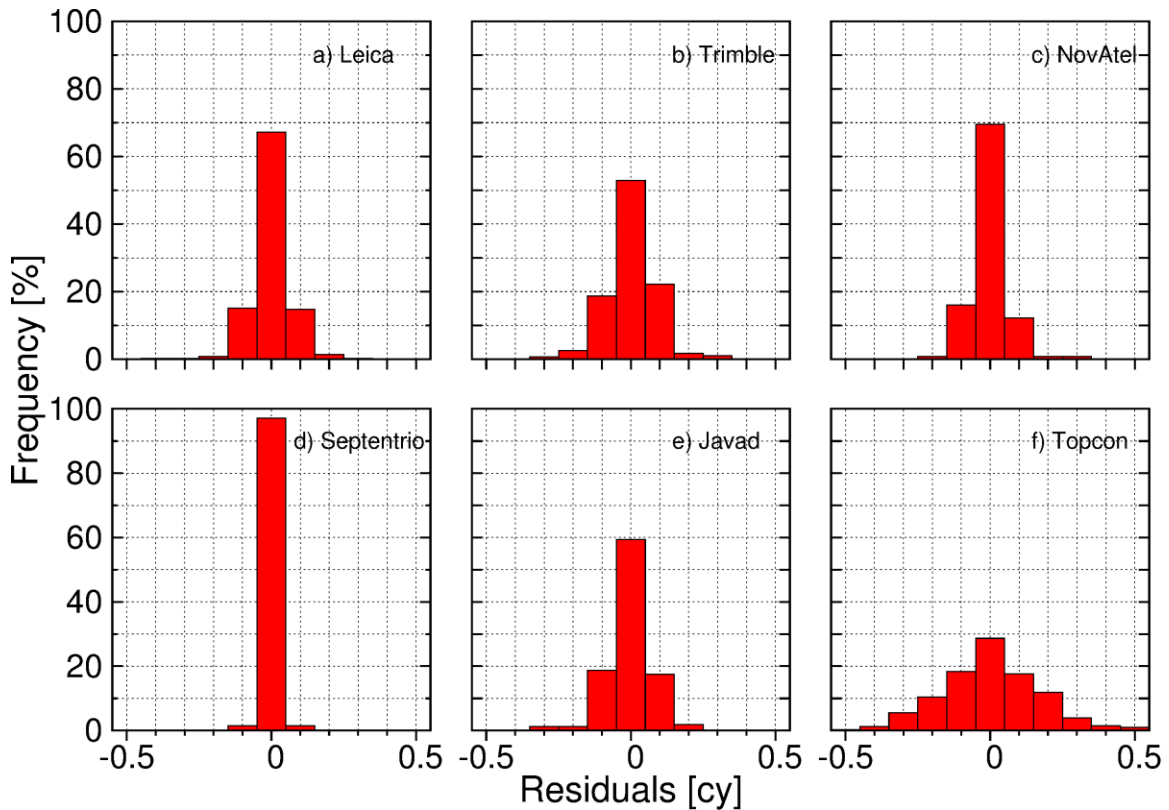
Figure 7.11: Residuals from ambiguity-fixed MW observations for each cluster defined in

Table 7.2.

The histograms from Figure 7.11 confirm that good consistency can be obtained when

using a homogeneous network of stations. For all of these clusters, more than 90% of the

estimated residuals are smaller than 0.15 widelane cycles ($\approx$13 cm). Therefore, using the

estimated MW satellite biases should allow any user, with equipment matching one of the

defined clusters, to obtain convergence of widelane ambiguities to integers. As expected,

the histogram for the group of Topcon receivers (Figure 7.11f) is much flatter, with only

65% of residuals below 0.15 cycles. This result again suggests that IFCBs vary between

models for Topcon receivers, or that antennas significantly affect IFCBs.

A potential downside of processing stations into independent clusters is that the estimated MW satellite biases may be associated with different datums for each cluster. A unified datum can be assured by simultaneous processing of the ionosphere-free carrier-phase and MW observables with proper ambiguity datum definition. This feature has however not yet been implemented.

It was shown in section 7.4 how the model of equation (7.13) could absorb the linear component of the narrowlane IFCBs. Combined with the QIF approach to ambiguity resolution, correct widelane integer values can be recovered for a baseline of mixed receiver types, even though ambiguities did not converge to integers (refer back to Figure 7.2). The baseline formed by stations BADH and KLOP was processed again using the same methodology described previously. The only difference is the application of the cluster-specific MW satellite biases estimated in this section. Figure 7.12 shows that the estimated ambiguities now converge to integer values, increasing the reliability of the ambiguity fixing procedure. Note that convergence time is not affected since it is dependent on the precision of the ambiguities which is the same in both scenarios.

Since this example was processed using a methodology similar to PPP, it is expected that comparable results could be obtained by processing of undifferenced signals, provided that satellite orbits and ionosphere-free satellite phase clocks can be estimated at the centimetre level.
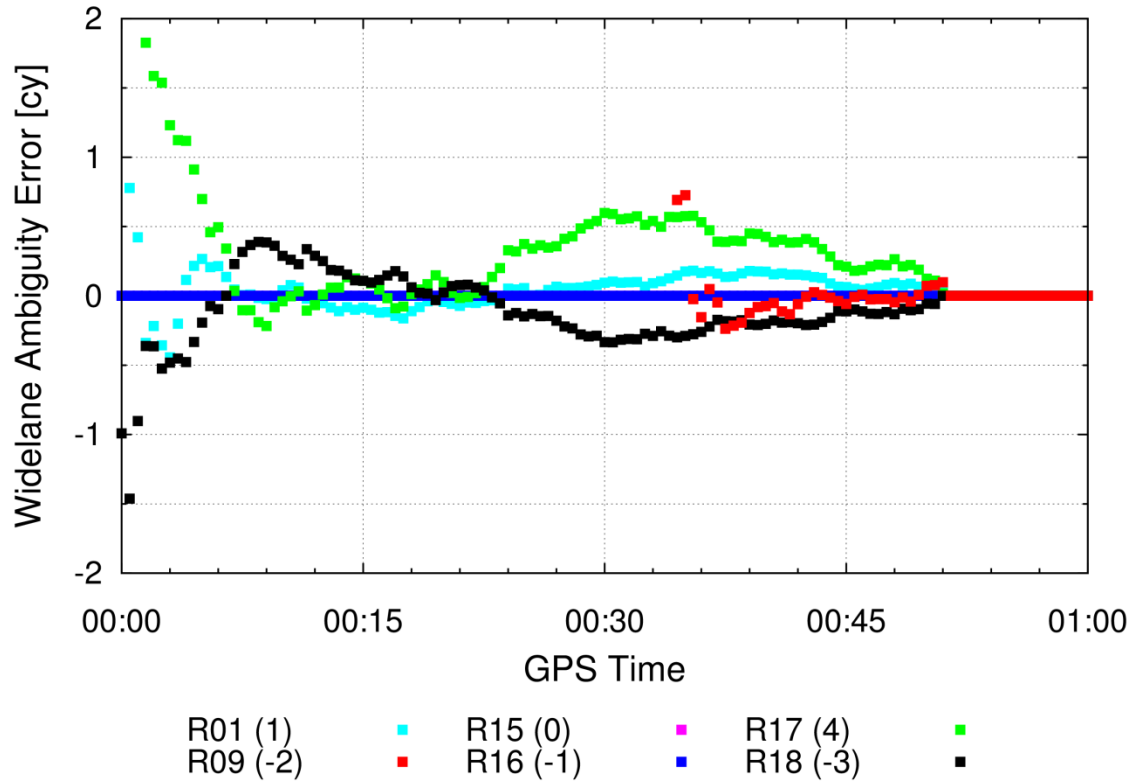
Figure 7.12: Convergence of the widelane ambiguities for baseline BADH-KLOP with the application of MW satellite biases.

7.7 Conclusion

Banville et al. [2013] demonstrated how selecting two GLONASS reference satellites with adjacent frequency channel numbers allows for estimation of ambiguities as formal integer values. In this paper, application of this concept to the MW signal was shown to also absorb the linear dependency of the narrowlane IFCBs with respect to frequency.

Therefore, if code observations from different frequencies had only such a dependency, widelane ambiguities for baselines of mixed receiver types would converge to integer values. However, an investigation of IFCBs confirmed that such biases are also affected by receiver and antenna types and, although the IFCBs of many stations can be modelled by a linear fit, non-negligible second-order effects must be accounted for.

Since stations with similar equipment have comparable IFCBs, six clusters of stations were formed to estimate MW satellite biases. For all clusters but one, over 90% of the estimated residuals were below 0.15 widelane cycles, confirming that undifferenced GLONASS ambiguity resolution can generally be achieved using a homogeneous network of stations. On the other hand, the consistency of IFCBs for some receiver types is not adequate to estimate meaningful MW satellite biases. This could be due to different IFCB patterns between receiver models, and by the diversity of antenna types connected to these receivers. While the quasi-ionosphere free (QIF) approach to ambiguity resolution can allow for correct ambiguities to be identified even in the presence of biases, not all receiver and/or antenna types can currently be accommodated by our approach. Examining the ionosphere-free IFCBs can be an effective means of screening out such stations.

Demonstration of the concepts presented in this paper was achieved by processing of a short baseline with mixed receiver types. Using a methodology similar to long-baseline differential processing and PPP, convergence of the estimated ambiguities to integer values was achieved. These preliminary results suggest that an implementation of a full

215

network solution for the estimation of GLONASS ionosphere-free satellite clocks and MW satellite biases is possible.

Acknowledgements

The authors would like to acknowledge the operators of the EUREF permanent network (EPN) and Bundesamt für Kartographie und Geodäsie (BKG) for archiving and providing the data used in this study.

References

Al-Shaery, A., S. Zhang, and C. Rizos (2013). "An enhanced calibration method of GLONASS inter-channel bias for GNSS RTK," *GPS Solutions*, Vol. 17, No. 2, pp. 165-173. doi: 10.1007/s10291-012-0269-5.

Banville, S., P. Collins, and F. Lahaye (2013). "GLONASS ambiguity resolution of mixed receiver types without external calibration," *GPS Solutions*, Vol. 17, No. 3, pp. 275-282. doi: 10.1007/s10291-013-0319-7.

Bruyninx, C. (2004). "The EUREF Permanent Network; a multidisciplinary network serving surveyors as well as scientists," *GeoInformatics*, No. 5, Vol. 7, pp. 32-35.

Cai, C., and Y. Gao (2013). "Modeling and assessment of combined GPS/GLONASS precise point positioning," *GPS Solutions*, Vol. 17, No. 2, pp. 223-236. doi: 10.1007/s10291-012-0273-9.

Chuang, S., W. Yi, W. Song, Y. Lou, Y. Yao, and R. Zhang (2013). "GLONASS pseudorange inter-channel biases and their effects on combined GPS/GLONASS precise point positioning," *GPS Solutions*, Vol. 17, No. 4, pp. 439-451. doi: 10.1007/s10291-013-0332-x.

Collins, P., S. Bisnath, F. Lahaye, and P. Héroux (2010). "Undifferenced GPS ambiguity resolution using the decoupled clock model and ambiguity datum fixing," *NAVIGATION: Journal of The Institute of Navigation*, Vol. 57, No. 2, Summer 2010, pp. 123-135.

Dach, R., U. Hugentobler, P. Fridez, and M. Meindl (2007). *Bernese GPS Software, Version 5.0*. Astronomical Institute, University of Bern, Bern, Switzerland, January 2007.

Ge, M., G. Gendt, M. Rothacher, C. Shi, and J. Liu (2008). "Resolution of GPS carrier-phase ambiguities in precise point positioning (PPP) with daily observations," *Journal of Geodesy*, Vol. 82, No. 7, pp. 389-399. doi: 10.1007/s00190-007-0187-4.

Habrich, H., G. Beutler, W. Gurtner, and M. Rothacher (1999). "Double difference ambiguity resolution for GLONASS/GPS carrier phase," *Proceedings of the 12th International Technical Meeting of the Satellite Division of The Institute of Navigation (ION GPS 1999)*, Nashville, Tenn., 14-17 September 1999, pp. 1609-1618.

Kim, D., and R. B. Langley (2007). "Ionosphere-nullification technique for long-baseline real-time kinematic applications," *NAVIGATION, Journal of The Institute of Navigation*, Vol. 54, No. 3, Fall 2007, pp. 227-240.

Kozlov, D., M. Tkachenko, and A. Tochilin (2000). "Statistical characterization of hardware biases in GPS+GLONASS receivers," *Proceedings of the 13th International Technical Meeting of the Satellite Division of The Institute of Navigation (ION GPS 2000)*, Salt Lake City, Utah, 19-22 September 2000, pp. 817-826.

Laurichesse, D., F. Mercier, J.-P. Berthias, P. Broca, and L. Cerri (2009). "Integer ambiguity resolution on undifferenced GPS phase measurements and its application to PPP and satellite precise orbit determination," *NAVIGATION: Journal of The Institute of Navigation*, Vol. 56, No. 2, Summer 2009, pp. 135-149.

Melbourne, W. G. (1985). "The case for ranging in GPS based geodetic systems," *Proceedings of 1st International Symposium on Precise Positioning with the Global Positioning System*, edited by Clyde Goad, U.S. Department of Commerce, Rockville, Md., 15-19 April, pp. 373-386.

Mervart, L. (1995). *Ambiguity resolution techniques in geodetic and geodynamic applications of the Global Positioning System*. Ph.D. Dissertation, Astronomical Institute, University of Berne, Switzerland, 155 pp.

Mireault, Y., P. Tétreault, F. Lahaye, P. Héroux, and J. Kouba (2008). "Online precise point positioning: A new, timely service from Natural Resources Canada," *GPS World*, Vol. 19, No. 9, September 2008, pp. 59-64.

Reussner, N., and L. Wanninger (2011). "GLONASS inter-frequency biases and their effects on RTK and PPP carrier-phase ambiguity resolution," *Proceedings of the 24th International Technical Meeting of the Satellite Division of The Institute of Navigation (ION GNSS 2011)*, Portland, Ore., 19-23 September 2011, pp. 712-716.

Sleewaegen, J. M., A. Simsky, W. de Wilde, F. Boon, and T. Willems (2012). "Demystifying GLONASS inter-frequency carrier phase biases," *InsideGNSS*, Vol. 7, No. 3, pp. 57-61.

Teunissen, P. J. G. (1993). *Least-squares estimation of the integer GPS ambiguities*. Technical Report, LGR Series 6, Delft Geodetic Computing Centre, Delft University of Technology, Delft, The Netherlands.

Teunissen, P. J. G. (1999b). "An optimality property of the integer least-squares estimator," *Journal of Geodesy*, Vol. 73, No. 11, pp. 587-593. doi: 10.1007/s001900050269.

Teunissen, P. J. G. (2001). "Integer estimation in the presence of biases," *Journal of Geodesy*, Vol. 75, No. 7-8, pp. 399-407. doi: 10.1007/s001900100191.

Wanninger, L. (2012). "Carrier-phase inter-frequency biases of GLONASS receivers," *Journal of Geodesy*, Vol. 86, No. 2, pp. 139-148. doi: 10.1007/s00190-011-0502-y.

Wübbena, G. (1985). "Software developments for geodetic positioning with GPS using TI 4100 code and carrier measurements," *Proceedings of 1st International Symposium on Precise Positioning with the Global Positioning System*, edited by Clyde Goad, U.S. Department of Commerce, Rockville, Md., 15-19 April, pp. 403-412.

CHAPTER 8

CONCLUSION

This final chapter briefly summarizes the context in which this research was performed, as well as its main findings and contributions. Finally, recommendations are made for future research and for users of the methods presented in this dissertation.

8.1 Summary

Popular positioning methodologies such as RTK or network RTK allow instantaneous centimetre-level accuracies but require the nearby presence of base stations. While the precise point positioning (PPP) methodology can rely on a sparse global network to reach a similar level of performance, a convergence period at least 30 minutes is typically required. Furthermore, when signal tracking is interrupted due to obstacles for instance, users must again wait for re-convergence of their positioning solutions. Such scenarios are highly undesirable for real-time applications, and mitigate the use of PPP in several applications. Recent developments led to the possibility of fixing undifferenced GPS ambiguities to integers, but convergence time is still on the order of 10 to 20 minutes.

In view of these challenges, the main objective of this research then became developing a methodology for reducing the length of this convergence period. Three

aspects were analyzed: 1) re-convergence capabilities based on cycle-slip correction; 2) incorporating external information on the ionosphere in the navigation filter; and 3) fixing undifferenced GLONASS ambiguities.

8.1.1 Cycle-Slip Correction

Once a PPP solution has converged to its expected accuracy, it is still vulnerable to all phenomena that could disrupt carrier-phase tracking, such as obstacles and ionospheric scintillation. For this purpose, the concept of cycle-slip correction was investigated.

8.1.1.1 Geometry-Based Cycle-Slip Correction

As a first step, the method of Kim and Langley [2001], in which single-epoch cycle-slip correction could be accomplished for a pair of GPS receivers, was generalized for the single-receiver case. Time-differenced carrier-phase and code observations were used in a least-squares adjustment to estimate the receiver displacement between epochs, the receiver clock offset variation, and the magnitude of the cycle slips. Cycle-slip parameters could then be fixed to integer values using popular ambiguity resolution techniques, and introduced in the PPP solution to provide continuous position solutions.

Still, instantaneous cycle-slip correction was found not to be a trivial task, especially with noisy code observations. For this purpose, a scheme for partial cycle-slip fixing was adopted, using a combination of the widelane and geometry-free linear combinations of carrier-phase observations. While it is demonstrated in this dissertation that linear combinations do not improve the success rate of the cycle-slip fixing process, this statement is only true when an attempt at fixing all cycle-slip parameters is made. With partial fixing (i.e., not fixing all cycle-slip parameters to integers), the use of linear combinations can be a beneficial factor. Practical examples illustrated the benefits of our partial fixing algorithm.

This instantaneous cycle-slip correction technique for PPP received special attention following the magnitude 8.8 earthquake that occurred on 27 February 2010 in Chile. It was demonstrated that a continuous position solution could have been obtained in real time even if the receiver temporarily lost lock on all satellites simultaneously, provided that communications with the station were maintained. This information is essential for incorporation into a tsunami-warning system [Blewitt et al., 2009].

8.1.1.2 Ionospheric Cycle Slips

Reliable detection of cycle slips is important from two points of view. First, it must detect real discontinuities in carrier-phase observations to ensure that the estimated

parameters are unbiased. Second, it must avoid falsely detecting cycle slips, which could trigger position discontinuities in PPP. In the presence of an active ionosphere, it was found that the latter condition could be problematic to satisfy using detection methods based on geometry-free linear combinations. An alternate means of detecting cycle slips, properly accounting for rapid ionospheric delay variations by estimating this quantity in a least-squares adjustment, was thus proposed based on the time-differenced model. It relies on a two-step process: a satellite-by-satellite screening and an integrated adjustment of all carrier-phase observations simultaneously. Application of this method to kinematic PPP solutions demonstrated up to decimetre-level improvements in three-dimensional position estimates, simply due to a more robust cycle-slip detection procedure.

According to the author's knowledge, no prior investigations on correcting cycle slips in the presence of high ionospheric activity had been performed. An in-depth analysis of the underlying stochastic model and integer validation procedure was also conducted to understand the intricacies of the method. It was demonstrated that the stochastic model (i.e., how the observations are weighted) has a critical influence on the shape of the pull-in regions. In other words, the closest integer vector depends not only on the cycle-slip parameter estimates, but also on the choice of observation weights. It was also demonstrated that the method of choice for integer validation must rely on two criteria: the proximity of the float estimates to an integer vector, and the strength of the mathematical model. Therefore, instead of using the simple ratio test for validating the selected integer candidates, another method based on Bayes' probability was adopted.

Simulations demonstrated that slightly over-constraining the ionospheric delay variation parameter could lead to improved cycle-slip correction capabilities.

Successful cycle-slip correction in the presence of decimetre-level ionospheric delay variations was demonstrated, which constitutes a major improvement over existing approaches. Another foreseeable application of this technique is the improved continuity of slant ionospheric delay estimates from GNSS receivers.

8.1.2 Ionospheric Corrections for PPP

One of the key elements for instantaneous convergence of RTK or network RTK solutions is the ability to cancel or precisely model the effects of the ionosphere. With PPP relying on a global network of stations, applying ionospheric corrections from global ionospheric maps was investigated to reduce the initial convergence period of PPP solutions.

8.1.2.1 Integer-Levelled Ionospheric Observables

Carrier-phase observations from GNSS receivers offer an accurate measure of the variation of the total electron content (TEC) along a satellite-receiver path. However, an

absolute measure of TEC is typically obtained in combination with the use of noisy code observations because of the ambiguous nature of carrier phases. Code measurements can sometimes be contaminated with important multipath effects and instrumental biases, leading to calibration errors in the determination of absolute TEC.

This dissertation described a new methodology, called "integer levelling," in which code observations are not directly needed to obtain a precise measure of TEC. Instead, integer ambiguities obtained in a PPP solution are used to remove the arc dependency of carrier-phase observations. Integer-levelled observations still contain receiver and satellite instrumental biases, similar to the well-known differential code biases, therefore requiring a mathematical model for retrieving absolute TEC. The main benefit of using integer-levelled observations as opposed to popular levelling techniques is the elimination of levelling errors introduced while fitting carrier phases to code observations. This idea had been contemplated by other researchers previously based on float estimates of the ambiguities, but no insights were offered on the presence of instrumental biases affecting the observations. Integer-levelled observations, based on an ambiguity datum, are biased by integer values originating from the minimal constraints imposed in the network satellite clock solution and on the user side.

Application of the integer-levelling procedure to observations of a regional network of stations on Vancouver Island in Canada led to improved consistency of slant TEC estimates among nearby stations. Unfortunately, the benefits of using integer-levelled observations can be obscured by other important error sources affecting the computation

224

of global ionospheric maps such as the use of a thin-shell representation of the ionosphere, sparse sampling, and interpolation methods. It is nonetheless expected that the new observables can improve the RMS of model fit, and perhaps be used for the investigation of new ionospheric modelling approaches by providing more precise measurements of TEC. Since ambiguity resolution in PPP can be achieved in real time, integer-levelled observations can be used to meet real-time or near-real-time needs in terms of TEC estimation. Furthermore, undifferenced ambiguity resolution for LEO satellites is performed routinely in some organizations, thereby offering a means of reducing levelling errors associated with occultation data.

8.1.2.2 PPP with Global Ionospheric Corrections

Global ionospheric maps (GIMs) produced by the International GNSS Service (IGS) are provided with differential code biases (DCBs). Those biases are a by-product of the TEC estimation process, and are also required to assure the compatibility of single-frequency observations with satellite clock corrections based on the ionosphere-free linear combination of (smoothed) code observations.

In PPP with ambiguity resolution based on the decoupled-clock model, satellite phase clock corrections are based purely on carrier-phase observations, the datum being defined by fixing certain ambiguity parameters in the adjustment process. As a consequence,

those satellite clock corrections contain integer biases that are absorbed in the ambiguity estimates of PPP users, allowing the integer properties of the ambiguities to be preserved. It then becomes obvious that using those biased ambiguity parameters to perform integer levelling will also lead to biased integer-levelled observations. Global ionospheric maps based on those observables would then have, as a by-product, (integer-biased) differential phase biases (DPBs) as opposed to DCBs.

Extending the ionosphere-free decoupled-clock model to allow explicit estimation of slant ionospheric delays can allow external information on the ionosphere to be included in the solution. Depending on the quality of this information, convergence time of PPP solutions can be reduced significantly. Still, ionospheric corrections must be consistent with the PPP model at the user end. This dissertation demonstrated that consistency can only be achieved by also providing to users DPBs based on integer-levelled observations (obtained based on the same satellite phase clock corrections). Failing to provide a consistent set of biases will destroy the integer nature of the carrier-phase ambiguities at the user end.

It was shown that, on a day with a quiet ionosphere, external ionospheric information from a global ionospheric map could potentially reduce convergence time of PPP solutions to 5 minutes (68% of the time). With a denser regional network, instantaneous ambiguity resolution can be obtained, leading to a level of performance similar to network RTK. This methodology (PPP with regional augmentation) is commonly referred to as PPP-RTK.

8.1.3 GLONASS Ambiguity Resolution

The last aspect considered in this dissertation for improving the convergence time of PPP solutions consisted of including GLONASS satellites in PPP solutions with ambiguity resolution capabilities. Several researchers have confirmed that a better geometry of satellites associated with processing of both GPS and GLONASS satellites leads to improved accuracy and reduced convergence time. However, due to receiver incompatibilities associated with the frequency division multiple access (FDMA) technology of GLONASS satellites, ambiguity resolution for GLONASS satellites is more complex than its GPS counterpart. Therefore, handling of both carrier-phase and code inter-frequency biases was analyzed.

8.1.3.1 Inter-Frequency Phase Biases

Since all GLONASS satellites in view transmit signals at slightly different frequencies, forming between-satellite differences of observations (in cycles) does not allow cancelling receiver clock errors. Equivalently, when expressed in units of metres, the ambiguity of the reference satellite remains an explicit parameter in the adjustment. As a result, the least-squares solution from the navigation filter is singular. This singularity can be removed by computing the ambiguity of the reference satellite using a combination of carrier-phase and code observations. However, those two observables are not necessarily synchronized within the receiver, and this synchronization offset is

different from one receiver manufacturer to another. From this characteristic arose the notion of inter-frequency phase biases, which are, in fact, only a consequence of timing considerations between receiver makes. Calibration values were computed to account for those biases and to allow for instantaneous ambiguity resolution to be performed with mixed receiver types in differential mode [Wanninger, 2012]. Nevertheless, those calibration values are firmware dependent and accurate metadata must be available to assure coherent solutions.

This dissertation proposed a new calibration-free approach to deal with the inter-frequency phase biases caused by the synchronization offset between phase and code observables. The idea is to explicitly estimate the ambiguity of the reference satellite in the least-squares solution rather than computing it using code measurements. In order for this approach to work, two reference satellites need to be selected, meaning that no ambiguity parameters are estimated for those satellites. Based on this methodology, mixed receiver types can be used for baseline processing without any *a priori* knowledge of inter-frequency biases. While the extra parameter to be estimated leads to a mathematically weaker model, tests have demonstrated that instantaneous ambiguity resolution can be reliably obtained in a combined GPS + GLONASS solution.

This new model for processing GLONASS observations is particularly useful when operating from a global network of stations, where valid metadata regarding receiver type and firmware version can be complex to maintain for all stations. Benefits are thus anticipated for the computation of GLONASS satellite clock corrections for PPP.

228

8.1.3.2 Inter-Frequency Code Biases

Ambiguity resolution in PPP typically requires the use of code observations to (either implicitly or explicitly) estimate slant ionospheric delays. This approach is problematic for GLONASS satellites because unmodelled inter-frequency code biases (IFCBs) propagate into those estimated delays, which, in turn, affect the ambiguity parameters. Since those IFCBs often exceed the wavelength of the carrier, they prevent undifferenced ambiguity resolution on GLONASS satellites.

It had already been reported that private companies (such as Trimble) were able to perform ambiguity resolution for GLONASS in PPP due to a network of stations based on homogeneous equipment (i.e., all stations are running Trimble receivers with identical firmware versions). In such a network, IFCBs can be absorbed by satellite clock corrections which in turn cancel such biases for users with compatible equipment. In an attempt to replicate such an approach, a thorough investigation of IFCBs was performed for this dissertation. It was demonstrated that IFCBs not only depend on receiver type and firmware version, but also on the antenna type connected to the receiver. Compatibility of IFCBs for certain types of receivers could be identified, allowing the definition of clusters of stations for which undifferenced ambiguity resolution would be achievable.

Based on those findings, satellite widelane biases were estimated and showed very good agreement between receivers of the same cluster. The estimated values were applied to processing of a long baseline (sharing similar challenges as PPP in terms of ambiguity resolution), and correct ambiguities could be identified. This work then paves the way to undifferenced ambiguity resolution for GLONASS based on a network of mixed receiver types. A combined GPS and GLONASS solution with ambiguity resolution capabilities for both systems could then be beneficial for reducing the convergence time of PPP solutions.

8.2 Recommendations

This section suggests possible ways to improve the methods described in this dissertation. It again focuses on the three main themes of this work: cycle-slip correction, ionosphere monitoring, and GLONASS ambiguity resolution.

8.2.1 Cycle-Slip Correction

Cycle-slip correction can offer instantaneous re-convergence of PPP solutions after signal tracking interruptions. However, implementation aspects of the time-differenced

model are not straightforward, and integrity measures must be put in place to assure that positioning solutions are not degraded by wrong integer candidate identification.

8.2.1.1 Observation Differencing

The cycle-slip detection and correction approach proposed herein is mainly based on time-differenced observations, meaning that an explicit subtraction of the observations made at two different epochs is performed. While this approach has the benefit of reducing time-correlated errors, the logic behind the implementation can become complex. For example, when signal tracking is lost on a satellite, signals can only be reacquired several epochs later. This involves the situation that observations from previous epochs must be stored in memory for a pre-defined period of time. Computing the time-differenced solution to detect or correct cycle slips then requires selecting the appropriate epochs of data to compute the time-differenced solution. Tracking on L_1 and L_2 can also be lost and reacquired at different epochs, which can further complicate the epoch selection. When a complete satellite tracking interruption occurs, one must make sure that the two epochs selected for the time-differenced solution are adequate. Since not all satellites are typically re-acquired at the same time, it might be preferable to wait until all satellites are tracked again to obtain a better geometry and thus improve the probability of correctly fixing the cycle slips. However, especially in real time, it is not

always obvious to know if a satellite will even be re-acquired, and delaying the cycle-slip correction procedure might not be desirable.

As proposed by other researchers, the cycle-slip correction process can be integrated in the PPP solution [Geng et al., 2010; Collins and Bisnath, 2011; Li, 2012]. Processing of undifferenced observations greatly simplifies the logistics since no explicit differencing of the observations is required. When a cycle slip is detected, a new ambiguity parameter can simply be set up in the least-squares adjustment. Constraining slant ionospheric delay variations (which must be explicitly estimated in the PPP solution) allows reducing the ambiguity search space and can allow for instantaneous re-fixing of ambiguities.

All theoretical developments made in this dissertation would still be applicable if undifferenced observations were used. Partial cycle-slip fixing based on the widelane combination, as suggested in Chapter 2, could be applied to constrain the position solution when the receiver is moving. The role of the *a priori* constraint on ionospheric parameters, analyzed in detail in Chapter 3, would be taking place through the process noise added on ionospheric parameters. If non-dispersive effects are adequately modelled, a similar level of performance for correcting ionospheric cycle slips would then be expected when processing undifferenced observations.

Even though there would still be cases where the time-differenced model would outperform the undifferenced approach because of the reduction of time-correlated errors,

232

I believe that ambiguity fixing in PPP will eventually replace cycle-slip correction in the same manner that on-the-fly ambiguity resolution dramatically reduced the need for this procedure in differential mode.

8.2.1.2 Integrity

Chapter 3 emphasized that incorrect identification of integer cycle-slip candidates can occur if the stochastic model is not properly defined. This implies that the precision of the observations used in the adjustment must reflect their true quality and that *a priori* constraints must be realistic. In practice, it is not a trivial task to define all of those quantities appropriately. Since fixing cycle slips to wrong values can have important consequences in some applications, it is thus recommended to use a conservative approach to cycle-slip correction. While the method proposed is a great tool in post-mission analysis of data, its use should be parsimonious in automated services. For example, repairing cycle slips with observations sampled at a 30-second interval is risky due to the sometimes unpredictable behavior of the ionosphere. Also associated with an active ionosphere are noisier measurements, which could compromise the integrity of the approach. Being aware of those pitfalls is the first step towards an appropriate use of this method, although further research on integrity monitoring could be of great benefit.

8.2.2 Ionospheric Corrections for PPP

This research has demonstrated that PPP processing is tightly linked with the ionosphere. Suggestions for future work include ideas for better monitoring of the ionosphere and for improved positioning solutions.

8.2.2.1 Changes in TEC Estimation Strategy

It was shown that PPP can provide measures of slant TEC that are much more precise than the ones obtained through current procedures. Due to other error sources in the generation of TEC maps, the adoption of integer-levelled observations has not yet gained significant momentum. As mathematical representations of the ionosphere, mapping functions and ground station density all improve over the years, I am convinced that more precise STEC measurements will be called for in the future.

Several implications of integer levelling should be tested to gain better understanding of this method. For example, it is well known that station DCBs can experience intra-day variations that impact particularly near-real-time applications where DCBs are not always being estimated. Since integer-levelled observations are based on an ambiguity datum rather than a datum defined by code measurements, it is expected that the stability of the corresponding DPBs should be improved. If this is the case, estimation of DPBs could be

further improved by imposing a constraint on their stability in a multi-day adjustment. Another implication of integer levelling referenced in this dissertation is the reduction of levelling errors for GPS receivers on LEO satellites, which should definitely be investigated.

Processing of GLONASS observations for the estimation of TEC parameters typically involves estimating one receiver-dependent parameter per frequency channel to account for inter-frequency code biases. For a network of 100 stations and a nominal constellation of 24 GLONASS satellites, this amounts to $99 \cdot 15 + 24 = 1509$ parameters (the biases for one receiver were assumed to be fixed). This large number of parameters can absorb ionospheric features and affect the final TEC estimates. When undifferenced ambiguity resolution for GLONASS can be achieved routinely, the integer levelling procedure can also be applied to this system. With integer-levelled observations, the total number of bias parameters for the above example is only $99 \cdot 2 + 24 = 222$, a reduction of 85%! Indeed, once the ambiguity contribution is removed from geometry-free carrier-phase observations, it is only necessary to estimate one receiver DPB parameter and a reference ambiguity parameter per station.

8.2.2.2 Global Ionospheric Corrections for PPP

While global ionospheric maps provide valuable information on the general trends of electron densities, the underlying models do not allow modelling of TEC to a level that could significantly improve high-precision positioning applications. Even in regions with a very dense number of ground stations, the use of a thin-shell representation of the ionosphere introduces considerable errors when computing STEC for satellites observed at low elevation angles above the horizon. This convenient but suboptimal mathematical representation of the ionosphere therefore prevents us from using the full potential of the data from the ground network. To meet the needs of PPP applications, it is imperative that more precise models be utilized in which STEC values from stations in the vicinity of a PPP user would contribute to significant mitigation of ionospheric errors (i.e., at a fraction of a TECU) for this user. This anticipated GIM would thus allow fast convergence of PPP solutions in regions of dense station coverage, while the same GIM would provide slower convergence capabilities in other regions. This approach differs from network RTK in that a user is free to move in and out of the network coverage area without loss of accuracy.

For obtaining both the highest accuracies and compatibility with the decoupled-clock model, it is imperative that integer-levelled observations be used for the computation of this next-generation GIM.

8.2.3 GLONASS Ambiguity Resolution

This dissertation described the theoretical elements required for the computation of satellite phase clocks for GLONASS based on a network of mixed receivers. However, several subsequent steps need to be performed before a solution is available to users. Of particular importance are the stability of IFCBs and the quality of GLONASS orbits.

8.2.3.1 Stability of IFCBs

Chapter 7 presented preliminary results regarding the estimation of GLONASS satellite widelane biases based on clusters of stations with compatible equipment. While it was confirmed that this approach allows for undifferenced GLONASS ambiguity resolution, this approach has two main drawbacks: 1) it leads to a significant increase in the number of parameters on the network side, and 2) more information needs to be transmitted to users. To overcome these limitations, an analysis of the temporal behavior of satellite widelane biases would need to be performed. The results of this analysis would reveal the frequency at which such biases should be estimated.

8.2.3.2 Orbit Accuracy

For ambiguity resolution to be successful, the error budget should remain below a quarter of a wavelength, namely 10 cm / 4 = 2.5 cm for the ionosphere-free combination. While this threshold can be attained for GPS through careful modelling, GLONASS orbits are typically not as accurate as GPS orbits. Apart from the network geometry, this is likely a consequence of the inability to fix double-differenced ambiguities in long-baseline GLONASS solutions.

The concepts presented in this dissertation regarding GLONASS ambiguity resolution are applicable to both PPP and long-baseline differential positioning. Implementing the methodology presented in Chapters 6 and 7 in orbit estimation software would then allow GLONASS ambiguity resolution over long baselines, and would ideally lead to an improvement in the quality of GLONASS orbits and satellite clocks.

8.3 Putting it All Together

(Re-)convergence of PPP solutions is greatly dependent on the ionosphere. During signal tracking interruptions, the ability of predicting slant ionospheric delay variations will dictate how quickly accurate positions can be retrieved. The same holds true for the

initial convergence period in which precise external information on the ionosphere can potentially allow for instantaneous ambiguity resolution.

Once carrier-phase ambiguities are fixed in PPP, this methodology also becomes a tool for precise monitoring of the ionosphere. With an increasing number of PPP users, a better sampling of the ionosphere becomes possible, and with proper means of passing this information back to other users, improvements in PPP convergence will follow.

Consolidated References

Abdel-Salam, M. A. (2005). *Precise Point Positioning Using Un-differenced Code and Carrier Phase Observations*. Ph.D. Dissertation, UCGE Reports No. 20229, University of Calgary, Canada, 206 pp.

Abidin, H. Z. (1993). "On the construction of the ambiguity searching space for on-the-fly ambiguity resolution," *NAVIGATION: Journal of The Institute of Navigation*, Vol. 40, No. 3, Fall, pp. 321-338.

Al-Shaery, A., S. Zhang, and C. Rizos (2013). "An enhanced calibration method of GLONASS inter-channel bias for GNSS RTK," *GPS Solutions*, Vol. 17, No. 2, pp. 165-173. doi: 10.1007/s10291-012-0269-5.

Baarda, W. (1968). "A testing procedure for use in geodetic networks." Publications on Geodesy, New Series, Vol. 2, No. 5, Netherlands Geodetic Commission, Delft, The Netherlands.

Banville, S., and H. Tang (2010). "Antenna rotation and its effects on kinematic precise point positioning." *Proceedings of the 23rd International Technical Meeting of the Satellite Division of The Institute of Navigation (ION GNSS 2010)*, Portland, Ore., 21-24 September, pp. pp. 2545-2552.

Banville, S., P. Collins, and F. Lahaye (2013). "GLONASS ambiguity resolution of mixed receiver types without external calibration," *GPS Solutions*, Vol. 17, No. 3, pp. 275-282. doi: 10.1007/s10291-013-0319-7.

Banville, S., and R. B. Langley (2009). "Improving real-time kinematic PPP with instantaneous cycle-slip correction." *Proceedings of the 22nd International Technical Meeting of the Satellite Division of The Institute of Navigation (ION GNSS 2009)*, Savannah, Ga., 22-25 September, pp. 2470-2478.

Banville, S., and R. B. Langley (2011). "Defining the basis of an integer-levelling procedure for estimating slant total electron content," *Proceedings of the 24th International Technical Meeting of the Satellite Division of The Institute of Navigation (ION GNSS 2011)*, Portland, Ore., 19-23 September, pp. 2542-2551.

Banville, S., R. B. Langley, and M. C. Santos (2009). "The Precise Point Positioning Software Centre: an insight into online PPP services." Poster presented at the International Association of Geodesy (IAG) 2009 Meeting, Buenos Aires, Argentina, 31 August - 4 September.

Banville, S., R. B. Langley, S. Saito, and T. Yoshihara (2010). "Handling cycle slips in GPS data during ionospheric plasma bubble events." *Radio Science*, Vol. 45, RS6007. doi: doi:10.1029/2010RS004415.

Banville, S., R. Santerre, M. Cocard, and R. B. Langley (2008). "Satellite and receiver phase bias calibration for undifferenced ambiguity resolution," *Proceedings of the 2008 National Technical Meeting of The Institute of Navigation*, San Diego, Calif., 28-30 January, pp. 711-719.

Banville, S., W. Zhang, R. Ghoddousi-Fard, and R. B. Langley (2012). "Ionospheric monitoring using 'integer-levelled' observations," *Proceedings of the 25th International Technical Meeting of the Satellite Division of The Institute of Navigation (ION GNSS 2012)*, Nashville, Tenn., 17-21 September, pp. 2692-2701.

Baselga, S. (2011). "Nonexistence of rigorous tests for multiple outlier detection in least-squares adjustment." *Journal of Surveying Engineering*, Vol. 137, No. 3, pp. 109-112. doi:10.1061/(ASCE)SU.1943-5428.0000048.

Bastos, L., and H. Landau (1988). "Fixing cycle slips in dual-frequency kinematic GPS-applications using Kalman filtering." *Manuscripta Geodaetica*, Vol. 13, No. 4, pp. 249-256.

Beran, T. (2008). *Single-frequency, single-receiver terrestrial and spaceborne point positioning*. Ph.D. dissertation, Technical Report 257, Department of Geodesy and Geomatics Engineering, University of New Brunswick, Fredericton, New Brunswick, Canada.

Bertiger, W., S. D. Desai, B. Haines, N. Harvey, A. W. Moore, S. Owen, and J. P. Weiss (2010). "Single receiver phase ambiguity resolution with GPS data," *Journal of Geodesy*, Vol. 84, No. 5, pp. 327-337. doi: 10.1007/s00190-010-0371-9.

Bertiger, W. I., Y. E. Bar-Sever, B. J. Haines, B. A. Iijima, S. M. Lichten, U. J. Lindqwister, A. J. Mannucci, R. J. Muellerschoen, T. N. Munson, A. W. Moore, L. J. Romans, B. D. Wilson, S. C. Wu, T. P. Yunck, G. Piesinger, and M. L. Whitehead (1997). "A real-time wide area differential GPS system." *NAVIGATION: Journal of The Institute of Navigation*, Vol. 44, No. 4, Winter, pp. 433-447.

Beutler, G., D. A. Davidson, R. B. Langley, R. Santerre, P. Vanicek, and D. E. Wells (1984). "Some theoretical and practical aspects of geodetic positioning using carrier phase difference observations of GPS satellites." Department of Geodesy and Geomatics Engineering Technical Report No. 109, University of New Brunswick, Fredericton, N.B., Canada.

Bisnath, S. B. (2000). "Efficient automated cycle-slip correction of dual-frequency kinematic GPS data." *Proceedings of the 13th International Technical Meeting of the Satellite Division of The Institute of Navigation (ION GPS 2000)*, Salt Lake City, Utah, 19-22 September, pp. 145-154.

Blewitt, G. (1989). "Carrier-phase ambiguity resolution for the global positioning system applied to geodetic baselines up to 2000 km." *Journal of Geophysical Research*, Vol. 94, No. B8, pp. 10187-10203. doi:10.1029/JB094iB08p10187.

Blewitt, G. (1990). "An automatic editing algorithm for GPS data." *Geophysical Research Letters,* Vol. 17, No. 3, pp. 199-202. doi:10.1029/GL017i003p00199.

Blewitt, G., W. C. Hammond, C. Kreemer, H.-P. Plag, S. Stein, and E. Okal (2009). "GPS for real-time earthquake source determination and tsunami warning systems," *Journal of Geodesy*, Vol. 83, No. 3-4, pp. 335–343. doi:10.1007/s00190-008-0262-5.

Boehm, J., J. Kouba, and H. Schuh (2009). "Forecast Vienna mapping functions 1 for real-time analysis of space geodetic observations." *Journal of Geodesy*, Vol. 83, No. 5, pp. 397-401. doi:10.1007/s00190-008-0216-y.

Brooks, B., and E. Holland (2010). "Researchers show how far South American cities moved in quake." The Ohio State University Research News. [On-line] 8 March, 2010. http://researchnews.osu.edu/archive/chilemoves.htm.

Brunini, C., and F. J. Azpilicueta (2009). "Accuracy assessment of the GPS-based slant total electron content," *Journal of Geodesy*, Vol. 83, No. 8, pp. 773-785. doi: 10.1007/s00190-008-0296-8.

Bruyninx, C. (2004). "The EUREF Permanent Network; a multidisciplinary network serving surveyors as well as scientists," *GeoInformatics*, No. 5, Vol. 7, pp. 32-35.

Cai, C., and Y. Gao (2008). "Estimation of GPS-GLONASS system time difference with application to PPP," *Proceedings of the 21st International Technical Meeting of the Satellite Division of The Institute of Navigation (ION GNSS 2008)*, Savannah, Ga., 16-19 September 2008, pp. 2880-2887.

Cai, C., and Y. Gao (2013). "Modeling and assessment of combined GPS/GLONASS precise point positioning," *GPS Solutions*, Vol. 17, No. 2, pp. 223-236. doi: 10.1007/s10291-012-0273-9.

Cai, C., Z. Liu, P. Xia, and W. Dai (2013). "Cycle slip detection and repair for undifferenced GPS observations under high ionospheric activity." *GPS Solutions*, Vol. 17, No. 2, pp. 247-260. doi:10.1007/s10291-012-0275-7.

Chen, W., C. Hu, S. Gao, Y. Chen, X. Ding, and S. C. Kowk (2004). "Precise estimation of absolute ionospheric delay based on GPS active network," *Proceedings of the 17th International Technical Meeting of the Satellite Division of The Institute of Navigation (ION GNSS 2004)*, Long Beach, Calif., 21-24 September, pp. 420-427.

Chuang, S., W. Yi, W. Song, Y. Lou, Y. Yao, and R. Zhang (2013). "GLONASS pseudorange inter-channel biases and their effects on combined GPS/GLONASS precise point positioning," *GPS Solutions*, Vol. 17, No. 4, pp. 439-451. doi: 10.1007/s10291-013-0332-x.

Ciraolo, L., F. Azpilicueta, C. Brunini, A. Meza, and S. M. Radicella (2007). "Calibration errors on experimental slant total electron content (TEC) determined with GPS," *Journal of Geodesy*, Vol. 81, No. 2, pp. 111-120. doi: 10.1007/s00190-006-0093-1.

Coco, D. S., C. E. Coker, S. R. Dahlke, and J. R. Clynch (1991). "Variability of GPS satellite differential group delay biases," *IEEE Transactions on Aerospace and Electronic Systems*, Vol. 27, No. 6, pp. 931-938. doi: 10.1109/7.104264.

Collin, F., and R. Warnant (1995). "Application of the wavelet transform for GPS cycle slip correction and comparison with Kalman filter." *Manuscripta Geodaetica*, Vol. 20, No. 3, pp. 161–172.

Collins, P. (2008). "Isolating and estimating undifferenced GPS integer ambiguities." *Proceedings of the 2008 National Technical Meeting of The Institute of Navigation*, San Diego, Calif., 28-30 January, pp. 720-732.

Collins, P. (2011). "Parameter estimability and an extended observation model for precise point positioning," Presented at the CRESS Graduate Student Presentation, York University, Toronto, Ont., 15 June.

Collins, P., F. Lahaye, and S. Bisnath (2012) "External ionospheric constraints for improved PPP-AR initialisation and a generalised local augmentation concept," *Proceedings of the 25th International Technical Meeting of the Satellite Division of The Institute of Navigation (ION GNSS 2012)*, Nashville, Tenn., 17-21 September 2012, pp. 3055-3065.

Collins, P., and S. Bisnath (2011). "Issues in ambiguity resolution for precise point positioning," *Proceedings of the 24th International Technical Meeting of the Satellite Division of The Institute of Navigation (ION GNSS 2011)*, Portland, Ore., 19-23 September 2011, pp. 679-687.

Collins, P., S. Bisnath, F. Lahaye, and P. Héroux (2010). "Undifferenced GPS ambiguity resolution using the decoupled clock model and ambiguity datum fixing," *NAVIGATION: Journal of The Institute of Navigation*, Vol. 57, No. 2, Summer 2010, pp. 123-135.

Collins, P., Y. Gao, F. Lahaye, P. Héroux, K. MacLeod, and K. Chen (2005). "Accessing and processing real-time GPS corrections for precise point positioning: some user considerations," *Proceedings of the 18th International Technical Meeting of the Satellite Division of The Institute of Navigation (ION GNSS 2005)*, Long Beach, Calif., 13-16 September 2005, pp. 1483-1491.

Colombo, O. L., M. Hernández-Pajares, J. M. Juan, J. Sanz, and J. Talaya (1999). "Resolving carrier-phase ambiguities on the fly, at more than 100 km from nearest reference site, with the help of ionospheric tomography," *Proceedings of the 12th International Technical Meeting of the Satellite Division of The Institute of Navigation (ION GPS 1999)*, 14-17 September, Nashville, Tenn., pp. 1635-1642.

Coster, A., and A. Komjathy (2008). "Space weather and the Global Positioning System," *Space Weather*, Vol. 6, No. 6, S06D04. doi: 10.1029/2008SW000400.

Dach, R., U. Hugentobler, P. Fridez, and M. Meindl (2007). *Bernese GPS Software, Version 5.0*. Astronomical Institute, University of Bern, Bern, Switzerland, January 2007.

Dai, L., R. Hatch, and R. Ronald (2011). "Integrated StarFire GPS with GLONASS for real-time precise navigation and positioning," *Proceedings of the 24th International Technical Meeting of the Satellite Division of The Institute of Navigation (ION GNSS 2011)*, Portland, Ore., 20-23 September 2011, pp. 1476-1485.

Dai, Z., S. Knedlik, and O. Loffeld (2009). "Instantaneous triple-frequency GPS cycle-slip detection and repair." *International Journal of Navigation and Observation*, Vol. 2009. doi:10.1155/2009/407231.

Defraigne, P., and Q. Baire (2011). "Combining GPS and GLONASS for time and frequency transfer," *Advances in Space Research*, Vol. 47, No. 2, pp. 265-275. doi: 10.1016/j.asr.2010.07.003.

de Jong, K., and P. J. G. Teunissen (2000). "Minimal detectable biases of GPS observations for a weighted ionosphere." *Earth Planets Space* Vol. 52, pp. 857–862.

de Jonge, P. J. (1998). *A Processing Strategy for the Application of the GPS in Networks*. Ph.D. dissertation, Publications on Geodesy 46, Delft University of Technology, Netherlands Geodetic Commission, Delft, The Netherlands.

de Jonge, P. J., and C. C. J. M. Tiberius (1996). "The LAMBDA method for integer ambiguity estimation: implementation aspects." LGR Series 12, Delft Geodetic Computing Center, Delft University of Technology, Delft, The Netherlands.

de Lacy, M.C., M. Reguzzoni, F. Sansò, and G. Venuti (2008). "The Bayesian detection of discontinuities in a polynomial regression and its application to the cycle-slip problem." *Journal of Geodesy*, Vol. 82, No. 9, pp. 527–542. doi:10.1007/s00190-007-0203-8.

de Lacy, M.C., M. Reguzzoni, and F. Sansò (2012). "Real-time cycle slip detection in triple-frequency GNSS." *GPS Solutions*, Vol. 16, No. 3, pp. 353–362. doi:10.1007/s10291-011-0237-5.

244

Dow, J. M., R. E. Neilan, and C. Rizos (2009). "The International GNSS Service in a changing landscape of global navigation satellite systems." *Journal of Geodesy*, Vol. 83, No. 3-4, pp. 191–198. doi:10.1007/s00190-008-0300-3.

Dragert, H., X. Chen, and J. Kouba (1995). "GPS monitoring of crustal strain in southwest British Columbia with the western Canada deformation array," G*eomatica*, Vol. 49, No. 3, pp. 301-313.

Drescher, R., X. Chen, H. Landau, A. Kipka, M. Glocker, and V. Gomez (2013). "Accelerating the convergence of Trimble CenterPoint RTX Positioning by using a global ionospheric model," *Presented at the GNSS PPP Workshop: Reaching Full Potential*, Ottawa, Ont., Canada, 12-14 June.

Enge, P., T. Walter, S. Pullen, C. Kee, Y. C. Chao, and Y.-J. Tsai (1996). "Wide area augmentation of the Global Positioning System," *Proceedings of the IEEE*, Vol. 84, No. 8, August 1996, pp.1063-1088. doi: 10.1109/5.533954.

Euler, H.-J., and B. Schaffrin (1991). "On a measure for the discernability between different ambiguity solutions in the static-kinematic GPS-mode." *IAG Symposia no. 107, Kinematic Systems in Geodesy, Surveying, and Remote Sensing*, Springer, Berlin Heidelberg, New York, pp. 285–295.

Euler, H.-J., and H. Landau (1992). "Fast GPS ambiguity resolution on-the-fly for real-time application," *Proceedings of the 6th International Geodetic Symposium on Satellite Positioning*, 17-20 March, Columbus, Ohio, pp. 650–659.

Felhauer, T. (1997). "On the impact of RF front-end group delay variations on GLONASS pseudorange accuracy," *Proceedings of the 10th International Technical Meeting of the Satellite Division of The Institute of Navigation (ION GPS 1997)*, Kansas City, Mo., 16-19 September 1997, pp. 1527-1532.

Feng, Y., and J. Wang (2011). "Computed success rates of various carrier phase integer estimation solutions and their comparison with statistical success rates." *Journal of Geodesy*, Vol. 85, No. 2, pp. 93–103. doi:10.1007/s00190-010-0418-y.

Fotopoulos, G. and M. E. Cannon (2001). "An overview of multiple-reference station methods for cm-level positioning," *GPS Solutions*, Vol. 4, No. 3, pp. 1-10. doi: 10.1007/PL00012849.

Gao, Y., F. Lahaye, P. Héroux, X. Liao, N. Beck, and M. Olynik (2001). "Modeling and estimation of C1–P1 bias in GPS receivers," *Journal of Geodesy*, Vol. 74, No. 9, pp. 621-626. doi: 10.1007/s001900000117.

Gao, Y., and X. Shen (2001). "Improving ambiguity convergence in carrier phase-based precise point positioning," *Proceedings of the 14th International Technical Meeting of the Satellite Division of The Institute of Navigation (ION GPS 2001)*, Salt Lake City, Utah, 11-14 September 2001, pp. 1532-1539.

Gao, Y., and Z. Li (1999). "Cycle slip detection and ambiguity resolution algorithms for dual-frequency GPS data processing." *Marine Geodesy*, Vol. 22, No. 3, pp. 169–181. doi:10.1080/014904199273443.

Ge, M., G. Gendt, M. Rothacher, C. Shi, and J. Liu (2008) "Resolution of GPS carrier-phase ambiguities in precise point positioning (PPP) with daily observations." *Journal of Geodesy*, Vol. 82, No. 7, pp. 389-399. doi:10.1007/s00190-007-0187-4.

Geng, J. (2009). "Rapid re-convergence in real-time precise point positioning with ambiguity resolution." *Proceedings of the 22nd International Technical Meeting of the Satellite Division of The Institute of Navigation (ION GNSS 2009)*, Savannah, Ga., 22-25 September, pp. 2437-2448.

Geng, J., X. Meng, A. Dodson, M. Ge, and F. Teferle (2010). "Rapid re-convergences to ambiguity-fixed solutions in precise point positioning." *Journal of Geodesy*, Vol. 84, No. 12, pp. 705–714. doi:10.1007/s00190-010-0404-4.

Grafarend, E., and B. Schaffrin (1976). "Equivalence of estimable quantities and invariants in geodetic networks," *Zeitschrift für Vermessungswesen*, Vol. 101, pp. 485-491.

Griffiths, J., and J. Ray (2009). "On the precision and accuracy of IGS orbits." *Journal of Geodesy*, Vol. 83, No. 3, pp. 277–287. doi:10.1007/s00190-008-0237-6.

Habrich, H., G. Beutler, W. Gurtner, and M. Rothacher (1999). "Double difference ambiguity resolution for GLONASS/GPS carrier phase," *Proceedings of the 12th International Technical Meeting of the Satellite Division of The Institute of Navigation (ION GPS 1999)*, Nashville, Tenn., 14-17 September 1999, pp. 1609-1618.

Hatch, R. (1990). "Instantaneous ambiguity resolution," *Proceedings of the International Symposium on Kinematic Systems for Geodesy, Surveying and Remote Sensing (KIS'90)*, 10-13 September, Banff, Alta., Canada, pp. 299-308.

Hauschild, A., and O. Montenbruck (2008). "Real-time clock estimation for precise orbit determination of LEO-satellites." *Proceedings of the 21st International Technical Meeting of the Satellite Division of The Institute of Navigation (ION GNSS 2008)*, Savannah, Ga., 16-19 September, pp. 581-589.

Hernández-Pajares, M., J. M. Juan, J. Sanz, R. Orus, A. Garcia-Rigo, J. Feltens, A. Komjathy, S. C. Schaer and A. Krankowski (2009). "The IGS VTEC maps: a reliable

source of ionospheric information since 1998," *Journal of Geodesy*, Vol. 83, No. 3-4, pp. 263-275. doi: 10.1007/s00190-008-0266-1

Héroux, P., Y. Gao, J. Kouba, F. Lahaye, Y. Mireault, P. Collins, K. Macleod, P. Tétreault, and K. Chen (2004). "Products and applications for precise point positioning - moving towards real-time," *Proceedings of the 17th International Technical Meeting of the Satellite Division of The Institute of Navigation (ION GNSS 2004)*, Long Beach, Calif., 21-24 September 2004, pp. 1832-1843.

Hofmann-Wellenhof, B., H. Lichtenegger, and J. Collins (1997). *Global Positioning System: Theory and Practice*. 4th ed., Springer, Berlin Heidelberg, New York.

Hugentobler, U., S. Schaer, T. Springer, G. Beutler, H. Bock, R. Dach, D. Ineichen, L. Mervart, M. Rothacher, U. Wild, A. Wiget, E. Brockmann, G. Weber, H. Habrich, and C. Boucher (2001). "CODE IGS analysis center technical report 2000." IGS Central Bureau (Eds.), IGS - 2000 Technical Reports, Jet Propulsion Laboratory Publications 02-012, California Institute of Technology, Pasadena, Calif., November.

IGS (2012). International GNSS Service (IGS) website. [On-line] 18 September 2012. http://igscb.jpl.nasa.gov/components/prods.html.

Jensen, A. B. O., and C. Mitchell (2011). "GNSS and the ionosphere: What's in store for the next solar maximum?" *GPS World*, Vol. 22, No. 2, pp. 40–48.

Jokinen, A., S. Feng, W. Schuster, W. Ochieng, L. Yang, C. Hide, T. Moore, and C. Hill (2013). "Fixed ambiguity precise point positioning (PPP) using tropospheric corrections based on numeric weather modeling (NWM)," *Proceedings of the ION 2013 Pacific PNT Meeting*, Honolulu, Hawaii, 23-25 April 2013, pp. 319-329.

Jorgensen, P. S. (1978). *Ionospheric Measurements from NAVSTAR Satellites*. Report prepared for Space and Missile Systems Organization, Air Force Systems Command, Los Angeles Air Force Station, Los Angeles, Calif. by Satellite Systems Division of the Aerospace Corporation, El Segundo, Calif., December, SAMSO-TR-79-29, 48 pp.

Kee, C., T. Walter, P. Enge, and B. Parkinson (1997). "Quality control algorithms on WAAS wide-area reference stations." *NAVIGATION: Journal of The Institute of Navigation*, Vol. 44, No. 1, Spring 1997, pp. 53–62.

Kim, D., and R. B. Langley (2000). "GPS ambiguity resolution and validation: methodologies, trends and issues." *Proceedings of the 7th GNSS Workshop – International Symposium on GPS/GNSS*, Seoul, Korea, 30 November – 2 December, pp. 213–221.

Kim, D., and R. B. Langley (2001). "Instantaneous real-time cycle-slip correction of dual-frequency GPS data." *Proceedings of the International Symposium on Kinematic*

Systems in Geodesy, Geomatics and Navigation, Banff, Alta., Canada, 5-8 June, pp. 255-264.

Kim, D., and R. B. Langley (2002) "Instantaneous real-time cycle-slip correction for quality control of GPS carrier-phase measurements," *NAVIGATION: Journal of The Institute of Navigation*, Vol. 49, No. 4, Winter, pp. 205–222.

Kim, D., and R. B. Langley (2007). "Ionosphere-nullification technique for long-baseline real-time kinematic applications," *NAVIGATION, Journal of The Institute of Navigation*, Vol. 54, No. 3, Fall 2007, pp. 227-240.

Knight, N.L., J. Wang, and C. Rizos (2010). "Generalized measures of reliability for multiple outliers." *Journal of Geodesy*, Vol. 84, No. 10, pp. 625–635. doi:10.1007/s00190-010-0392-4.

Komjathy, A. (1997). *Global Ionospheric Total Electron Content Mapping Using the Global Positioning System*. Ph. D. dissertation, Technical Report 188, Department of Geodesy and Geomatics Engineering, University of New Brunswick, Fredericton, New Brunswick, Canada.

Komjathy, A., L. Sparks, A. J. Mannucci, and X. Pi (2003). "On the ionospheric impact of recent storm events on satellite-based augmentation systems in middle and low-latitude sectors." *Proceedings of the 16th International Technical Meeting of the Satellite Division of The Institute of Navigation (ION GPS/GNSS 2003)*, Portland, Ore., 9-12 September, pp. 2769–2776.

Komjathy, A., L. Sparks, B. Wilson, and A. J. Mannucci (2005). "Automated daily processing of more than 1000 ground-based GPS receivers to study intense ionospheric storms," *Radio Science*, Vol. 40, RS6006. doi:10.1029/2005RS003279.

Kouba, J. (2002). "Relativistic time transformations in GPS," *GPS Solutions*, Vol. 5, No. 4, pp. 1–9. doi: 10.1007/PL00012907.

Kouba, J. (2004). "Improved relativistic transformations in GPS," *GPS Solutions*, Vol. 8, No. 3, pp. 170–180. doi: 10.1007/s10291-004-0102-x.

Kouba, J. (2008). "Implementation and testing of the gridded Vienna mapping function 1 (VMF1)." *Journal of Geodesy*, Vol. 82, No. 4-5, pp. 193-205. doi:10.1007/s00190-007-0170-0.

Kouba, J. (2009). "Guide to using International GNSS Service (IGS) products." [On-line] 20 May 2012. http://igscb.jpl.nasa.gov/.

Kouba, J. (2010). "IGS observations during the February 27, 2010 M 8.8 Chilean earthquake." [On-line] 8 March 2010. http://www.igs.org/overview/pubs/2010-8.8-Chilean-Earthquake/.

Kouba, J., and P. Héroux (2001). "Precise point positioning using IGS orbit and clock products." *GPS Solutions*, Vol. 5, No. 2, pp. 12-28. doi:10.1007/PL00012883.

Kozlov, D., M. Tkachenko, and A. Tochilin (2000). "Statistical characterization of hardware biases in GPS+GLONASS receivers," *Proceedings of the 13th International Technical Meeting of the Satellite Division of The Institute of Navigation (ION GPS 2000)*, Salt Lake City, Utah, 19-22 September 2000, pp. 817-826.

Krankowski, A. (2011). "IGS ionosphere working group technical report 2011," In International GNSS Service Technical Report 2011, Astronomical Institute, University of Bern, [On-line] 18 September 2012. ftp://igs.org/pub/resource/pubs/2011_techreport.pdf

Landau, H., and H.-J. Euler (1992). "On-the-fly ambiguity resolution for precise differential positioning," *Proceedings of the 5th International Technical Meeting of the Satellite Division of The Institute of Navigation (ION GPS 1992)*, Albuquerque, N.M., 16-18 September 1992, pp. 607-613.

Landau, H., M. Brandl, X. Chen, R. Drescher, M. Glocker, A. Nardo, M. Nitschke, D. Salazar, U. Weinbach, F. Zhang (2013). "Towards the inclusion of Galileo and BeiDou/Compass satellites in Trimble CenterPoint RTX," *Proceedings of the 26th International Technical Meeting of the Satellite Division of The Institute of Navigation (ION GNSS+ 2013)*, Nashville, Tenn., 16-20 September 2013, pp. 1215-1223.

Landau, H., U. Vollath, and X. Chen (2002). "Virtual reference station systems," *Journal of Global Positioning Systems*, Vol. 1, No. 2, pp. 137-143.

Lannes, A., and J.-L. Prieur (2013). "Calibration of the clock-phase biases of GNSS networks: the closure-ambiguity approach," *Journal of Geodesy*, Vol. 87, No. 8, pp. 709-731. doi: 10.1007/s00190-013-0641-4.

Lanyi, G. E., and T. Roth (1988). "A comparison of mapped and measured total ionospheric electron content using Global Positioning System and beacon satellite observations," *Radio Science*, Vol. 23, No. 4, pp. 483-492. doi:10.1029/RS023i004p00483.

Laurichesse, D. (2011). "The CNES real-time PPP with undifferenced integer ambiguity resolution demonstrator," *Proceedings of the 24th International Technical Meeting of the Satellite Division of The Institute of Navigation (ION GNSS 2011)*, Portland, Ore., 19-23 September 2011, pp. 654-662.

Laurichesse, D., and F. Mercier (2007). "Integer ambiguity resolution on undifferenced GPS phase measurements and its application to PPP." *Proceedings of the 20th International Technical Meeting of the Satellite Division of The Institute of Navigation (ION GNSS 2007)*, Fort Worth, Texas, 25-28 September, pp. 839-848.

Laurichesse, D., F. Mercier, J.-P. Berthias, P. Broca, and L. Cerri (2009). "Integer ambiguity resolution on undifferenced GPS phase measurements and its application to PPP and satellite precise orbit determination," *NAVIGATION: Journal of The Institute of Navigation*, Vol. 56, No. 2, Summer 2009, pp. 135-149.

Leandro, R., H. Landau, M. Nitschke, M. Glocker, S. Seeger, X. Chen, A. Deking, M. Ben Tahar, F. Zhang, K. Ferguson, R. Stolz, N. Talbot, G. Lu, T. Allison, M. Brandl, V. Gomez, W. Cao, and A. Kipka (2011). "RTX positioning: the next generation of cm-accurate real-time GNSS positioning," *Proceedings of the 24th International Technical Meeting of the Satellite Division of The Institute of Navigation (ION GNSS 2011)*, Portland, Ore., 19-23 September 2011, pp. 1460-1475.

Leandro, R. F., M. C. Santos, and R. B. Langley (2007). "PPP-based ionosphere activity monitoring," *Proceedings of the 20th International Technical Meeting of the Satellite Division of The Institute of Navigation (ION GNSS 2007)*, Fort Worth, Texas, 25-28 September, pp. 2849-2853.

Li, X. (2012) "Improving real-time PPP ambiguity resolution with ionospheric characteristic consideration," *Proceedings of the 25th International Technical Meeting of the Satellite Division of The Institute of Navigation (ION GNSS 2012)*, Nashville, Tenn., 17-21 September 2012, pp. 3027-3037.

Liu, Z. (2011). "A new automated cycle slip detection and repair method for a single dual-frequency GPS receiver." *Journal of Geodesy*, Vol. 85, No. 3, pp. 171–183. doi:10.1007/s00190-010-0426-y.

Mader, G. (1986). "Dynamic positioning using GPS carrier phase measurements," *Manuscripta Geodaetica*, Vol. 11, No. 4, pp. 272-277.

Mader, G. (1999). "GPS antenna calibration at the National Geodetic Survey," *GPS Solutions*, Vol. 3, No. 1, pp. 50-58. doi: 10.1007/PL00012780.

Mader, G., J. Beser, A. Leick, and J. Li (1995). "Processing GLONASS carrier phase observations - theory and first experience," *Proceedings of the 8th International Technical Meeting of the Satellite Division of The Institute of Navigation (ION GPS 1995)*, Palm Springs, Calif., 12-15 September 1995, pp. 1041-1047.

Mahalanobis, P. C. (1936). "On the generalised distance in statistics." *Proceedings of the National Institute of Sciences of India*, Vol. 2, No. 1, pp. 49–55.

Melbourne, W. G. (1985). "The case for ranging in GPS based geodetic systems," *Proceedings of 1ˢᵗ International Symposium on Precise Positioning with the Global Positioning System*, edited by Clyde Goad, U.S. Department of Commerce, Rockville, Md., 15-19 April, pp. 373-386.

Melgar, D., and Y. Bock (2013). "Near-field tsunami models with rapid earthquake source inversions from land- and ocean-based observations: The potential for forecast and warning," *Journal of Geophysical Research: Solid Earth*, Vol. 118, No. 11, pp. 5939-5955. doi: 10.1002/2013JB010506.

Mervart, L. (1995). *Ambiguity resolution techniques in geodetic and geodynamic applications of the Global Positioning System*. Ph.D. Dissertation, Astronomical Institute, University of Berne, Switzerland, 155 pp.

Mervart, L., Z. Lukes, C. Rocken, and T. Iwabuchi (2008). "Precise point positioning with ambiguity resolution in real-time." *Proceedings of the 21st International Technical Meeting of the Satellite Division of The Institute of Navigation (ION GNSS 2008)*, Savannah, Ga., 16-19 September, pp. 397-405.

Michaud, S., and R. Santerre (2001). "Time-relative positioning with a single civil GPS receiver." *GPS Solutions*, Vol. 5, No. 2, pp. 71-77. doi:10.1007/PL00012888.

Mireault, Y., P. Tétreault, F. Lahaye, P. Héroux, and J. Kouba (2008). "Online precise point positioning: A new, timely service from Natural Resources Canada," *GPS World*, Vol. 19, No. 9, September 2008, pp. 59-64.

Odijk, D. (2002). *Fast precise GPS positioning in the presence of ionospheric delays*. Ph.D. dissertation, Publications on Geodesy 52, Delft University of Technology, Netherlands Geodetic Commission, Delft, The Netherlands.

Odijk, D., and S. Verhagen (2007). "Recursive detection, identification and adaptation of model errors for reliable high-precision GNSS positioning and attitude determination." *3rd International Conference on Recent Advances in Space Technologies (RAST '07)*, Istanbul, pp. 624–629. doi:10.1109/RAST.2007.4284068.

Parkinson, B. W. (1994). "GPS eyewitness: The early years," *GPS World*, Vol. 5, No. 9, pp. 32-45.

Petit, G., and B. Luzum (Eds.) (2010). "IERS conventions (2010). IERS technical note no. 36," Frankfurt am Main: Verlag des Bundesamts für Kartographie und Geodäsie, 179 pp. [On-line] 11 July 2014.
http://www.iers.org/IERS/EN/Publications/TechnicalNotes/tn36.html

Pratt, M., B. Burke, and P. Misra (1997). "Single-epoch integer ambiguity resolution with GPS L1-L2 carrier phase measurements," *Proceedings of the 10th International*

Technical Meeting of the Satellite Division of The Institute of Navigation (ION GPS 1997), Kansas City, Mo., 16-19 September 1997, pp. 1737-1746.

Remondi, B. W. (1984). *Using the Global Positioning System (GPS) phase observable for relative geodesy: modeling, processing, and results*. Ph. D. dissertation, Center for Space Research, The University of Texas at Austin, Austin, Texas, 360 pp.

Reussner, N., and L. Wanninger (2011). "GLONASS inter-frequency biases and their effects on RTK and PPP carrier-phase ambiguity resolution," *Proceedings of the 24th International Technical Meeting of the Satellite Division of The Institute of Navigation (ION GNSS 2011)*, Portland, Ore., 19-23 September 2011, pp. 712-716.

Rizos, C. (2002) "Network RTK research and implementation – a geodetic perspective," *Journal of Global Positioning Systems*, Vol.1, No.2, pp. 144-150.

Rocken, C., L. Mervart, J. Johnson, Z. Lukes, T. Springer, T. Iwabuchi, and S. Cummins (2011). "A new real-time global GPS and GLONASS precise positioning correction service: Apex," *Proceedings of the 24th International Technical Meeting of the Satellite Division of The Institute of Navigation (ION GNSS 2011)*, Portland, Ore., 20-23 September 2011, pp. 1825-1838.

Schaer, S. (1999). *Mapping and Predicting the Earth's Ionosphere Using the Global Positioning System.* Ph.D. dissertation, Astronomical Institute, University of Berne, Switzerland, 205 pp.

Schaer, S., W. Gurtner, and F. Feltens (1998). "IONEX: the IONosphere map Exchange format version 1, February 25, 1998," *Proceedings of the 1998 IGS Analysis Centers Workshop*, ESOC, Darmstadt, Germany, 9-11 February.

Schmitz, M., G. Wübbena and G. Boettcher (2002). "Tests of phase center variations of various GPS antennas, and some results." *GPS Solutions*, Vol. 6, No. 1-2, pp. 18-27. doi: 10.1007/s10291-002-0008-4.

Skone, S., and K. Knudsen (2000). "Impact of ionospheric scintillations on SBAS performance." *Proceedings of the 13th International Technical Meeting of the Satellite Division of The Institute of Navigation (ION GPS 2000)*, Salt Lake City, Utah, 19-22 September, pp. 284–293.

Skone, S., K. Knudsen, and M. de Jong (2001). "Limitations in GPS receiver tracking performance under ionospheric scintillation conditions." *Physics and Chemistry of the Earth, Part A: Solid Earth and Geodesy*, Vol. 26, No. 6-8, pp. 613-621. doi:10.1016/S1464-1895(01)00110-7.

Sleewaegen, J. M., A. Simsky, W. de Wilde, F. Boon, and T. Willems (2012). "Demystifying GLONASS inter-frequency carrier phase biases," *InsideGNSS*, Vol. 7, No. 3, pp. 57-61.

Song, Y. T., I. Fukumori, C. K. Shum, and Y. Yi (2012). "Merging tsunamis of the 2011 Tohoku-Oki earthquake detected over the open ocean," *Geophysical Research Letters*, Vol. 39, No. 5, L05606. doi: 10.1029/2011GL050767.

Stephens, P., A. Komjathy, B. Wilson, and A. Mannucci (2011). "New leveling and bias estimation algorithms for processing COSMIC/FORMOSAT-3 data for slant total electron content measurements," *Radio Science*, Vol. 46, RS0D10. doi:10.1029/2010RS004588.

Takac, F. (2009) "GLONASS inter-frequency biases and ambiguity resolution," *InsideGNSS*, Vol. 4, No. 2, pp. 24-28.

Takasu, T., and A. Yasuda (2008). "Cycle slip detection and fixing by MEMS-IMU/GPS integration for mobile environment RTK-GPS," *Proceedings of the 21st International Technical Meeting of the Satellite Division of The Institute of Navigation (ION GNSS 2008)*, Savannah, Ga., 16-19 September 2008, pp. 64-71.

Teunissen, P. J. G. (1985). "Zero order design: generalized inverses, adjustment, the datum problem and S-transformations," In: Grafarend E. W., and Sansò F (eds) Optimization and Design of Geodetic Networks, Springer-Verlag, pp 11-55.

Teunissen, P. J. G. (1990). "Quality control in integrated navigation systems." *IEEE Aerospace and Electronic Systems Magazine*, Vol. 5, No. 7, pp. 35–41. doi:10.1109/62.134219.

Teunissen, P. J. G. (1991). "On the minimal detectable biases of GPS phase ambiguity slips." *Proceedings of DGPS'91, the First International Symposium on Real Time Differential Applications of the Global Positioning System*, Braunschweig, Germany, Vol. 2, pp. 679–686.

Teunissen, P. J. G. (1993). *Least-squares estimation of the integer GPS ambiguities*. Technical Report, LGR Series 6, Delft Geodetic Computing Centre, Delft University of Technology, Delft, The Netherlands.

Teunissen, P. J. G. (1994). "A new method for fast carrier phase ambiguity estimation." *Proceedings of the IEEE Position, Location and Navigation Symposium (PLANS '94),* Las Vegas, Nev., 11-15 April, pp. 562-573.

Teunissen, P. J. G. (1997). "A canonical theory for short baselines. Part IV: Precision versus reliability." *Journal of Geodesy*, Vol. 71, No. 9, pp. 513–525. doi:10.1007/s001900050119.

Teunissen, P. J. G. (1998). "On the integer normal distribution of the GPS ambiguities." *Artificial Satellites*, Vol. 33, No. 2, pp. 49–64.

Teunissen, P. J. G. (1999a). "Minimal detectable biases of GPS data." *Journal of Geodesy*, Vol. 72, No. 4, pp. 236–244. doi:10.1007/s001900050163.

Teunissen, P. J. G. (1999b). "An optimality property of the integer least-squares estimator." *Journal of Geodesy*, Vol. 73, No. 11, pp. 587-593. doi:10.1007/s001900050269.

Teunissen, P. J. G. (2000). "The success rate and precision of the GPS ambiguities." *Journal of Geodesy*, Vol. 74, No. 3-4, pp. 321–326. doi:10.1007/s001900050289.

Teunissen, P. J. G. (2001). "Integer estimation in the presence of biases." *Journal of Geodesy*, Vol. 75, No. 7-8, pp. 399-407. doi:10.1007/s001900100191.

Teunissen, P. J. G. (2005). "GNSS ambiguity resolution with optimally controlled failure-rate." *Artificial Satellites*, Vol. 40, No. 4, pp. 219–227.

Teunissen, P. J. G., and A. Kleusberg (Eds.) (1998). *GPS for Geodesy*, 2nd ed., Springer, Berlin Heidelberg, New York.

Teunissen, P. J. G., and D. Odijk (1997). "Ambiguity dilution of precision: definition, properties and application," *Proceedings of the 10th International Technical Meeting of the Satellite Division of The Institute of Navigation (ION GPS 1997),* Kansas City, Mo., 16-19 September 1997, pp. 891-899.

Teunissen, P. J. G., D. Odijk, and B. Zhang (2010). "PPP-RTK: results of CORS network-based PPP with integer ambiguity resolution," *Journal of Aeronautics, Astronautics and Aviation, Series A*, Vol. 42, No. 4, pp. 223-230.

Teunissen, P. J. G., and M. A. Salzmann (1989). "A recursive slippage test for use in state-space filtering," *Manuscripta Geodaetica*, Vol. 14, No. 6, pp. 383–390.

Teunissen, P. J. G., P. Joosten, and C. C. J. M. Tiberius (1999). "Geometry-free ambiguity success rates in case of partial fixing." *Proceedings of the 1999 National Technical Meeting of The Institute of Navigation*, San Diego, Calif., 25-27 January, pp. 201–207.

Teunissen, P. J. G., P. Joosten, and C. C. J. M. Tiberius (2000). "Bias robustness of GPS ambiguity resolution." *Proceedings of the 13th International Technical Meeting of the Satellite Division of The Institute of Navigation (ION GPS-2000)*, Salt Lake City, Utah, 19-22 September, pp. 104–112.

Teunissen, P. J. G., and S. Verhagen (2009). "The GNSS ambiguity ratio-test revisited: a better way of using it." *Survey Review*, Vol. 41, No. 312, pp. 138–151. doi:10.1179/003962609X390058.

Themens, D. R., P. T. Jayachandran, R. B. Langley, J. W. MacDougall, and M. J. Nicolls (2013) "Determining receiver biases in GPS-derived total electron content in the auroral oval and polar cap region using ionosonde measurements," *GPS Solutions*, Vol. 17, No. 3, pp. 357-369. doi: 10.1007/s10291-012-0284-6.

Ulmer, K., P. Hwang, B. Disselkoen, and M. Wagner (1995). "Accurate azimuth from a single PLGR+GLS DoD GPS receiver using time relative positioning." *Proceedings of the 8th International Technical Meeting of the Satellite Division of The Institute of Navigation (ION GPS 1995)*, Palm Springs, Calif., 12-15 September, pp. 1733-1741.

Van Meerbergen, G., A. Simsky, and F. Boon (2010). "A novel decision directed Kalman filter to improve RTK performance." *Proceedings of the 23rd International Technical Meeting of the Satellite Division of The Institute of Navigation (ION GNSS 2010)*, Portland, Ore., 21-24 September, pp. 3268–3276.

Verhagen, S. (2004). "Integer ambiguity validation: an open problem?" *GPS Solutions*, Vol. 8, No. 1, pp. 36–43. doi:10.1007/s10291-004-0087-5.

Verhagen, S., and P. J. G. Teunissen (2006). "On the probability density function of the GNSS ambiguity residuals." *GPS Solutions*, Vol. 10, No. 1, pp. 21–28. doi:10.1007/s10291-005-0148-4.

Wang, J., C. Rizos, M. P. Stewart, and A. Leick (2001). "GPS and GLONASS integration: modeling and ambiguity resolution issues," *GPS Solutions*, Vol. 5, No. 1, pp. 55-64. doi: 10.1007/PL00012877.

Wang, J., and Y. Feng (2013). "Reliability of partial ambiguity fixing with multiple GNSS constellations," *Journal of Geodesy*, Vol. 87, No. 1, pp. 1-14. doi: 10.1007/s00190-012-0573-4.

Wanninger, L. (2012). "Carrier-phase inter-frequency biases of GLONASS receivers," *Journal of Geodesy*, Vol. 86, No. 2, pp. 139-148. doi: 10.1007/s00190-011-0502-y.

Wanninger, L., and S. Wallstab-Freitag (2007). "Combined processing of GPS, GLONASS, and SBAS code phase and carrier phase measurements," *Proceedings of the 20th International Technical Meeting of the Satellite Division of The Institute of Navigation (ION GNSS 2007)*, Fort Worth, Texas, 25-28 September 2007, pp. 866-875.

Weber, G., D. Dettmering, and H. Gebhard (2005). "Networked transport of RTCM via Internet protocol (NTRIP)." In: Sanso F. (Ed.): A Window on the Future, Proceedings of

the IAG General Assembly, Sapporo, Japan, 2003, Springer Verlag, Symposia Series, Vol. 128, 2005, pp. 60-64, doi:10.1007/3-540-27432-4_11.

Wells, D. E., and E. J. Krakiwsky (1971). *The Method of Least-squares*. Department of Geodesy and Geomatics Engineering Lecture Notes 18, University of New Brunswick, Fredericton, N.B., Canada.

Wild, U., G. Beutler, W. Gurtner, and M. Rothacher (1989). "Estimating the ionosphere using one or more dual frequency GPS receivers," *Proceedings of the Fifth International Geodetic Symposium on Satellite Positioning*, Vol. 2, Las Cruces, N.M., 13-17 March, pp. 724-736.

Wilson, B. D., and A. J. Mannucci (1993). "Instrumental biases in ionospheric measurements derived from GPS data," *Proceedings of the 6th International Technical Meeting of the Satellite Division of The Institute of Navigation (ION GPS 1993)*, Salt Lake City, Utah, 22-24 September, pp. 1343-1351.

Wu, J., S. Wu, G. Hajj, W. Bertiger, and S. Lichten (1993). "Effects of antenna orientation on GPS carrier phase." *Manuscripta Geodaetica*, Vol. 18, No. 2, pp. 91–98.

Wübbena, G. (1985). "Software developments for geodetic positioning with GPS using TI 4100 code and carrier measurements," *Proceedings of 1st International Symposium on Precise Positioning with the Global Positioning System*, edited by Clyde Goad, U.S. Department of Commerce, Rockville, Md., 15-19 April, pp. 403-412.

Wübbena, G., A. Bagge, and M. Schmitz (2001). "RTK networks based on Geo++® GNSMART - concepts, implementation, results," *Proceedings of the 14th International Technical Meeting of the Satellite Division of The Institute of Navigation (ION GPS 2001)*, Salt Lake City, Utah, 11-14 September 2001, pp. 368-378.

Wübbena, G., M. Schmitz, and A. Bagge (2005). "PPP-RTK: precise point positioning using state-space representation in RTK networks," *Proceedings of the 18th International Technical Meeting of the Satellite Division of The Institute of Navigation (ION GNSS 2005)*, Long Beach, Calif., 13-16 September 2005, pp. 2584-2594.

Wübbena, G., and S. Willgalis (2001). "State space approach for precise real time positioning in GPS reference networks," *Proceedings of the International Symposium on Kinematic Systems in Geodesy, Geomatics and Navigation (KIS 2001)*, Banff, Alta., Canada, June 5-8, 2001.

Xu, P. (2006). "Voronoi cells, probabilistic bounds and hypothesis testing in mixed integer linear models." *IEEE Transactions on Information Theory*, Vol. 52, No. 7, pp. 3122–3138. doi:10.1109/TIT.2006.876356.

256

Yamada, H., T. Takasu, N. Kubo, and A. Yasuda (2010). "Evaluation and calibration of receiver inter-channel biases for RTK-GPS/GLONASS," *Proceedings of the 23rd International Technical Meeting of the Satellite Division of The Institute of Navigation (ION GNSS 2010)*, Portland, Ore., 21-24 September 2010, pp. 1580-1587.

Zhang, X., and P. Li (2013). "Assessment of correct fixing rate for precise point positioning ambiguity resolution on a global scale," *Journal of Geodesy*, Vol. 87, No. 6, pp. 579-589. doi: 10.1007/s00190-013-0632-5.

Zhang, X., and X. Li (2012). "Instantaneous re-initialization in real-time kinematic PPP with cycle slip fixing." *GPS Solutions*, Vol. 16, No. 3, pp. 315–327. doi:10.1007/s10291-011-0233-9.

Zumberge, J. F., M. B. Heflin, D. C. Jefferson, M. M. Watkins, and F. H. Webb (1997). "Precise point positioning for the efficient and robust analysis of GPS data from large networks," *Journal of Geophysical Research*, Vol. 102, No. B3, pp. 5005–5017. doi: 10.1029/96JB03860.

APPENDIX I

THE DECOUPLED-CLOCK MODEL

This appendix explains how datum parameters propagate into estimable parameters in the decoupled-clock model and the extended decoupled-clock model. The concepts presented are based on *S-Basis* theory; see, .e.g., Teunissen [1985], de Jonge [1998], or Lannes and Prieur [2013]. Application of *S-Basis* theory for the derivation of the decoupled-clock model has originally been presented by Collins [2011].

I.1 Functional Model

The main principle underlying the decoupled-clock model (DCM) is that instrumental biases constitute, in fact, timing biases. Hence, different observables call for distinct clock parameters. Those observable-dependent clock-like parameters can absorb instrumental biases, and the integer nature of carrier-phase ambiguities can thus be recovered. A simplified functional model for the DCM can be written as:

$$\tilde{\Phi}_{IF}^{j} = \left(dT_{\Phi_{IF}} - dt_{\Phi_{IF}}^{j}\right) + \lambda_{NL}N_1^{j} - \beta_{IF}\lambda_{WL}N_{WL}^{j}$$

$$\tilde{P}_{IF}^{j} = \left(dT_{P_{IF}} - dt_{P_{IF}}^{j}\right) \tag{I.1}$$

$$\Phi_{MW}^{j} = \left(b_{\Phi_{MW}} - b_{\Phi_{MW}}^{j}\right) + \lambda_{WL}N_{WL}^{j}$$

where

$$\lambda_{NL} = \alpha_{IF}\lambda_1 + \beta_{IF}\lambda_2. \qquad (I.2)$$

Readers are referred to Chapter 5 for a definition of the quantities involved. Without loss

of generality, the range parameter (ρ^j) and the slant tropospheric delay parameter (T^j),

were omitted in equation (I.1). As a consequence, the ionosphere-free carrier-phase and

code measurements are replaced by misclosures, denoted by a tilde symbol. Furthermore,

the noise terms (ε) were neglected for simplicity.

Equation (I.1) shows that different receiver and satellite clock parameters have been

introduced for the ionosphere-free carrier-phase, the ionosphere-free code and the

Melbourne-Wübbena observables (note the different subscripts). By doing so, it is

possible to avoid the propagation of observable-specific equipment delays into ambiguity

parameters, thereby preserving their integer nature. On the other hand, specifying

observable-dependent clock parameters leads to a singular system of equations since it is

not possible to directly estimate both ambiguity and phase-clock parameters. This issue

can be resolved by defining an ambiguity datum, as described next.

I.2 Defining an Ambiguity Datum

In the presence of a rank-deficient system of equations, it is possible to separate

parameters into two groups: estimable parameters ($\boldsymbol{x}_E$) and non-estimable (datum)

parameters ($\boldsymbol{x}_D$). The system of equations can then be expressed as:

$$l = A_E x_E + A_D x_D \tag{I.3}$$

where l is the vector of observations, and A_E and A_D are the design matrices corresponding to the parameters x_E and x_D, respectively. Equation (I.3) can be solved for x_E as:

$$\widehat{\overline{x}}_E = (A_E^T A_E)^{-1} A_E^T (l - A_D x_D) = (A_E^T A_E)^{-1} A_E^T l - \underbrace{(A_E^T A_E)^{-1} A_E^T A_D}_{C} x_D \tag{I.4}$$

where the overbar and hat symbols denote biased and estimated quantities, respectively. Equation (I.4) demonstrates that the estimable parameters will be biased by a linear combination (C) of the non-estimable parameters.

There are several ways to define which parameters are estimable or non-estimable, but one has to keep in mind that all estimable parameters will be contaminated by a combination of the non-estimable parameters. In the decoupled-clock model, it is desirable that estimable parameters be contaminated by integer ambiguities, such that the estimable ambiguity parameters will be integer-biased, which still allows for ambiguity resolution to be performed.

To illustrate this concept, we will consider a "network" of a single station (A) observing two satellites (1 and 2), as well as a PPP user (B) observing the same satellites. The following system of equations can thus be formed:

$$
\begin{bmatrix}
\widetilde{\Phi}_{\mathrm{IF}}^{1}(A) \\
\widetilde{P}_{IF}^{1}(A) \\
\Phi_{\mathrm{MW}}^{1}(A) \\
\widetilde{\Phi}_{\mathrm{IF}}^{2}(A) \\
\widetilde{P}_{IF}^{2}(A) \\
\Phi_{\mathrm{MW}}^{2}(A) \\
\widetilde{\Phi}_{\mathrm{IF}}^{1}(B) \\
\widetilde{P}_{IF}^{1}(B) \\
\Phi_{\mathrm{MW}}^{1}(B) \\
\widetilde{\Phi}_{\mathrm{IF}}^{2}(B) \\
\widetilde{P}_{IF}^{2}(B) \\
\Phi_{\mathrm{MW}}^{2}(B)
\end{bmatrix}
= \boldsymbol{A}_E \cdot
\begin{bmatrix}
dt_{\Phi_{IF}}^{1} \\
dt_{P_{IF}}^{1} \\
b_{\Phi_{MW}}^{1} \\
dt_{\Phi_{IF}}^{2} \\
dt_{P_{IF}}^{2} \\
b_{\Phi_{MW}}^{2} \\
dT_{\Phi_{IF}}(B) \\
dT_{P_{IF}}(B) \\
b_{\Phi_{MW}}(B) \\
N_{1}^{2}(B) \\
N_{WL}^{2}(B)
\end{bmatrix}
+ \boldsymbol{A}_D \cdot
\begin{bmatrix}
dT_{\Phi_{IF}}(A) \\
dT_{P_{IF}}(A) \\
b_{\Phi_{MW}}(A) \\
N_{1}^{1}(A) \\
N_{WL}^{1}(A) \\
N_{1}^{2}(A) \\
N_{WL}^{2}(A) \\
N_{1}^{1}(B) \\
N_{WL}^{1}(B)
\end{bmatrix}.
\tag{I.5}
$$

While there are 12 observations, a total of 20 parameters need to be considered. To remove the rank deficiency, the decoupled-clock model requires that one ambiguity be fixed for each ionosphere-free phase clock and Melbourne-Wübbena phase bias parameter. In our example, 6 ambiguities were thus defined as datum parameters. Since timing is relative, the receiver clock/bias parameters of station A were also held fixed. The design matrices $\boldsymbol{A}_E$ and $\boldsymbol{A}_D$ are defined in equations (I.6) and (I.7):

$$
\boldsymbol{A}_E = \begin{bmatrix}
-1 & 0 & 0 & 0 & 0 & 0 & 0 & 0 & 0 & 0 & 0 \\
0 & -1 & 0 & 0 & 0 & 0 & 0 & 0 & 0 & 0 & 0 \\
0 & 0 & -1 & 0 & 0 & 0 & 0 & 0 & 0 & 0 & 0 \\
0 & 0 & 0 & -1 & 0 & 0 & 0 & 0 & 0 & 0 & 0 \\
0 & 0 & 0 & 0 & -1 & 0 & 0 & 0 & 0 & 0 & 0 \\
0 & 0 & 0 & 0 & 0 & -1 & 0 & 0 & 0 & 0 & 0 \\
-1 & 0 & 0 & 0 & 0 & 0 & 1 & 0 & 0 & 0 & 0 \\
0 & -1 & 0 & 0 & 0 & 0 & 0 & 1 & 0 & 0 & 0 \\
0 & 0 & -1 & 0 & 0 & 0 & 0 & 0 & 1 & 0 & 0 \\
0 & 0 & 0 & -1 & 0 & 0 & 1 & 0 & 0 & \lambda_{NL} & -\beta_{IF} \\
0 & 0 & 0 & 0 & -1 & 0 & 0 & 1 & 0 & 0 & 0 \\
0 & 0 & 0 & 0 & 0 & -1 & 0 & 0 & 1 & 0 & \lambda_{WL}
\end{bmatrix}
\tag{I.6}
$$

$$A_D = \begin{bmatrix} 1 & 0 & 0 & \lambda_{NL} & -\beta_{IF}\lambda_2 & 0 & 0 & 0 & 0 \\ 0 & 1 & 0 & 0 & 0 & 0 & 0 & 0 & 0 \\ 0 & 0 & 1 & 0 & \lambda_{WL} & 0 & 0 & 0 & 0 \\ 1 & 0 & 0 & 0 & 0 & \lambda_{NL} & -\beta_{IF}\lambda_2 & 0 & 0 \\ 0 & 1 & 0 & 0 & 0 & 0 & 0 & 0 & 0 \\ 0 & 0 & 1 & 0 & 0 & 0 & \lambda_{WL} & 0 & 0 \\ 0 & 0 & 0 & 0 & 0 & 0 & 0 & \lambda_{NL} & -\beta_{IF}\lambda_2 \\ 0 & 0 & 0 & 0 & 0 & 0 & 0 & 0 & 0 \\ 0 & 0 & 0 & 0 & 0 & 0 & 0 & 0 & \lambda_{WL} \\ 0 & 0 & 0 & 0 & 0 & 0 & 0 & 0 & 0 \\ 0 & 0 & 0 & 0 & 0 & 0 & 0 & 0 & 0 \\ 0 & 0 & 0 & 0 & 0 & 0 & 0 & 0 & 0 \end{bmatrix} \tag{I.7}$$

The propagation of non-estimable parameters into estimable parameters can then be computed from equation (I.4). The linear combination coefficients of the transformation matrix C are presented in Table I.1. As expected, all estimated clock/bias and ambiguity parameters are biased by the non-estimable (datum) parameters, as denoted by the overbar symbol. As a consequence, the decoupled-clock model leads to integer-biased ionosphere-free phase clock and Melbourne-Wübbena phase bias parameters. Importantly, a fundamental characteristic of this approach is that all estimated ambiguity parameters are only biased by datum ambiguities, which preserves their integer definition.

Table I.1: Propagation of non-estimable parameters (columns) into estimable parameters (rows) for the decoupled-clock model.

	Station A							Station B	
	$dT_{\Phi_{IF}}$	$dT_{P_{IF}}$	$b_{\Phi_{MW}}$	N_1^1	N_{WL}^1	N_1^2	N_{WL}^2	N_1^1	N_{WL}^1
$\overline{dt}_{\Phi_{IF}}^1$	-1	0	0	$-\lambda_{NL}$	$\beta_{IF}\lambda_2$	0	0	0	0
$\overline{dt}_{P_{IF}}^1$	0	-1	0	0	0	0	0	0	0
$\overline{b}_{\Phi_{MW}}^1$	0	0	-1	0	$-\lambda_{WL}$	0	0	0	0
$\overline{dt}_{\Phi_{IF}}^2$	-1	0	0	0	0	$-\lambda_{NL}$	$\beta_{IF}\lambda_2$	0	0
$\overline{dt}_{P_{IF}}^2$	0	-1	0	0	0	0	0	0	0
$\overline{b}_{\Phi_{MW}}^2$	0	0	-1	0	0	0	$-\lambda_{WL}$	0	0
$\overline{dT}_{\Phi_{IF}}(B)$	-1	0	0	$-\lambda_{NL}$	$\beta_{IF}\lambda_2$	0	0	λ_{NL}	$-\beta_{IF}\lambda_2$
$\overline{dT}_{P_{IF}}(B)$	0	-1	0	0	0	0	0	0	0
$\overline{b}_{\Phi_{MW}}(B)$	0	0	-1	0	$-\lambda_{WL}$	0	0	0	λ_{WL}
$\overline{N}_1^2(B)$	0	0	0	1	0	-1	0	-1	0
$\overline{N}_{WL}^2(B)$	0	0	0	0	1	0	-1	0	-1

I.3 The Extended Decoupled-Clock Model

The propagation of datum parameters in the extended decoupled-clock model (EDCM) can be demonstrated in a similar fashion. First, let us recall the basic equations of this model, based on equations (5.1) and (5.3):

$$\widetilde{\Phi}_{IF}^j = \left(dT_{\Phi_{IF}} - dt_{\Phi_{IF}}^j\right) + \lambda_{NL}N_1^j - \beta_{IF}\lambda_{WL}N_{WL}^j \tag{I.8}$$

$$\tilde{P}_{IF}^j = \left(dT_{P_{IF}} - dt_{P_{IF}}^j\right)$$

$$\tilde{\Phi}_{WL}^j = \left(dT_{\Phi_{IF}} - dt_{\Phi_{IF}}^j\right) + \frac{f_1}{f_2}I^j + \lambda_{WL}N_{WL}^j + \frac{f_1 f_2}{f_1^2 - f_2^2}\left(DPB_r - DPB^j\right)$$

$$\tilde{P}_{NL}^j = \left(dT_{P_{NL}} - dt_{\Phi_{IF}}^j\right) + b_{\Phi_{MW}}^j + \frac{f_1}{f_2}I^j + \frac{f_1 f_2}{f_1^2 - f_2^2}\left(DPB_r - DPB^j\right)$$

where the range parameter (ρ^j), the slant tropospheric delay parameter (T^j), and the noise terms (ε) were again omitted for simplicity. Equation (I.8) also contains scaled differential phase biases, necessary for consistency. Assuming that widelane observations contain receiver widelane phase biases ($b_{\Phi_{WL}}$) and that ionosphere-free phase clocks contain receiver ionosphere-free phase biases ($b_{\Phi_{IF}}$), we can derive:

$$
\begin{aligned}
b_{\Phi_{WL}} - b_{\Phi_{IF}} &= \left[\frac{f_1}{f_1 - f_2}b_{\Phi_1} - \frac{f_2}{f_1 - f_2}b_{\Phi_2}\right] - \left[\frac{f_1^2}{f_1^2 - f_2^2}b_{\Phi_1} - \frac{f_2^2}{f_1^2 - f_2^2}b_{\Phi_2}\right] \\[2mm]
&= \left[\frac{f_1}{f_1 - f_2} - \frac{f_1^2}{f_1^2 - f_2^2}\right]b_{\Phi_1} - \left[\frac{f_2}{f_1 - f_2} - \frac{f_2^2}{f_1^2 - f_2^2}\right]b_{\Phi_2} \\[2mm]
&= \underbrace{\left[\frac{f_1 f_2}{f_1^2 - f_2^2}\right]}_{\vartheta}\left(b_{\Phi_1} - b_{\Phi_2}\right) \\[2mm]
&= \vartheta \cdot DPB_r
\end{aligned}
\tag{I.9}
$$

where DPB is the differential phase bias. Equation (I.9) can also be used to derive the satellite DPB, where only a sign difference would occur. Since both the satellite Melbourne-Wübbena bias ($b_{\Phi_{MW}}^j$), assumed to contain widelane phase biases, and ionosphere-free phase clock ($dt_{\Phi_{IF}}^j$) are applied to the narrowlane code observables, the same DPB quantities appear in the functional model of this observable.

To illustrate the propagation of datum parameters in the EDCM, we will refer back to the example of stations A and B tracking satellites 1 and 2, defined in the previous section. We will also assume that only the PPP user (station B) uses the EDCM, while the network solution again relies on the decoupled-clock model of equation (I.1). The following system of equations can thus be formed:

$$
\begin{bmatrix}
\tilde{\Phi}_{IF}^1(A) \\
\tilde{P}_{IF}^1(A) \\
\tilde{\Phi}_{MW}^1(A) \\
\tilde{\Phi}_{IF}^2(A) \\
\tilde{P}_{IF}^2(A) \\
\tilde{\Phi}_{MW}^2(A) \\
\tilde{\Phi}_{IF}^1(B) \\
\tilde{P}_{IF}^1(B) \\
\tilde{\Phi}_{WL}^1(B) \\
\tilde{P}_{NL}^1(B) \\
\tilde{\Phi}_{IF}^2(B) \\
\tilde{P}_{IF}^2(B) \\
\tilde{\Phi}_{WL}^2(B) \\
\tilde{P}_{NL}^2(B)
\end{bmatrix}
= \boldsymbol{A}_E \cdot
\begin{bmatrix}
dt_{\Phi_{IF}}^1 \\
dt_{P_{IF}}^1 \\
b_{\Phi_{MW}}^1 \\
dt_{\Phi_{IF}}^2 \\
dt_{P_{IF}}^2 \\
b_{\Phi_{MW}}^2 \\
dT_{\Phi_{IF}}(B) \\
dT_{P_{IF}}(B) \\
dT_{P_{NL}}(B) \\
N_1^2(B) \\
N_{WL}^2(B) \\
I^1(B) \\
I^2(B)
\end{bmatrix}
+ \boldsymbol{A}_D \cdot
\begin{bmatrix}
dT_{\Phi_{IF}}(A) \\
dT_{P_{IF}}(A) \\
b_{\Phi_{MW}}(A) \\
N_1^1(A) \\
N_{WL}^1(A) \\
N_1^2(A) \\
N_{WL}^2(A) \\
N_1^1(B) \\
N_{WL}^1(B) \\
DPB^1 \\
DPB^2 \\
DPB_r(B)
\end{bmatrix}.
\tag{I.10}
$$

Equation (I.10) contains two additional estimable unknowns with respect to equation (I.5), i.e. the slant ionospheric delays from station B to satellites 1 and 2. It also contains three extra non-estimable or datum parameters, which are the satellite DPBs and the DPB of station B. The design matrices $\boldsymbol{A}_E$ and $\boldsymbol{A}_D$ are defined in equation (I.11) and (I.12):

$$\boldsymbol{A_E} = \begin{bmatrix}
-1 & 0 & 0 & 0 & 0 & 0 & 0 & 0 & 0 & 0 & 0 & 0 & 0 \\
0 & -1 & 0 & 0 & 0 & 0 & 0 & 0 & 0 & 0 & 0 & 0 & 0 \\
0 & 0 & -1 & 0 & 0 & 0 & 0 & 0 & 0 & 0 & 0 & 0 & 0 \\
0 & 0 & 0 & -1 & 0 & 0 & 0 & 0 & 0 & 0 & 0 & 0 & 0 \\
0 & 0 & 0 & 0 & -1 & 0 & 0 & 0 & 0 & 0 & 0 & 0 & 0 \\
0 & 0 & 0 & 0 & 0 & -1 & 0 & 0 & 0 & 0 & 0 & 0 & 0 \\
-1 & 0 & 0 & 0 & 0 & 0 & 1 & 0 & 0 & 0 & 0 & 0 & 0 \\
0 & -1 & 0 & 0 & 0 & 0 & 0 & 1 & 0 & 0 & 0 & 0 & 0 \\
-1 & 0 & 0 & 0 & 0 & 0 & 1 & 0 & 0 & 0 & 0 & \frac{f_1}{f_2} & 0 \\
-1 & 0 & 1 & 0 & 0 & 0 & 0 & 0 & 1 & 0 & 0 & \frac{f_1}{f_2} & 0 \\
0 & 0 & 0 & -1 & 0 & 0 & 1 & 0 & 0 & \lambda_{NL} & -\beta_{IF} & 0 & 0 \\
0 & 0 & 0 & 0 & -1 & 0 & 0 & 1 & 0 & 0 & 0 & 0 & 0 \\
0 & 0 & 0 & -1 & 0 & 0 & 1 & 0 & 0 & 0 & \lambda_{WL} & 0 & \frac{f_1}{f_2} \\
0 & 0 & 0 & -1 & 0 & 1 & 0 & 0 & 1 & 0 & 0 & 0 & \frac{f_1}{f_2}
\end{bmatrix}$$

$$(\text{I.11})$$

$$
\boldsymbol{A_D} =
\begin{bmatrix}
1 & 0 & 0 & \lambda_{NL} & -\beta_{IF}\lambda_2 & 0 & 0 & 0 & 0 & 0 & 0 & 0 \\
0 & 1 & 0 & 0 & 0 & 0 & 0 & 0 & 0 & 0 & 0 & 0 \\
0 & 0 & 1 & 0 & \lambda_{WL} & 0 & 0 & 0 & 0 & 0 & 0 & 0 \\
1 & 0 & 0 & 0 & 0 & \lambda_{NL} & -\beta_{IF}\lambda_2 & 0 & 0 & 0 & 0 & 0 \\
0 & 1 & 0 & 0 & 0 & 0 & 0 & 0 & 0 & 0 & 0 & 0 \\
0 & 0 & 1 & 0 & 0 & 0 & \lambda_{WL} & 0 & 0 & 0 & 0 & 0 \\
0 & 0 & 0 & 0 & 0 & 0 & 0 & \lambda_{NL} & -\beta_{IF}\lambda_2 & 0 & 0 & 0 \\
0 & 0 & 0 & 0 & 0 & 0 & 0 & 0 & 0 & 0 & 0 & 0 \\
0 & 0 & 0 & 0 & 0 & 0 & 0 & 0 & \lambda_{WL} & -\vartheta & 0 & \vartheta \\
0 & 0 & 0 & 0 & 0 & 0 & 0 & 0 & 0 & -\vartheta & 0 & \vartheta \\
0 & 0 & 0 & 0 & 0 & 0 & 0 & 0 & 0 & 0 & 0 & 0 \\
0 & 0 & 0 & 0 & 0 & 0 & 0 & 0 & 0 & 0 & 0 & 0 \\
0 & 0 & 0 & 0 & 0 & 0 & 0 & 0 & 0 & 0 & -\vartheta & \vartheta \\
0 & 0 & 0 & 0 & 0 & 0 & 0 & 0 & 0 & 0 & -\vartheta & \vartheta
\end{bmatrix}
$$

$$(\text{I.12})$$

The propagation of non-estimable parameters into estimable parameters can again be computed from equation (I.4). The values of all common parameters between the DCM and EDCM are identical and were presented in Table I.1. The new parameters can be defined as:

$$\overline{dT}_{P_{NL}}(B) = dT_{P_{NL}}(B) - \Delta dT_{P_{NL}}(B) \tag{I.13}$$

with

$$\Delta dT_{P_{NL}}(B) = b_{\Phi_{MW}} - dT_{\Phi_{IF}} - \lambda_{NL}[N_1^1(A) - N_1^1(B)] \\ + \alpha_{IF}\lambda_1[N_{WL}^1(A) - N_{WL}^1(B)] \tag{I.14}$$

and,

$$\bar{I}^j(B) = I^j(B) - \beta_{IF}\left(\bar{b}_{\Phi_{GF}} - \bar{b}_{\Phi_{GF}}^j\right) \tag{I.15}$$

with

$$\bar{b}_{\Phi_{GF}} = DPB_r(B) + (\lambda_1 - \lambda_2) \cdot [N_1^1(B) - N_1^1(A)] + \lambda_2 \cdot [N_{WL}^1(B) - N_{WL}^1(A)] \\ \bar{b}_{\Phi_{GF}}^j = DPB^j - (\lambda_1 - \lambda_2) \cdot N_1^j(A) - \lambda_2 \cdot N_{WL}^j(A). \tag{I.16}$$

Equations (I.15) and (I.16) are essentially the same as equations (5.4) and (5.5).

Curriculum Vitae

Candidate's full name: Simon Banville
Date of birth: 30 August 1982

Universities attended:

2008-2014   Doctor of philosophy candidate, University of New Brunswick
2005-2007   Master of science, Laval University
2001-2005   Bachelor of science, Laval University

Publications:

Banville, S., P. Collins, W. Zhang, and R. B. Langley (2014). "Global and regional ionospheric corrections for faster PPP convergence," *NAVIGATION: Journal of The Institute of Navigation*, Vol. 61, No. 2, Summer 2014, pp. 115-124.

Banville, S., P. Collins, and F. Lahaye (2013). "Concepts for undifferenced GLONASS ambiguity resolution," *Proceedings of the 26th International Technical Meeting of the Satellite Division of The Institute of Navigation (ION GNSS+ 2013)*, Nashville, Tenn., 16-20 September 2013, pp. 1186-1197.

Banville, S., P. Collins, and F. Lahaye (2013). "GLONASS ambiguity resolution of mixed receiver types without external calibration," *GPS Solutions*, Vol. 17, No. 3, pp. 275-282. doi: 10.1007/s10291-013-0319-7.

Banville, S., and R. B. Langley (2013). "Mitigating the impact of ionospheric cycle slips in GNSS observations," *Journal of Geodesy*, Vol. 87, No. 2, pp. 179-193. doi: 10.1007/s00190-012-0604-1.

Banville, S., W. Zhang, and R. B. Langley (2013). "Monitoring the ionosphere with integer-levelled GPS measurements," *GPS World*, Vol. 24, No. 3, March 2013, pp. 43-49.

Zhang, W., R. B. Langley, A. Komjathy, and S. Banville (2013). "Eliminating potential errors caused by the thin shell assumption: an extended 3D UNB ionospheric modeling technique," *Proceedings of the 26th International Technical Meeting of the Satellite Division of The Institute of Navigation (ION GNSS+ 2013)*, Nashville, Tenn., 16-20 September 2013, pp. 2447-2462.

Banville, S., and R. B. Langley (2012) "Cycle-slip correction for single-frequency PPP," Proceedings of the 25th International Technical Meeting of the Satellite Division of The

Institute of Navigation (ION GNSS 2012), Nashville, Tenn., 17-21 September, pp. 3753-3761.

Langley, R. B., S. Banville, and P. Steigenberger (2012). "First results: precise positioning with Galileo prototype satellites," *GPS World*, Vol. 23, No. 9, pp. 45-49.

Banville, S., W. Zhang, R. Ghoddousi-Fard, and R. B. Langley (2012). "Ionospheric monitoring using 'integer-levelled' observations," *Proceedings of the 25th International Technical Meeting of the Satellite Division of The Institute of Navigation (ION GNSS 2012)*, Nashville, Tenn., 17-21 September, pp. 2692-2701.

Banville, S., and R. B. Langley (2011). "Defining the basis of an integer-levelling procedure for estimating slant total electron content," *Proceedings of the 24th International Technical Meeting of the Satellite Division of The Institute of Navigation (ION GNSS 2011)*, Portland, Ore., 19-23 September, pp. 2542-2551.

Banville, S., and R. B. Langley (2010). "Instantaneous cycle-slip correction for real-time PPP applications," *NAVIGATION: Journal of The Institute of Navigation*, Vol. 57, No. 4, Winter 2010-2011, pp. 325-334.

Banville, S., R. B. Langley, S. Saito, and T. Yoshihara (2010). "Handling cycle slips in GPS data during ionospheric plasma bubble events." *Radio Science*, Vol. 45, RS6007. doi: doi:10.1029/2010RS004415.

Banville, S., and H. Tang (2010). "Antenna rotation and its effects on kinematic precise point positioning." *Proceedings of the 23rd International Technical Meeting of the Satellite Division of The Institute of Navigation (ION GNSS 2010)*, Portland, Ore., 21-24 September, pp. pp. 2545-2552.

Banville, S., and R. B. Langley (2009). "Improving real-time kinematic PPP with instantaneous cycle-slip correction." *Proceedings of the 22nd International Technical Meeting of the Satellite Division of The Institute of Navigation (ION GNSS 2009)*, Savannah, Ga., 22-25 September, pp. 2470-2478.

Banville, S., R. B. Langley, and M. C. Santos (2009). "The Precise Point Positioning Software Centre: an insight into online PPP services." Poster presented at the International Association of Geodesy (IAG) 2009 Meeting, Buenos Aires, Argentina, 31 August - 4 September.

Banville, S., R. Santerre, M. Cocard, and R. B. Langley (2008), "Satellite and receiver phase bias calibration for undifferenced ambiguity resolution," *Proceedings of the 2008 National Technical Meeting of The Institute of Navigation* (ION NTM 2008), San Diego, Calif., 28-30 January 2008, pp. 711-719.